

# The *UBV* Color Evolution of Classical Novae. III. Time-Stretched Color-Magnitude Diagram of Novae in Outburst

IZUMI HACHISU<sup>1</sup> AND MARIKO KATO<sup>2</sup>

<sup>1</sup>*Department of Earth Science and Astronomy, College of Arts and Sciences, The University of Tokyo, 3-8-1 Komaba, Meguro-ku, Tokyo 153-8902, Japan*

<sup>2</sup>*Department of Astronomy, Keio University, Hiyoshi, Kouhoku-ku, Yokohama 223-8521, Japan*

## ABSTRACT

We propose a modified color-magnitude diagram for novae in outburst, i.e.,  $(B - V)_0$  versus  $(M_V - 2.5 \log f_s)$ , where  $f_s$  is the timescaling factor of a (target) nova against a comparison (template) nova,  $(B - V)_0$  is the intrinsic  $B - V$  color, and  $M_V$  is the absolute  $V$  magnitude. We dub it the time-stretched color-magnitude diagram. We carefully reanalyzed 20 novae based on the time-stretching method and revised their extinctions  $E(B - V)$ , distance moduli in the  $V$  band  $(m - M)_V$ , distances  $d$ , and timescaling factors  $f_s$  against the template nova LV Vul. We have found that these 20 nova outburst tracks broadly follow one of the two template tracks, LV Vul/V1668 Cyg or V1500 Cyg/V1974 Cyg group, in the time-stretched color-magnitude diagram. In addition, we estimate the white dwarf masses and  $(m - M)_V$  of the novae by directly fitting the absolute  $V$  model light curves ( $M_V$ ) with observational apparent  $V$  magnitudes ( $m_V$ ). A good agreement in the two estimates of  $(m - M)_V$  confirms the consistency of the time-stretched color-magnitude diagram. Our distance estimates are in good agreement with the results of Gaia Data Release 2.

*Keywords:* novae, cataclysmic variables — stars: individual (V574 Pup, V679 Car, V1369 Cen, V5666 Sgr) — stars: winds

## 1. INTRODUCTION

A nova is a thermonuclear explosion event on a mass-accreting white dwarf (WD) in a close binary. When the mass of the hydrogen-rich envelope on the WD reaches a critical value, hydrogen ignites at the bottom of the hydrogen-rich envelope to trigger a nova explosion. Then, the envelope expands to a red-giant size and emits strong winds (Kato & Hachisu 1994). After the maximum expansion of the photosphere (when the maximum wind mass-loss rate is attained), the photospheric radius begins to shrink and the photospheric temperature rises with time. The main emitting wavelength region thus shifts from optical to UV and supersoft X-ray (see, e.g., Figure 23 of Hachisu & Kato 2006, for V1974 Cyg). A large part of the hydrogen-rich envelope is blown in the wind. The wind stops and the nova enters a supersoft X-ray source (SSS) phase. The envelope mass decreases further by nuclear burning. When it decreases to below the critical mass (minimum mass for steady hydrogen shell-burning), nuclear burning extinguishes. The WD cools down and the nova outburst

ends. These evolutions of novae are briefly summarized in Hachisu & Kato (2017).

Evolutions of nova outbursts can be followed by the optically thick wind theory. Kato & Hachisu (1994) calculated nova evolution for various WD masses (from  $0.5 M_\odot$  to  $1.38 M_\odot$ ) and showed that the main parameter which determines the speed class of novae is the WD mass. A nova on a more massive WD evolves faster because the ignition mass (envelope mass at the epoch when hydrogen ignites) is much smaller and is blown off in the wind in a much shorter time.

The acceleration mechanism of the wind is the so-called continuum radiation-driven (Friedjung 1966). The matter in the envelope is accelerated deep inside the photosphere, in other words, at/near the iron peak of the radiative opacity ( $\log T$  (K)  $\sim 5.2$ ). So, it is called the optically thick winds. This mechanism is common among all the WD masses ranging from  $\sim 0.5 M_\odot$  to  $1.38 M_\odot$  (Kato & Hachisu 1994).

Nova spectra in the decay phase are dominated by free-free emission (Gallagher & Ney 1976; Ennis et al. 1977; Krautter et al. 1984; Naik et al. 2009) until the nova entered the nebular phase where strong emission lines such as [O III] are dominant. Free-free emission

of novae is originating from the expanding hot and optically thin gaseous plasma, that is, outside the photosphere of the optically thick winds. Free-free emission light curves of novae are theoretically calculated from the wind-mass loss rate  $\dot{M}_{\text{wind}}$ , photospheric velocity  $v_{\text{ph}}$ , and photospheric radius  $R_{\text{ph}}$ , that is,  $F_{\nu} \propto \dot{M}_{\text{wind}}^2 / v_{\text{ph}}^2 R_{\text{ph}}$  (Hachisu & Kato 2006), where  $F_{\nu}$  is the flux of free-free emission at the frequency  $\nu$ . It should be noted that the flux of free-free emission  $F_{\nu}$  is almost independent of the frequency  $\nu$  in the optical and near-infrared (NIR) region.

Hachisu & Kato (2006) calculated free-free emission light curves for various WD masses (from  $0.5 M_{\odot}$  to  $1.38 M_{\odot}$ ) and envelope chemical compositions. Since the flux of free-free emission  $F_{\nu}$  is almost independent of the frequency  $\nu$ , the light curve shapes are very similar among the optical and NIR bands until the nebular phase or dust formation started. For example, the  $V$ ,  $J$ ,  $H$ ,  $2.3\mu\text{m}$ , and  $3.6\mu\text{m}$  band light curves of V1668 Cyg show an almost identical light curve shape, which are well reproduced by a theoretical light curve until the optically-thin dust shell formation makes a deviation from the theoretical one (see, e.g., Figure 18 of Hachisu & Kato 2006).

Hachisu & Kato (2006) further found that the theoretical free-free emission light curves and UV (1455 Å) light curves show a scaling law among various WD masses and chemical compositions. The UV 1455 Å band is a narrow (1445–1465 Å) and emission line-free band invented by Cassatella et al. (2002) and represents continuum flux of UV. All the UV 1455 Å model light curves also follow the same timescaling law as that of free-free emission light curves. In other words, if we properly squeeze the timescales of novae, these theoretical light curves converge into one (see Figure 18 of Hachisu & Kato 2006). The main part of theoretical free-free emission light curve decays as  $F_{\nu} \propto t^{-1.75}$ . Hachisu & Kato (2006) called this property the universal decline law of classical novae.

Because the decline rate of optical light curve is a good indicator of the WD mass, we can estimate the WD mass from comparison of the theoretical light curve with the observed optical one. If multiwavelength light curves are available, we are able to determine the WD mass more accurately. Using multiwavelength light curves in optical, UV 1455 Å, and supersoft X-ray turn-on/turnoff times, Hachisu & Kato (2006, 2010, 2016a) determined the WD masses of V1974 Cyg and V1668 Cyg. The UV 1455 Å band flux represents the photospheric emission in the wind phase while the supersoft X-ray flux does in the post-wind phase. These multiwavelength data are so useful because their dependences on the

WD mass and chemical composition are different. It should be noted that the soft X-ray light curves do not obey the timescaling law (see, e.g., Figure 6 of Hachisu & Kato 2010). We are further able to discriminate these two parameters from multiwavelength light curve fitting. Thus, Hachisu & Kato (2015, 2016a) determined the WD masses within error of  $\pm 0.01 M_{\odot}$  by simultaneously reproducing the observed multiwavelength light curves for a number of novae.

Hachisu & Kato (2010) introduced the timescaling factor  $f_s$ , which is the timescale ratio of a target nova against a template nova. Using this  $f_s$ , we can compare various nova light curves in a quantitative way. They showed that, if a large part of the nova light/color curves overlap each other by properly squeezing/stretching their timescales, the absolute brightness ( $M_V$ ) of the target nova is related to the absolute brightness ( $M'_V$ ) of the other (template) nova by  $M_V = M'_V + 2.5 \log f_s$ . This means that the time-stretched absolute light curves of the two novae overlap each other in the  $(t/f_s)$ - $(M_V - 2.5 \log f_s)$  plane. They adopted V1668 Cyg and V1974 Cyg as template novae, of which the distances and extinctions are known. Using this property, Hachisu & Kato (2010, 2015, 2016a) determined the absolute magnitude  $M_V$  for each free-free emission light curve of different WD mass and chemical composition. They called this method the time-stretching method. By directly fitting the theoretical light curves of  $M_V$  with the observed  $m_V$ , we can also estimate the WD mass  $M_{\text{WD}}$  and distance modulus in the  $V$  band of  $\mu_V \equiv (m - M)_V$  for a target nova. Hachisu & Kato (2018b) confirmed that the time-stretching method is applicable to fast and very fast novae in our Galaxy, LMC, and M31.

There are also common properties in the color evolution in nova outbursts. Hachisu & Kato (2014, hereafter Paper I) found that many novae in outburst evolve on a common path in the  $(B - V)_0$ - $(U - B)_0$  color-color diagram. Here,  $(B - V)_0$  and  $(U - B)_0$  are the intrinsic colors of  $B - V$  and  $U - B$ , respectively. The evolution path starts from the nova-giant sequence and then moves to the free-free emission phase followed by the emission line dominant nebular phase. (See, e.g., their Figure 28.)

Hachisu & Kato (2016b, Paper II) found that many novae follow similar evolution path in the  $(B - V)_0$ - $M_V$  color-magnitude diagram. Here,  $M_V$  is the absolute  $V$  magnitude in the  $V$  band. They extensively examined the color-magnitude tracks of 40 novae in outburst and found several distinct “template tracks” in the  $(B - V)_0$ - $M_V$  diagram. They proposed six template tracks of novae and dubbed them the V1500 Cyg, V1668 Cyg,

V1974 Cyg, LV Vul, FH Ser, and PU Vul type tracks. The difference among the groups may be related to the envelope mass, which is closely related to the nova evolution speed, but was not fully clarified. They categorized 40 novae into one of these six subgroups, depending on their similarity of the tracks in the  $(B - V)_0 - M_V$  diagram. They are not fully successful, however, to explain why each nova has a similar  $M_V$  in the  $(B - V)_0 - M_V$  diagram.

Nova light curves show a similar property in the  $(t/f_s) - (M_V - 2.5 \log f_s)$  plane. The color-magnitude evolution should also be treated in the same way, that is, based on the time-stretching method. In the present work, we propose the  $(B - V)_0 - (M_V - 2.5 \log f_s)$  color magnitude diagram. We call this “time-stretched color-magnitude diagram” in order to distinguish it from the usual  $(B - V)_0 - M_V$  diagram. The time-stretching method is useful because many nova light curves follow a universal decline law. Once their absolute  $V$  magnitude is time-stretched, nova light curves overlap each other in the  $(t/f_s) - (M_V - 2.5 \log f_s)$  light curve (Hachisu & Kato 2010). Here, we stretch/squeeze the timescale of a target nova as  $t' = t/f_s$  and overlap its light curve to the comparison (template) nova. Then, we have the relation of

$$\begin{aligned} (M_V[t])_{\text{template}} &= (M'_V[t'])_{\text{target}} \\ &= (M_V[t/f_s] - 2.5 \log f_s)_{\text{target}} \end{aligned} \quad (1)$$

between  $(t', M'_V)$  and  $(t, M_V)$  coordinates systems (see Appendix A of Hachisu & Kato 2016a), where  $M_V[t]$  means that  $M_V$  is a function of time  $t$ . The color  $(B - V)_0$  is not affected by this time-stretch because the both fluxes of  $B$  and  $V$  are shifted by the same quantities,  $-2.5 \log f_s$  (Hachisu & Kato 2018a). We thus examine each nova evolution in the  $(B - V)_0 - (M_V - 2.5 \log f_s)$  diagram. The above two reasons, Equation (1) and that the color  $(B - V)_0$  is not affected by time-stretch, are the theoretical background for the property that each nova track overlaps in the time-stretched color-magnitude diagram.

To summarize the theoretical background, both the colors  $(B - V)_0$  and  $(U - B)_0$  are not affected by time-stretch. Therefore, the  $(t/f_s) - (B - V)_0$  and  $(t/f_s) - (U - B)_0$  color curves overlap each other after time-stretch. As a result, many novae in outburst evolve on a common path in the usual  $(B - V)_0 - (U - B)_0$  color-color diagram. This is the reason why Hachisu & Kato (2014) found a common track in the  $(B - V)_0 - (U - B)_0$  diagram. On the other hand, the  $(t/f_s) - M_V$  light curves do not overlap because the absolute  $M_V$  magnitudes are different among novae. This is the reason why Hachisu & Kato (2016b) did not find common tracks

in the  $(B - V)_0 - M_V$  diagram. If we use the  $(B - V)_0 - (M_V - 2.5 \log f_s)$  diagram, we could find common tracks because the  $(t/f_s) - (M_V - 2.5 \log f_s)$  light curves overlap each other after time-stretch.

In this work, we examine nova evolution in the time-stretched color-magnitude diagram. We adopt total 20 novae, including 12 novae that were already analyzed in Paper II, but reanalyzed here in a new light of the time-stretched color-magnitude diagram. Our aim is to provide a uniform set of 20 novae analyzed by the same time-stretched color-magnitude diagram method.

Our paper is organized as follows. First we describe our method for four well-studied novae in Section 2. Then, we apply this method to four recent novae V574 Pup, V679 Car, V1369 Cen, and V5666 Sgr to determine their various physical parameters in Sections 3, 4, 5, and 6, respectively. In Section 7, we reanalyze twelve novae, which were studied in Paper II on the usual color-magnitude diagram. We confirm that all the novae follow one of the two template tracks, V1500 Cyg or LV Vul, in the time-stretched color-magnitude diagram. In Section 8, we compared our distance estimates with the Gaia Data Release 2. Conclusions follows in Section 9.

## 2. METHOD AND TEMPLATE NOVAE

### 2.1. Method

First, we need to know the intrinsic color and time-stretching factor  $f_s$  in order to analyze a particular nova light curve. The procedure is summarized as follows:

**1.** Calculate the intrinsic colors of  $(B - V)_0$  and  $(U - B)_0$  as

$$(B - V)_0 = (B - V) - E(B - V), \quad (2)$$

and

$$(U - B)_0 = (U - B) - 0.64E(B - V), \quad (3)$$

where the factor of 0.64 is taken from Rieke & Lebofsky (1985). The color excess  $E(B - V)$  is taken from literature, if available.

**2.** Determine the time-stretching factor  $f_s$  of a target nova from a comparison with a template nova in the light/color curves (see, e.g., Figure 19). We adopt the template nova from one of LV Vul, V1500 Cyg, V1668 Cyg, and V1974 Cyg, of which the distance modulus  $\mu_V \equiv (m - M)_V$  and extinction  $E(B - V)$  are well determined. We use LV Vul as the template nova unless otherwise specified. The timescaling factor  $f_s$  is measured against the timescale of LV Vul. In the light/color curves, we stretch/squeeze the timescale of the target nova (horizontal shift in a logarithmic timescale) and also shift the magnitude in the vertical direction. The light curve of the target nova overlaps the template nova

**Table 1.** Extinctions, distance moduli, and distances for selected novae

Object	Outburst year	$E(B - V)$	$(m - M)_V$	$d$ (kpc)	$\log f_s^a$	$(m - M')_V$	Ref. <sup>b</sup>
CI Aql	2000	1.0	15.7	3.3	-0.22	15.15	3
V1419 Aql	1993	0.52	15.0	4.7	+0.15	15.35	4
V679 Car	2008	0.69	16.1	6.2	+0.0	16.1	4
V705 Cas	1993	0.45	13.45	2.6	+0.45	14.55	4
V1065 Cen	2007	0.45	15.0	5.3	+0.0	15.0	2
V1369 Cen	2013	0.11	10.25	0.96	+0.17	10.65	4
IV Cep	1971	0.65	14.5	3.1	+0.0	14.5	2
T CrB	1946	0.056	10.1	0.96	-1.32	13.4	3
V407 Cyg	2010	1.0	16.1	3.9	-0.37	15.2	3
V1500 Cyg	1975	0.45	12.3	1.5	-0.22	11.75	1
V1668 Cyg	1978	0.30	14.6	5.4	+0.0	14.6	1
V1974 Cyg	1992	0.30	12.2	1.8	+0.03	12.3	1
V2362 Cyg	2006	0.60	15.4	5.1	+0.25	16.05	4
V2468 Cyg	2008	0.65	16.2	6.9	+0.38	17.15	4
V2491 Cyg	2008	0.45	17.4	15.9	-0.34	16.55	4
YY Dor	2010	0.12	18.9	50.0	-0.72	17.1	3
V446 Her	1960	0.40	11.95	1.38	+0.0	11.95	4
V533 Her	1963	0.038	10.65	1.28	+0.08	10.85	4
V838 Her	1991	0.53	13.7	2.6	-1.22	10.65	3
V959 Mon	2012	0.38	13.15	2.5	+0.14	13.5	2
RS Oph	2006	0.65	12.8	1.4	-1.02	10.25	3
V2615 Oph	2007	0.90	15.95	4.3	+0.20	16.45	4
V574 Pup	2004	0.45	15.0	5.3	+0.10	15.25	4
U Sco	2010	0.26	16.3	12.6	-1.32	13.0	3
V745 Sco	2014	0.70	16.6	7.8	-1.32	13.3	3
V1534 Sco	2014	0.93	17.6	8.8	-1.22	14.55	3
V496 Sct	2009	0.45	13.7	2.9	+0.30	14.45	4
V5114 Sgr	2004	0.47	16.65	10.9	-0.12	16.35	4
V5666 Sgr	2014	0.50	15.4	5.8	+0.25	16.0	4
V382 Vel	1999	0.25	11.5	1.4	-0.29	10.75	4
LV Vul	1968	0.60	11.85	1.0	+0.0	11.85	1,2,4
PW Vul	1984	0.57	13.0	1.8	+0.35	13.85	4
LMCN 2009a	2014	0.12	18.9	50.0	-0.52	17.6	3
LMCN 2012a	2012	0.12	18.9	50.0	-1.22	15.85	3
LMCN 2013	2013	0.12	18.9	50.0	-0.42	17.85	3
SMCN 2016	2016	0.08	16.8	20.4	-0.72	15.0	3
M31N 2008-12a	2015	0.30	24.8	780	-1.32	21.5	3

<sup>a</sup>  $f_s$  is the timescale against that of LV Vul.

<sup>b</sup> 1 - Hachisu & Kato (2016b), 2 - Hachisu & Kato (2018a), 3 - Hachisu & Kato (2018b), 4 - present paper,

by stretching horizontally (in the time-direction) by a factor of  $f_s$  and by shifting vertically by  $\Delta V$ , we estimate the distance modulus of the target nova,

$$(m - M)_{V,\text{target}} = ((m - M)_V + \Delta V)_{\text{template}} - 2.5 \log f_s. \quad (4)$$

Hachisu & Kato (2010) called this method the time-stretching method. We usually increase/decrease the horizontal shift by a step of  $\delta(\Delta \log t) = \delta(\log f_s) = 0.01$  and the vertical shift by a step of  $\delta(\Delta V) = 0.1$  mag, and determine the best one by eye. The model light curves obey the universal decline law. This phase corresponds to the optically thick wind phase before the

nebular phase started. In fact, many novae show a good agreement with the model light curve in the optically thick phase. Moreover, we find that the  $V$  light curve of a target nova often show a good agreement with that of a template nova even in the nebular (optically thin) phase. In such a case, we use all the phases to determine the timescaling factor (see, e.g., Figure 2).

**3.** Determine the WD mass and absolute brightness from the comparison with model light curves calculated by Hachisu & Kato (2010, 2015, 2016a). These light curves are obtained for various WD masses and chemical compositions. The distance modulus in the  $V$  band,  $(m - M)_V$ , is determined independently of procedure

**Table 2.** White dwarf masses of selected novae

Object	$\log f_s$	$M_{\text{WD}}$	$M_{\text{WD}}$	$M_{\text{WD}}$	$M_{\text{WD}}$	Chem.comp.
		$f_s^a$	UV 1455 Å <sup>b</sup>	$t_{\text{SSS-on}}^c$	$t_{\text{SSS-off}}^d$	
		( $M_{\odot}$ )	( $M_{\odot}$ )	( $M_{\odot}$ )	( $M_{\odot}$ )	
CI Aql	-0.22	1.18	—	—	—	interp. <sup>e</sup>
V1419 Aql	+0.15	0.90	—	—	—	CO3
V679 Car	+0.0	0.98	—	—	—	CO3
V705 Cas	+0.45	0.78	0.78	—	—	CO4
V1065 Cen	+0.0	0.98	—	—	—	CO3
V1369 Cen	+0.17	0.90	—	—	—	CO3
IV Cep	+0.0	0.98	—	—	—	CO3
T CrB	-1.32	1.38	—	—	—	interp.
V407 Cyg	-0.37	1.22	—	—	—	interp.
V1500 Cyg	-0.22	1.20	—	—	—	Ne2
V1668 Cyg	+0.0	0.98	0.98	—	—	CO3
V1974 Cyg	+0.03	0.98	0.98	0.98	0.98	CO3
V2362 Cyg	+0.25	0.85	—	—	—	interp.
V2468 Cyg	+0.38	0.85	—	—	—	CO4
V2491 Cyg	-0.34	1.35	—	1.35	1.35	Ne2
YY Dor	-0.72	1.29	—	—	—	interp.
V446 Her	+0.0	0.98	—	—	—	CO3
V533 Her	+0.08	1.03	—	—	—	Ne2
V838 Her	-1.22	1.35	1.35	—	—	Ne2
V838 Her	-1.22	1.37	1.37	—	—	Ne3
V959 Mon	+0.14	0.95	—	0.95	—	CO3
V959 Mon	+0.14	1.05	—	1.05	—	Ne2
V959 Mon	+0.14	1.1	—	1.10	—	Ne3
RS Oph	-1.02	1.35	1.35	1.35	1.35	evol. <sup>f</sup>
V2615 Oph	+0.20	0.90	—	—	—	CO3
V574 Pup	+0.10	1.05	—	1.05	1.05	Ne2
U Sco	-1.32	1.37	—	1.37	1.37	evol.
V745 Sco	-1.32	1.38	—	1.385	1.385	evol.
V1534 Sco	-1.22	1.37	—	—	—	interp.
V496 Sct	+0.30	0.85	—	—	—0	CO3
V5114 Sgr	-0.12	1.15	—	—	—	Ne2
V5666 Sgr	+0.25	0.85	—	—	—	CO3
V382 Vel	-0.29	1.23	—	—	1.23	Ne2
LV Vul	+0.0	0.98	—	—	—	CO3
PW Vul	+0.35	0.83	0.83	—	—	CO4
LMC N 2009a	-0.52	1.25	—	1.25	1.25	Ne3
LMC N 2012a	-1.22	1.37	—	—	—	interp.
LMC N 2013	-0.42	1.23	—	—	—	interp.
SMC N 2016	-0.72	1.29	—	—	1.3	Ne3
SMC N 2016	-0.72	1.29	—	—	1.25	Ne2
M31N 2008-12a	-1.32	1.38	—	1.38	1.38	evol.

<sup>a</sup> WD mass estimated from the  $f_s$  timescale.

<sup>b</sup> WD mass estimated from the UV 1455 Å fit.

<sup>c</sup> WD mass estimated from the  $t_{\text{SSS-on}}$  fit.

<sup>d</sup> WD mass estimated from the  $t_{\text{SSS-off}}$  fit.

<sup>e</sup> “interp.”: WD mass estimated from a linear interpolation of  $\log f_s$  vs. WD mass relation (see Hachisu & Kato 2018b).

<sup>f</sup> “evol.”: WD mass estimated from the time-evolution calculation with a Henyey type code (see, e.g., Hachisu & Kato 2018b).

No.2.

**4.** The above procedures in No.2 and No.3 are independent methods. Thus, good agreement of the two  $(m - M)_V$  confirms our method. We obtain the distance  $d$  to the target nova from the relation of

$$(m - M)_V = 3.1E(B - V) + 5 \log(d/10 \text{ pc}), \quad (5)$$

where the factor  $R_V = A_V/E(B - V) = 3.1$  is the ratio of total to selective extinction (e.g., [Rieke & Lebofsky 1985](#)).

**5.** We apply the same time-stretching method to the  $U$ ,  $B$ ,  $I_C$ , and  $K_s$  bands, if they are available, that is,

$$(m - M)_{U,\text{target}} = ((m - M)_U + \Delta U - 2.5 \log f_s)_{\text{template}}, \quad (6)$$

$$(m - M)_{B,\text{target}} = ((m - M)_B + \Delta B - 2.5 \log f_s)_{\text{template}}, \quad (7)$$

$$(m - M)_{I,\text{target}} = ((m - M)_I + \Delta I_C - 2.5 \log f_s)_{\text{template}}, \quad (8)$$

$$(m - M)_{K,\text{target}} = ((m - M)_K + \Delta K_s - 2.5 \log f_s)_{\text{template}}, \quad (9)$$

where the timescaling factor  $f_s$  is unique and the same as that in Equation (4). Thus, we independently obtain the five distance moduli in the  $U$ ,  $B$ ,  $V$ ,  $I_C$ , and  $K_s$  bands (for example, Figure 18). Then, we obtain the relation between the distance  $d$  and color excess  $E(B - V)$  to the target nova where we use the relation of

$$(m - M)_U = 4.75E(B - V) + 5 \log(d/10 \text{ pc}), \quad (10)$$

$$(m - M)_B = 4.1E(B - V) + 5 \log(d/10 \text{ pc}), \quad (11)$$

$$(m - M)_I = 1.5E(B - V) + 5 \log(d/10 \text{ pc}), \quad (12)$$

$$(m - M)_K = 0.35E(B - V) + 5 \log(d/10 \text{ pc}), \quad (13)$$

and  $A_U/E(B - V) = 4.75$ ,  $A_B/E(B - V) = 4.1$ ,  $A_I/E(B - V) = 1.5$ , and  $A_K/E(B - V) = 0.35$  are taken from [Rieke & Lebofsky \(1985\)](#). We plot these relations of Equations (10), (11), (5), (12), and (13) in the reddening-distance plane. If these lines cross at the same point, this point gives correct values of reddening  $E(B - V)$  and distance  $d$  (for example, Figure 7(a)).

**6.** Using  $E(B - V)$ ,  $(m - M)_V$ , and  $f_s$  obtained in the above procedures, we plot the  $(B - V)_0 - M_V$  color-magnitude diagram and the  $(B - V)_0 - (M_V - 2.5 \log f_s)$  time-stretched color-magnitude diagram of the target

nova (for example, Figures 8 and 9, respectively). We derive the relation of

$$(m - M')_{V,\text{target}} \equiv (m_V - (M_V - 2.5 \log f_s))_{\text{target}} = ((m - M)_V + \Delta V)_{\text{template}}, \quad (14)$$

from Equations (1) and (4).

**7.** If the track of the target nova overlaps to the LV Vul (or V1500 Cyg, V1668 Cyg, V1974 Cyg) template track in the time-stretched color-magnitude diagram, we regard that our set of  $f_s$ ,  $E(B - V)$ ,  $(m - M)_V$ , and distance  $d$  are reasonable.

## 2.2. Reddening and distance

In what follows, we use LV Vul, V1500 Cyg, V1668 Cyg, and V1974 Cyg as template novae, because their distances and extinctions have been well determined. Figure 1 shows the distance-reddening relations toward the four template novae, (a) LV Vul, (b) V1500 Cyg, (c) V1668 Cyg, and (d) V1974 Cyg. We have already analyzed them in our previous papers (e.g., [Hachisu & Kato 2016a,b](#)), but here we reanalyze them because new distance-reddening relations are recently available (e.g., [Green et al. 2018](#); [Chen et al. 2018](#)). To summarize, we use five results: (1) [Marshall et al. \(2006\)](#) published a three-dimensional (3D) extinction map of our Galaxy. The range is  $-100^\circ 0 \leq l \leq 100^\circ 0$  and  $-10^\circ 0 \leq b \leq +10^\circ 0$  and the resolution of grids is  $\Delta l = 0^\circ 25$  and  $\Delta b = 0^\circ 25$ , where  $(l, b)$  is the galactic coordinates. (2) [Sale et al. \(2014\)](#) presented a 3D reddening map with the region of  $30^\circ \leq l < 215^\circ$  and  $|b| < 5^\circ$ . Their data are based on the INT Photometric H-Alpha Survey (IPHAS) photometry. (3) [Green et al. \(2015\)](#) published a 3D reddening map with a wider range of three quarters of the sky and with much finer grids of  $3'4$  to  $13'7$  whose distance resolution is 25%. The data of distance-reddening relation were recently revised by [Green et al. \(2018\)](#). (4) [Özdörmez et al. \(2016\)](#) obtained distance-reddening relations toward 46 novae based on the unique position of the red clump giants in the color-magnitude diagram. Recently, [Özdörmez et al. \(2018\)](#) added the data of recent novae. (5) [Chen et al. \(2018\)](#) presented 3D interstellar dust reddening maps of the galactic plane in three colors,  $E(G - K_s)$ ,  $E(G_{\text{BP}} - G_{\text{RP}})$ , and  $E(H - K_s)$ . We use the conversion of  $E(B - V) = 0.75E(G_{\text{BP}} - G_{\text{RP}})$  from [Chen et al. \(2018\)](#). The maps have a spatial angular resolution of 6 arcmin and covers the galactic longitude  $0 < l < 360^\circ$  and latitude  $|b| < 10^\circ$ . The maps are constructed from parallax estimates from the Gaia Data Release 2 (Gaia DR2) combined with the photometry from the Gaia DR2 and the infrared photometry from the 2MASS and WISE surveys.

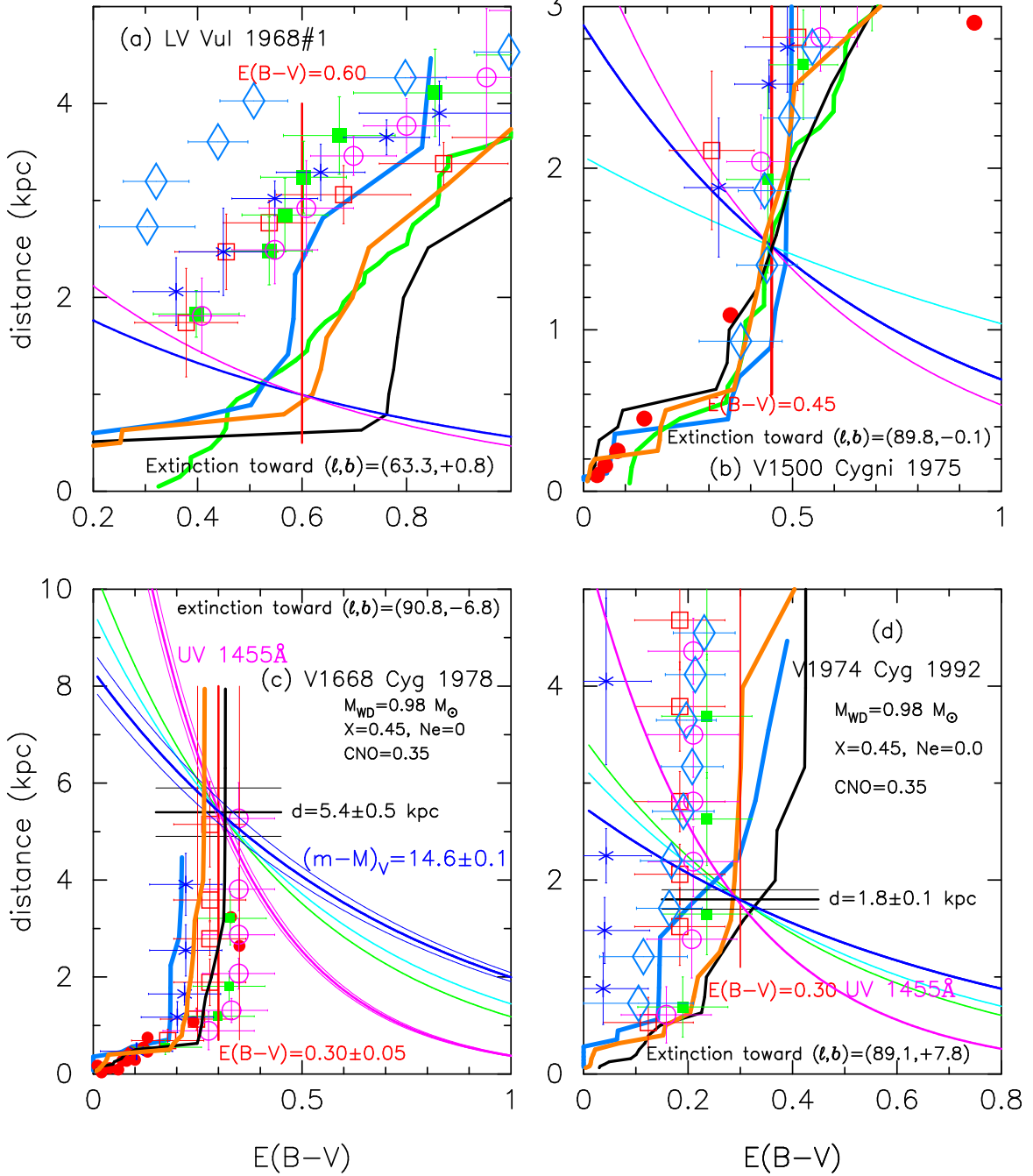


**Figure 1.** Distance-reddening relations toward our template novae: (a) LV Vul, (b) V1500 Cyg, (c) V1668 Cyg, and (d) V1974 Cyg. The thick solid blue lines denote (a)  $(m - M)_V = 11.85$ , (b)  $(m - M)_V = 12.3$ , (c)  $(m - M)_V = 14.6$ , and (d)  $(m - M)_V = 12.2$ . The vertical solid red lines represent the color excess of each nova. The open cyan-blue diamonds denote the distance-reddening relations given by Özdörmez et al. (2016). The solid black/orange lines represent the distance-reddening relations given by Green et al. (2015, 2018), respectively. The thick solid cyan-blue lines denote the relations given by Chen et al. (2018). The four sets (open red squares, filled green squares, blue asterisks, and open magenta circles) of data with error bars show the distance-reddening relations of Marshall et al. (2006) in four nearby directions of each nova. In panels (a) and (b), the green solid lines indicate the distance-reddening relations given by Sale et al. (2014). In panels (a) and (b), the thin solid magenta line denotes the  $B$  band distance modulus. In panel (b), the solid cyan line represents the  $I$  band distance modulus. In panels (c) and (d), the filled red circles denote the distances and reddenings of nearby stars given by Young et al. (1976) and Slovak & Vogt (1979), respectively. In panels (c) and (d), the solid magenta lines represent the distance-reddening relation from the UV 1455Å light curve fitting, and the thin solid green/cyan lines depict the distance moduli of  $U/B$  bands, respectively. See text for more details.

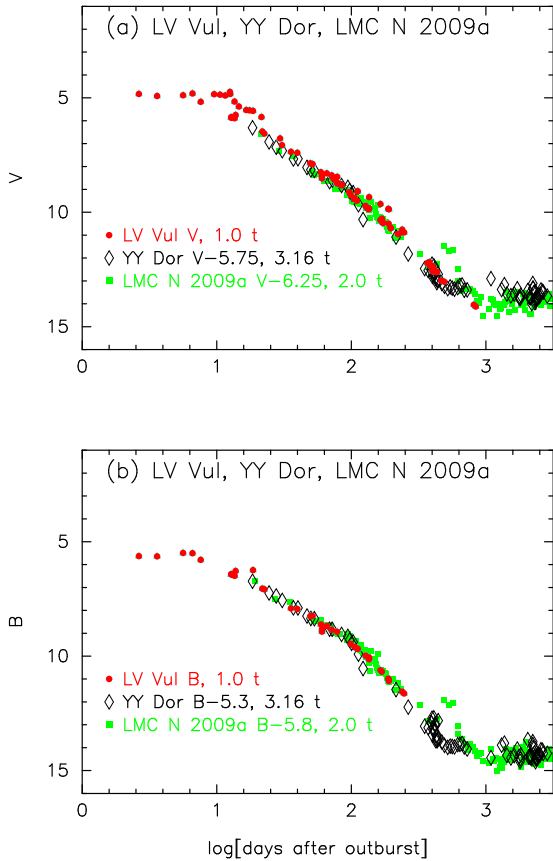


**Figure 2.** The (a)  $V$  and (b)  $B$  light curves of LV Vul, YY Dor (2004), and LMC N 2009a on logarithmic timescales. Each light curve is horizontally moved by  $\Delta \log t = \log f_s$  and vertically shifted by  $\Delta V$  (or  $\Delta B$ ) with respect to that of LV Vul, as indicated in the figure by, for example, “YY Dor  $V-5.75$ ,  $3.16 t$ ,” (“YY Dor  $B-5.3$ ,  $3.16 t$ ,”), where  $\Delta V = -5.75$  ( $\Delta B = -5.3$ ) and  $f_s = 3.16$ .

These five 3D dust maps often show large discrepancies (see, e.g., Figure 1(a)). The 3D dust maps essentially give an averaged value of a relatively broad region and thus, the pinpoint reddening could be different from it, because the resolutions of these dust maps are considerably larger than molecular cloud structures observed in the interstellar medium. For example, Figure 1(a) shows a large discrepancy among the various relations. The orange line (Green et al. 2018) is quite consistent with our values, i.e., the crossing point of  $(m - M)_V = 11.85$  (blue line) and  $E(B - V) = 0.60$  (vertical solid red line). This will be discussed in detail in Section 2.3.1.

### 2.3. Template nova light curves

Here, we reexamine the four template novae LV Vul, V1500 Cyg, V1668 Cyg, and V1974 Cyg, with the new distance-reddening relations (Green et al. 2018;

Chen et al. 2018) and fix the distances and extinctions for later use.

#### 2.3.1. LV Vul 1968#1

The reddening toward LV Vul was estimated by Fernie (1969) to be  $E(B - V) = 0.6 \pm 0.2$  from the color excesses of 14 B stars near the line of sight. Tempesti (1972) obtained  $E(B - V) = 0.55$  from the color at optical maximum; i.e.,  $E(B - V) = (B - V)_{\max} - (B - V)_{0,\max} = 0.9 - 0.35 = 0.55$ . He adopted  $(B - V)_{0,\max} = +0.35$  (Schmidt 1957) instead of  $(B - V)_{0,\max} = +0.23$  (van den Bergh & Younger 1987). Hachisu & Kato (2014) obtained  $E(B - V) = 0.60 \pm 0.05$  by fitting with the typical color-color evolution track of nova outbursts. Slavin et al. (1995) obtained the distance toward LV Vul to be  $d = 0.92 \pm 0.08$  kpc by a nebular expansion parallax method.

Figure 2 shows the (a)  $V$  and (b)  $B$  light curves of LV Vul as well as YY Dor (2004) and LMC N 2009a. The LV Vul data are the same as those in Figure 4 of Paper II. The light curves of YY Dor and LMC N 2009a are time-stretched against LV Vul. These two novae are analyzed by Hachisu & Kato (2018b) and the various properties are summarized in their Tables 1, 2, and 3. They determined the timescaling factors of YY Dor and LMC N 2009a against LV Vul, which are plotted in Figure 2. In this case, we shift up/down the YY Dor and LMC N 2009a light curves in a step of  $\delta(\Delta V) = 0.1$  mag (or  $\delta(\Delta B) = 0.1$  mag) and find the best fit one by eye. We use all the part of the light curve if they overlap each other. If not, we use only the part of the optically thick wind phase before the nebular (or dust blackout) phase started. Fortunately, the three light curves of LV Vul, YY Dor, and LMC N 2009a broadly overlap each other even during the nebular phase as shown in Figure 2.

YY Dor and LMC N 2009a belong to the Large Magellanic Cloud (LMC) and their distances are well constrained. We adopt  $\mu_{0,\text{LMC}} = 18.493 \pm 0.048$  (Pietrzyński et al. 2013). The reddenings toward YY Dor is assumed to be  $E(B - V) = 0.12$ , which is the typical reddening toward the LMC (Imara & Blitz 2007). The distance modulus in the  $V$  band is  $(m - M)_V = \mu_0 + A_V = 18.49 + 3.1 \times 0.12 = 18.86$  toward the LMC novae.

Applying the obtained  $f_s$  and  $\Delta V$  to Equation (4), we have the relation of

$$\begin{aligned}
 (m - M)_{V,\text{LV Vul}} &= ((m - M)_V + \Delta V)_{\text{YY Dor}} - 2.5 \log 3.16 \\
 &= 18.86 - 5.75 \pm 0.2 - 1.25 = 11.86 \pm 0.2 \\
 &= ((m - M)_V + \Delta V)_{\text{LMCN 2009a}} - 2.5 \log 2.0 \\
 &= 18.86 - 6.25 \pm 0.2 - 0.75 = 11.86 \pm 0.2. \quad (15)
 \end{aligned}$$



Thus, we obtain  $(m - M)_V = 11.86 \pm 0.1$  for LV Vul, being consistent with our previous results of  $(m - M)_V = 11.85 \pm 0.1$  (Hachisu & Kato 2018b).

In the same way, we obtain  $\Delta B$  from Figure 2(b). Using this  $\Delta B$  and  $f_s$ , we obtain

$$\begin{aligned} (m - M)_{B, LV \text{ Vul}} &= ((m - M)_B + \Delta B)_{YY \text{ Dor}} - 2.5 \log 3.16 \\ &= 18.98 - 5.3 \pm 0.2 - 1.25 = 12.43 \pm 0.2 \\ &= ((m - M)_B + \Delta B)_{LMCN \text{ 2009a}} - 2.5 \log 2.0 \\ &= 18.98 - 5.8 \pm 0.2 - 0.75 = 12.43 \pm 0.2, \quad (16) \end{aligned}$$

from Equation (7). Here, we adopt  $(m - M)_B = 18.49 + 4.1 \times 0.12 = 18.98$  for the LMC novae. Thus, we obtain  $(m - M)_B = 12.43 \pm 0.1$  for LV Vul.

We determine the stretching factor  $f_s$  by horizontally shifting the light and color curves. Its step is  $\delta \log f_s = 0.01$  as explained in Section 2.1. Usually we use three  $BVI_C$  light curves and  $(B - V)_0$  color curve to overlap them with those of the template novae against a unique  $f_s$ . The error of  $\log f_s$  depends on how well these light/color curves overlap. Typically we have 0.03–0.05 for the error of  $\log f_s$ . This error is not independent but propagates to the error of vertical fit of  $\Delta V$ . We estimate the typical total error of  $\epsilon(\Delta V - 2.5 \log f_s) = (\pm 0.2) + (\pm 0.1)$ . In the case of LV Vul,  $\log f_s$  is rather well determined against YY Dor and LMC N 2009a, that is, the error of  $\epsilon(\log f_s) = \pm 0.02$  (see Section 5.1 of Hachisu & Kato 2018b). Therefore, the total error is about  $\epsilon(\Delta V - 2.5 \log f_s) = (\pm 0.2) + (\pm 0.05)$ . In what follows, we include the error of the  $f_s$  determination in the error of vertical fit  $\Delta V$ , because the vertical fit always reflect the error of  $f_s$  determination.

We plot these two distance-reddening relations of Equations (5) and (11) in Figure 1(a) by the thin solid blue and magenta lines, respectively. The crossing point of the blue, magenta, orange, and vertical red lines, i.e.,  $d = 1.0$  kpc and  $E(B - V) = 0.60$ , is in reasonable agreement with  $d = 0.92 \pm 0.08$  kpc (Slavin et al. 1995) and  $E(B - V) = 0.60 \pm 0.05$  (Hachisu & Kato 2014, 2016b). Thus, we confirm that the distance modulus in the  $V$  band is  $(m - M)_V = 11.85 \pm 0.1$ , the reddening is  $E(B - V) = 0.60 \pm 0.05$ , and the distance is  $d = 1.0 \pm 0.2$  kpc. These values are listed in Table 1.

### 2.3.2. V1500 Cyg 1975

The distance to V1500 Cyg was discussed by many authors. Young et al. (1976) estimated the distance to be  $1.4 \pm 0.1$  kpc for  $E(B - V) = 0.45$  (Tomkin et al. 1976) from the distance-reddening law toward the nova (depicted by the filled red circles in Figure 1(b)). We add Marshall et al.’s (2006) relations for four directions close to V1500 Cyg, that is,  $(l, b) = (89^\circ 75', 0^\circ 00')$

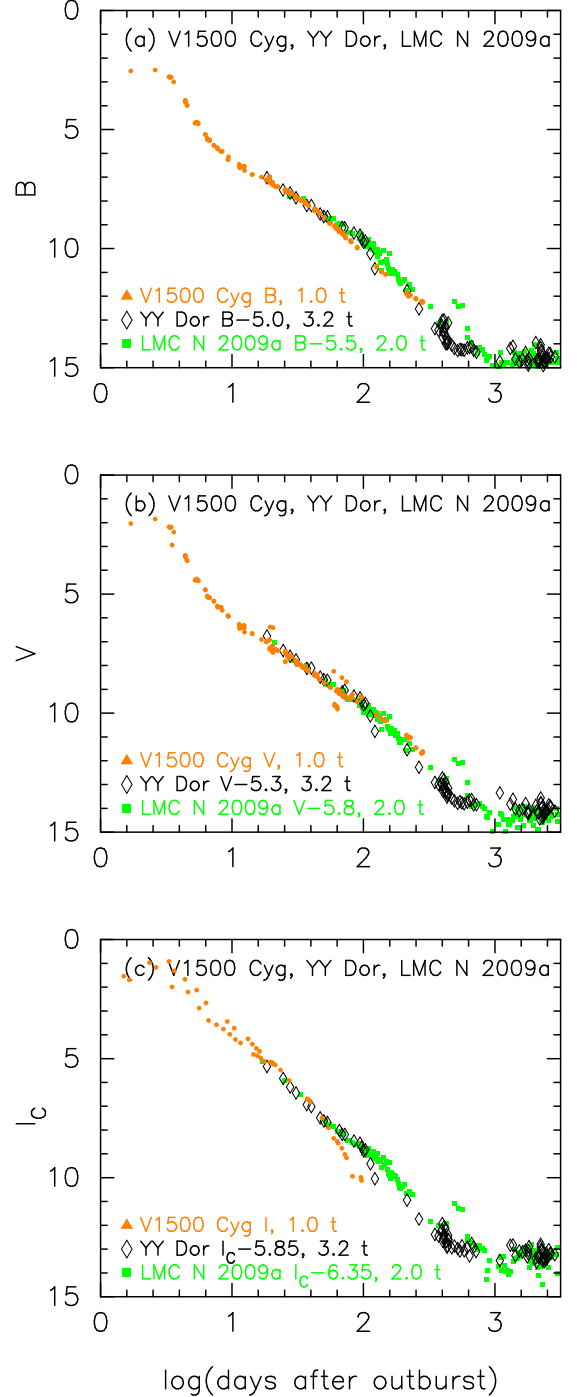


**Figure 3.** The (a)  $B$ , (b)  $V$ , and (c)  $I$  light curves of V1500 Cyg as well as YY Dor and LMC N 2009a. The  $BV$  data of V1500 Cyg are taken from Williamon (1977), Tempesti (1979), Pfau (1976), and Arhipova & Zaitseva (1976). The  $I$  data of V1500 Cyg are taken from Belokon & Larionov (1977) and The & van der Klis (1976). We plot the  $I_C$  data for YY Dor and LMC N 2009a because no  $I$  data are available.

(red open squares), (90°00, 0°00) (green filled squares), (89°75, -0°25) (blue asterisks), and (90°00, -0°25) (magenta open circles). We further add the relations of Green et al. (2015, 2018), Sale et al. (2014), Özdörmez et al. (2016), and Chen et al. (2018). Green et al.'s and Sale et al.'s relations (black and green lines) give  $d = 1.5$  kpc for  $E(B - V) = 0.45$ .

A firm upper limit to the apparent distance modulus was obtained as  $(m - M)_V \leq 12.5$  by Ando & Yamashita (1976) from the galactic rotational velocities of interstellar H and K absorption lines. The nebular expansion parallax method also gives an estimate of the distance. Becker & Duerbeck (1980) first imaged an expanding nebular ( $0'.25 \text{ yr}^{-1}$ ) of V1500 Cyg and estimated a distance of 1350 pc from the expansion velocity of  $v_{\text{exp}} = 1600 \text{ km s}^{-1}$ . However, Wade et al. (1991) resolved an expanding nebula and obtained a much lower expansion rate of  $0'.16 \text{ yr}^{-1}$ ; they estimated the distance to be 1.56 kpc, with a much smaller expansion velocity of  $v_{\text{exp}} = 1180 \text{ km s}^{-1}$  (Cohen 1985). Slavin et al. (1995) obtained a similar expanding angular velocity of the nebula ( $0'.16 \text{ yr}^{-1}$ ) and obtained a distance of 1550 pc from  $v_{\text{exp}} = 1180 \text{ km s}^{-1}$ . Therefore, the distance is reasonably determined to be  $d = 1.5 \pm 0.1$  kpc from the nebular expansion parallax method.

Hachisu & Kato (2014) obtained  $(m - M)_V = 12.3$  for V1500 Cyg by the time-stretching method together with the light curves of GK Per and V603 Aql (see Figure 40 and Equation (A1) of Paper I). We plot  $(m - M)_V = 12.3$  (blue solid line) and  $E(B - V) = 0.45$  (vertical red solid line) in Figure 1(b). The crossing point of these two lines is consistent with the distance-reddening relations of Green et al. (2015, 2018), Sale et al. (2014), Özdörmez et al. (2016), and Chen et al. (2018) except Marshall et al. (2006). Thus, we confirm  $d = 1.5 \pm 0.1$  kpc,  $E(B - V) = 0.45 \pm 0.05$ , and  $(m - M)_V = 12.3 \pm 0.1$ . The timescaling factor of V1500 Cyg is determined to be  $f_s = 0.60$  against LV Vul. We list these values in Table 1.

We check the distance moduli of V1500 Cyg with the LMC novae, YY Dor and LMC N 2009a, based on the time-stretching method. Figure 3 shows the *BVI* light curves of V1500 Cyg as well as YY Dor and LMC N 2009a. Here we use the *I* band data of V1500 Cyg because no *I<sub>C</sub>* data are available. We apply Equation (7) for the *B* band to Figure 3(a) and obtain

$$\begin{aligned} (m - M)_{B, V1500 \text{ Cyg}} &= ((m - M)_B + \Delta B)_{\text{YY Dor}} - 2.5 \log 3.2 \\ &= 18.98 - 5.0 \pm 0.2 - 1.25 = 12.73 \pm 0.2 \\ &= ((m - M)_B + \Delta B)_{\text{LMC N 2009a}} - 2.5 \log 2.0 \\ &= 18.98 - 5.5 \pm 0.2 - 0.75 = 12.73 \pm 0.2, \quad (17) \end{aligned}$$

where we adopt  $(m - M)_B = 18.49 + 4.1 \times 0.12 = 18.98$  for the LMC novae. Thus, we obtain  $(m - M)_{B, V1500 \text{ Cyg}} = 12.73 \pm 0.1$ .

For the *V* light curves in Figure 3(b), we similarly obtain

$$\begin{aligned} (m - M)_{V, V1500 \text{ Cyg}} &= ((m - M)_V + \Delta V)_{\text{YY Dor}} - 2.5 \log 3.2 \\ &= 18.86 - 5.3 \pm 0.2 - 1.25 = 12.31 \pm 0.2 \\ &= ((m - M)_V + \Delta V)_{\text{LMC N 2009a}} - 2.5 \log 2.0 \\ &= 18.86 - 5.8 \pm 0.2 - 0.75 = 12.31 \pm 0.2, \quad (18) \end{aligned}$$

where we adopt  $(m - M)_V = 18.49 + 3.1 \times 0.12 = 18.86$  for the LMC novae. Thus, we obtain  $(m - M)_{V, V1500 \text{ Cyg}} = 12.31 \pm 0.1$ .

We apply Equation (8) to Figure 3(c) and obtain

$$\begin{aligned} (m - M)_{I, V1500 \text{ Cyg}} &= ((m - M)_I + \Delta I_C)_{\text{YY Dor}} - 2.5 \log 3.2 \\ &= 18.66 - 5.85 \pm 0.3 - 1.25 = 11.56 \pm 0.3 \\ &= ((m - M)_I + \Delta I_C)_{\text{LMC N 2009a}} - 2.5 \log 2.0 \\ &= 18.66 - 6.35 \pm 0.3 - 0.75 = 11.56 \pm 0.3, \quad (19) \end{aligned}$$

where we adopt  $(m - M)_I = 18.49 + 1.5 \times 0.12 = 18.66$  for the LMC novae. Thus, we obtain  $(m - M)_{I, V1500 \text{ Cyg}} = 11.56 \pm 0.2$ .

We plot three distance moduli in the *B*, *V*, and *I<sub>C</sub>* bands in Figure 1(b) by the magenta, blue, and cyan lines, that is,  $(m - M)_B = 12.73$ ,  $(m - M)_V = 12.31$ , and  $(m - M)_I = 11.56$ , together with Equations (11), (5), and (12), respectively. These three lines cross at  $d = 1.5$  kpc and  $E(B - V) = 0.45$ . This crossing point is an independent confirmation of the distance and reddening.

### 2.3.3. V1668 Cyg 1978

Figure 4 shows the *UBV* light curves of V1668 Cyg and LV Vul. The timescale of V1668 Cyg is the same as LV Vul, that is,  $f_s = 1.0$  against LV Vul. If the chemical composition of V1668 Cyg is similar to that of LV Vul, both the WD masses should be similar. The peak of V1668 Cyg is slightly brighter than that of LV Vul. In general, the peak brightness depends mainly on the WD mass and initial envelope mass. The peak magnitude is brighter for the more massive ignition mass even if the WD masses are the same. Such a tendency was discussed in detail in Hachisu & Kato (2010) (see their Figure 2 for the physical explanation). The initial envelope mass, that is, the ignition mass, is closely related to the mass accretion rate on the WD. The larger the mass accretion rate, the smaller the ignition mass (see, e.g., Figure 3 of Kato et al. 2014). We suppose that the mass accretion rate is smaller in V1668 Cyg than in LV Vul even if the two WD masses are similar.

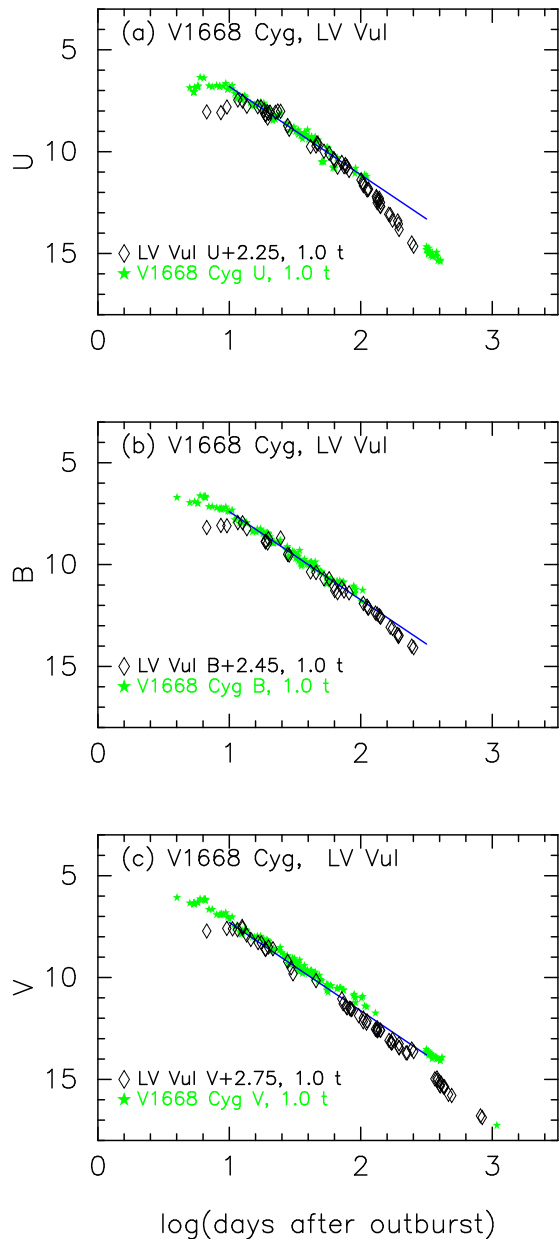


**Figure 4.** The (a)  $U$ , (b)  $B$ , and (c)  $V$  light curves of V1668 Cyg and LV Vul on a logarithmic timescale. Each light curve is vertically shifted by  $\Delta U$  (or  $\Delta B$  or  $\Delta V$ ) with respect to that of V1668 Cyg as indicated in the figure. The timescales of the two novae are the same. The solid blue lines denote the slope of  $F_\nu \propto t^{-1.75}$ , which represents well the optically thick wind phase (Hachisu & Kato 2006). The  $UBV$  data of V1668 Cyg and LV Vul are the same as Figures 1 and 4 of Hachisu & Kato (2016b), respectively.

These two nova light curves well overlap except for the peak brightnesses. The distance moduli of LV Vul are well determined in Section 2.3.1, so the distance moduli of V1668 Cyg are calculated to be  $(m-M)_U = 12.84 + 2.25 \pm 0.1 = 15.1 \pm 0.1$ ,  $(m-M)_B = 12.45 + 2.45 \pm 0.1 =$

$14.9 \pm 0.1$ , and  $(m-M)_V = 11.85 + 2.75 \pm 0.1 = 14.6 \pm 0.1$  from the time-stretching method. These three distance moduli cross at  $d = 5.4$  kpc and  $E(B-V) = 0.30$  in the distance-reddening plane of Figure 1(c).

Hachisu & Kato (2006, 2016a) calculated free-free emission model light curves based on the optically thick wind model (Kato & Hachisu 1994) for various WD masses and chemical compositions and fitted their free-free emission model light curves with the  $V$  and  $y$  light curves of V1668 Cyg. They further fitted their black-body emission UV 1455Å model light curves with the *International Ultraviolet Explorer (IUE)* UV 1455Å observation, and estimated the WD mass. This is a narrow-band (1445–1465 Å) flux that represents well the continuum UV fluxes of novae (Cassatella et al. 2002).

Assuming the chemical composition of CO nova 3 for V1668 Cyg, Hachisu & Kato (2016a) obtained the best fit model of  $0.98 M_\odot$  WD with both the  $V$  and UV 1455 Å light curves. (Such model light curve fittings are also plotted in Figure 23 in Appendix A.2.) We plot the distance-reddening relation of  $(m-M)_V = 14.6 \pm 0.1$  (thick solid blue line flanked by two thin blue lines in Figure 1(c)) and another distance-reddening relation of the UV 1455Å fit (thick solid magenta line flanked by two thin solid magenta lines) of

$$2.5 \log F_{1455}^{\text{mod}} - 2.5 \log F_{1455}^{\text{obs}} = 5 \log \left( \frac{d}{10 \text{ kpc}} \right) + 8.3 \times E(B-V), \quad (20)$$

where  $F_{1455}^{\text{mod}}$  is the model flux at the distance of 10 kpc and  $F_{1455}^{\text{obs}}$  the observed flux. Here we assume an absorption of  $A_\lambda = 8.3 \times E(B-V)$  at  $\lambda = 1455$  Å (Seaton 1979).

We further plot other distance-reddening relations toward V1668 Cyg in Figure 1(c): given by Slovak & Vogt (1979) (filled red circles), by Marshall et al. (2006), by Green et al. (2015, 2018), and by Chen et al. (2018). Marshall et al.’s are for four nearby directions:  $(l, b) = (90^\circ 75', -6^\circ 75')$  (red open squares),  $(91^\circ 00', -6^\circ 75')$  (green filled squares),  $(90^\circ 75', -7^\circ 00')$  (blue asterisks), and  $(91^\circ 00', -7^\circ 00')$  (magenta open circles). These trends/lines broadly cross at  $d = 5.4 \pm 0.5$  kpc and  $E(B-V) = 0.30 \pm 0.05$  except that of Chen et al. (2018). The extinction almost saturates at the distance of  $d \gtrsim 3$  kpc as shown in Figure 1(c). This is consistent with the galactic 2D dust absorption map of  $E(B-V) = 0.29 \pm 0.02$  in the direction toward V1668 Cyg at the NASA/IPAC Infrared Science Archive<sup>1</sup>, which is calculated on the basis of data

<sup>1</sup> <http://irsa.ipac.caltech.edu/applications/DUST/>

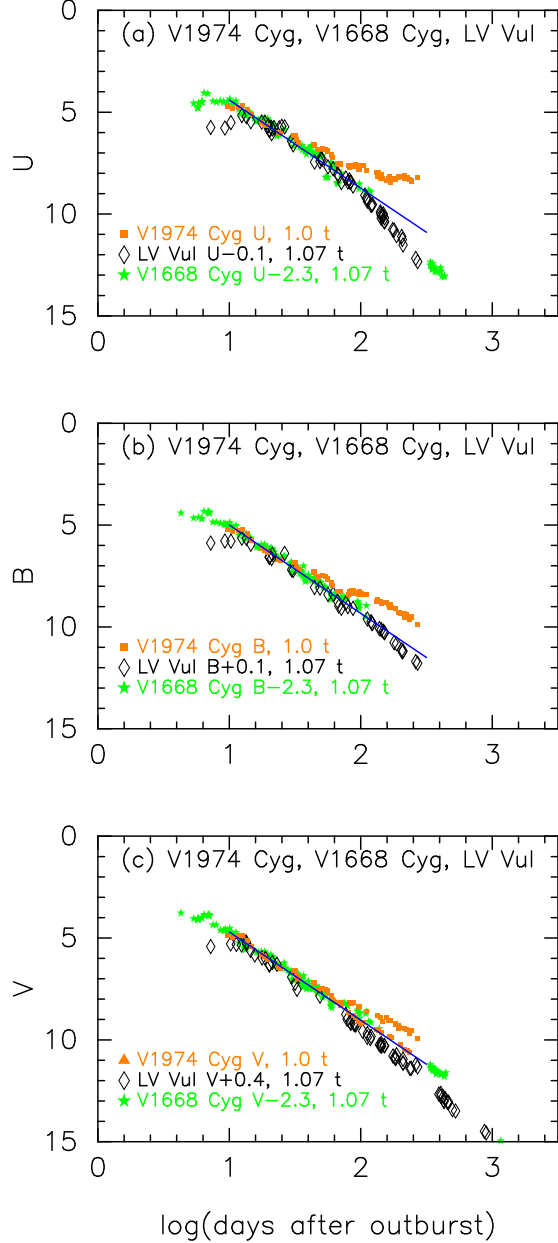


**Figure 5.** The  $UBV$  light curves of V1974 Cyg are plotted together with those of LV Vul and V1668 Cyg. The solid blue lines denote the slope of  $F_\nu \propto t^{-1.75}$ , which represents well the optically thick wind phase (Hachisu & Kato 2006). The  $UBV$  data of V1974 Cyg are taken from Chochol et al. (1993). The  $UBV$  data of LV Vul and V1668 Cyg are the same as those in Figure 4.

from Schlafly & Finkbeiner (2011). Thus, we confirm  $E(B - V) = 0.30 \pm 0.05$ .

#### 2.3.4. V1974 Cyg 1992

We obtain the reddening and distance from the time-stretching method. We plot the  $UBV$  light curves of V1974 Cyg together with those of LV Vul and

V1668 Cyg in Figure 5. The  $UBV$  light curves well overlap until the nebular phase started on Day  $\sim 60$ . We use only the part of optically thick wind (or optically thick ejecta) phase, which are represented by the decline trend of  $F_\nu \propto t^{-1.75}$  (Hachisu & Kato 2006). The timescaling factor of  $f_s = 1.07$  against LV Vul is well determined from the fitting of UV 1455Å light curve between V1668 Cyg and V1974 Cyg (see, e.g., Figure 39(a) in Appendix B.6).

We apply Equation (6) for the  $U$  band to Figure 5(a) and obtain

$$\begin{aligned}
 (m - M)_{U, V1974 \text{ Cyg}} &= ((m - M)_U + \Delta U)_{LV \text{ Vul}} - 2.5 \log 1.07 \\
 &= 12.85 - 0.1 \pm 0.2 - 0.08 = 12.67 \pm 0.2 \\
 &= ((m - M)_U + \Delta U)_{V1668 \text{ Cyg}} - 2.5 \log 1.07 \\
 &= 15.1 - 2.3 \pm 0.2 - 0.08 = 12.72 \pm 0.2, \quad (21)
 \end{aligned}$$

where we adopt  $(m - M)_{U, LV \text{ Vul}} = 11.85 + (4.75 - 3.1) \times 0.60 = 12.85$ , and  $(m - M)_{U, V1668 \text{ Cyg}} = 14.6 + (4.75 - 3.1) \times 0.30 = 15.10$ . Thus, we obtain  $(m - M)_{U, V1974 \text{ Cyg}} = 12.7 \pm 0.1$ . For the  $B$  light curves in Figure 5(b), we similarly obtain

$$\begin{aligned}
 (m - M)_{B, V1974 \text{ Cyg}} &= ((m - M)_B + \Delta B)_{LV \text{ Vul}} - 2.5 \log 1.07 \\
 &= 12.45 + 0.1 \pm 0.2 - 0.08 = 12.47 \pm 0.2 \\
 &= ((m - M)_B + \Delta B)_{V1668 \text{ Cyg}} - 2.5 \log 1.07 \\
 &= 14.9 - 2.3 \pm 0.2 - 0.08 = 12.52 \pm 0.2, \quad (22)
 \end{aligned}$$

where we adopt  $(m - M)_{B, LV \text{ Vul}} = 11.85 + 1.0 \times 0.6 = 12.45$  and  $(m - M)_{B, V1668 \text{ Cyg}} = 14.6 + 1.0 \times 0.3 = 14.9$ . Thus, we obtain  $(m - M)_{B, V1974 \text{ Cyg}} = 12.5 \pm 0.1$ . We apply Equation (4) to Figure 5(c) and obtain

$$\begin{aligned}
 (m - M)_{V, V1974 \text{ Cyg}} &= ((m - M)_V + \Delta V)_{LV \text{ Vul}} - 2.5 \log 1.07 \\
 &= 11.85 + 0.4 \pm 0.2 - 0.08 = 12.17 \pm 0.2 \\
 &= ((m - M)_V + \Delta V)_{V1668 \text{ Cyg}} - 2.5 \log 1.07 \\
 &= 14.6 - 2.3 \pm 0.2 - 0.08 = 12.22 \pm 0.2. \quad (23)
 \end{aligned}$$

Thus, we obtain  $(m - M)_{V, V1974 \text{ Cyg}} = 12.2 \pm 0.1$ . These three distance moduli, that is,  $(m - M)_U = 12.7$ ,  $(m - M)_B = 12.5$ , and  $(m - M)_V = 12.2$  together with Equations (10), (11), and (5), cross at  $d = 1.8$  kpc and  $E(B - V) = 0.30$  as shown in Figure 1(d).

Hachisu & Kato (2016a) modeled the  $V$ , UV 1455Å, and supersoft X-ray light curves and fitted a  $0.98 M_\odot$  WD model with the observed  $V$ , UV 1455Å, and X-ray fluxes assuming the chemical composition of CO nova 3 (see, e.g., Figure 33(a) for such a model light curve fit). The supersoft X-ray flux was calculated assuming that the photospheric emission is approximated by blackbody emission in the supersoft X-ray band. The  $V$  model

light curve gives a distance modulus in the  $V$  band of  $(m - M)_V = 12.2$  (blue line) as shown in Figure 1(d), while the UV 1455 Å light curve fit gives a relation of magenta line.

These two lines (blue and magenta lines) cross at  $d \approx 1.8$  kpc and  $E(B - V) \approx 0.29$  as shown in Figure 1(d). The figure also depicts other distance-reddening relations toward V1974 Cyg, whose galactic coordinates are  $(l, b) = (89^\circ 1338, 7^\circ 8193)$ . The four sets of data points with error bars correspond to the distance-reddening relations in four directions close to V1974 Cyg:  $(l, b) = (89^\circ 00, 7^\circ 75)$  (red open squares),  $(89^\circ 25, 7^\circ 75)$  (green filled squares),  $(89^\circ 00, 8^\circ 00)$  (blue asterisks), and  $(89^\circ 25, 8^\circ 00)$  (magenta open circles), the data for which are taken from Marshall et al. (2006). We also add distance-reddening relations given by Green et al. (2015, 2018) (black/orange lines), Özdörmez et al. (2016) (open cyan-blue diamonds with error bars), and Chen et al. (2018) (cyan-blue line). The orange line is consistent with the crossing point at  $d \approx 1.8$  kpc and  $E(B - V) \approx 0.30$ .

Chochol et al. (1997) estimated the distance to V1974 Cyg as  $d = 1.77 \pm 0.11$  kpc by a nebular expansion parallax method. This distance is consistent with our value of  $d = 1.8 \pm 0.1$  kpc. The reddening was also estimated by many researchers. For example, Austin et al. (1996) obtained the reddening toward V1974 Cyg mainly on the basis of the UV and optical line ratios for days 200 through 500, i.e.,  $E(B - V) = 0.3 \pm 0.1$ . The NASA/IPAC galactic 2D dust absorption map gives  $E(B - V) = 0.35 \pm 0.01$  in the direction toward V1974 Cyg. This slightly larger value of reddening indicates that the reddening toward V1974 Cyg does not saturate yet at the distance of 1.8 kpc, as shown in Figure 1(d). These are all consistent with our estimates, that is,  $(m - M)_V = 12.2 \pm 0.1$ ,  $d = 1.8 \pm 0.1$  kpc, and  $E(B - V) = 0.3 \pm 0.05$ . These values are listed in Table 1.

#### 2.4. Template nova tracks in the time-stretched color-magnitude diagram

Hachisu & Kato (2016b) proposed six template tracks of novae with well-determined distance modulus in the  $V$  band  $(m - M)_V$  and color excess  $E(B - V)$ . They dubbed them the V1500 Cyg, V1668 Cyg, V1974 Cyg, LV Vul, FH Ser, and PU Vul tracks as shown in Figure 6(a). Here, we adopt  $E(B - V) = 0.60$  and  $(m - M)_V = 11.85$  for LV Vul from Section 2.3.1,  $E(B - V) = 0.45$  and  $(m - M)_V = 12.3$  for V1500 Cyg from Section 2.3.2,  $E(B - V) = 0.30$  and  $(m - M)_V = 14.6$  for V1668 Cyg from Section 2.3.3,  $E(B - V) = 0.30$  and  $(m - M)_V = 14.3$  for V1974 Cyg from Section 2.3.4,

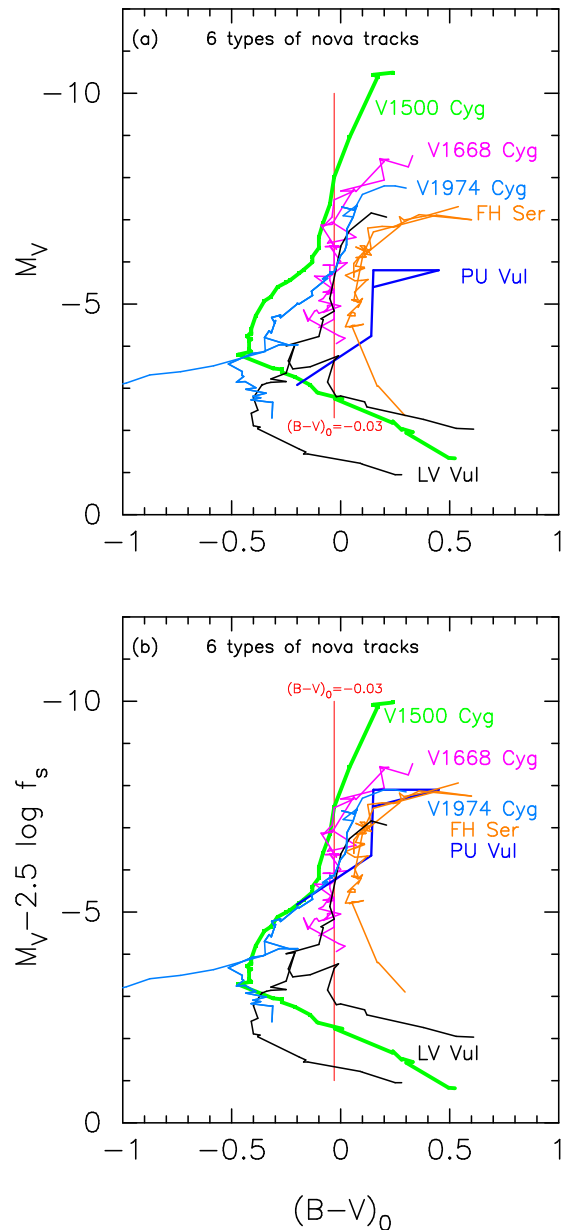


**Figure 6.** (a) Six typical nova tracks in the color-magnitude diagram: from left to right: V1500 Cyg (thick solid green lines), V1668 Cyg (solid magenta lines), V1974 Cyg (solid sky-blue lines), LV Vul (solid black lines), FH Ser (solid orange lines), and PU Vul (thick solid blue lines). The vertical solid red line indicates  $(B - V)_0 = -0.03$ , the color of optically thick free-free emission. (b) The time-stretched color-magnitude diagram of six typical nova tracks. Here,  $f_s$  is the timescaling factor against that of LV Vul.

$E(B - V) = 0.60$  and  $(m - M)_V = 11.7$  for FH Ser and  $E(B - V) = 0.30$  and  $(m - M)_V = 14.3$  for PU Vul both from Hachisu & Kato (2016b). They categorized 40 novae into one of these six subgroups, depending on their similarity in the  $(B - V)_0 - M_V$  diagram.

The LV Vul and V1974 Cyg tracks split into two branches just after the nebular phase started. As already discussed in our previous papers (see, e.g., Figure 10 and Section 3.3 of Hachisu & Kato 2014), strong emission lines such as [O III] contribute to the blue edge of  $V$  filter. A small difference in the  $V$  filter response function makes a large difference in the  $V$  magnitude and results in a large difference in the  $B - V$  color. This is the reason why the track splits into two (or three or even four) branches among various observatories.

In the present work, we propose the  $(B - V)_0 - (M_V - 2.5 \log f_s)$  diagram, that is, Figure 6(b). In this new color-magnitude diagram, the above six nova tracks are shifted up or down. Here, we show the above six tracks of V1500 Cyg, V1974 Cyg, V1668 Cyg, LV Vul, FH Ser, and PU Vul, adopting  $(m - M')_V = 11.75$  for V1500 Cyg,  $(m - M')_V = 12.3$  for V1974 Cyg,  $(m - M')_V = 11.85$  for LV Vul,  $(m - M')_V = 14.6$  for V1668 Cyg,  $(m - M')_V = 12.45$  for FH Ser, and  $(m - M')_V = 16.4$  for PU Vul.

The tracks of V1500 Cyg and V1974 Cyg are different from each other in the early phase but almost overlap in the middle part of the tracks. They turn from toward the blue to toward the red at the similar place, that is, the turning corner. Therefore, we regard that V1974 Cyg belongs to the V1500 Cyg type in the time-stretched color-magnitude diagram.

Also, the V1668 Cyg track almost follows the template track of LV Vul. Thus, these two template tracks can be merged into the same group. The track of FH Ser is close to that of V1668 Cyg and LV Vul. The track of PU Vul is close to that of V1500 Cyg. Thus, the six tracks seem to closely converge into one of the two groups, LV Vul/V1668 Cyg or V1500 Cyg/V1974 Cyg, in the time-stretched color-magnitude diagram.

The main difference between them is that the V1668 Cyg/LV Vul group novae evolve almost straight down along  $(B - V)_0 \sim -0.03$  during  $(M_V - 2.5 \log f_s) = -7$  and  $-4$ , while the V1500 Cyg/V1974 Cyg group novae evolve blueward up to  $(B - V)_0 \sim -0.5$  during  $(M_V - 2.5 \log f_s) = -5$  and  $-3$ . This tendency is clear, e.g., in the case of V2362 Cyg (Figure 13(d)).

### 3. V574 PUP 2004

Hachisu & Kato (2010) analyzed the optical and X-ray light curves of V574 Pup. They assumed  $A_V = 2.2$  after Burlak (2008), which will be revised later. Hachisu & Kato (2015) determined the absolute magnitude of theoretical  $V$  light curve for various WD masses and chemical compositions. Using their theoretical light curves, we reexamine the light/color curves of V574 Pup,

Ness et al. (2007a) obtained  $E(B - V) = 0.50$  during the SSS phase from the relation of  $E(B - V) = N_H/4.8 \times 10^{21} \text{ cm}^{-2}$  (Bohlin et al. 1978) together with their estimate of  $N_H = (2.5 \pm 0.6) \times 10^{21} \text{ cm}^{-2}$  calculated with an X-ray model spectrum fitting. Here,  $N_H$  is the neutral hydrogen column density. Naik et al. (2010) derived the distance of  $d = 5.5$  kpc from the maximum magnitude versus rate of decline (MMRD) relation of della Valle & Livio (1995) and obtained the reddening of  $E(B - V) = A_V/3.1 = 1.95/3.1 = 0.63$  from the empirical relation of  $(B - V)_{0,\text{max}} = +0.23 \pm 0.06$  at optical  $V$  maximum (van den Bergh & Younger 1987).

#### 3.1. Distance-reddening relations toward V574 Pup

We obtain the distance and reddening toward V574 Pup based on the time-stretching method. Figure 7(a) shows four distance moduli in the  $B$ ,  $V$ ,  $I_C$ , and  $K_s$  bands by the thin solid magenta, blue, cyan, cyan-blue lines, that is,  $(m - M)_B = 15.43$ ,  $(m - M)_V = 15.0$ ,  $(m - M)_I = 14.22$ , and  $(m - M)_K = 13.68$ , which are obtained in Appendix A.1, together with Equations (11), (5), (12), and (13). These four lines cross at  $d = 5.3$  kpc and  $E(B - V) = 0.45$ . Thus, we obtain the reddening toward V574 Pup,  $E(B - V) = 0.45 \pm 0.05$ , the distance of V574 Pup,  $d = 5.3 \pm 0.5$  kpc, and the timescaling factor,  $f_s = 1.26$  against LV Vul. The distance modulus in the  $V$  band is  $(m - M)_V = 15.0 \pm 0.1$ . These values are listed in Table 1.

We further check our estimates of the distance modulus in the  $V$  band  $(m - M)_V = 15.0 \pm 0.1$  and extinction  $E(B - V) = 0.45 \pm 0.05$ . Figure 7(a) shows the distance-reddening relations toward V574 Pup, whose galactic coordinates are  $(l, b) = (242^\circ 56' 95'', -1^\circ 99' 33'')$ . The thick solid black/orange lines denote the distance-reddening relations given by Green et al. (2015, 2018), respectively. The open cyan-blue diamonds with error bars are taken from Özdörmez et al. (2016). The thick solid cyan-blue line denotes the result of Chen et al. (2018). These four distance-reddening relations based on the dust map are consistent with each other until  $d \lesssim 5$  kpc.

Green et al.'s black/orange lines are roughly consistent with our results of  $d = 5.3 \pm 0.5$  kpc and  $E(B - V) = 0.45 \pm 0.05$ . The NASA/IPAC galactic 2D dust absorption map gives  $E(B - V) = 0.60 \pm 0.02$  toward V574 Pup, which is slightly larger than our value of  $E(B - V) = 0.45 \pm 0.05$ . This is because the reddening increases further beyond the position of V574 Pup as shown in Figure 7(a).

#### 3.2. Color-magnitude diagram

Using  $E(B - V) = 0.45$  and  $(m - M)_V = 15.0$ , we plot the color-magnitude diagram of V574 Pup in Fig-

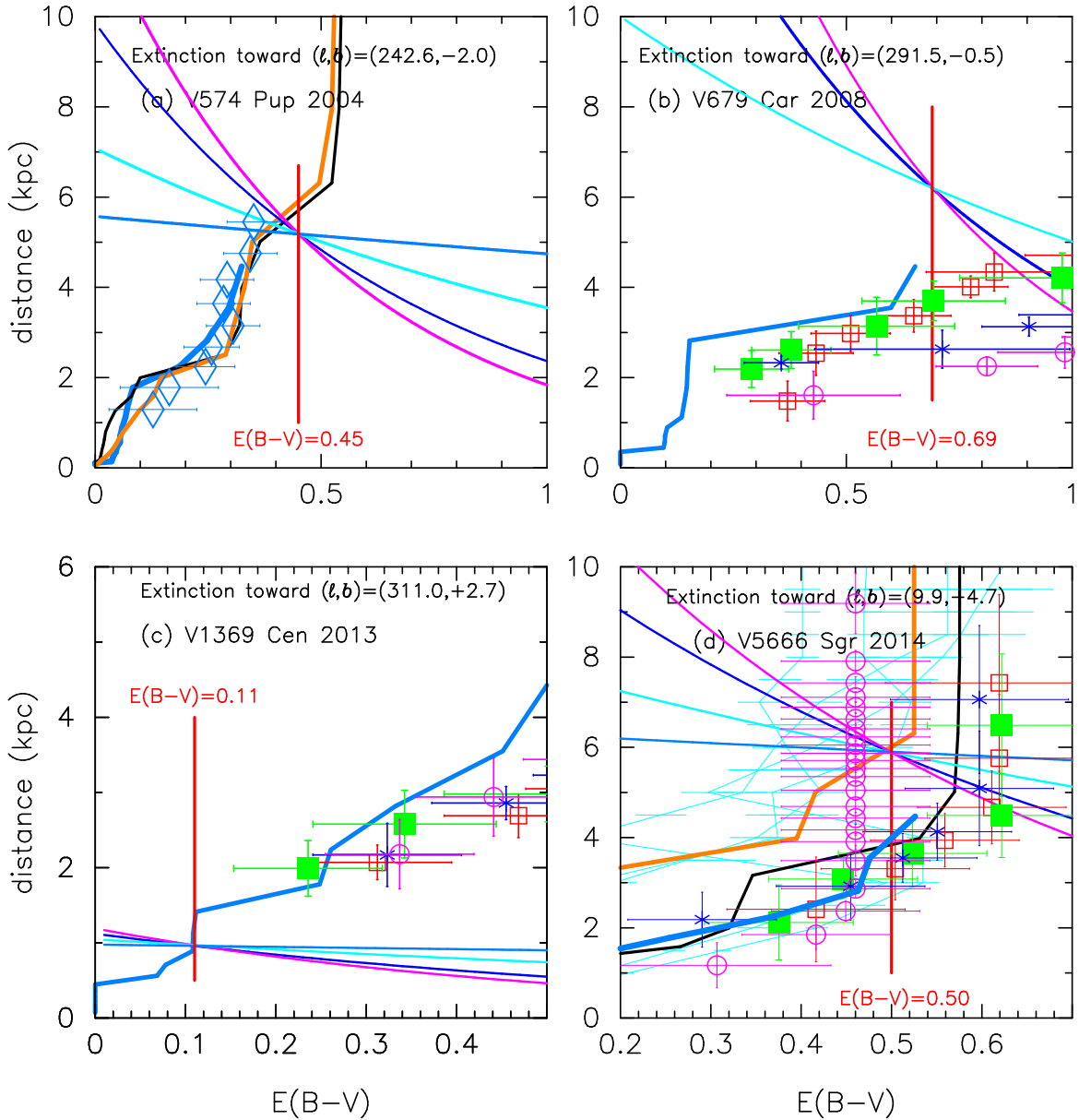


**Figure 7.** Same as Figure 1, but for (a) V574 Pup, (b) V679 Car, (c) V1369 Cen, and (d) V5666 Sgr. In panel (d), the four very thin solid cyan lines with error bars indicate the distance-reddening relations given by [Schultheis et al. \(2014\)](#).

ure 8(a). We add tracks of V1500 Cyg (solid green line), LV Vul (solid orange line), and V1974 Cyg (solid magenta line) for comparison. The data of V574 Pup are scattered in the early phase owing to its oscillatory behavior but close to that of V1974 Cyg (solid magenta line). Therefore, V574 Pup belongs to the V1974 Cyg type in the  $(B-V)_0$ - $M_V$  color-magnitude diagram. The track in the early oscillatory phase shows a circular movement similar to that of V705 Cas as shown in Figure 37(b) of Paper II.

In Figure 9(a), adopting  $E(B-V) = 0.45$  and  $(m - M')_V = 15.25$  in Equation (A6), we obtain the time-stretched color-magnitude diagram of V574 Pup. The

text “ $(m - M')_V = 15.25(-0.25)$ ” in the figure means that  $(m - M')_V = 15.25$  and  $(m - M)_V = 15.25 - 0.25 = 15.0$ .

We note the starting epoch of the nebular phase in Figures 8(a) and 9(a). A nebular phase could be identified by the first clear appearance of the nebular emission lines [O III] or [Ne III] which are stronger than permitted lines. The nebular phase of V574 Pup started at  $m_V \sim 12$  from the spectra of the Small Medium Aperture Telescope System (SMARTS) database<sup>2</sup> ([Walter et al.](#)

<sup>2</sup> <http://www.astro.sunysb.edu/fwalter/SMARTS/NovaAtlas/atlas.html>

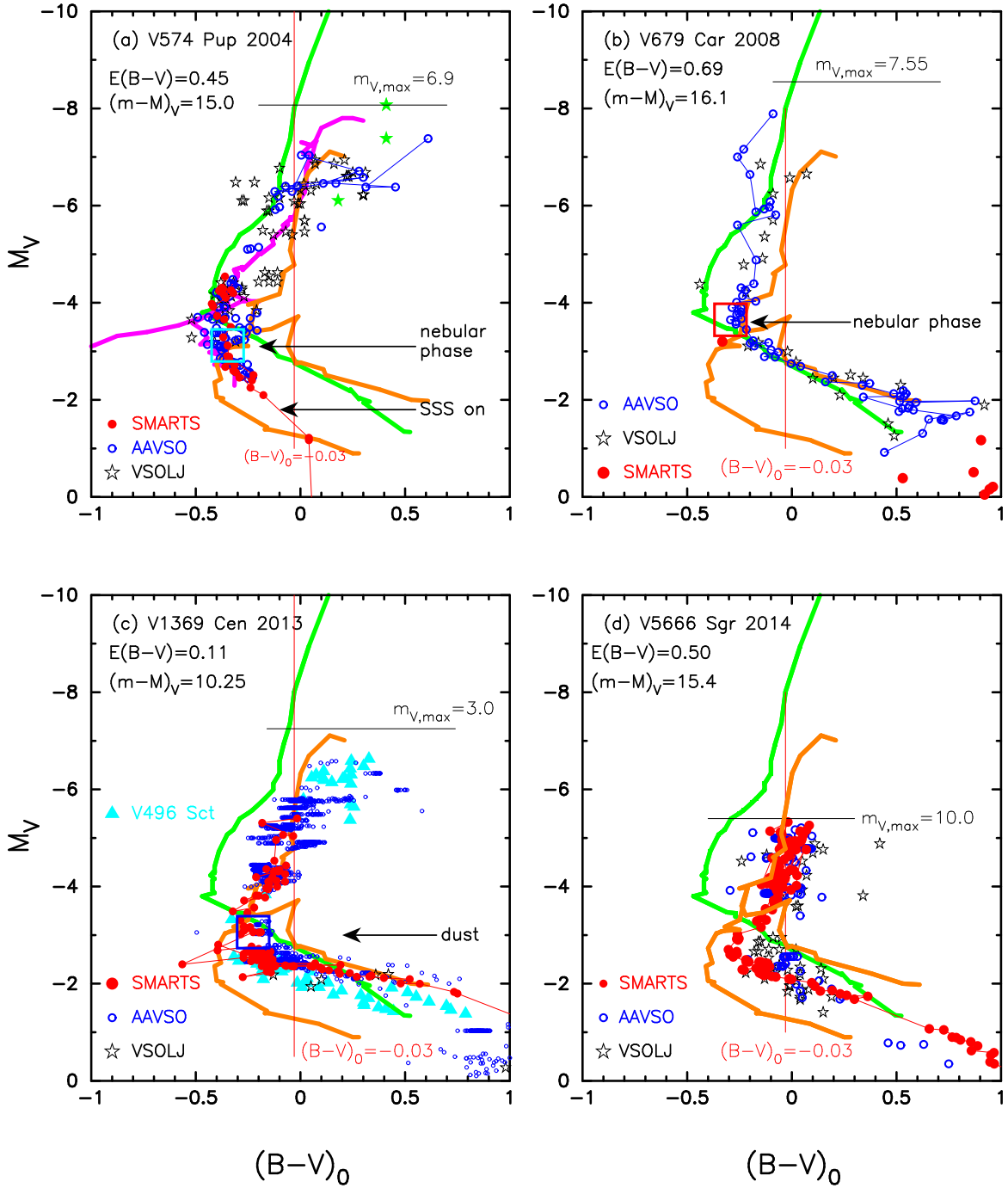


**Figure 8.** Color-magnitude diagram for (a) V574 Pup, (b) V679 Car, (c) V1369 Cen, and (d) V5666 Sgr. The thick solid green, magenta, and orange lines denote the template tracks of V1500 Cyg, V1974 Cyg, and LV Vul, respectively. In panel (a), we show the start of the nebular phase by the large open cyan square, while in panel (b), the red square. In panel (a), we add the start of the supersoft X-ray source (SSS) phase by “SSS on.” In panel (c), we add the data of V496 Sct (filled cyan triangles), which are taken from Section 7.12 and Appendix B.12. We also show the start of the dust black out phase by the large open blue square.



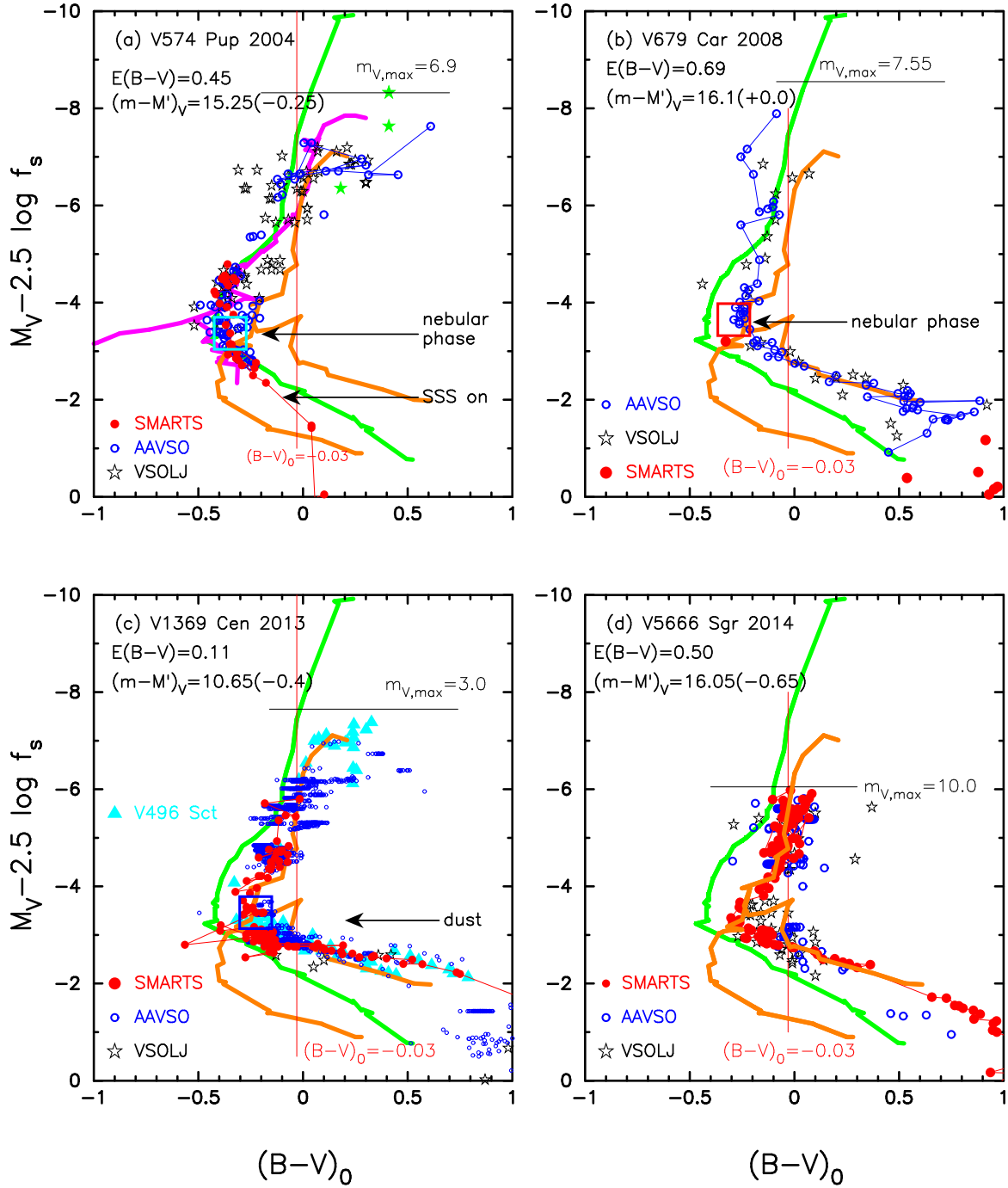


**Figure 9.** Time-stretched color-magnitude diagram for (a) V574 Pup, (b) V679 Car, (c) V1369 Cen, and (d) V5666 Sgr. Here,  $f_s$  is the timescaling factor against that of LV Vul. The green, magenta, and orange lines denote the template tracks of V1500 Cyg, V1974 Cyg, and LV Vul, respectively. Each symbol is the same as that in Figure 8.

2012), which is denoted by the large open cyan square in Figures 8(a) and 9(a). After the onset of the nebular phase, the track turns to the right (red). This is because the strong emission lines of [O III] contribute to the blue edge of the  $V$  filter and its large contribution makes the  $B - V$  color redder.

Ness et al. (2007a) discussed that the SSS phase started between May and July in 2005. This epoch corresponds to  $m_V \sim 13.2$  and denoted by “SSS on” in Figures 8(a) and 9(a). The  $(B - V)_0$  color seems to keep a constant value of  $\sim 0.0$  during the SSS phase, as shown in Figure 19(b).

In Figure 9(a), the track of V574 Pup almost follows those of V1500 Cyg and V1974 Cyg except for the early oscillation phase. Thus, we conclude that V574 Pup belongs to the V1500 Cyg/V1974 Cyg type in the time-stretched color-magnitude diagram.

### 3.3. Model light curve fitting

Kato & Hachisu (1994) calculated evolutions of nova outbursts based on the optically thick wind theory. Their numerical models provide various physical quantities such as the photospheric temperature, radius, velocity, and wind mass-loss rate of a nova hydrogen-rich envelope (mass of  $M_{\text{env}}$ ) for a specified WD mass ( $M_{\text{WD}}$ ) and chemical composition of the envelope. Hachisu & Kato (2015) calculated the absolute  $V$  magnitude light curves based on Kato & Hachisu’s envelope models. Their model  $V$  light curve is composed of photospheric emission and free-free emission. The photospheric emission is approximated by blackbody emission at the photosphere, while the free-free emission is calculated from the photospheric radius, velocity, and wind mass-loss rate (Hachisu & Kato 2015). Fitting the absolute  $V$  magnitudes ( $M_V$ ) of model light curve with the observed apparent  $V$  magnitudes ( $m_V$ ), we are able to specify the  $(m - M)_V$  (and even  $M_{\text{WD}}$ ) for the nova. Such results are presented in Hachisu & Kato (2015, 2016a, 2018a,b).

Hachisu & Kato (2010) estimated the WD mass of V574 Pup to be  $1.05 M_{\odot}$ . In Figure 19(a), we plot the  $1.05 M_{\odot}$  WD model (solid black line for  $V$  magnitudes and solid red line for soft X-ray fluxes) with the chemical composition of Ne nova 3 (Hachisu & Kato 2016a). We use the absolute  $V$  magnitudes of the  $1.05 M_{\odot}$  WD model calculated in Hachisu & Kato (2016a). We add a  $0.98 M_{\odot}$  WD model (solid green lines both for  $V$  and soft X-ray) with the chemical composition of CO nova 3 (Hachisu & Kato 2016a) for comparison, the timescale of which is stretched by a factor of  $f_s = 1.17$ . The absolute  $V$  light curve of the  $1.05 M_{\odot}$  WD model reasonably follows the observed apparent  $V$  light curves of

V574 Pup for  $(m - M)_V = 15.0$ . In these models, the optically thick winds stop at the open black circle (at the right edge of the solid black line).

The model supersoft X-ray light curve also shows good fit with the X-ray observation, i.e., turn-on and turnoff times. The X-ray data are the same as those of Hachisu & Kato (2010). Thus, the  $1.05 M_{\odot}$  WD model is consistent with the X-ray data. We list the WD mass of V574 Pup in Table 2.

## 4. V679 CAR 2008

V679 Car was discovered by Katarzyna Malek at mag 7.9 on UT 2008 November 26.26 (JD 2454795.76). It reached mag 7.55 on UT 2008 November 27.27 (JD 2454796.77) (Waagen et al. 2008). The spectrum showed that the object is a classical nova of the Fe II type. Recently, Franckowiak et al. (2018) suggested that V679 Car is a candidate for GeV gamma-ray detected nova with *Fermi*/Large Area Telescope (LAT).

### 4.1. Distance-reddening relations toward V679 Car

We plot three distance moduli in the  $B$ ,  $V$ , and  $I_C$  bands in Figure 7(b) by the magenta, blue, and cyan lines, that is,  $(m - M)_B = 16.8$ ,  $(m - M)_V = 16.1$ , and  $(m - M)_I = 15.0$  in Appendix A.2 together with Equations (11), (5), and (12), respectively. These three lines cross at  $d = 6.2$  kpc and  $E(B - V) = 0.69$ . Thus, we obtain the reddening toward V679 Car,  $E(B - V) = 0.69 \pm 0.05$ , the distance of V574 Pup,  $d = 6.2 \pm 0.7$  kpc, and the timescaling factor,  $f_s = 1.0$  against LV Vul. The distance modulus in the  $V$  band is  $(m - M)_V = 16.1 \pm 0.1$ . These values are listed in Table 1.

We check the distance and reddening toward V679 Car, whose galactic coordinates are  $(l, b) = (291^{\circ}4697, -0^{\circ}5479)$ , on the basis of dust extinction maps calculated by Marshall et al. (2006) and Chen et al. (2018). Figure 7(b) shows the relations given by Marshall et al. (2006):  $(l, b) = (291^{\circ}25, -0^{\circ}50)$  by open red squares,  $(291^{\circ}50, -0^{\circ}50)$  by filled green squares,  $(291^{\circ}25, -0^{\circ}75)$  by blue asterisks, and  $(291^{\circ}50, -0^{\circ}75)$  by open magenta circles. The filled green squares of Marshall et al. (2006) are the closest direction toward V679 Car among the four nearby directions. The solid cyan-blue line denotes the relation given by Chen et al. (2018). Neither Green et al.’s (2015, 2018) nor Özdörmez et al.’s (2016) data are available toward this direction. The three relations of  $(m - M)_B = 16.8$  (magenta line),  $(m - M)_V = 16.1$  (blue line), and  $(m - M)_I = 15.0$  (cyan line) cross at  $d = 6.2$  kpc and  $E(B - V) = 0.69$ . This crossing point is significantly different from the closest relation (filled green squares) given by Marshall et al. (2006). However, Chen et al.’s relation (solid cyan-blue

line) seems to show possible agreement with our crossing point, although the data end at  $d = 4.5$  kpc.

This large discrepancy can be understood as follows: Marshall et al.'s 3D dust map gives an averaged value of a relatively broad region, and thus a pinpoint reddening toward the nova could be different from the values of the 3D dust maps, because the resolution of the dust map is considerably larger than molecular cloud structures observed in the interstellar medium. For example, Marshall et al.'s 3D dust map gave a significantly different value for the reddening of LV Vul as shown in Figure 1(a).

#### 4.2. Color-magnitude diagram

The  $V$  light and  $(B - V)_0$  color curve shapes of V679 Car are similar to those of LV Vul and V1668 Cyg as shown in Figures 22 and 23. This suggests that the color-magnitude diagram of V679 Car is also similar to them. Adopting  $E(B - V) = 0.69$  and  $(m - M)_V = 16.1$ , we plot the color-magnitude track in Figure 8(b) together with V1500 Cyg (solid green line) and LV Vul (solid orange line). The SMARTS spectra of V679 Car show that the nebular phase started between JD 2454845.71 (UT 2009 January 14.21) and JD 2454860.67 (UT 2009 January 29.17), corresponding to  $m_V = 12.45$  and  $B - V = 0.40$ , which is denoted by the large open red square in Figure 8(b). The start of the nebular phase usually corresponds to the turning point from toward blue to toward red (from toward left to toward right) as already discussed in Section 3. The track of V679 Car broadly locates on the track of LV Vul (orange line), although the  $(B - V)_0$  colors of the early phase are rather scattered and slightly bluer than that of LV Vul. After this turning point, the track of V679 Car follows that of LV Vul. We conclude that V679 Car belongs to the LV Vul type in the color-magnitude diagram (Paper II).

Adopting  $E(B - V) = 0.69$  and  $(m - M')_V = 16.1$  from Equation (A12), we plot the time-stretched color-magnitude diagram of V679 Car in Figure 9(b). The  $(B - V)_0$  intrinsic color is not affected by time-stretch (see Hachisu & Kato 2018a). Because  $f_s = 1.0$ , the time-stretched color-magnitude track is the same as in Figure 8(b), but the track of V1500 Cyg is shifted down. The overlap of the track to the LV Vul track supports our values of  $E(B - V) = 0.69$  and  $(m - M')_V = 16.1$ , that is,  $f_s = 1.0$ ,  $E(B - V) = 0.69 \pm 0.05$ ,  $(m - M)_V = 16.1 \pm 0.1$ , and  $d = 6.2 \pm 0.7$  kpc. We list our results in Table 1.

#### 4.3. Model light curve fitting with V679 Car

Figure 23(a) shows the model light curve of a  $0.98 M_\odot$  WD (solid red lines) with the envelope chemical composition of CO Nova 3 (Hachisu & Kato 2016a). Taking

the distance modulus in the  $V$  band of  $(m - M)_V = 16.1$ , we reasonably fit the model absolute  $V$  light curve with the observed apparent  $V$  magnitudes of V679 Car. Thus, our obtained value of  $(m - M)_V = 16.1$  is consistent with the model light curve. We also add the  $0.98 M_\odot$  WD model (solid green lines) with the same envelope chemical composition of CO nova 3 but a slightly larger initial envelope mass, assuming  $(m - M)_V = 14.6$  for V1668 Cyg. This model fits with the  $V$  and UV 1455Å light curves of V1668 Cyg as already discussed in our previous paper (Hachisu & Kato 2016a).

Our model light curve of the  $0.98 M_\odot$  WD predicts the SSS phase between day 250 and day 600 as shown in Figure 23(a). V679 Car was observed with *Swift* eight times, but no SSS phase was detected (Schwarz et al. 2011). The epochs of the *Swift* observations are indicated by the downward magenta arrows. The second and third arrows almost overlap. We expect detection of supersoft X-rays at the last one or two. Non-detection may be owing to a large extinction toward V679 Car, as large as  $E(B - V) = 0.69$ , corresponding to  $N_H = 8.3 \times 10^{21} E(B - V) = 0.6 \times 10^{22} \text{ cm}^{-2}$  (Liszt 2014), or see also Figure 3 in Schwarz et al. (2011),

#### 5. V1369 CEN 2013

V1369 Cen was discovered by J. Seach at mag 5.5 on UT 2013 December 2.692 (JD 2456629.192) (Guido et al. 2013) and reached  $m_{V,\text{max}} \approx 3.0$  on JD 2456639.18 (VSOLJ data by S. Kiyota, however, we omit his  $m_V = 2.8$  on JD 2456637.21 because it is too bright compared with other data). Mason et al. (2018) obtained the reddening to be  $E(B - V) = 0.15$  from the Na I D2  $\lambda 5890$  interstellar absorption line and the best fit column density of  $N_H = 7.2 \times 10^{21} \text{ cm}^{-2}$  derived from the model of the interstellar Ly $\alpha$  absorption. This value of  $N_H$  would be a typo of  $N_H = 7.2 \times 10^{20} \text{ cm}^{-2}$ , because of  $E(B - V) = N_H / 4.8 \times 10^{21} \text{ cm}^{-2}$  (Bohlin et al. 1978).

This nova is characterized by pre-nova X-ray observation and GeV gamma-ray detection. Kuulkers et al. (2013) reported a pre-nova X-ray detection between UT 2002 February 20 16:57 and 21:08 with an absorbed 0.3-10 keV flux of  $(1.0 \pm 0.1) \times 10^{-12} \text{ erg s}^{-1} \text{ cm}^2$  and  $N_H = (2 \pm 1) \times 10^{21} \text{ cm}^{-2}$  for a non-isothermal collisional plasma. Cheung et al. (2013) reported a gamma-ray detection during UT 2013 December 7-10 with an average flux of  $F(E > 100 \text{ MeV}) \sim (2.1 \pm 0.6) \times 10^{-7} \text{ ph cm}^{-2} \text{ s}^{-1}$ .

#### 5.1. Distance and reddening toward V1369 Cen

We obtain the distance and reddening toward the nova based on the time-stretching method. We plot four distance moduli in the  $B$ ,  $V$ ,  $I_C$ , and  $K_s$  bands in Figure

7(c), which are obtained in Appendix A.3. These four (magenta, blue, cyan, cyan-blue) lines cross at the distance of 0.96 kpc and the reddening of  $E(B - V) = 0.11$ . Thus, we obtain the distance  $d = 0.96 \pm 0.1$  kpc, the reddening  $E(B - V) = 0.11 \pm 0.03$ , and the timescaling factor  $f_s = 1.48$  against LV Vul.

Izzo et al. (2013) obtained an extinction of  $E(B - V) = 0.11 \pm 0.08$  from the relation given by Poznanski et al. (2012) or  $E(B - V) = 0.14$  from the relation given by Munari & Zwitter (1997), both between the widths of Na I D doublet and the extinction. Shore et al. (2014) obtained the extinction of  $E(B - V) \sim 0.1$ , using UV interstellar spectra. They also estimated the distance of  $d \sim 2.4$  kpc comparing the UV fluxes with those of V339 Del. As already mentioned, Mason et al. (2018) obtained the reddening of  $E(B - V) = 0.15$  from the Na I D2  $\lambda 5890$  interstellar absorption line and the best fit neutral hydrogen column density derived from the model of the interstellar Ly $\alpha$  absorption.

We further examine the reddening and distance based on various distance-reddening relations. Figure 7(c) shows the distance-reddening relations toward V1369 Cen, whose galactic coordinates are  $(l, b) = (310^\circ 9816, +2^\circ 7274)$ . We plot Marshall et al.’s (2006) relations:  $(l, b) = (310^\circ 75, +2^\circ 50)$  by open red squares,  $(311^\circ 00, +2^\circ 50)$  by filled green squares,  $(310^\circ 75, +2^\circ 75)$  by blue asterisks, and  $(311^\circ 00, +2^\circ 75)$  by open magenta circles. The open magenta circles are the closest direction among the four nearby directions. Green et al.’s or Özdörmez et al.’s data are not available. We add the relation (cyan-blue line) given by Chen et al. (2018), which is consistent with our crossing point of  $E(B - V) = 0.11$  and  $d = 0.96$  kpc. Although Marshall et al.’s relations do not reach  $E(B - V) \lesssim 0.2$ , it seems that its trend of linear extension toward  $E(B - V) = 0.11$  are roughly consistent with our crossing point at  $d = 0.96 \pm 0.1$  kpc and  $E(B - V) = 0.11 \pm 0.03$ .

### 5.2. Color-magnitude diagram

Adopting  $E(B - V) = 0.11$  and  $(m - M)_V = 10.25$ , we plot the color-magnitude diagram of V1369 Cen in Figure 8(c). We also plot the tracks of V1500 Cyg (solid green line), LV Vul (solid orange line), and V496 Sct (filled cyan triangles). The data of V496 Sct are the same as those in Figures 72(b) and 73 of Paper II. The track of V1369 Cen and V496 Sct almost follow that of LV Vul in the early phase until the dust-shell formation, which is denoted by the large open blue square. After that, the track of V1369 Cen underlies the track of LV Vul.

Figure 9(c) shows the time-stretched color-magnitude diagram of V1369 Cen. We adopt  $E(B - V) = 0.11$  and

$(m - M)_V = 10.65$  from Equation (A14). Now, the track of V1369 Cen and V496 Sct almost follow that of LV Vul. Thus, we conclude that V1369 Cen belongs to the LV Vul type in the time-stretched color-magnitude diagram. This overlapping of V1369 Cen track to that of LV Vul suggests that our adopted values of  $E(B - V) = 0.11$ ,  $f_s = 1.48$ , and  $(m - M)_V = 10.65$  are reasonable.

### 5.3. Model light curve fitting

Figure 27(a) shows the model absolute  $V$  light curve of a  $0.90 M_\odot$  WD (thick solid red line) with the envelope chemical composition of CO Nova 3 (Hachisu & Kato 2016a). Here, we assume  $(m - M)_V = 10.25$ . The chemical composition of V1369 Cen ejecta is not known, so we assume CO Nova 3 because V1369 Cen showed an optically-thin dust blackout similar to V1668 Cyg, of which the chemical composition is represented roughly by CO Nova 3 (Hachisu & Kato 2006, 2016a).

In free-free emission dominant spectra, optical and near-infrared (NIR), i.e.,  $B$ ,  $V$ , and  $I_C$  light curves should have the same shape (see, e.g., Hachisu & Kato 2006). The V1369 Cen data show such a property in the middle phase of light curves and are in good agreement with the model light curve. The observed  $B$  and  $V$  magnitudes departed from the theoretical light curve at  $t \gtrsim 100$  day because of strong contributions of emission lines to the  $B$  and  $V$  bands in the nebular phase (see Paper I). This model light curve again confirms our result of  $(m - M)_V = 10.25$ . The WD mass is around  $0.9 M_\odot$ .

Our  $0.90 M_\odot$  WD model also predicts a supersoft X-ray source phase from Day 340 until Day 960 (thin solid red line in Figure 27(a)). Page et al. (2014) reported an X-ray spectrum on UT 2014 March 8 (JD 2456724.5). This epoch (Day  $\sim 100$ ) corresponds to the deepest dust blackout (see Figure 24), and is much earlier than the X-ray turn-on time in our model. Mason et al. (2018) presented the X-ray count rates of V1369 Cen obtained with *Swift*. We plot the X-ray data taken from the *Swift* Web site<sup>3</sup> (Evans et al. 2009) in Figure 27(a). The blue pluses represent the hard X-ray (1.5–10 keV) and the magenta crosses denote the soft X-ray (0.3–1.5 keV) components. No clear supersoft X-rays were detected until Day 370. We may conclude that the X-rays detected on Day  $\sim 100$  are not from the WD surface but shock-origin.

## 6. V5666 SGR 2014

V5666 Sgr was discovered by S. Furuyama at mag 8.7 on UT 2014 January 26.857 (JD 2456684.357)

<sup>3</sup> <http://www.swift.ac.uk/>

(Furuyama & Pearce 2014). It reached  $m_V = 10.0$  on JD 2456697.3 (estimated from S. Kiyota's  $m_V = 9.8$  of VSOLJ). The nova was identified by A. Arai as an Fe II type (Furuyama & Pearce 2014).

We estimate the distance moduli of V5666 Sgr in the four bands, i.e.,  $(m - M)_B = 15.87$ ,  $(m - M)_V = 15.38$ ,  $(m - M)_I = 14.59$ , and  $(m - M)_K = 14.07$  in Appendix A.4. We plot these four relations by the magenta, blue, cyan, and cyan-blue lines in Figure 7(d). These four lines cross at  $d = 5.8$  kpc and  $E(B - V) = 0.50$ . Thus, we adopt  $d = 5.8 \pm 0.6$ ,  $E(B - V) = 0.50 \pm 0.05$ , and the timescaling factor  $f_s = 1.78$  against LV Vul.

Figure 7(d) also shows various distance-reddening relations toward V5666 Sgr, whose galactic coordinates are  $(l, b) = (9^\circ 8835, -4^\circ 6567)$ . We add Marshall et al.'s (2006) relations:  $(l, b) = (9^\circ 75, -4^\circ 50)$  by open red squares,  $(10^\circ 00, -4^\circ 50)$  by filled green squares,  $(9^\circ 75, -4^\circ 75)$  by blue asterisks, and  $(10^\circ 00, -4^\circ 75)$  by open magenta circles, each with error bars. The closest direction among the four nearby directions is that of open magenta circles. We also add the relations given by Green et al. (2015, 2018) (solid black and orange lines, respectively) and the relation by Chen et al. (2018) (solid cyan-blue line). Özdörmez et al.'s data are not available. The orange line is consistent with our results of  $d = 5.8 \pm 0.6$  kpc and  $E(B - V) = 0.50 \pm 0.05$ .

Schultheis et al. (2014) determined interstellar extinction as a function of distance in the galactic bulge covering  $-10^\circ 0 < l < 10^\circ 0$  and  $-10^\circ 0 < b < 5^\circ 0$ , using data from the VISTA Variables in the Via Lactea (VVV) survey together with the Besançon stellar population synthesis model of the Galaxy. The resolution is  $0^\circ 1 \times 0^\circ 1$  and the distance is extended up to 10 kpc in a 0.5 kpc step. We plot four Schulteis et al.'s distance-reddening relations toward near the direction of V5666 Sgr, i.e.,  $(l, b) = (9^\circ 8, -4^\circ 6)$ ,  $(9^\circ 8, -4^\circ 7)$ ,  $(9^\circ 9, -4^\circ 6)$ , and  $(9^\circ 9, -4^\circ 7)$  by very thin solid cyan lines in Figure 7(d), where we adopt the relations of  $A_{K_s} = 0.364 E(B - V)$  (Saito et al. 2013) and  $A_{K_s} = 0.528 E(J - K_s)$  (Nishiyama et al. 2009) in the conversion of  $E(B - V)$  from their  $E(J - K_s)$  in their Table 1. The four lines show zigzag patterns, although the reddening should increase monotonically with the distance. In this sense, Schulteis et al.'s relation may not be appropriate in the middle distance. Our crossing point,  $d = 5.8$  kpc and  $E(B - V) = 0.50$ , however, is consistent with theirs.

Adopting  $E(B - V) = 0.50$  and  $(m - M)_V = 15.4$ , we plot the color-magnitude diagram of V5666 Sgr in Figure 8(d). In the same figure, we add the tracks of V1500 Cyg (solid green line) and LV Vul (solid orange line). Although the track of V5666 Sgr almost follows

that of LV Vul, its position is slightly lower than that of LV Vul.

Figure 9(d) shows the time-stretched color-magnitude diagram of V5666 Sgr. We adopt  $E(B - V) = 0.50$  and  $(m - M')_V = 16.05$  in Equation (A21). Now, the track of V5666 Sgr follows well that of LV Vul. Thus, we conclude that V5666 Sgr belongs to the LV Vul type in the time-stretched color-magnitude diagram. This overlap supports our results of  $E(B - V) = 0.50$  and  $(m - M')_V = 16.05$ , that is,  $E(B - V) = 0.50 \pm 0.05$ ,  $(m - M)_V = 15.4 \pm 0.1$ ,  $f_s = 1.78$ , and  $d = 5.8 \pm 0.6$  kpc. We list our results in Table 1.

We further confirm  $(m - M)_V = 15.4$  from our model light curve fitting. Taking  $(m - M)_V = 15.4$ , we plot a  $0.85 M_\odot$  WD model with the chemical composition of CO nova 3 (Hachisu & Kato 2016a) in Figure 31(a). The  $0.85 M_\odot$  WD (solid red lines) model does not match with the early phase of oscillatory flat peak, but reasonably fit with the mid and later phases, where free-free emission dominates in the  $B$ ,  $V$ , and  $I_C$  magnitudes. Thus, we again confirm  $(m - M)_{V, V5666 \text{ Sgr}} = 15.4 \pm 0.2$ . The estimated WD mass is about  $M_{\text{WD}} = 0.85 M_\odot$  for the chemical composition of CO Nova 3.

## 7. REVISITING 12 NOVAE IN THE TIME-STRETCHED COLOR-MAGNITUDE DIAGRAM

In what follows, we reexamine 12 novae studied in Paper II with a new light of time-stretched color-magnitude diagram.

### 7.1. V446 Her 1960

For the reddening toward V446 Her, Hachisu & Kato (2014) obtained the arithmetic average of the values in literature to be  $E(B - V) = 0.41 \pm 0.15$ . Recently, Özdörmez et al. (2016) proposed another average of  $E(B - V) = 0.37 \pm 0.04$  including the result of Selvelli & Gilmozzi (2013),  $E(B - V) = 0.38 \pm 0.04$ , from the archival 2200Å feature. See Paper II and Özdörmez et al. (2016) for a summary of other estimates on the distance and reddening. In the present paper, we adopt  $E(B - V) = 0.40 \pm 0.05$  after Hachisu & Kato (2014). We obtain the distance of  $d = 1.38 \pm 0.2$  kpc from Equation (5),  $E(B - V) = 0.40 \pm 0.05$ ,  $f_s = 1.0$  against LV Vul, and  $(m - M)_V = 11.95 \pm 0.1$  in Appendix B.1.

Figure 10(a) shows various distance-reddening relations toward V446 Her, whose galactic coordinates are  $(l, b) = (45^\circ 4092, +4^\circ 7075)$ . The vertical solid red line denotes the reddening of  $E(B - V) = 0.40$ . The solid blue line denotes the distance modulus in the  $V$  band, i.e.,  $(m - M)_V = 11.95$  and Equation (5). These two

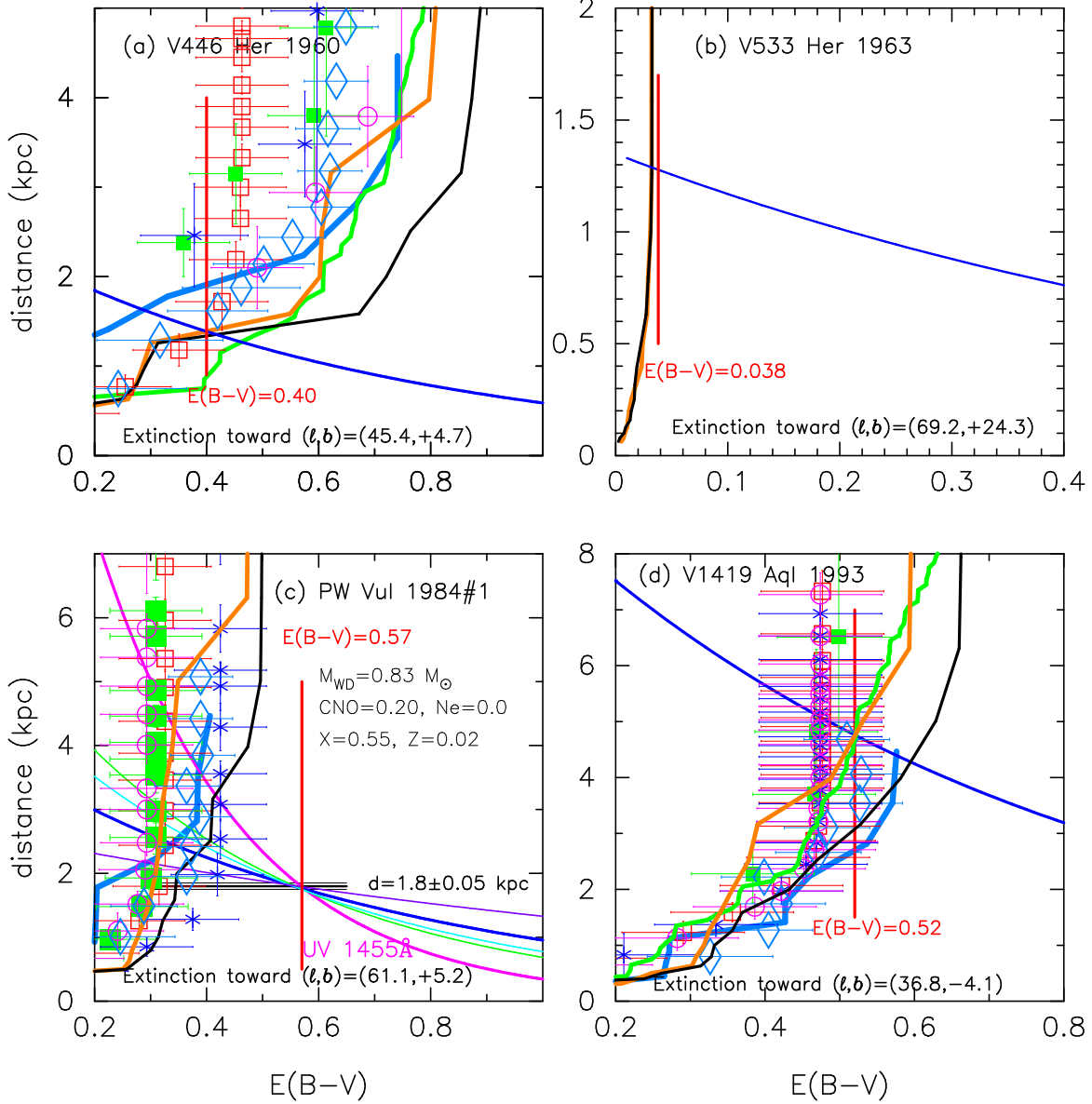


**Figure 10.** Same as Figure 1, but for (a) V446 Her, (b) V533 Her, (c) PW Vul, and (d) V1419 Aql. In panel (c), the solid magenta line represents the UV 1455Å flux fitting. The thin solid green, cyan, and blue-magenta lines denotes the relations of  $(m-M)_U = 13.92$ ,  $(m-M)_B = 13.55$ ,  $(m-M)_V = 13.0$ , and  $(m-M)_I = 12.12$ , respectively.

lines cross at  $E(B-V) = 0.40$  and  $d = 1.38$  kpc. We further plot Marshall et al.’s (2006) relations in four directions close to the direction of V446 Her; toward  $(l, b) = (45^\circ 25, 4^\circ 50)$  by open red squares,  $(45^\circ 50, 4^\circ 50)$  by filled green squares,  $(45^\circ 25, 4^\circ 75)$  by blue asterisks, and  $(45^\circ 50, 4^\circ 75)$  by open magenta circles. The closest direction in the galactic coordinates is that of open magenta circles among the four nearby directions. The solid black/orange lines denote the distance-reddening relations given by Green et al. (2015, 2018), respectively. The solid green line represents the relation given by Sale et al. (2014). The open cyan diamonds depict the relation of Özdörmez et al. (2016).

The cyan-blue line represents the relation given by Chen et al. (2018). Our crossing point at  $E(B-V) = 0.40$  and  $d = 1.38$  kpc is consistent with Marshall et al.’s (open magenta circles) and Green et al.’s (solid black/orange lines) relations. Our crossing point is also consistent with the distance-reddening relation given by Özdörmez et al. (2016). Cohen (1985) obtained the distance of V446 Her by the expansion parallax method to be  $d = (v_{\text{exp}} \times t) / r_{\text{shell}} = (1235 \text{ km s}^{-1} \times 24 \text{ yr}) / 4''.5 = 1.35$  kpc. Our value of  $d = 1.38 \pm 0.2$  kpc is consistent with Cohen’s value. Thus, we confirm again that our obtained values of  $(m-M)_V = 11.95 \pm 0.1$ ,

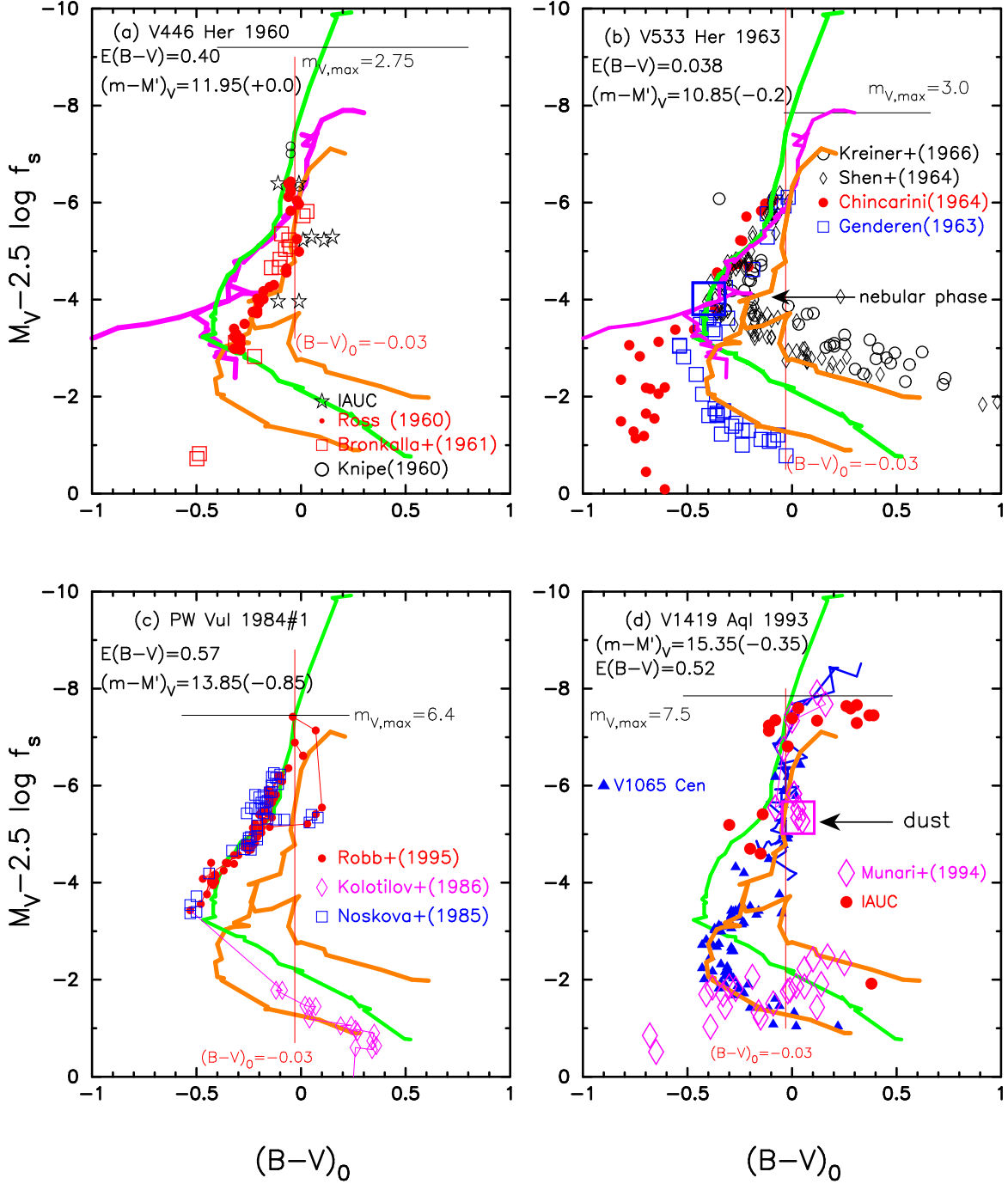


**Figure 11.** Same as Figure 9, but for (a) V446 Her, (b) V533 Her, (c) PW Vul, and (d) V1419 Aql. The data are the same as those in Papers I & II. The solid orange lines show the template track of LV Vul while the solid green lines show that of V1500 Cyg. In panels (a) and (b), we add the tracks of V1974 Cyg (solid magenta lines). In panel (d), we add the track of V1668 Cyg (solid blue lines) and V1065 Cen (filled blue triangles). In panel (b), we depict the start of the nebular phase by the large open blue square. In panel (d), we denote the start of the dust blackout by the large open magenta square.

$E(B - V) = 0.40 \pm 0.05$ , and  $d = 1.38 \pm 0.2$  kpc are reasonable.

Adopting  $E(B - V) = 0.40$  and  $(m - M')_V = 11.95$  in Equation (B28), we obtain the time-stretched color-magnitude diagram of V446 Her in Figure 11(a). The track of V446 Her is just on the LV Vul track (solid orange line). Therefore, V446 Her belongs to the LV Vul type. This overlapping to the LV Vul track supports our values of  $E(B - V) = 0.40$  and  $(m - M')_V = 11.95$ , that is,  $f_s = 1.0$ ,  $E(B - V) = 0.40 \pm 0.05$ ,  $(m - M)_V = 11.95 \pm 0.1$ , and  $d = 1.38 \pm 0.2$  kpc. We list our results in Table 1.

Taking  $(m - M)_V = 11.95$  for V446 Her, we add a  $0.98 M_\odot$  WD model (solid red line) with the chemical composition of CO nova 3 (Hachisu & Kato 2016a) in Figure 32(a). The model absolute  $V$  light curve reasonably fits with the observed apparent  $V$  light curve of V446 Her. This confirms that the distance modulus of  $(m - M)_V = 11.95$  is reasonable. In the same figure, we depict another  $0.98 M_\odot$  WD model with  $(m - M)_V = 14.6$  for V1668 Cyg (solid black lines). The difference between these two models represents the difference in the initial hydrogen-rich envelope mass; the initial envelope mass  $M_{\text{env},0}$  of the solid red line is slightly smaller than that of the solid black line.

### 7.2. V533 Her 1963

V533 Her was studied in Paper II on the  $(B - V)_0 - M_V$  diagram but we here examine it on the time-stretched color-magnitude diagram. Hachisu & Kato (2016b) took  $E(B - V) = 0.038 \pm 0.002$  from the NASA/IPAC galactic absorption map. We adopt their value of  $E(B - V) = 0.038$ . We determine the distance modulus in the  $V$  band to be  $(m - M)_V = 10.65 \pm 0.1$  together with  $f_s = 1.20$  against LV Vul in Appendix B.2, and plot it by the solid blue line in Figure 10(b). The vertical solid red line is the color excess of  $E(B - V) = 0.038$ . These two lines cross at  $d = 1.28$  kpc (and  $E(B - V) = 0.038$ ). Thus, we obtain the distance of  $d = 1.28 \pm 0.2$  kpc.

Figure 10(b) also shows a few distance-reddening relations toward V533 Her, whose galactic coordinates are  $(l, b) = (69^\circ 1887, +24^\circ 2733)$ . None of Marshall et al.'s, Sale et al.'s, Özdörmez et al.'s, and Chen et al.'s relations is available. The solid black/orange lines denote the distance-reddening relations given by Green et al. (2015, 2018), respectively. Our crossing point is broadly consistent with Green et al.'s distance-reddening relations.

Adopting  $E(B - V) = 0.038$  and  $(m - M')_V = 10.85$  in Equation (B30), we obtain the time-stretched color-magnitude diagram of V533 Her in Figure 11(b). We

also add the template tracks of LV Vul (thick solid orange lines), V1500 Cyg (thick solid green line), and V1974 Cyg (solid magenta lines). The V533 Her track broadly follows the mid part of V1974 Cyg tracks at least until the onset of the nebular phase (see also Figure 33(a) and (b)). We regard that V533 Her belongs to the V1500 Cyg type in the time-stretched color-magnitude diagram. This supports our values of  $(m - M')_V = 10.85$  and  $E(B - V) = 0.038$ , that is,  $(m - M)_V = 10.65 \pm 0.1$ ,  $E(B - V) = 0.038 \pm 0.01$ , and  $f_s = 1.20$ . Our results are listed in Table 1.

We again discuss the effect of different responses in the color filters. The color-magnitude track of V533 Her bifurcates at the onset of the nebular phase around UT 1963 April 19 (Chincarini & Rosino 1964), i.e., at  $m_V = 7.2$  denoted by the large open blue square in Figure 11(b). We plot four color-magnitude data taken from Kreiner et al. (1966), Shen et al. (1964), van Genderen (1963), and Chincarini (1964), from upper to lower (or from right to left), and one of the three major branches immediately turns to the right. After the onset of the nebular phase, strong emission lines [O III] began to contribute to the blue edge of  $V$  filter. The response of each  $V$  filter is different to each other at the blue edge and this difference makes a significant difference in the  $V$  magnitude. This effect can be clearly seen in Figures 3, 4, and 5 of Kreiner et al. (1966), in which the  $V$  magnitude started to branch off after UT 1963 April 10 while the  $B$  magnitude did not among the various observers.

We check our obtained value of  $(m - M)_V = 10.65$  by fitting with our model  $V$  light curve in Figure 33(a). We add a  $1.03 M_\odot$  WD model (solid red line) with the chemical composition of Ne nova 2 (Hachisu & Kato 2010). Taking  $(m - M)_V = 10.65$  for V533 Her, the absolute model  $V$  light curve reproduces the observed apparent  $V$  light curve of V533 Her (filled red circles). This confirms that the distance modulus of  $(m - M)_V = 10.65$  is reasonable.

### 7.3. PW Vul 1984#1

PW Vul was examined in Paper II on the  $(B - V)_0 - M_V$  diagram. Here, we reexamine it on the time-stretched color-magnitude diagram. In Appendix B.3, we obtain  $(m - M)_V = 13.0 \pm 0.2$  together with  $f_s = 2.24$  against LV Vul based on the time-stretching method. Taking  $(m - M)_V = 13.0$  for PW Vul, we plot a  $0.83 M_\odot$  WD model (solid red line) with the chemical composition of CO nova 4 (Hachisu & Kato 2015) in Figure 34(a). The model absolute  $V$  light curve reasonably fits with the observed apparent  $V$  light curve of PW Vul after  $t >$



60 day. This confirms that the distance modulus of  $(m - M)_V = 13.0$  is reasonable.

We also fit our UV 1455Å light curve model of the  $0.83 M_\odot$  WD with the observation as shown in Figure 34(a). We obtain  $F_{1455}^{\text{mod}} = 15$  and  $F_{1455}^{\text{obs}} = 6$  in units of  $10^{-12} \text{ erg cm}^{-2} \text{ s}^{-1} \text{ \AA}^{-1}$  at the upper bound of Figure 34(a). With these values, we plot the distance-reddening relation of Equation (20) in Figure 10(c) by the solid magenta line. The solid blue line of  $(m - M)_V = 13.0$  and this magenta line cross at  $d = 1.8 \text{ kpc}$  and  $E(B - V) = 0.57$ . These light curve fittings are essentially the same as in the previous work (Hachisu & Kato 2015). Thus, we obtain the distance of  $d = 1.8 \pm 0.2 \text{ kpc}$  from Equation (5),  $E(B - V) = 0.57 \pm 0.05$ , and  $(m - M)_V = 13.0 \pm 0.2$ . This distance estimate is consistent with the distance estimated by Downes & Duerbeck (2000),  $d = 1.8 \pm 0.05 \text{ kpc}$ , with the nebular expansion parallax method. We list the results in Table 1.

For comparison, in Figure 34(a), we depict a  $0.98 M_\odot$  WD model (solid blue lines) with the chemical composition of CO nova 3 (Hachisu & Kato 2015), assuming that  $(m - M)_V = 14.6$  for V1668 Cyg. With the same stretching factor of  $f_s = 2.24$ , both the  $V$  and UV 1455Å light curves almost overlap between PW Vul and V1668 Cyg. This confirms that the optical light curves and UV 1455Å light curves follow the same timescaling law as already explained in Section 1.

We check the distance and reddening based on various distance-reddening relations. Hachisu & Kato (2015) obtained  $E(B - V) = 0.55 \pm 0.05$  from the fitting in the color-color diagram (Paper I), being consistent with the crossing point mentioned above. Figure 10(c) shows various distance-reddening relations toward PW Vul, whose galactic coordinates are  $(l, b) = (61^\circ 0983, +5^\circ 1967)$ . We plot the constraint of  $d = 1.8 \pm 0.05 \text{ kpc}$  by Downes & Duerbeck (2000) (solid horizontal black lines). We further add other distance-reddening relations toward PW Vul. The vertical solid red line is  $E(B - V) = 0.57$ . We plot the distance-reddening relations (solid black/orange lines) given by Green et al. (2015, 2018), respectively. We also plot four distance-reddening relations of Marshall et al. (2006); toward  $(l, b) = (61^\circ 00, +5^\circ 00)$  denoted by open red squares,  $(61^\circ 25, +5^\circ 00)$  by filled green squares,  $(61^\circ 00, +5^\circ 25)$  by blue asterisks, and  $(61^\circ 25, +5^\circ 25)$  by open magenta circles, each with error bars. The closest direction in the galactic coordinates is that of blue asterisks. The open cyan-blue diamonds represent the relation given by Özdörmez et al. (2016). Our crossing point at  $d = 1.8 \text{ kpc}$  and  $E(B - V) = 0.57$  is  $\Delta E(B - V) = 0.15 \text{ mag}$  larger than the trends of Marshall et al.'s blue asterisks data. To summarize, our set

of  $d = 1.8 \text{ kpc}$  and  $E(B - V) = 0.57$  is not consistent with all the 3D dust maps given by Marshall et al. (2006), Özdörmez et al. (2016), Green et al. (2015, 2018), and Chen et al. (2018). This is the first and only the case that our crossing point is largely different from the several 3D dust maps. We discuss the reason of such a large discrepancy below.

The 3D dust maps basically give an averaged value of a relatively broad region, so the pinpoint reddening could be different from the values of the 3D dust maps. The pinpoint estimate of the reddening toward PW Vul indicates  $E(B - V) = 0.55 \pm 0.05$  as already discussed in Hachisu & Kato (2015). For example, Andreä et al. (1991) obtained  $E(B - V) = 0.58 \pm 0.06$  from He II  $\lambda 1640/\lambda 4686$  ratio and  $E(B - V) = 0.55 \pm 0.1$  from the interstellar absorption feature at  $2200\text{\AA}$  for the reddening toward PW Vul. Saizar et al. (1991) reported  $E(B - V) = 0.60 \pm 0.06$  from He II  $\lambda 1640/\lambda 4686$  ratio. Hachisu & Kato (2014) estimated the reddening to be  $E(B - V) = 0.55 \pm 0.05$  from the color-color diagram fit of PW Vul. As for the distance to PW Vul, Downes & Duerbeck (2000) obtained  $d = 1.8 \pm 0.05 \text{ kpc}$  with the nebular expansion parallax method. These pinpoint constraints are all consistent with our crossing point of  $E(B - V) = 0.57 \pm 0.05$ ,  $(m - M)_V = 13.0 \pm 0.2$ , and  $d = 1.8 \pm 0.2 \text{ kpc}$ .

We further obtain the distance moduli of  $UBVI$  bands and check their crossing points in the distance-reddening plane. We obtain  $(m - M)_U = 13.92$ ,  $(m - M)_B = 13.55$ , and  $(m - M)_V = 13.0$  (and  $(m - M)_I = 12.12$ ) in Appendix B.3, and plot them in Figure 10(c) by the thin solid green, cyan, thick solid blue (and thin solid blue-magenta) lines, respectively. These lines cross at  $E(B - V) = 0.57$  and  $d = 1.8 \text{ kpc}$ , confirming again our results.

Adopting  $E(B - V) = 0.57$  and  $(m - M')_V = 13.85$  in Equation (B32), we obtain the time-stretched color-magnitude diagram of PW Vul in Figure 11(c). Here, we plot the data taken from Noskova et al. (1985), Kolotilov & Noskova (1986), and Robb & Scarfe (1995). PW Vul follows the V1500 Cyg track except for the very early phase. Therefore, PW Vul belongs to the V1500 Cyg type in the time-stretched color-magnitude diagram. This overlapping to the V1500 Cyg track supports our estimates of  $E(B - V) = 0.57$  and  $(m - M')_V = 13.85$ , that is,  $f_s = 2.24$ ,  $E(B - V) = 0.57 \pm 0.05$ ,  $(m - M)_V = 13.0 \pm 0.2$ , and  $d = 1.8 \pm 0.2 \text{ kpc}$ . We list our results in Table 1.

#### 7.4. V1419 Aql 1993

V1419 Aql was examined in Paper II on the  $(B - V)_0 - M_V$  diagram. Here, we reexamine it on the time-

stretched color-magnitude diagram. We determine the distance modulus in the  $V$  band to be  $(m - M)_V = 15.0 \pm 0.2$  together with  $f_s = 1.41$  against LV Vul in Appendix B.4. For the reddening toward V1419 Aql, Hachisu & Kato (2014, 2016b) obtained  $E(B - V) = 0.50 \pm 0.05$  from the fitting in the color-color diagram (Paper I). On the other hand, the NASA/IPAC galactic 2D dust absorption map gives  $E(B - V) = 0.55 \pm 0.01$  in the direction toward V1419 Aql. See Hachisu & Kato (2014, 2016b) and Özdörmez et al. (2016) for a summary of other estimates on the extinction and distance of V1419 Aql. We adopt the arithmetic mean of these two values, i.e.,  $E(B - V) = 0.52 \pm 0.05$  in the present paper. Then, we obtain the distance of  $d = 4.7 \pm 0.5$  kpc from Equation (5).

We check the distance and reddening toward V1419 Aql, whose galactic coordinates are  $(l, b) = (36^\circ 8110, -4^\circ 1000)$ , based on various distance-reddening relations in Figure 10(d). The solid blue line denotes the distance modulus of  $(m - M)_V = 15.0$  and Equation (5). The vertical solid red line is  $E(B - V) = 0.52$ . These two lines cross at  $d = 4.7$  kpc (and  $E(B - V) = 0.52$ ). We add the distance-reddening relations (solid black/orange lines) given by Green et al. (2015, 2018), respectively. We also plot four distance-reddening relations of Marshall et al. (2006); toward  $(l, b) = (36^\circ 75, -4^\circ 00)$  denoted by open red squares,  $(37^\circ 00, -4^\circ 00)$  by filled green squares,  $(36^\circ 75, -4^\circ 25)$  by blue asterisks, and  $(37^\circ 00, -4^\circ 25)$  by open magenta circles, each with error bars. The closest direction is that of open red squares. The solid green line is the relation given by Sale et al. (2014). The open cyan-blue diamonds with error bars are the relation given by Özdörmez et al. (2016). The solid cyan-blue line is the relation given by Chen et al. (2018). Our set of  $E(B - V) = 0.52$  and  $d = 4.7$  kpc is broadly consistent with the distance-reddening relations of Marshall et al. (2006), Sale et al. (2014), Green et al. (2018), and Özdörmez et al. (2016). Thus, we confirm that our adopted values of  $E(B - V) = 0.52 \pm 0.05$ ,  $(m - M)_V = 15.0 \pm 0.2$ , and  $d = 4.7 \pm 0.5$  kpc are reasonable. We list our results in Table 1.

Adopting  $E(B - V) = 0.52$  and  $(m - M)_V = 15.35$  in Equation (B40), we obtain the time-stretched color-magnitude diagram of V1419 Aql in Figure 11(d). Here, we plot the data taken from Munari et al. (1994b) and IAU Circular Nos. 5794, 5802, 5807, and 5829. The track of V1419 Aql is considerably affected by dust formation, the start of which is denoted by the large magenta square. We regard that V1419 Aql belongs to the LV Vul type because the V1419 Aql track follows a part of the V1668 Cyg track (blue lines) until the dust blackout started. For comparison, we also plot the V1065 Cen

track (filled blue triangles) that shows a similar shallow dust blackout (see Figures 4 and 6 of Hachisu & Kato 2018a). The track of V1065 Cen almost follows the lower branch of LV Vul, while the track of V1419 Aql is not clear owing to dust blackout.

Finally, we plot a  $0.90 M_\odot$  WD model with the chemical composition of CO nova 3 (Hachisu & Kato 2016a) by the solid red lines in Figure 37(a). The  $V$  model light curve reasonably fits with the  $V$  light curve of V1419 Aql during  $\log t$  (day) = 1.0 – 1.5. This confirms our value of  $(m - M)_V = 15.0$ .

### 7.5. V705 Cas 1993

V705 Cas was examined in Paper II, but we reexamine it on the time-stretched color-magnitude diagram. For the reddening toward V705 Cas, we adopt  $E(B - V) = 0.45 \pm 0.05$  after Hachisu & Kato (2014). We do not repeat the discussion. Papers I & II give a summary on the distance and reddening toward V705 Cas,  $(l, b) = (113^\circ 6595, -4^\circ 0959)$ . We obtain the timescaling factor of  $f_s = 2.8$  against LV Vul and the distance of  $d = 2.6 \pm 0.3$  kpc from Equation (5),  $E(B - V) = 0.45 \pm 0.05$ , and  $(m - M)_V = 13.45 \pm 0.2$  in Appendix B.5. Using the expansion parallax method, Eyres et al. (1996) and Diaz et al. (2001) obtained  $d = 2.5$  kpc and  $d = 2.9 \pm 0.4$  kpc, respectively. These distances are all consistent with our value of  $d = 2.6 \pm 0.3$  kpc. We list our results in Table 1.

Next, we discuss the model light curve fitting. We obtain  $(m - M)_V = 13.45$  based on the time-stretching method in Appendix B.5. Assuming that  $(m - M)_V = 13.45$ , we plot a  $0.78 M_\odot$  WD model (solid magenta lines) with the chemical composition of CO nova 4 (Hachisu & Kato 2015) in Figure 38(a). The model absolute  $V$  and UV 1455Å light curves of the  $0.78 M_\odot$  WD reasonably fit with the observed apparent  $V$  and UV 1455Å light curves of V705 Cas. This model light curve fitting is essentially the same as Figure 15 of Hachisu & Kato (2015) and we again confirm that the distance modulus of  $(m - M)_V = 13.45$  is reasonable for V705 Cas. In the same figure, we add a  $0.83 M_\odot$  WD model (solid blue lines) with the same chemical composition of CO nova 4, assuming that  $(m - M)_V = 13.0$  for PW Vul.

We reanalyze the distance and reddening toward V705 Cas based on various distance-reddening relations in Figure 12(a). The solid blue line shows  $(m - M)_V = 13.45$  and Equation (5). The solid magenta line is the UV 1455Å fit of our  $0.78 M_\odot$  WD model. The UV 1455Å light curve fit gives the relation of Equation (20) together with  $F_{1455}^{\text{obs}} = 6.0$  and  $F_{1455}^{\text{mod}} = 12.5$  in units of  $10^{-12} \text{ erg cm}^{-2} \text{ s}^{-1} \text{ \AA}^{-1}$  at the upper bound of Figure

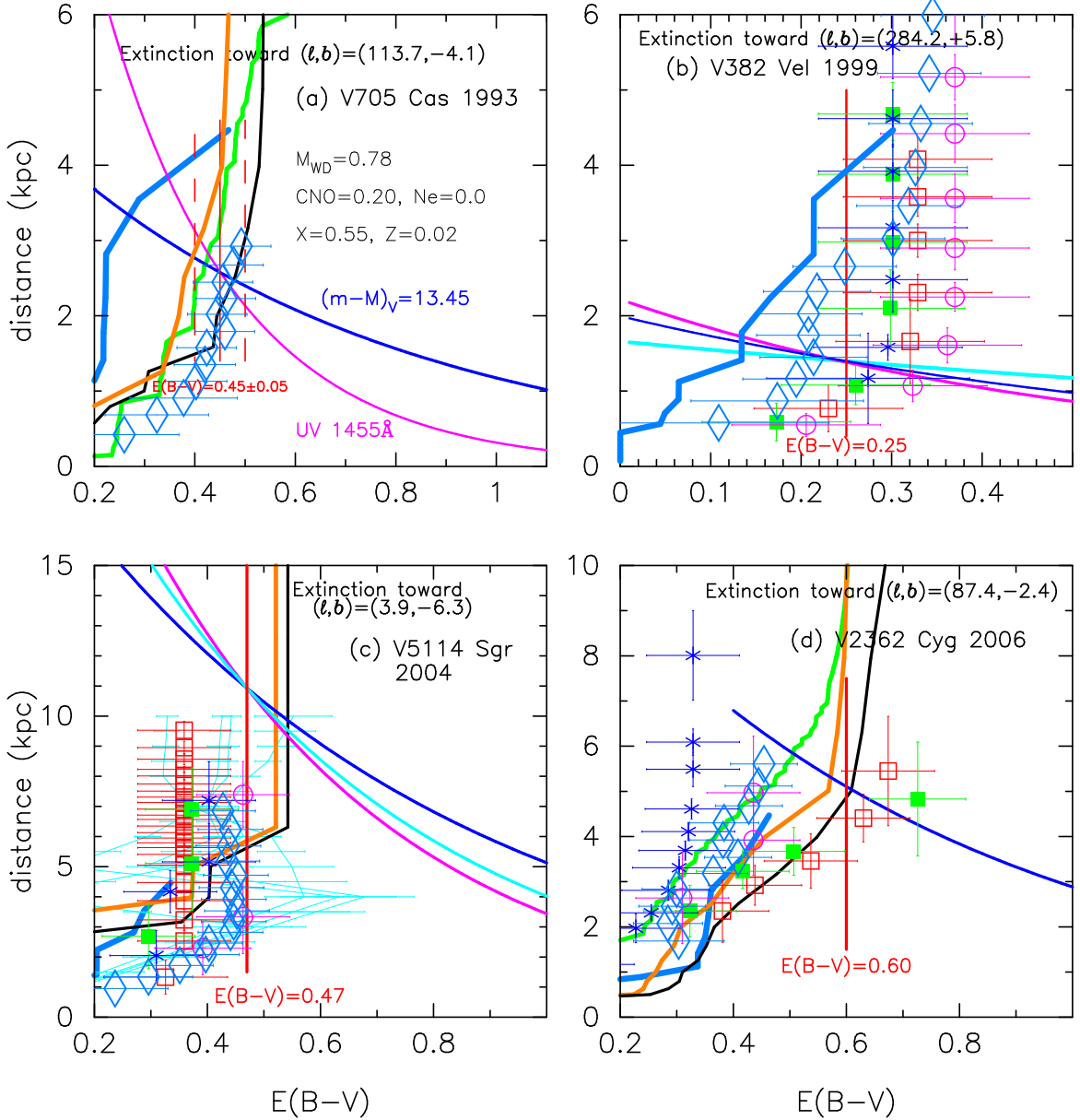


**Figure 12.** Various distance-reddening relations for (a) V705 Cas, (b) V382 Vel, (c) V5114 Sgr, and (d) V2362 Cyg. The vertical thick solid red lines represent the color excess of each nova. The solid black/orange lines represent the distance-reddening relations given by Green et al. (2015, 2018), respectively. Four sets (open red squares, filled green squares, blue asterisks, and open magenta circles) of data, each with error bars, show distance-reddening relations given by Marshall et al. (2006) in four nearby directions of each nova. The open cyan-blue diamonds with error bars are the relation given by Özdörmez et al. (2016, 2018). The thick solid green line represents the relation given by Sale et al. (2014). The thick solid cyan-blue line represents the relation given by Chen et al. (2018). In panel (c), the four very thin cyan lines with error bars denote the four nearby distance-reddening relations given by Schultheis et al. (2014).

38(a). We also plot the relations given by Green et al. (2015, 2018) by the solid black/orange lines, respectively. No data of Marshall et al. (2006) are available in this direction. The solid green line represent the relation given by Sale et al. (2014). The open cyan-blue diamonds with error bars denote the relation given by Özdörmez et al. (2016). The solid cyan-blue line de-

notes the relation given by Chen et al. (2018). The blue, magenta, and red lines cross at  $E(B - V) = 0.45$  and  $d = 2.6$  kpc. This crossing point is also consistent with the distance-reddening relation given by Green et al. (2015, black line), Sale et al. (2014, green line), and Özdörmez et al. (2016, cyan-blue diamonds).

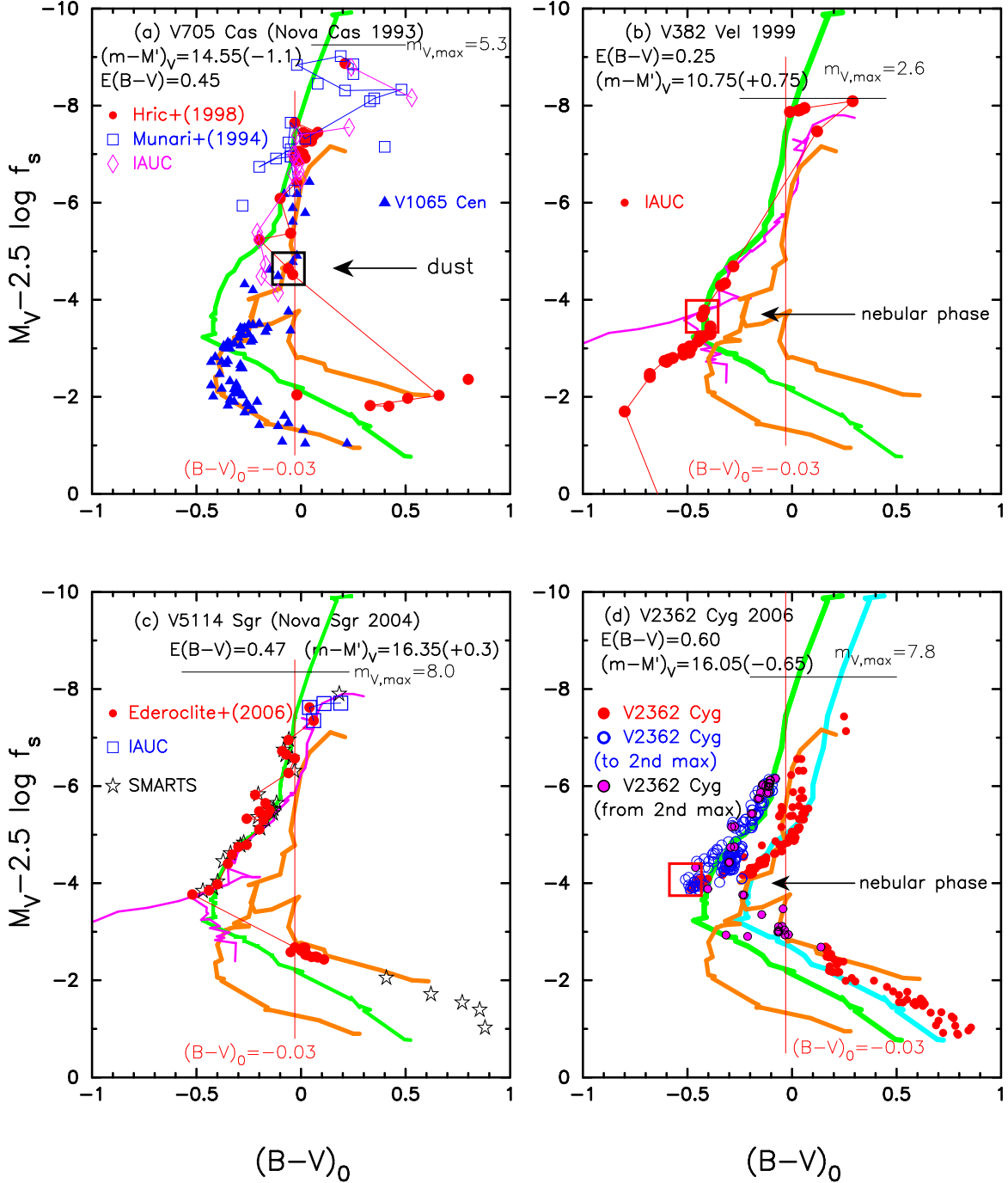


**Figure 13.** Same as Figure 9, but for (a) V705 Cas, (b) V382 Vel, (c) V5114 Sgr, and (d) V2362 Cyg. The solid orange, green, and magenta lines indicate the template tracks of LV Vul, V1500 Cyg, and V1974 Cyg, respectively. The onset of nebular phase is indicated by a large open red square. The start of dust blackout is denoted by a large open black square. In panel (d), we add the track of V1500 Cyg shifted redward by  $\Delta(B-V) = 0.20$  (solid cyan lines). We indicate the rising/decay phase of the secondary maximum by blue open circles/filled magenta circles with black outlines, respectively.

Adopting  $E(B - V) = 0.45$  and  $(m - M')_V = 14.55$  in Equation (B42), we obtain the time-stretched color-magnitude diagram of V705 Cas in Figure 13(a). Here, we plot the data taken from Munari et al. (1994a), Hric et al. (1998), and IAU Circular Nos. 5905, 5912, 5914, 5920, 5928, 5929, 5945, and 5957. The track of V705 Cas is also affected by dust formation as denoted by the large black square. We also plot the V1065 Cen track (see Figures 4 and 6 of Hachisu & Kato 2018a) in Figure 13(a). V1065 Cen shows a similar dust blackout to V705 Cas but its depth of dust blackout is much shallower (see Figure 51) than that of V705 Cas. The V1065 Cen track comes back soon after the dust blackout and follows again the LV Vul track, so that V1065 Cen belongs to the LV Vul type in the time-stretched color-magnitude diagram. We regard that V705 Cas also belongs to the LV Vul type because the V705 Cas track almost follows that of LV Vul and V1065 Cen until the dust blackout started. The early pulse (oscillation) in the  $V$  light curve makes a loop in the color-magnitude diagram. This kind of loops were also seen in multiple-peak novae like V723 Cas and V5558 Sgr as discussed by Hachisu & Kato (2016b). We list our results in Table 1.

### 7.6. V382 Vel 1999

V382 Vel was also studied in Paper II on the  $(B - V)_0 - M_V$  diagram. In this subsection, we examine it on the  $(B - V)_0 - (M_V - 2.5 \log f_s)$  diagram. For the reddening toward V382 Vel,  $(l, b) = (284^\circ 1674, +5^\circ 7715)$ , Steiner et al. (1999) obtained  $E(B - V) = A_V/3.1 = 0.8/3.1 = 0.26$  from an equivalent width of 0.024 nm of the interstellar Ca II K line. Orio et al. (2002) obtained the hydrogen column density toward V382 Vel to be  $N_H \sim 2 \times 10^{21} \text{ cm}^{-2}$  from X-ray spectrum fittings. This value can be converted with  $E(B - V) = N_H/4.8 \times 10^{21} \sim 0.4$  (Bohlin et al. 1978),  $E(B - V) = N_H/5.8 \times 10^{21} \sim 0.34$  (Güver & Özel 2009), and  $E(B - V) = N_H/6.8 \times 10^{21} \sim 0.3$  (Liszt 2014). On the other hand, della Valle et al. (2002) obtained  $E(B - V) = 0.05$  from various line ratios and  $E(B - V) = 0.09$  from Na I D interstellar absorption features. Shore et al. (2003) obtained  $E(B - V) = 0.20$  from the resemblance of IUE spectra to that of V1974 Cyg. Shore et al. (2003) and Ness et al. (2005) obtained  $N_H = 1.2 \times 10^{21} \text{ cm}^{-2}$ , corresponding to  $E(B - V) = N_H/4.8 \times 10^{21} = 0.25$ ,  $E(B - V) = N_H/5.8 \times 10^{21} = 0.21$ , and  $E(B - V) = N_H/6.8 \times 10^{21} = 0.18$ . Hachisu & Kato (2014) obtained  $E(B - V) = 0.15 \pm 0.05$  by fitting the color-color track of V382 Vel with the general track of novae. To summarize, there are two estimates,  $E(B - V) = 0.1 \pm 0.05$  and  $E(B - V) = 0.25 \pm 0.05$ .

We obtain three distance moduli of  $B$ ,  $V$ , and  $I_C$  bands in Appendix B.6 based on the time-stretching method. We plot these distance moduli in Figure 12(b) by the magenta, blue, and cyan lines, that is,  $(m - M)_B = 11.7$ ,  $(m - M)_V = 11.48$ , and  $(m - M)_I = 11.09$  together with Equations (11), (5), and (12). These three lines broadly cross at  $d = 1.4$  kpc and  $E(B - V) = 0.25$ . Thus, we obtain the timescaling factor  $f_s = 0.51$  against LV Vul, the reddening toward V382 Vel,  $E(B - V) = 0.25 \pm 0.05$ , and the distance to V382 Vel,  $d = 1.4 \pm 0.2$  kpc. The distance modulus in the  $V$  band is  $(m - M)_V = 11.5 \pm 0.2$ . These values are listed in Table 1.

Adopting  $E(B - V) = 0.25$  and  $(m - M')_V = 10.75$  in Equation (B44), we plot the time-stretched color-magnitude diagram of V382 Vel in Figure 13(b). The nebular phase had started at least by the end of 1999 June, i.e.,  $\sim 40$  days after the optical maximum (della Valle et al. 2002). We plot this phase ( $M_V = m_V - (m - M)_V \approx 7.09 - 11.5 = -4.41$ ) by the large open red square in Figure 13(b). The track of V382 Vel follows the V1500 Cyg/V1974 Cyg tracks at least until the nebular phase started. Thus, we regard that V382 Vel belongs to the V1500 Cyg type in the time-stretched color-magnitude diagram. This overlapping to the tracks of V1500 Cyg/V1974 Cyg supports our values of  $E(B - V) = 0.25$  and  $(m - M')_V = 10.75$ , that is,  $E(B - V) = 0.25 \pm 0.05$ ,  $(m - M)_V = 11.5 \pm 0.2$ ,  $f_s = 0.51$ , and  $d = 1.4 \pm 0.2$  kpc.

Taking  $(m - M)_V = 11.5$  for V382 Vel, we plot the  $V$  model light curve (total flux of free-free plus photospheric emission: solid red line) of a  $1.23 M_\odot$  WD with the envelope chemical composition of Ne nova 2 (Hachisu & Kato 2010, 2016a) in Figure 39(a). The model  $V$  light curve reasonably reproduces the observation (filled red circles). This model light curve fitting gives the same result as in Figure 27 of Hachisu & Kato (2016a). Thus, we again confirm that the distance modulus of  $(m - M)_V = 11.5 \pm 0.2$  is reasonable.

We further examine the distance and reddening toward V382 Vel,  $(l, b) = (284^\circ 1674, +5^\circ 7715)$ , based on various distance-reddening relations in Figure 12(b). We plot the four sets of distance-reddening relation calculated by Marshall et al. (2006); toward  $(l, b) = (284^\circ 00, +5^\circ 75)$  denoted by open red squares,  $(284^\circ 25, +5^\circ 75)$  by filled green squares,  $(284^\circ 00, +6^\circ 00)$  by blue asterisks, and  $(284^\circ 25, +6^\circ 00)$  by open magenta circles. The filled green squares are the closest direction among the four nearby directions. The open cyan-blue diamonds with error bars denote the relation given by Özdörmez et al. (2016). The solid cyan-blue line denotes the relation given by Chen et al. (2018). The ver-

tical solid red line is the color excess of  $E(B-V) = 0.25$ . Our crossing point at  $d = 1.4$  kpc and  $E(B-V) = 0.25$  is broadly consistent with Marshall et al.’s and Özdörmez et al.’s relations within error bars.

The distance toward V382 Vel was recently estimated by Tomov et al. (2015) to be  $d = (v_{\text{exp}} \times t)/r_{\text{shell}} = (1800 \pm 100 \text{ km s}^{-1} \times 12 \text{ yr})/(6''.0 \pm 0''.25) \approx 0.8 \pm 0.1$  kpc with the expansion parallax method. This value is much smaller than our estimate of  $d = 1.4 \pm 0.2$  kpc. However, the distance obtained with the expansion parallax method depends largely on the assumed velocity,  $v_{\text{exp}}$ . If we adopt other velocities estimated in the early outburst phase  $v_{\text{exp}} \sim 3500 \text{ km s}^{-1}$  (e.g., della Valle et al. 2002) or  $v_{\text{exp}} \sim 2900 \text{ km s}^{-1}$  (e.g., Ness et al. 2005), we have large distances such as  $d \sim 1.5$  kpc or  $d \sim 1.2$  kpc, respectively.

### 7.7. V5114 Sgr 2004

V5114 Sgr was studied in Paper II on the  $(B-V)_0$ - $M_V$  diagram. In this subsection, we reexamine it but on the  $(B-V)_0$ - $(M_V - 2.5 \log f_s)$  diagram. We obtain three distance moduli in the  $U$ ,  $B$ , and  $V$  bands in Appendix B.7. We plot these three distance moduli in Figure 12(c) by the magenta, cyan, and blue lines, that is,  $(m-M)_U = 17.45$ ,  $(m-M)_B = 17.15$ , and  $(m-M)_V = 16.65$  together with Equations (10), (11), and (5), respectively. These three lines do not exactly but broadly cross at  $d = 10.9$  kpc and  $E(B-V) = 0.47$ . Thus, we obtain the timescaling factor of  $f_s = 0.76$  against LV Vul, the reddening of  $E(B-V) = 0.47 \pm 0.05$ , and the distance of  $d = 10.9 \pm 1$  kpc. These values are listed in Table 1.

Various reddening estimates were summarized in Paper II and their arithmetic mean was calculated to be  $E(B-V) = 0.51 \pm 0.09$ . The NASA/IPAC galactic dust absorption map gives  $E(B-V) = 0.49 \pm 0.02$  in the direction toward V5114 Sgr. Hachisu & Kato (2014) derived the reddening of  $E(B-V) = 0.45 \pm 0.05$  on the basis of the general track of color-color evolution of novae. These are all consistent with our new value of  $E(B-V) = 0.47 \pm 0.05$ .

Next, we reanalyze the distance and reddening toward V5114 Sgr,  $(l, b) = (3^\circ 9429, -6^\circ 3121)$ , based on various distance-reddening relations in Figure 12(c). The vertical solid red line is  $E(B-V) = 0.47$ . We plot four distance-reddening relations of Marshall et al. (2006); toward  $(l, b) = (3^\circ 75, -6^\circ 50)$  denoted by open red squares,  $(4^\circ 00, -6^\circ 50)$  by filled green squares,  $(3^\circ 75, -6^\circ 25)$  by blue asterisks, and  $(4^\circ 00, -6^\circ 25)$  by open magenta circles, each with error bars. The closest direction in the galactic coordinates is that of open magenta circles. The black/orange lines are the rela-

tions given by Green et al. (2015, 2018), respectively. The cyan-blue line is the relation given by Chen et al. (2018). We further add the 3D reddening map given by Schulteis et al. (2014). We plot four Schulteis et al.’s distance-reddening relations toward near the direction of V5114 Sgr:  $(l, b) = (3^\circ 9, -6^\circ 4)$ ,  $(3^\circ 9, -6^\circ 3)$ ,  $(4^\circ 0, -6^\circ 4)$ , and  $(4^\circ 0, -6^\circ 3)$  by the very thin solid cyan lines. The lines show zigzag patterns in this case, although the reddening must increase monotonically with the distance. In this sense, Schulteis et al.’s distance-reddening relation may not be appropriate in the middle part of the lines. Our set of  $E(B-V) = 0.47$  and  $d = 10.9$  kpc is consistent with the trend of Marshall et al.’s data (open magenta circles), although  $\Delta E(B-V) \sim 0.05 - 0.1$  mag smaller than Green et al.’s.

Adopting  $E(B-V) = 0.47$  and  $(m-M')_V = 16.35$  in Equation (B49), we obtain the time-stretched color-magnitude diagram of V5114 Sgr in Figure 13(c). Here, we plot the data taken from Ederoclite et al. (2006), IAU Circular Nos. 8306 and 8310, and SMARTS. V5114 Sgr follows those of V1500 Cyg/V1974 Cyg. Therefore, we regard that V5114 Sgr belongs to the V1500 Cyg type in the time-stretched color-magnitude diagram. This overlapping supports our estimates of  $E(B-V) = 0.47$  and  $(m-M')_V = 16.35$ , that is,  $f_s = 0.76$ ,  $E(B-V) = 0.47 \pm 0.05$ ,  $(m-M)_V = 16.65 \pm 0.1$ , and  $d = 10.9 \pm 1$  kpc. We list our results in Table 1.

Taking  $(m-M)_V = 16.65$  for V5114 Sgr, we plot the  $V$  model light curve (solid red line) of a  $1.15 M_\odot$  WD with the envelope chemical composition of Ne nova 2 (Hachisu & Kato 2010, 2016a) in Figure 41(a). The model  $V$  light curve reasonably reproduces the observation (filled red circles). This again confirms that the distance modulus of  $(m-M)_V = 16.65 \pm 0.1$  is reasonable.

### 7.8. V2362 Cyg 2006

V2362 Cyg was also studied in Paper II. Here, we reexamine it on the  $(B-V)_0$ - $(M_V - 2.5 \log f_s)$  diagram. V2362 Cyg shows a prominent secondary maximum (e.g., Kimeswenger et al. 2008; Munari et al. 2008b, see Figure 43). The origin of the secondary maximum was discussed by Hachisu & Kato (2009).

The color excess of V2362 Cyg was estimated by various authors (see Section 3.22 of Paper II). We adopt  $E(B-V) = 0.60 \pm 0.05$  after Hachisu & Kato (Paper II). Then, the timescaling factor is obtained to be  $f_s = 1.78$  against LV Vul and the distance is  $d = 5.1 \pm 0.5$  kpc from Equation (5) together with  $(m-M)_V = 15.4 \pm 0.2$  in Appendix B.8.

Adopting  $E(B - V) = 0.60$  and  $(m - M')_V = 16.05$  from Equation (B54), we plot the time-stretched color-magnitude diagram of V2362 Cyg in Figure 13(d). We also add the template tracks of LV Vul (thick solid orange line) and V1500 Cyg (thick solid green line). We further add another track of V1500 Cyg (thick solid cyan line) which is shifted toward red by  $\Delta(B - V) = 0.20$  mag.

V2362 Cyg shows an interesting evolution in the color-magnitude diagram. V2362 Cyg goes down along the LV Vul track (orange line) or the red-shifted V1500 Cyg track (cyan line) just after the optical maximum. In the secondary maximum phase, it goes up along the original track of V1500 Cyg (solid green line) as denoted by open blue circles, and then goes down along the same V1500 Cyg track (solid green line) as denoted by filled magenta circles with black outlines. After the onset of the nebular phase, the track turns to the right and follows again the upper LV Vul track (orange line) or the red-shifted V1500 Cyg track (cyan line).

These distinct two tracks are a hint to resolve the reason why the two types of V1500 Cyg and LV Vul tracks are clearly separated in the time-stretched color-magnitude diagram. Munari et al. (2008b) wrote “the emission spectrum at second maximum was quite different from that at first maximum, reflecting the much higher temperature of the underlying continuum. At second maximum, Fe II emission lines were not seen and were replaced by N II, N III, O II, [O I], and He I.” The strong emission lines (He II/N III as well as Balmer lines such as H $\gamma$ , H $\delta$ , H $\epsilon$ ) contribute to the  $B$ -band and make  $B - V$  blue in the secondary maximum phase. Thus, the difference in the  $(B - V)_0$  color is real rather than the difference in the  $V$  filter response. We can conclude that the two tracks reflect the difference in the ionization state which originates from the temperature difference of the underlying continuum. We call the redder location the LV Vul type and the bluer location the V1500 Cyg type. The separation is  $\Delta(B - V)_0 \sim 0.2$  mag. Overlapping of these tracks of V2362 Cyg with the two templates novae, LV Vul and V1500 Cyg, supports our values of  $(m - M')_V = 16.05$  and  $E(B - V) = 0.60$ , that is,  $f_s = 1.78$ ,  $E(B - V) = 0.60 \pm 0.05$ ,  $(m - M)_V = 15.4 \pm 0.2$ , and  $d = 5.1 \pm 0.5$  kpc. We list our results in Table 1.

We reexamine the distance-reddening relation toward V2362 Cyg,  $(l, b) = (87^\circ 37' 24, -2^\circ 35' 74)$ , based on several distance-reddening relations in Figure 12(d). The solid blue line denotes the distance-reddening relation of Equation (5) together with  $(m - M)_V = 15.4$ . The vertical solid red line is the color excess of V2362 Cyg estimated in Paper II. These two

lines cross at  $d = 5.1$  kpc (and  $E(B - V) = 0.60$ ). We plot the four sets of distance-reddening relation calculated by Marshall et al. (2006); toward  $(l, b) = (87^\circ 25, -2^\circ 25)$  denoted by open red squares,  $(87^\circ 50, -2^\circ 25)$  by filled green squares,  $(87^\circ 25, -2^\circ 50)$  by blue asterisks, and  $(87^\circ 50, -2^\circ 50)$  by open magenta circles. The open red squares are the closest direction toward V2362 Cyg among the four nearby directions. The solid black/orange lines denote the distance-reddening relations given by Green et al. (2015, 2018), respectively. The solid green line represent the relation given by Sale et al. (2014) and the open cyan-blue diamonds with error bars indicate the relation given by Özdörmez et al. (2016). The solid cyan-blue line is the relation given by Chen et al. (2018). Our crossing point at  $d = 5.1$  kpc and  $E(B - V) = 0.60$  is roughly consistent with Marshall et al.’s (open red squares) and Green et al.’s (solid black/orange lines) relations, although the reddenings given by Sale et al. (2014) and Özdörmez et al. (2016) slightly deviates from the crossing point. Thus, we confirm again that our estimated values of  $(m - M)_V = 15.4 \pm 0.2$ ,  $E(B - V) = 0.60 \pm 0.05$ , and  $d = 5.1 \pm 0.5$  kpc are reasonable.

### 7.9. V2615 Oph 2007

V2615 Oph was also studied in Paper II on the  $(B - V)_0 - M_V$  diagram. In this subsection, we reexamine it on the  $(B - V)_0 - (M_V - 2.5 \log f_s)$  diagram.

We obtain three distance moduli in the  $B$ ,  $V$ , and  $I_C$  bands in Appendix B.9. We plot these three distance moduli in Figure 14(a) by the thin solid magenta, blue, and cyan lines. These three lines cross at  $d = 4.3$  kpc and  $E(B - V) = 0.90$ . Therefore, we adopt  $E(B - V) = 0.90 \pm 0.05$ . See Paper II for other various estimates on the reddening and distance. Thus, we obtain the timescaling factor of  $f_s = 1.58$  against LV Vul and the distance of  $d = 4.3 \pm 0.4$  kpc,  $E(B - V) = 0.90 \pm 0.05$ , and  $(m - M)_V = 15.95 \pm 0.2$ .

We reanalyze the distance and reddening toward V2615 Oph,  $(l, b) = (4^\circ 14' 75, +3^\circ 30' 15)$ , based on various distance-reddening relations in Figure 14(a). We plot four distance-reddening relations of Marshall et al. (2006); toward  $(l, b) = (4^\circ 00, +3^\circ 25)$  denoted by open red squares,  $(4^\circ 25, +3^\circ 25)$  by filled green squares,  $(4^\circ 00, +3^\circ 50)$  by blue asterisks, and  $(4^\circ 25, +3^\circ 50)$  by open magenta circles, each with error bars. The direction toward V2615 Oph is between those of open red squares and filled green squares. We add the distance-reddening relations (solid black/orange lines) given by Green et al. (2015, 2018), respectively. We further add four distance-reddening relations (very thin solid cyan lines) given by Schultheis et al. (2014). The

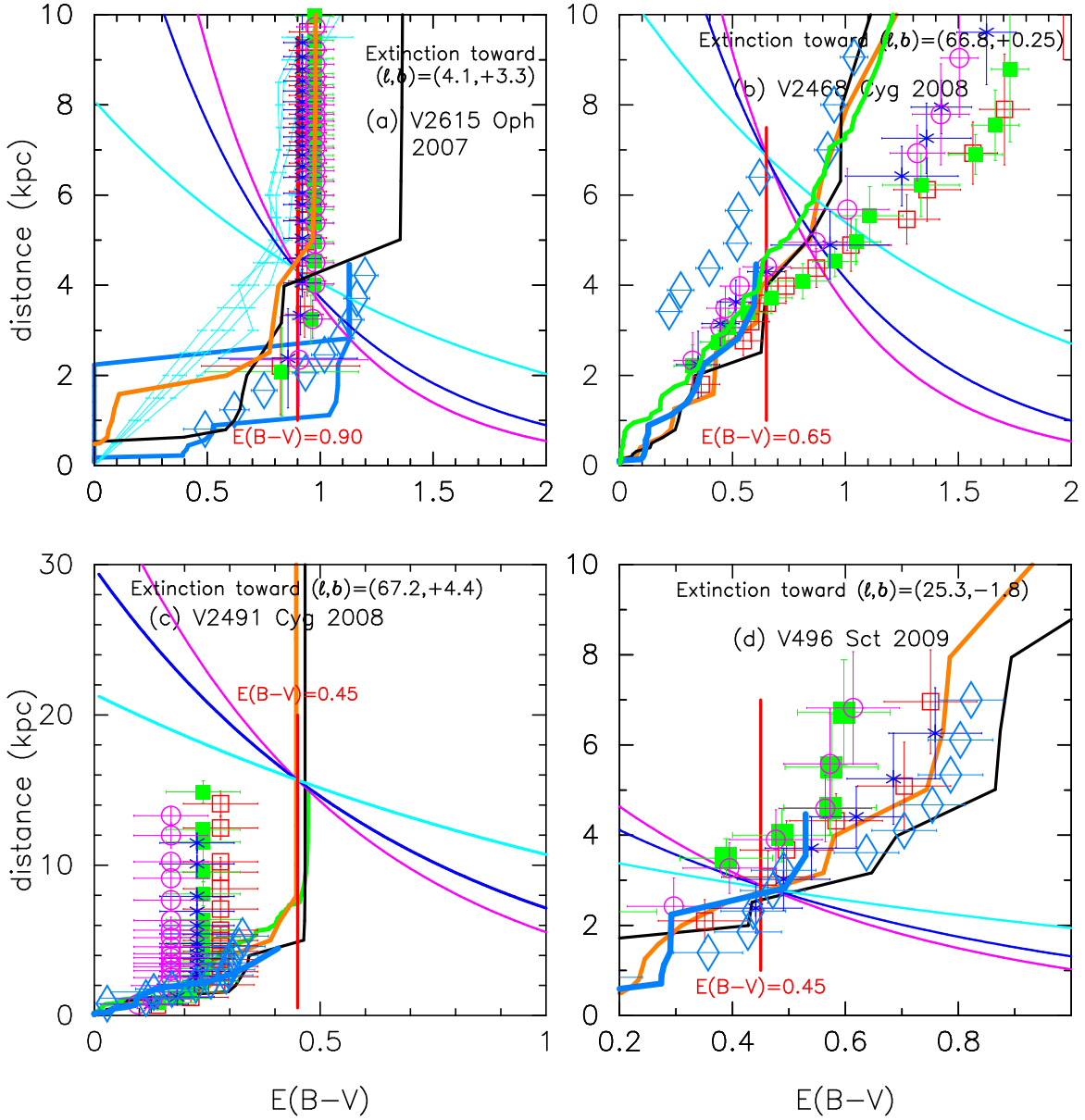


**Figure 14.** Same as Figures 1 and 7, but for (a) V2615 Oph, (b) V2468 Cyg, (c) V2491 Cyg, and (d) V496 Sct.

open cyan-blue diamonds are the relation given by Özdörmez et al. (2016). The cyan-blue line represents the relation given by Chen et al. (2018); one is toward  $(4^{\circ}15', +3^{\circ}25')$  and the other is toward  $(4^{\circ}15', +3^{\circ}35')$ . Our crossing point at  $E(B-V) = 0.90$  and  $d = 4.3$  kpc is consistent with the both trends of Marshall et al. and Green et al. The NASA/IPAC galactic 2D dust absorption map gives  $E(B-V) = 0.87 \pm 0.02$  toward V2615 Oph, being consistent with our value of  $E(B-V) = 0.90 \pm 0.05$ . We list our results in Table 1.

Adopting  $E(B-V) = 0.90$  and  $(m-M)_V = 16.45$  in Equation (B56), we obtain the time-stretched color-magnitude diagram of V2615 Oph in Figure 15(a). Here, we add the time-stretched track of V1065 Cen by the

filled cyan triangles. The track of V2615 Oph is similar to that of V1065 Cen until the dust blackout. It broadly follows the LV Vul track. Therefore, V2615 Oph belongs to the LV Vul type in the time-stretched color-magnitude diagram. This overlapping supports our estimates of  $E(B-V) = 0.90$  and  $(m-M)_V = 16.45$ , that is,  $f_s = 1.58$ ,  $E(B-V) = 0.90 \pm 0.05$ ,  $(m-M)_V = 15.95 \pm 0.2$ , and  $d = 4.3 \pm 0.4$  kpc.

Taking  $(m-M)_V = 15.95$  for V2615 Oph, we plot the  $V$  model light curve (solid red line) of a  $0.90 M_{\odot}$  WD with the envelope chemical composition of CO nova 3 (Hachisu & Kato 2016a) in Figure 44(a). The model  $V$  light curve reasonably reproduces the observation (filled



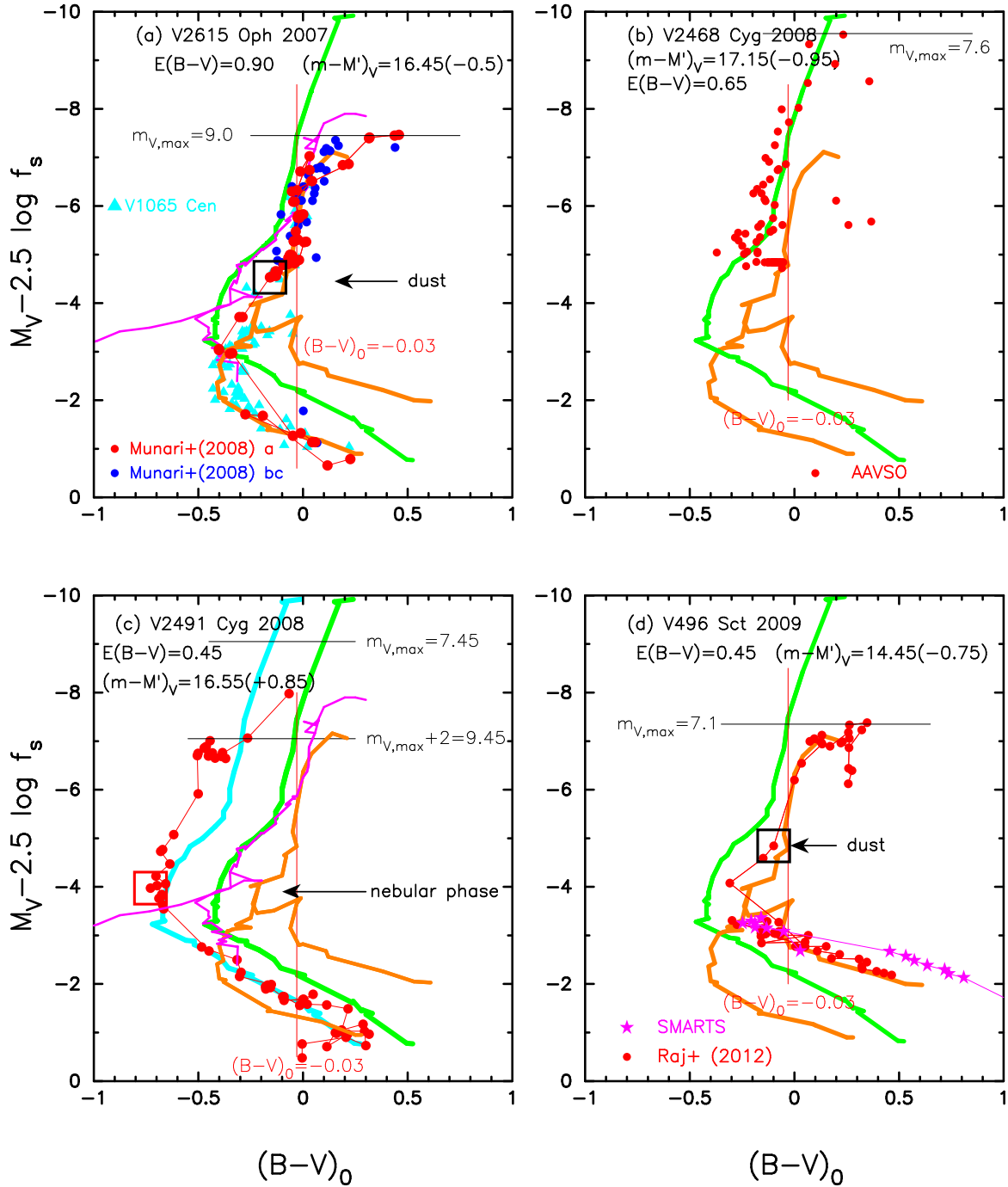


**Figure 15.** Same as Figure 9, but for (a) V2615 Oph, (b) V2468 Cyg, (c) V2491 Cyg, and (d) V496 Sct. The solid orange, green, and magenta lines indicate the template tracks of LV Vul, V1500 Cyg, and V1974 Cyg, respectively. The onset of nebular phase is indicated by a large open red square while the onset of dust blackout is indicated by a large open black square. In panel (c), we add the track of V1500 Cyg shifted blueward by  $\Delta(B-V) = -0.25$  (solid cyan lines).

red circles). This confirms that the distance modulus of  $(m - M)_V = 15.95 \pm 0.2$  is reasonable.

### 7.10. V2468 Cyg 2008

V2468 Cyg was studied in Paper II. Here, we reexamine it on the  $(B - V)_0 - (M_V - 2.5 \log f_s)$  diagram.

We obtain three distance moduli in the  $B$ ,  $V$ , and  $I_C$  bands in Appendix B.10. We plot these three distance moduli in Figure 14(b) by the thin solid magenta, blue, and cyan lines. These three lines cross at  $d = 6.9$  kpc and  $E(B - V) = 0.65$ . We adopt  $f_s = 2.4$  against LV Vul,  $E(B - V) = 0.65 \pm 0.05$ , and  $(m - M)_V = 16.2 \pm 0.2$ . The previous values in Paper II are  $E(B - V) = 0.75 \pm 0.05$ ,  $(m - M)_V = 15.6 \pm 0.2$ , and  $d = 4.5 \pm 0.5$  kpc, being smaller than our new values. The main difference is the improvement in the timescaling factor. See the discussion in Paper II for a summary of other estimates on the reddening and distance toward V2468 Cyg.

Figure 14(b) also shows several distance-reddening relations toward V2468 Cyg,  $(l, b) = (66^\circ 8084, +0^\circ 2455)$ . We plot four distance-reddening relations of Marshall et al. (2006); toward  $(l, b) = (66^\circ 75, +0^\circ 00)$  denoted by open red squares,  $(67^\circ 00, +0^\circ 00)$  by filled green squares,  $(66^\circ 75, +0^\circ 25)$  by blue asterisks, and  $(67^\circ 00, +0^\circ 25)$  by open magenta circles, each with error bars. The closest direction in the galactic coordinates is that of blue asterisks. We add the distance-reddening relations (solid black/orange lines) given by Green et al. (2015, 2018), respectively. The solid green line represents the relation given by Sale et al. (2014) and the open cyan-blue diamonds with error bars are given by Özdörmez et al. (2016). The cyan-blue line represents the relation given by Chen et al. (2018). Our crossing point at  $E(B - V) = 0.65$  and  $d = 6.9$  kpc is consistent with the distance-reddening relation given by Özdörmez et al. Thus, we confirm that our set of  $E(B - V) = 0.65 \pm 0.05$  and  $d = 6.9 \pm 0.8$  kpc are reasonable. We list our results in Table 1.

Adopting  $E(B - V) = 0.65$  and  $(m - M)_V = 17.15$  in Equation (B61), we obtain the time-stretched color-magnitude diagram of V2468 Cyg in Figure 15(b). Here, we plot the data of V2468 Cyg taken from AAVSO. Although the color data are rather scattered, V2468 Cyg broadly follows the V1500 Cyg track. Therefore, V2468 Cyg belongs to the V1500 Cyg type. This overlapping supports our estimates of  $E(B - V) = 0.65$  and  $(m - M)_V = 17.15$ , that is,  $f_s = 2.4$ ,  $E(B - V) = 0.65 \pm 0.05$ ,  $(m - M)_V = 16.2 \pm 0.2$ , and  $d = 6.9 \pm 0.8$  kpc.

Taking  $(m - M)_V = 16.2$  for V2468 Cyg, we plot the  $V$  model light curve (solid red line) of a  $0.85 M_\odot$  WD with the envelope chemical composition of CO nova 4

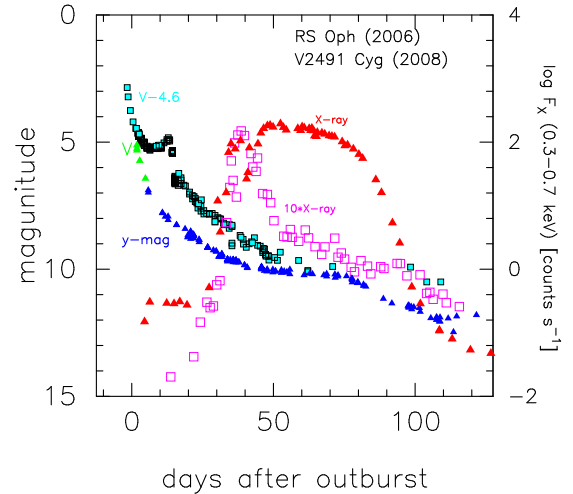


**Figure 16.** The  $V$  (filled cyan squares with black outlines) and X-ray (open magenta squares) light curves of V2491 Cyg are plotted on a linear timescale together with the  $V$  (filled green triangles) and  $y$  (filled blue triangles), and supersoft X-ray (filled red triangles) light curves of RS Oph. The  $V$  magnitudes of V2491 Cyg are shifted upward by 4.6 mag to match the absolute magnitudes of V2491 Cyg to those of RS Oph. The open magenta triangles represent 10 times the supersoft X-ray fluxes of V2491 Cyg. The data of RS Oph are the same as those in Hachisu et al. (2006b, 2008b) and Hachisu et al. (2007).

(Hachisu & Kato 2015) in Figure 46(a). The model  $V$  light curve reasonably reproduces the upper bound of observation (filled red circles) during  $\log t$  (day)  $\sim 1 - 2$ . This suggests that the distance modulus of  $(m - M)_V = 16.2 \pm 0.2$  is reasonable.

### 7.11. V2491 Cyg 2008#2

V2491 Cyg was studied in Paper II on the  $(B - V)_0 - M_V$  diagram. In this subsection, we reexamine it on the  $(B - V)_0 - (M_V - 2.5 \log f_s)$  diagram. V2491 Cyg showed a small secondary maximum (e.g., Hachisu & Kato 2009). This nova is also characterized by the detection of pre-outburst X-ray emission (Ibarra & Kuulkers 2008; Ibarra et al. 2008). Hachisu & Kato (2016b) adopted  $E(B - V) = 0.23$  after Munari et al. (2011) while we here adopt a different value of  $E(B - V) = 0.45$ . These two values are significantly different, so we explained the reason below.

Figure 14(c) plots three distance moduli in the  $B$ ,  $V$ , and  $I_C$  bands obtained from the time-stretching method in Appendix B.11 by the magenta, blue, and cyan lines, that is,  $(m - M)_B = 17.83$ ,  $(m - M)_V = 17.41$ , and  $(m - M)_I = 16.62$  together with Equations (11), (5), and (12). These three lines broadly cross at  $d = 15.9$  kpc and  $E(B - V) = 0.45$ .

Figure 14(c) also shows several distance-reddening relations toward V2491 Cyg,  $(l, b) = (67^\circ 2287, +4^\circ 3532)$ . We plot the distance-reddening relations given by Marshall et al. (2006); toward  $(l, b) = (67^\circ 00, 4^\circ 25)$  denoted by open red squares,  $(67^\circ 25, 4^\circ 25)$  by filled green squares,  $(67^\circ 00, 4^\circ 50)$  by blue asterisks, and  $(67^\circ 25, 4^\circ 50)$  by open magenta circles. The closest direction in the galactic coordinates is that denoted by filled green squares. The solid green line represents the relation given by Sale et al. (2014), black/orange lines by Green et al. (2015, 2018). The open cyan-blue diamonds with error bars denote the relation given by Özdörmez et al. (2016) and the solid cyan-blue line represents the relation given by Chen et al. (2018).

Marshall et al.’s distance-reddening relations (green squares and blue asterisks) match the smaller value of  $E(B - V) = 0.23 \pm 0.01$ . On the other hand, Green et al.’s and Sale et al.’s relations are consistent with the larger value of  $E(B - V) = 0.45 \pm 0.05$ , which is consistent with our new estimate of  $E(B - V) = 0.45 \pm 0.05$ .

The reddening toward V2491 Cyg was obtained by Lynch et al. (2008b) to be  $E(B - V) = 0.3$  from O I lines, which was revised by Rudy et al. (2008b) to be  $E(B - V) = 0.43$  from the O I lines at  $0.84 \mu\text{m}$  and  $1.13 \mu\text{m}$ . Munari et al. (2011) obtained  $E(B - V) = 0.23 \pm 0.01$  from an average of  $E(B - V) = 0.24$  from Na I 5889.953 line profiles,  $E(B - V) = (B - V)_{\text{max}} - (B - V)_{0, \text{max}} = 0.46 - (0.23 \pm 0.06) = 0.23 \pm 0.06$ , and  $E(B - V) = (B - V)_{t_2} - (B - V)_{0, t_2} = 0.20 - (-0.02 \pm 0.04) = 0.22 \pm 0.04$ , from the intrinsic colors at maximum and  $t_2$  time (van den Bergh & Younger 1987). The distance modulus and distance to V2491 Cyg were estimated by Munari et al. (2011) as  $(m - M)_V = m_{V, \text{max}} - M_{V, \text{max}} = 7.45 - (-9.06) = 16.51$  from the MMRD relation (Cohen 1988) together with  $t_2 = 4.8$  days, and then derived the distance of  $d = 14$  kpc. On the other hand, the NASA/IPAC Galactic 2D dust absorption map gives  $E(B - V) = 0.48 \pm 0.03$  in the direction toward V2491 Cyg. To summarize, there are two estimates on the reddening, i.e.,  $E(B - V) = 0.23 \pm 0.01$  and  $E(B - V) = 0.43 \pm 0.05$ . Our value is consistent with the larger one. We here adopt  $E(B - V) = 0.45 \pm 0.05$  and  $d = 15.9 \pm 2$  kpc. The distance modulus in the  $V$  band is  $(m - M)_V = 17.4 \pm 0.2$ . These values are listed in Table 1.

Using  $E(B - V) = 0.45$  and  $(m - M)_V = 16.55$  from Equation (B66), we plot the time-stretched color-magnitude diagram of V2491 Cyg in Figure 15(c). We add the template tracks of LV Vul (thick solid orange line), V1500 Cyg (thick solid green line), and V1974 Cyg (solid magenta line). We also add the V1500 Cyg track

shifted toward blue by  $\Delta(B - V) = -0.25$  (thick solid cyan line). V2491 Cyg approximately follows the blue-shifted V1500 Cyg track (cyan line) except for during the tiny secondary maximum. The track turns to the right after the onset of the nebular phase (Paper II). This redward excursion is due to large contribution of the strong emission lines [O III] to the  $V$  magnitude as already discussed in the previous subsections.

Munari et al. (2011) suggested the low metallicity of  $[\text{Fe}/\text{H}] = -0.25$  for V2491 Cyg. This sub-solar metallicity is roughly consistent with  $-0.5 < [\text{Fe}/\text{H}] < -0.3$  at the galacto-centric distance ( $\sim 14$  kpc) of V2491 Cyg. Hachisu & Kato (2018b) clarified that the color-magnitude tracks of LMC novae are located at the bluer side by  $\Delta(B - V) = -0.3$  than those of galactic novae. For example, the color-magnitude track of YY Dor overlaps with the V1668 Cyg track shifted by  $\Delta(B - V) = -0.3$ . They supposed that this blue-shift is caused by the lower metallicity of LMC stars,  $[\text{Fe}/\text{H}] = -0.55$  (see, e.g., Piatti & Geisler 2013). The LMC N 2009a track is in good agreement with the 0.2 mag blue-shifted V1500 Cyg and 0.15 mag blue-shifted U Sco tracks (Hachisu & Kato 2018b). This bluer feature of the LMC N 2009a track is also due to the lower metallicity. The blue-shifted nature of the V2491 Cyg track is consistent with the nature of LMC novae (Hachisu & Kato 2018b).

It should be noted that the empirical relations proposed by van den Bergh & Younger (1987), i.e.,  $(B - V)_0 = 0.23 \pm 0.06$  at maximum and  $(B - V)_0 = -0.02 \pm 0.04$  at  $t_2$ , are not applicable to novae of sub-solar metallicity as clearly shown in Figure 15(c). This is one of the reason why Munari et al. (2011) obtain the smaller reddening of  $E(B - V) = 0.23 \pm 0.01$ .

Munari et al. (2011) obtained the abundance of ejecta to be  $X = 0.573$ ,  $Y = 0.287$ ,  $Z = 0.140$  by mass weight, with those of individual elements being  $X_{\text{N}} = 0.074$ ,  $X_{\text{O}} = 0.049$ , and  $X_{\text{Ne}} = 0.015$  (see also Tarasova 2014b, for another abundance estimate). This abundance is close to that of Ne nova 2 (Hachisu & Kato 2010). Taking  $(m - M)_V = 17.4$  for V2491 Cyg, we plot the  $V$  model light curve of  $1.35 M_{\odot}$  (solid red lines) and  $1.30 M_{\odot}$  (solid green lines) WDs with the envelope chemical composition of Ne nova 2 in Figure 48(a). The model  $V$  light curve reasonably reproduces the observation (filled red circles) except during the secondary maximum. This suggests that the distance modulus of  $(m - M)_V = 17.4 \pm 0.2$  is reasonable.

Our model light curve fitting suggests that the WD mass is approximately  $1.35 M_{\odot}$ . The WD mass of RS Oph has been estimated to be  $\sim 1.35 M_{\odot}$  by Hachisu et al. (2006b, 2007) and Hachisu & Kato

(2018b). It is interesting to compare the  $V$  (or  $y$ ) and supersoft X-ray light curves of these two novae (Figure 16). The starting time of the SSS phases are almost the same between the two novae while the duration of the SSS phase is rather different and much longer in the recurrent nova RS Oph than in the classical nova V2491 Cyg.

### 7.12. V496 Sct 2009

V496 Sct was studied in Paper II on the  $(B - V)_0 - M_V$  diagram. In this subsection, we reexamine it on the  $(B - V)_0 - (M_V - 2.5 \log f_s)$  diagram.

We obtain the distance moduli of  $BVI_C$  bands in Appendix B.12 and plot them by the magenta, blue, and cyan lines, i.e.,  $(m - M)_B = 14.15$ ,  $(m - M)_V = 13.71$ , and  $(m - M)_I = 13.02$ , in Figure 14(d). These three lines broadly cross each other at  $d = 2.9$  kpc and  $E(B - V) = 0.45$ . Thus, we determine the distance and reddening to be  $d = 2.9 \pm 0.3$  kpc and  $E(B - V) = 0.45 \pm 0.05$ . The distance modulus in the  $V$  band is  $(m - M)_V = 13.7 \pm 0.2$ .

Hachisu & Kato (2016b) obtained  $E(B - V) = 0.50 \pm 0.05$  by assuming that the intrinsic  $B - V$  color curve of V496 Sct is the same as those of FH Ser and NQ Vul. See Paper II for a summary for the other estimates on the reddening. We reanalyze the distance and reddening toward V496 Sct,  $(l, b) = (25^\circ 28' 38'', -1^\circ 7' 67' 8'')$ , based on various distance-reddening relations in Figure 14(d). We plot four distance-reddening relations of Marshall et al. (2006); toward  $(l, b) = (25^\circ 25', -1^\circ 75')$  denoted by open red squares,  $(25^\circ 50', -1^\circ 75')$  by filled green squares,  $(25^\circ 25', -2^\circ 00')$  by blue asterisks, and  $(25^\circ 50', -2^\circ 00')$  by open magenta circles, each with error bars. The closest direction in the galactic coordinates is that of open red squares. We add the distance-reddening relations (solid black/orange lines) given by Green et al. (2015, 2018), respectively. The open cyan-blue diamonds with error bars represent the relation given by Özdörmez et al. (2016). The solid cyan-blue line denotes the relation given by Chen et al. (2018). Our set of  $d = 2.9$  kpc and  $E(B - V) = 0.45$  is consistent with the trends of Marshall et al., Green et al., Özdörmez et al., and Chen et al. Our results are listed in Table 1.

Adopting  $E(B - V) = 0.45$  and  $(m - M')_V = 14.45$  in Equation (B71), we obtain the time-stretched color-magnitude diagram of V496 Sct in Figure 15(d). Here, we plot the data taken from Raj et al. (2012) and SMARTS (Walter et al. 2012). V496 Sct follows the LV Vul track until the dust blackout. Note that, even after the dust blackout, V496 Sct comes back and follows the LV Vul track again (upper branch after the

onset of nebular phase). Therefore, V496 Sct belongs to the LV Vul type in the time-stretched color-magnitude diagram. This overlapping supports our estimates of  $E(B - V) = 0.45$  and  $(m - M')_V = 14.45$ , that is,  $f_s = 2.0$ ,  $E(B - V) = 0.45 \pm 0.05$ ,  $(m - M)_V = 13.7 \pm 0.2$ , and  $d = 2.9 \pm 0.3$  kpc.

Taking  $(m - M)_V = 13.7$  for V496 Sct, we plot the  $V$  model light curve (solid red line) of a  $0.85 M_\odot$  WD with the envelope chemical composition of CO nova 3 (Hachisu & Kato 2016a) in Figure 50(a). The model  $V$  light curve reasonably reproduces the observation (filled red circles). This confirms that the distance modulus of  $(m - M)_V = 13.7 \pm 0.2$  is reasonable.

## 8. DISCUSSION

### 8.1. Comparison with Gaia DR2 distances

Recently, Schaefer (2018) listed distances of 64 novae from Gaia data release 2 (DR2) in his Table 1. Among them, seven novae dubbed the “very well observed light curve ( $< 30\%$  error)” coincide with our analyzed novae in Table 1. These distances are compared with the present results (Gaia DR2) as follows: CI Aql, 3.3 kpc (3.19 kpc); V705 Cas, 2.6 kpc (2.16 kpc); V1974 Cyg, 1.8 kpc (1.63 kpc); V446 Her, 1.38 kpc (1.36 kpc); V533 Her, 1.28 kpc (1.20 kpc); V382 Vel 1.4 kpc (1.80 kpc), PW Vul 1.8 kpc (2.42 kpc). These values are in good agreement within each error box.

## 9. CONCLUSIONS

We have obtained the following results:

1. We improved the timescaling factor  $f_s$  of each nova by overlapping not only  $V$  light curves but also  $(B - V)_0$  and  $(U - B)_0$  color curves. Applying the improved  $f_s$  to the time-stretching method, we revised the distance modulus in the  $V$  band  $\mu_V = (m - M)_V$ . The results are summarized in Table 1.
2. We also reexamine the color excess  $E(B - V)$  from the multi-band time-stretching method. We obtain the distance moduli in the  $UBVI_C K_s$  bands,  $(m - M)_U$ ,  $(m - M)_B$ ,  $(m - M)_V$ ,  $(m - M)_I$ , and  $(m - M)_K$ , of each nova. The crossing point of these distance-reddening relations gives a reasonable reddening and distance toward the nova. The results are also summarized in Table 1.
3. With the improved values of  $f_s$ ,  $(m - M)_V$ , and  $E(B - V)$ , we obtain the  $(B - V)_0 - (M_V - 2.5 \log f_s)$  color-magnitude diagram. We call it the time-stretched color-magnitude diagram. In general, each nova evolves from the upper right (red) to the lower left (blue) and then turns back toward the right (red) at the onset of the

nebular phase. We found two representative tracks in this diagram, the tracks of LV Vul and V1500 Cyg. The template LV Vul goes down along the line of  $(B - V)_0 = -0.03$ , the color of optically thick free-free emission, in the middle part of the track. The template V1500 Cyg track is almost parallel to, but located at the bluer side of  $\Delta(B - V)_0 \sim -0.2$  mag than the LV Vul track. This difference is caused by the difference in the ionization state which originates from the temperature difference of the underlying continuum.

4. Among the eight novae studied in Sections 2–6, V1668 Cyg (see Figure 11(d)), V679 Car, V1369 Cen, and V5666 Sgr follow the template track of LV Vul while V1974 Cyg (see Figure 9(a)) and V574 Pup follow the template track of V1500 Cyg.

5. We reanalyzed additional 12 novae in Section 7 on the time-stretched color-magnitude diagram. Among the 12 novae, V446 Her, V1419 Aql, V705 Cas, V2615 Oph, and V496 Sct broadly follow the LV Vul (or V1668 Cyg) template track, while V533 Her, PW Vul, V382 Vel, V5114 Sgr, V2468 Cyg, and V2491 Cyg follow the template track of V1500 Cyg (or V1974 Cyg). Only V2362 Cyg follows the track of LV Vul in the first decline and then follows the V1500 Cyg track during the secondary maximum (a large rebrightening). Thus, we establish the two representative tracks in the  $(B - V)_0 - (M_V - 2.5 \log f_s)$  diagram.

6. The location of V2491 Cyg track is about 0.25 mag bluer than that of the original V1500 Cyg track (Figure 15(c)). This bluer location is due to a lower metallicity of the nova ejecta (e.g., subsolar by  $[\text{Fe}/\text{H}] = -0.25$ ) as suggested by Munari et al. (2011). This kind of low metallicity effect is already discussed in Hachisu & Kato (2018b) for LMC novae.

7. We estimated the white dwarf masses and  $(m - M)_V$  of the novae by directly fitting the absolute  $V$  model light curves ( $M_V$ ) with observational apparent  $V$  magnitudes ( $m_V$ ). The obtained results of  $(m - M)_V$  are in good agreement with the estimates by the time-stretched color-magnitude diagram method.

8. The white dwarf masses are estimated from the  $V$ , UV 1455Å, and supersoft X-ray light curve fittings, assuming an appropriate chemical composition of ejecta. They are  $0.98 M_\odot$  (LV Vul, CO3),  $1.2 M_\odot$  (V1500 Cyg, Ne2),  $0.98 M_\odot$  (V1668 Cyg, CO3),  $0.98 M_\odot$  (V1974 Cyg, CO3),  $1.05 M_\odot$  (V574 Pup, Ne3),  $0.98 M_\odot$  (V679 Car, CO3),  $0.90 M_\odot$  (V1369 Cen, CO3),  $0.85 M_\odot$  (V5666 Sgr, CO3),  $0.98 M_\odot$  (V446 Her, CO3),  $1.03 M_\odot$  (V533 Her, Ne2),  $0.83 M_\odot$  (PW Vul, CO4),  $0.90 M_\odot$  (V1419 Aql, CO3),  $0.78 M_\odot$  (V705 Cas, CO4),  $1.23 M_\odot$  (V382 Vel, Ne2),  $1.15 M_\odot$  (V5114 Sgr, Ne2),  $0.85 M_\odot$  (V2362 Cyg, interpolation),  $0.90 M_\odot$  (V2615 Oph, CO3),  $0.85 M_\odot$  (V2468 Cyg, CO3),  $1.35 M_\odot$  (V2491 Cyg, Ne2), and  $0.85 M_\odot$  (V496 Sct, CO3). These results are summarized in Table 2.

9. Our distance estimates are in good agreement with the results of Gaia Data Release 2.

We express our gratitude to T. Iijima and the Astronomical Observatory of Padova (Asiago) for the warm hospitality during which we initiated the present work. We are grateful to the late A. Cassatella for providing us with UV 1455 Å data for *IUE* novae. We thank the American Association of Variable Star Observers (AAVSO) and the Variable Star Observers League of Japan (VSOLJ) for the archival data of various novae. We are also grateful to the anonymous referee for useful comments regarding how to improve the manuscript. This research has been supported in part by Grants-in-Aid for Scientific Research (15K05026, 16K05289) from the Japan Society for the Promotion of Science.

## APPENDIX

### A. TIME-STRETCHED LIGHT CURVES OF V574 PUP, V679 CAR, V1369 CEN, AND V5666 SGR

#### A.1. V574 Pup 2004

Figure 17 shows (a) the  $V$  light curve and (b)  $(B - V)_0$  color curve of V574 Pup on a linear timescale. We deredden the color with  $E(B - V) = 0.45$  as obtained in Section 3.1. The  $BV$  data are taken from the Small Medium Aperture Telescope System (SMARTS) data base (Walter et al. 2012), American Association of Variable Star Observers (AAVSO), and the Variable Star Observers League of Japan (VSOLJ). The  $B - V$  data of AAVSO (open blue circles) are systematically bluer by 0.2 mag compared with the other two colors of SMARTS and VSOLJ, so we shift them toward red by 0.2 mag in Figure 17(b). Such differences come from slightly different responses of  $V$  filters at different observatories (see, e.g., discussion in Hachisu & Kato 2006). The horizontal solid red line indicates the  $B - V$  color of optically thick free-free emission, i.e.,  $(B - V)_0 = -0.03$  (see Paper I). The typical error of SMARTS

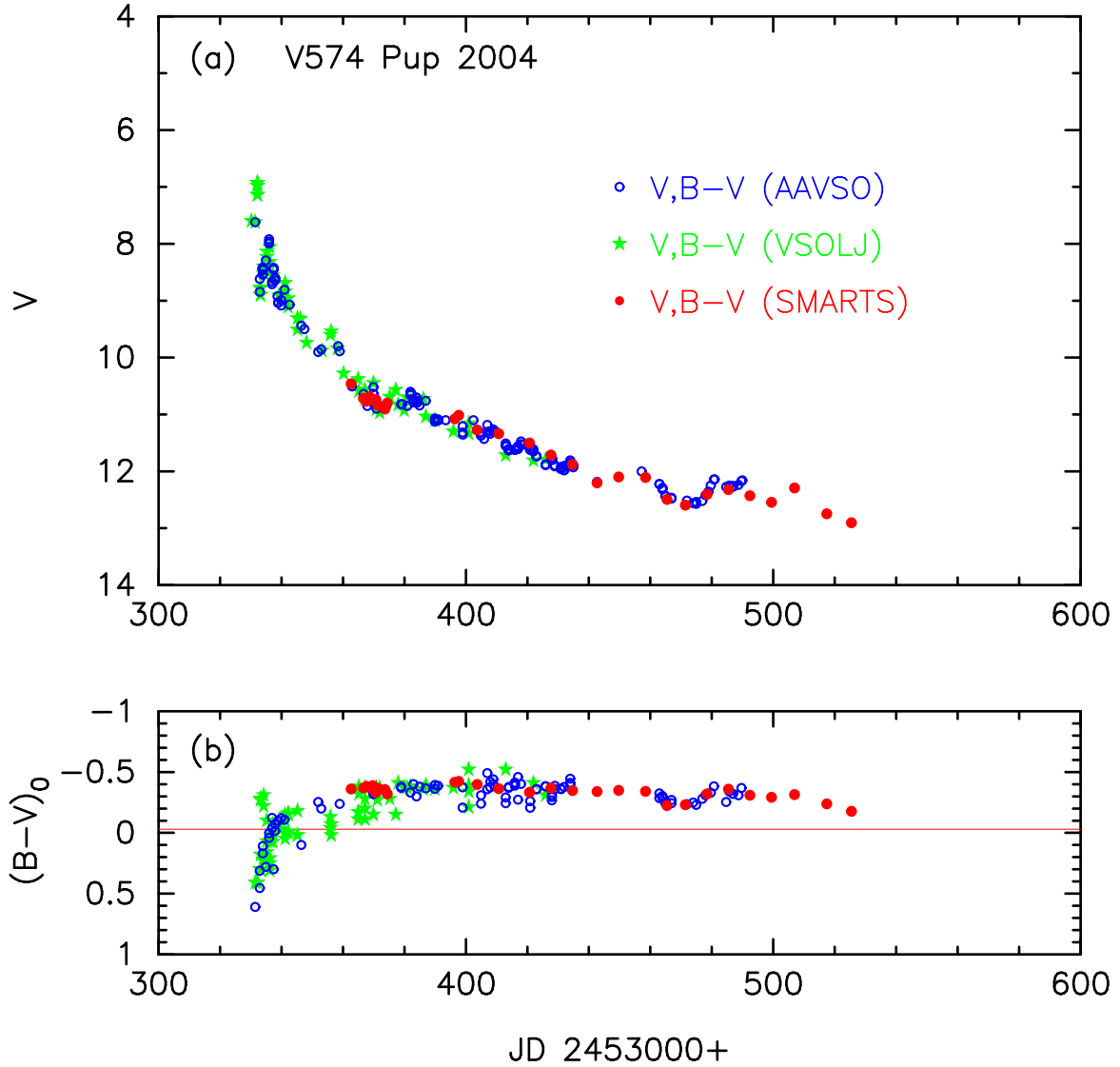


**Figure 17.** (a) The  $V$  light and (b)  $(B-V)_0$  color curves of V574 Pup. The  $BV$  data are taken from AAVSO (open blue circles), VSOLJ (filled green stars), and SMARTS (filled red circles). In panel (b), the  $(B-V)_0$  are dereddened using Equation (2) with  $E(B-V) = 0.45$ . The  $B-V$  data of AAVSO are systematically shifted toward red by 0.2 mag. The horizontal solid red line denotes  $(B-V)_0 = -0.03$ , which is the intrinsic  $B-V$  color of optically thick free-free emission.

$BVRI$  data is about 0.001 mag, being much smaller than the size of each symbol. The error of AAVSO and VSOLJ data are not reported.

Figure 18 shows the (a)  $B$ , (b)  $V$ , (c)  $I_C$ , and (d)  $K_s$  light curves of V574 Pup together with YY Dor and LMC N 2009a. Here, we assume that V574 Pup outburst on JD 2453326.0 (day 0). Hachisu & Kato (2018b) have already analyzed YY Dor and LMC N 2009a and their various properties are summarized in their Tables 1, 2, and 3. We increase/decrease the horizontal shift by a step of  $\delta(\Delta \log t) = \delta \log f_s = 0.01$  and the vertical shift by a step of  $\delta(\Delta V) = 0.1$  mag, and determine the best overlapping one by eye. As mentioned in Section 1, the model light curves obey the universal decline law. This phase corresponds to the optically thick wind phase before the nebular phase started. Therefore, we should use only the optically thick phase. However, we usually use all the phases if they overlap each other even after the nebular phase in order to determine the timescaling factor accurately as much as possible. If not, we use only the part of optically thick wind phase before the nebular (or dust blackout) phase started. It should be noted that the timescaling factor of  $f_s$  is common among these four band light curves. In the case of Figure 18, the four band light curves well overlap each other even after the nebular phase started. For the  $B$  band,

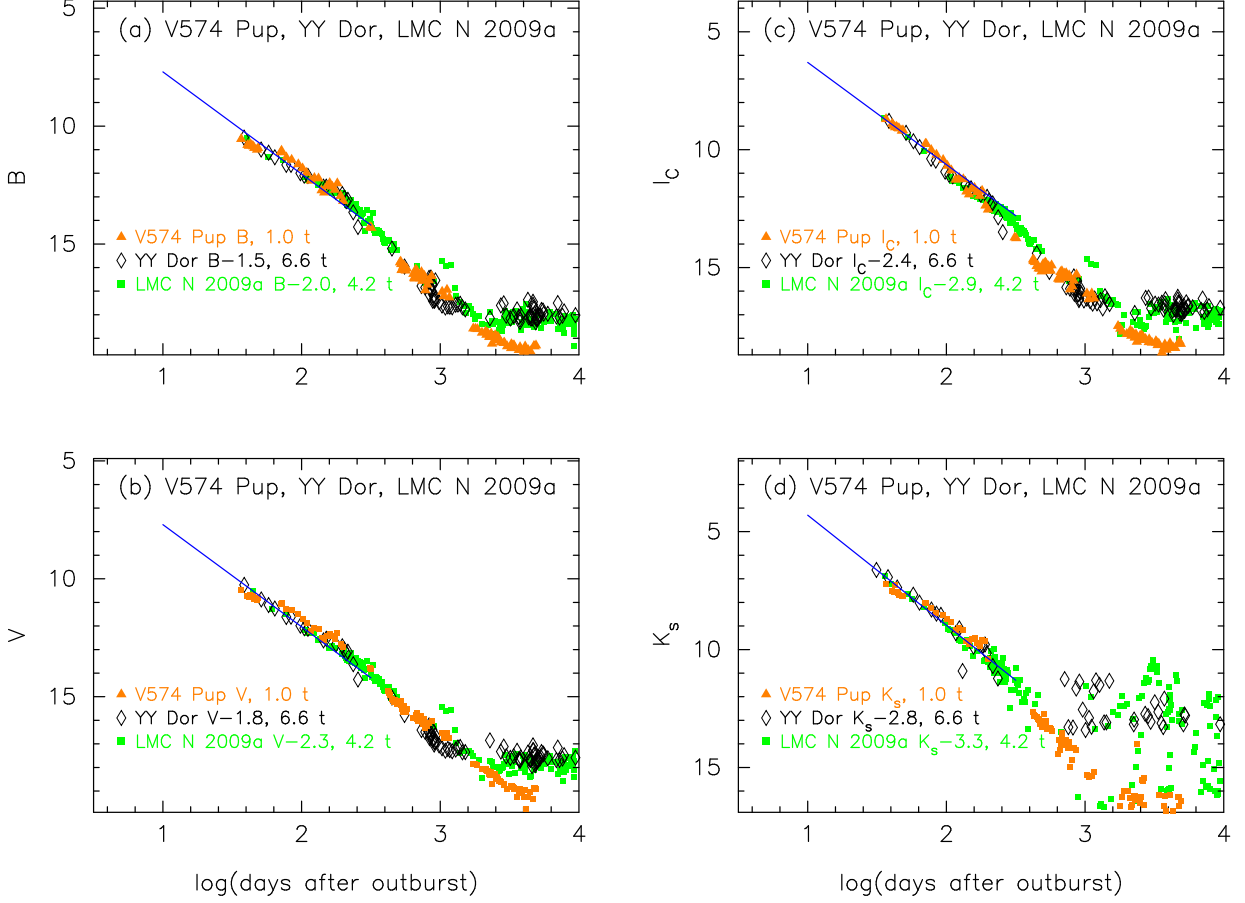


**Figure 18.** Same as Figure 2, but for the (a)  $B$ , (b)  $V$ , (c)  $I_C$ , and (d)  $K_s$  light curves of V574 Pup, YY Dor, and LMC N 2009a. The solid blue lines denote the slope of  $F_\nu \propto t^{-1.75}$ , which represents well the optically thick wind phase (Hachisu & Kato 2006). The  $BV$  data of YY Dor and LMC N 2009a are taken from SMARTS. The  $BV$  data of V574 Pup are the same as those in Figure 17. The  $I_C K_s$  data of V574 Pup, YY Dor, and LMC N 2009a are taken from SMARTS.

we apply Equation (7) to Figure 18(a) and obtain

$$\begin{aligned}
 (m - M)_{B, V574 \text{ Pup}} &= ((m - M)_B + \Delta B)_{YY \text{ Dor}} - 2.5 \log 6.6 \\
 &= 18.98 - 1.5 \pm 0.2 - 2.05 = 15.43 \pm 0.2 \\
 &= ((m - M)_B + \Delta B)_{LMC \text{ N } 2009a} - 2.5 \log 4.2 \\
 &= 18.98 - 2.0 \pm 0.2 - 1.55 = 15.43 \pm 0.2,
 \end{aligned} \tag{A1}$$

where we adopt  $(m - M)_B = 18.49 + 4.1 \times 0.12 = 18.98$  for the LMC novae. Thus, we obtain  $(m - M)_{B, V574 \text{ Pup}} = 15.43 \pm 0.1$ .

For the  $V$  light curves in Figure 18(b), we similarly obtain

$$\begin{aligned}
 (m - M)_{V, V574 \text{ Pup}} &= ((m - M)_V + \Delta V)_{YY \text{ Dor}} - 2.5 \log 6.6 \\
 &= 18.86 - 1.8 \pm 0.2 - 2.05 = 15.01 \pm 0.2 \\
 &= ((m - M)_V + \Delta V)_{LMC \text{ N } 2009a} - 2.5 \log 4.2 \\
 &= 18.86 - 2.3 \pm 0.2 - 1.55 = 15.01 \pm 0.2,
 \end{aligned} \tag{A2}$$

where we adopt  $(m - M)_V = 18.49 + 3.1 \times 0.12 = 18.86$  for the LMC novae. Thus, we obtain  $(m - M)_{V, V574 \text{ Pup}} = 15.0 \pm 0.1$ .

We apply Equation (8) for the  $I_C$  band to Figure 18(c) and obtain

$$(m - M)_{I, V574 \text{ Pup}}$$

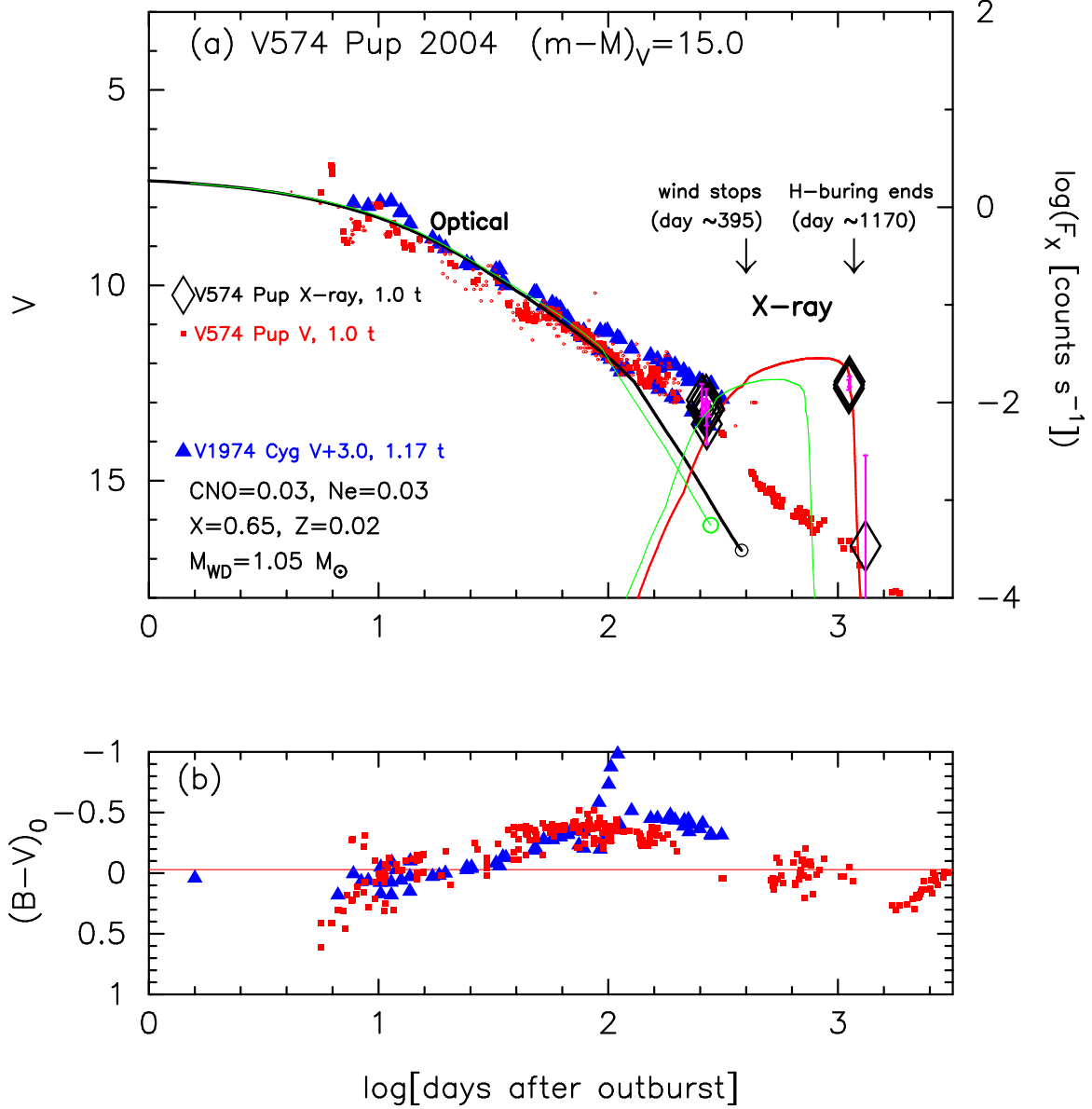


**Figure 19.** The (a)  $V$  and X-ray light curves and (b)  $(B - V)_0$  color curves of V574 Pup (filled red squares) as well as V1974 Cyg (filled blue triangles) on a logarithmic timescale. The large open black diamonds with error bars (vertical magenta lines) denote the soft X-ray flux obtained by Ness et al. (2007a). The  $BV$  data of V574 Pup are the same as those in Figure 17. The other data are the same as those in Hachisu & Kato (2016a). In panel (a), assuming that  $(m - M)_V = 15.0$  for V574 Pup, we add a model  $V$  light curve (solid black line) of a  $1.05 M_\odot$  WD with the envelope chemical composition of Ne nova 3 (Hachisu & Kato 2016a). We also add a  $0.98 M_\odot$  WD (left solid green line) with the chemical composition of CO nova 3 (Hachisu & Kato 2016a), assuming that  $(m - M)_V = 12.2$  for V1974 Cyg (with a stretching factor of  $f_s = 1.17$  against V574 Pup). We also add model X-ray light curves of  $1.05 M_\odot$  (solid red line) and  $0.98 M_\odot$  (right solid green line) WDs. Optically thick winds stop at the right edge of each model light curve (denoted by an open circle).

$$\begin{aligned}
 &= ((m - M)_I + \Delta I_C)_{\text{YY Dor}} - 2.5 \log 6.6 \\
 &= 18.67 - 2.4 \pm 0.3 - 2.05 = 14.22 \pm 0.3 \\
 &= ((m - M)_I + \Delta I_C)_{\text{LMC N 2009a}} - 2.5 \log 4.2 \\
 &= 18.67 - 2.9 \pm 0.3 - 1.55 = 14.22 \pm 0.3,
 \end{aligned} \tag{A3}$$

$(m - M)_I = 18.49 + 1.5 \times 0.12 = 18.67$  for the LMC novae. Thus, we obtain  $(m - M)_{I, \text{V574 Pup}} = 14.22 \pm 0.2$ .



For the  $K_s$  light curves in Figure 18(d), we apply Equation (9) and obtain

$$\begin{aligned}
 (m - M)_{K,V574 \text{ Pup}} &= ((m - M)_K + \Delta K_s)_{YY \text{ Dor}} - 2.5 \log 6.6 \\
 &= 18.53 - 2.8 \pm 0.4 - 2.05 = 13.68 \pm 0.4 \\
 &= ((m - M)_K + \Delta K_s)_{LMC \text{ N } 2009a} - 2.5 \log 4.2 \\
 &= 18.53 - 3.3 \pm 0.4 - 1.55 = 13.68 \pm 0.4,
 \end{aligned} \tag{A4}$$

$(m - M)_{K,YY \text{ Dor}} = 18.49 + 0.35 \times 0.12 = 18.53$  for the LMC novae. Thus, we obtain  $(m - M)_{K,V574 \text{ Pup}} = 13.68 \pm 0.2$ .

Figure 19 shows the  $V$  light curve and  $(B - V)_0$  color curve of V574 Pup on a logarithmic timescale in comparison with V1974 Cyg. The V1974 Cyg data are taken from Figure 38 of Paper II. We add visual magnitudes (small red dots) of V574 Pup, which are taken from AAVSO. The  $V$  light curves of these two novae do not exactly but broadly overlap each other. Note that there are two different values of V1974 Cyg  $V$  magnitudes in the nebular phase. This is because the response of each  $V$  filter is different between these two observations. We set the  $V$  light curve of V574 Pup to overlap with the lower (fainter) branch of the V1974 Cyg light curves. We also take into account the  $(B - V)_0$  color evolution in Figure 19(b) to determine the horizontal shift of  $\Delta \log t = \log f_s$ . We set  $\log f_s$  to overlap the two  $(B - V)_0$  color evolution as much as possible.

Applying the obtained  $f_s$  and  $\Delta V$  to Equation (4), we have the relation of

$$\begin{aligned}
 (m - M)_{V,V574 \text{ Pup}} &= ((m - M)_V + \Delta V)_{V1974 \text{ Cyg}} - 2.5 \log 1.17 \\
 &= 12.2 + 3.0 \pm 0.2 - 0.175 = 15.025 \pm 0.3,
 \end{aligned} \tag{A5}$$

where we adopt  $(m - M)_{V,V1974 \text{ Cyg}} = 12.2$  in Section 2.3.4. Thus, we obtain  $f_s = 1.07 \times 1.17 = 1.26$  against LV Vul (see Table 1) and  $(m - M)_V = 15.0 \pm 0.3$  for V574 Pup.

Using  $(m - M)_V = 15.0 \pm 0.3$  and  $f_s = 1.26$ , we have the relation of

$$\begin{aligned}
 (m - M')_{V,V574 \text{ Pup}} &\equiv (m_V - (M_V - 2.5 \log f_s))_{V574 \text{ Pup}} \\
 &= ((m - M)_V + 2.5 \log f_s)_{V574 \text{ Pup}} \\
 &= 15.0 \pm 0.3 + 2.5 \times 0.10 = 15.25 \pm 0.3.
 \end{aligned} \tag{A6}$$

## A.2. V679 Car 2008

Figure 20 shows the (a)  $V$  and (b)  $(B - V)_0$  evolutions of V679 Car on a linear timescale. The  $BV$  data are taken from AAVSO (open blue circles), VSOLJ (filled green stars), and SMARTS (filled red circles). Here,  $(B - V)_0$  are dereddened with  $E(B - V) = 0.69$  as obtained in Section 4.1, but the  $B - V$  data of VSOLJ (filled green stars) are systematically shifted toward red by 0.25 mag to overlap them to the other color data. The typical error of SMARTS  $BVRI$  data is about 0.003 mag, being much smaller than the size of each symbol. The error of AAVSO and VSOLJ data are not reported.

Figure 21 shows the  $B$ ,  $V$ , and  $I_C$  light curves of V679 Car together with those of the LMC novae YY Dor and LMC N 2009a. Here, we assume that the V679 Car outburst started on JD 2454794.5 (day 0). As in Figure 21(c), the  $I_C$  light curve of V679 Car overlaps with those of YY Dor and LMC N 2009a only in the first 60 days because of the different contributions of line emission in the nebular phase. Thus, we use only the  $V$  light curves that overlap longer period to determine the timescaling factor  $f_s$ .

We apply Equation (7) for the  $B$  band to Figure 21(a) and obtain

$$\begin{aligned}
 (m - M)_{B,V679 \text{ Car}} &= ((m - M)_B + \Delta B)_{YY \text{ Dor}} - 2.5 \log 5.2 \\
 &= 18.98 - 0.4 \pm 0.2 - 1.8 = 16.78 \pm 0.2 \\
 &= ((m - M)_B + \Delta B)_{LMC \text{ N } 2009a} - 2.5 \log 3.3 \\
 &= 18.98 - 0.9 \pm 0.2 - 1.3 = 16.78 \pm 0.2.
 \end{aligned} \tag{A7}$$

Thus, we obtain  $(m - M)_{B,V679 \text{ Car}} = 16.78 \pm 0.1$ .

For the  $V$  light curves in Figure 21(b), we similarly obtain

$$(m - M)_{V,V679 \text{ Car}}$$

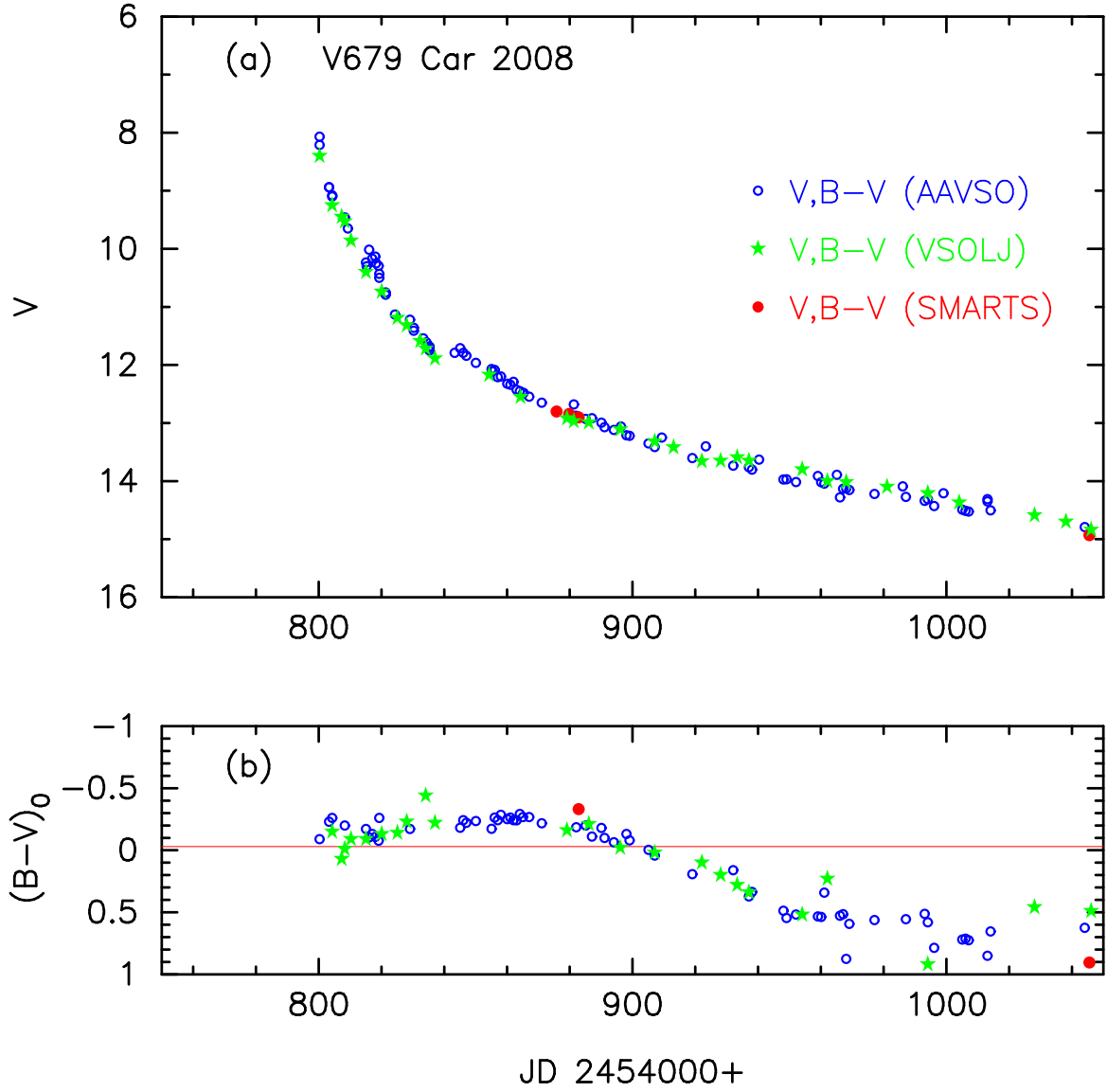


**Figure 20.** Same as Figure 17, but for V679 Car. In panel (b), the  $(B - V)_0$  data are dereddened with  $E(B - V) = 0.69$  but the  $B - V$  data of VSOLJ (filled green stars) are systematically shifted toward red by 0.25 mag to overlap them to the other color data.

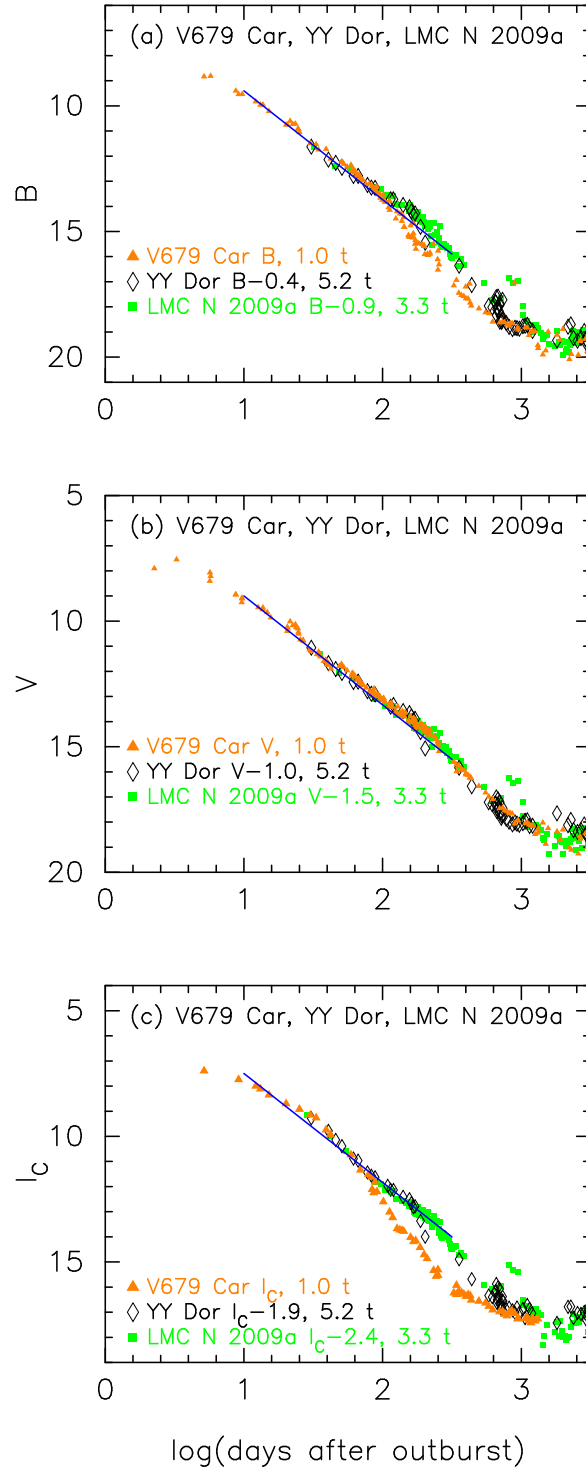
$$\begin{aligned}
 &= ((m - M)_V + \Delta V)_{\text{YY Dor}} - 2.5 \log 5.2 \\
 &= 18.86 - 1.0 \pm 0.2 - 1.8 = 16.06 \pm 0.2 \\
 &= ((m - M)_V + \Delta V)_{\text{LMC N 2009a}} - 2.5 \log 3.3 \\
 &= 18.86 - 1.5 \pm 0.2 - 1.3 = 16.06 \pm 0.2.
 \end{aligned} \tag{A8}$$

Thus, we obtain  $(m - M)_{V, \text{V679 Car}} = 16.06 \pm 0.1$ .

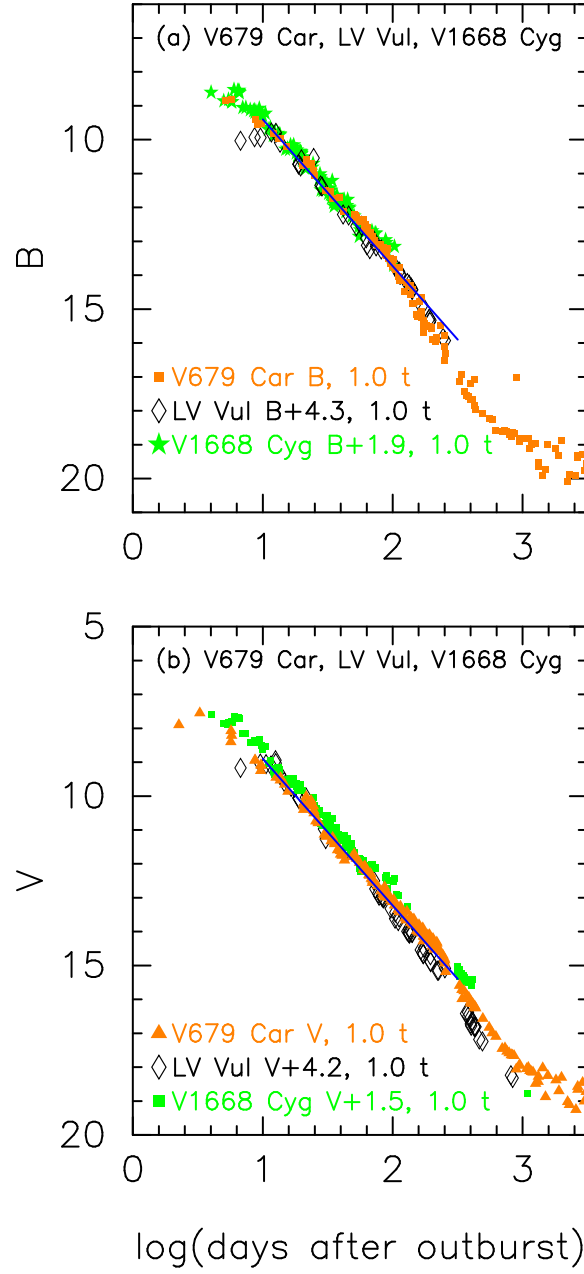
We apply Equation (8) to Figure 21(c) and obtain

$$\begin{aligned}
 &(m - M)_{I, \text{V679 Car}} \\
 &= ((m - M)_I + \Delta I_C)_{\text{YY Dor}} - 2.5 \log 5.2 \\
 &= 18.67 - 1.9 \pm 0.3 - 1.8 = 14.97 \pm 0.3 \\
 &= ((m - M)_I + \Delta I_C)_{\text{LMC N 2009a}} - 2.5 \log 3.3 \\
 &= 18.67 - 2.4 \pm 0.3 - 1.3 = 14.97 \pm 0.3.
 \end{aligned} \tag{A9}$$

Thus, we obtain  $(m - M)_{I, \text{V679 Car}} = 14.97 \pm 0.2$ .



**Figure 21.** The (a)  $B$ , (b)  $V$ , and (c)  $I_C$  light curves of V679 Car as well as YY Dor and LMC N 2009a. The solid blue lines denote the slope of  $F_\nu \propto t^{-1.75}$ . The  $BV$  data of V679 Car are the same as those in Figure 20. The  $I_C$  data of V679 Car, YY Dor, and LMC N 2009a are taken from AAVSO, VSOLJ, and SMARTS.



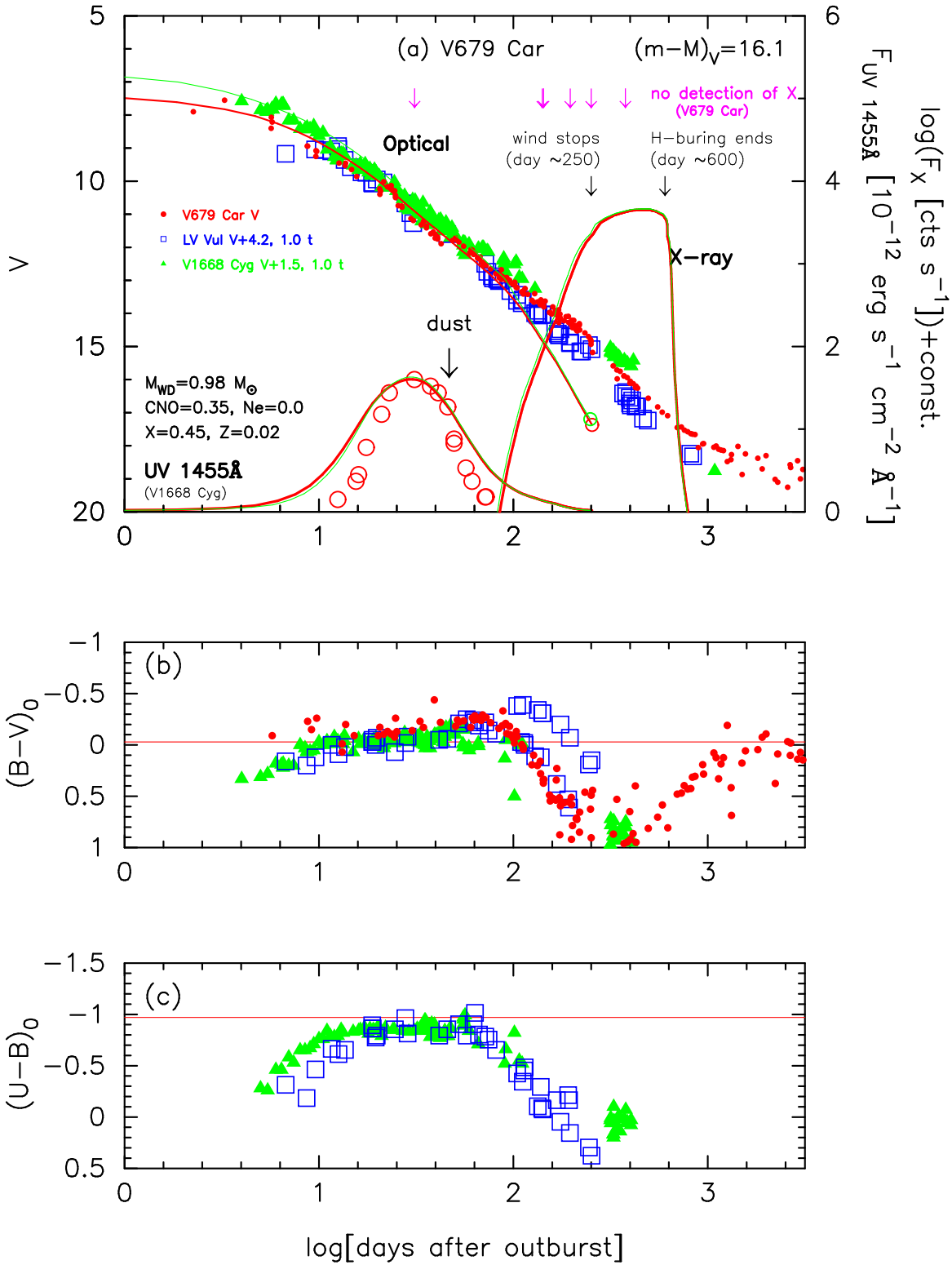
**Figure 22.** The (a)  $B$  and (b)  $V$  light curves of V679 Car as well as LV Vul and V1668 Cyg. The  $BV$  data of V679 Car are the same as those in Figure 20. The  $BV$  data of LV Vul and V1668 Cyg are taken from various literature and the same as those in Paper I.

Figure 22 show the comparison with the galactic novae LV Vul and V1668 Cyg in the (a)  $B$  and (b)  $V$  light curves. Note that we do not time-stretch these two novae because their timescales are almost the same as that of V679 Car.

Applying Equation (7) for the  $B$  band to Figure 22(a), we have the relation of

$$\begin{aligned}
 (m - M)_{B, \text{V679 Car}} &= ((m - M)_B + \Delta B)_{\text{LV Vul}} - 2.5 \log 1.0 \\
 &= 12.45 + 4.3 \pm 0.2 + 0.0 = 16.75 \pm 0.2 \\
 &= ((m - M)_B + \Delta B)_{\text{V1668 Cyg}} - 2.5 \log 1.0 \\
 &= 14.9 + 1.9 \pm 0.2 + 0.0 = 16.8 \pm 0.2.
 \end{aligned} \tag{A10}$$

Thus, we obtain  $(m - M)_{B, \text{V679 Car}} = 16.78 \pm 0.2$ , being consistent with Equation (A7).



**Figure 23.** Same as Figure 19, but for V679 Car. We add the light/color curves of LV Vul and V1668 Cyg. We also add the observed UV 1455Å flux data of V1668 Cyg. The timescales of LV Vul and V1668 Cyg are the same as that of V679 Car. The UV 1455Å flux of V1668 Cyg sharply drops at Day 60 owing to a shallow dust blackout (denoted by the arrow labeled “dust”). No supersoft X-ray phase of V679 Car was detected with *Swift* as denoted by downward magenta arrows (Schwarz et al. 2011). We add two  $0.98 M_{\odot}$  WD model (solid red/green lines) with the chemical composition of CO nova 3 (Hachisu & Kato 2016a), which reproduces the V light curves of V679 Car (red) and V1668 Cyg (green), respectively. These two models also reproduce the UV 1455Å light curve of V1668 Cyg. The difference of these two models (red and green) exists only in their initial envelope masses. See text for more details.

Applying Equation (4) to Figure 22(b), we have the relation of

$$\begin{aligned}
(m - M)_{V, V679 \text{ Car}} &= (m - M)_{V, LV \text{ Vul}} + \Delta V - 2.5 \log 1.0 \\
&= 11.85 + 4.2 \pm 0.2 + 0.0 = 16.05 \pm 0.2 \\
&= (m - M)_{V, V1668 \text{ Cyg}} + \Delta V - 2.5 \log 1.0 \\
&= 14.6 + 1.5 \pm 0.2 + 0.0 = 16.1 \pm 0.2.
\end{aligned} \tag{A11}$$

Thus, we obtain  $f_s = 1.0$  against LV Vul and  $(m - M)_V = 16.08 \pm 0.1$  for V679 Car, again being consistent with Equation (A8). Thus, we confirm that both the time-stretching methods for the galactic novae and LMC novae give the same results for the  $B$  and  $V$  bands of V679 Car.

Figure 23 shows the same  $V$  light curve as in Figure 22(b), but also shows the color evolution. We confirm that we do not need to stretch the light/color curves because its timescale is almost the same as those of LV Vul and V1668 Cyg. We shift the  $V$  light curves of LV Vul by 4.2 mag and V1668 Cyg by 1.5 mag downward in order to overlap these  $V$  light curves.

The  $(B - V)_0$  color evolution in Figure 23(b) is also used to constrain the horizontal shift of  $\Delta \log t = \log f_s = 0.0$ . The  $(B - V)_0$  color evolution of LV Vul splits into two branches just after the nebular phase started as shown in Figure 23(b). This is because each response function of  $V$  filters is slightly different from each other between these two observations. We set the  $(B - V)_0$  color evolution of V679 Car to overlap with the lower branch of LV Vul in Figure 23(b). The timescaling factor of  $f_s = 1.0$  gives a good match between the two  $(B - V)_0$  color curves.

From Equations (1), (4), and (A11), we have the relation of

$$\begin{aligned}
(m - M')_{V, V679 \text{ Car}} &\equiv (m_V - (M_V - 2.5 \log f_s))_{V679 \text{ Car}} \\
&= ((m - M)_V + \Delta V)_{LV \text{ Vul}} \\
&= 11.85 + 4.2 \pm 0.2 = 16.05 \pm 0.2.
\end{aligned} \tag{A12}$$

### A.3. V1369 Cen 2013

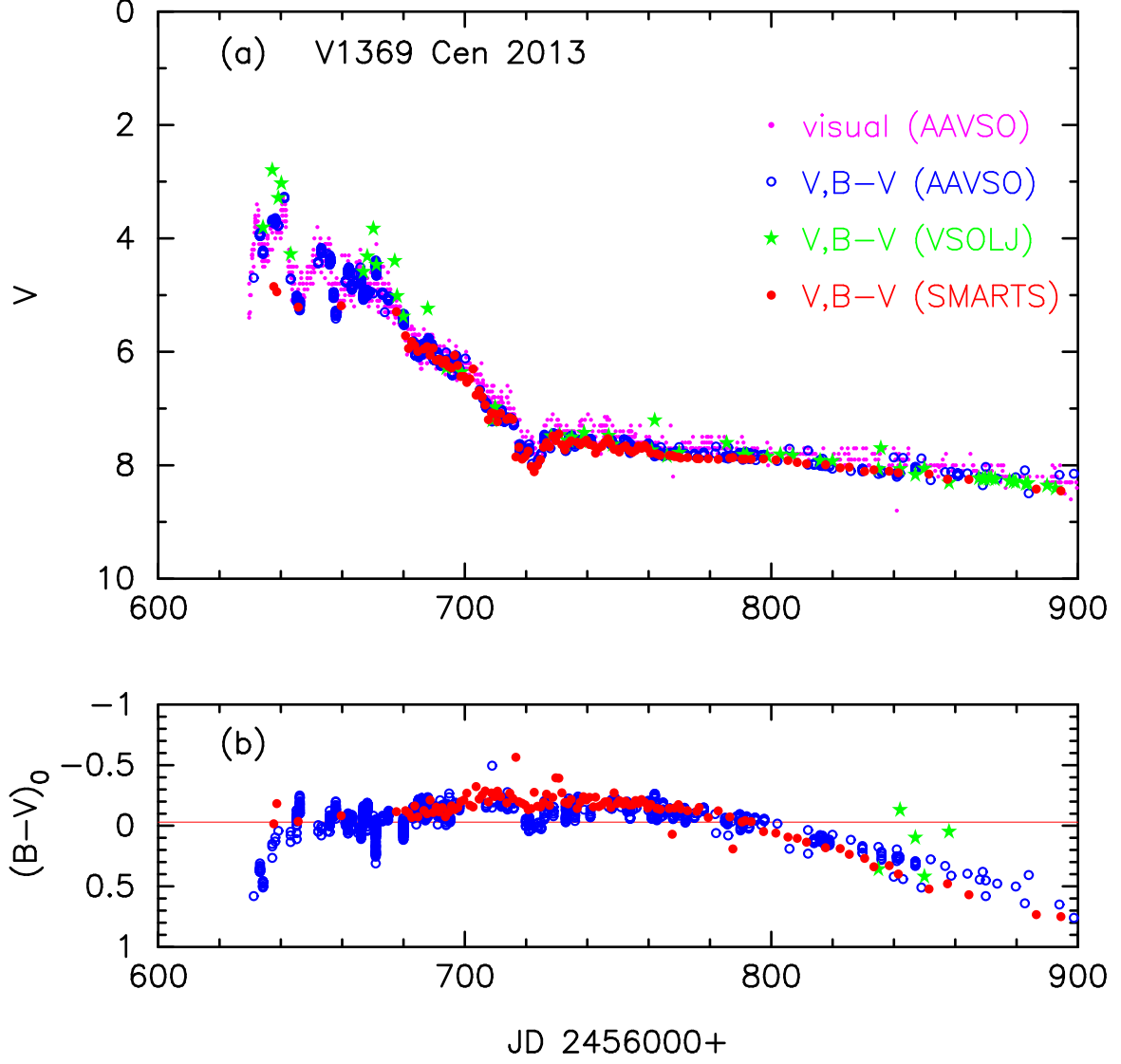
Figure 24 shows the (a)  $V$  light and (b)  $(B - V)_0$  color curves of V1369 Cen, where  $(B - V)_0$  are dereddened with  $E(B - V) = 0.11$  as obtained in Section 5. The  $V$  data of AAVSO (blue open circles), VSOLJ (filled green stars), and SMARTS (filled red circles) are very similar to each other.

Figure 25 shows the light/color curves of V1369 Cen as well as LV Vul and V496 Sct on a logarithmic timescale. Here we assume that the nova outbursted on JD 2456627.5 (Day 0). We add a straight solid black line labeled “ $t^{-3}$ ” that indicates the homologously expanding ejecta, i.e., free expansion, after the optically thick winds stop (see, e.g., Woodward et al. 1997; Hachisu & Kato 2006). Both the V1369 Cen and V496 Sct light curves have wavy structures in the early phase, but we overlap these three novae light/color curves as much as possible. In the middle phase, both V1369 Cen and V496 Sct show a sharp and shallow dip due to dust blackout. In the later nebular phase, the  $V$  light curves of V1369 Cen and V496 Sct well overlap the upper branch of LV Vul. The  $V$  light curve of LV Vul splits into two branches in the nebular phase due to the different responses of their  $V$  filters as discussed in Paper II. This is because strong [O III] lines contributes to the blue edge of  $V$  filter in the nebular phase and small differences among the response functions of  $V$  filters make large differences in the  $V$  magnitudes. The  $(B - V)_0$  color curves of LV Vul also splits into two branches for  $\log t \gtrsim 2.0$ , that is, in the nebular phase. The  $V$  light curve of V1369 Cen follows V496 Sct and the upper branch of LV Vul, while the  $(B - V)_0$  color curve of V1369 Cen follows V496 Sct and the lower branch of LV Vul.

Applying Equation (4) to Figure 25, we have the relation of

$$\begin{aligned}
(m - M)_{V, V1369 \text{ Cen}} &= (m - M + \Delta V)_{V, LV \text{ Vul}} - 2.5 \log 1.48 \\
&= 11.85 - 1.2 \pm 0.2 - 0.425 = 10.23 \pm 0.2 \\
&= (m - M + \Delta V)_{V, V496 \text{ Sct}} - 2.5 \log 0.74 \\
&= 13.7 - 3.8 \pm 0.2 + 0.325 = 10.23 \pm 0.2.
\end{aligned} \tag{A13}$$

Thus, we obtain  $f_s = 1.48$  against LV Vul and  $(m - M)_V = 10.23 \pm 0.2$  for V1369 Cen. These values are summarized in Table 1



**Figure 24.** Same as Figure 17, but for V1369 Cen. (a) The visual (magenta dots),  $V$  (blue open circles) data of AAVSO, and  $V$  data of VSOLJ (filled green stars) and SMARTS (filled red circles) well overlap each other. (b) The  $(B - V)_0$  color is dereddened with  $E(B - V) = 0.11$ .

From Equations (1), (4), and (A13), we have the relation of

$$\begin{aligned}
 (m - M')_{V, V1369 \text{ Cen}} & \\
 & \equiv (m_V - (M_V - 2.5 \log f_s))_{V1369 \text{ Cen}} \\
 & = ((m - M)_V + \Delta V)_{LV \text{ Vul}} \\
 & = 11.85 - 1.2 \pm 0.2 = 10.65 \pm 0.2.
 \end{aligned} \tag{A14}$$

We further compare with other novae having similar light curves to V1369 Cen, i.e., V496 Sct and V5666 Sgr. Figure 26 shows the time-stretched light curves of  $B$ ,  $V$ ,  $I_C$ , and  $K_s$  bands. The light curves well overlap except for the  $K_s$  band. Applying Equation (7) for the  $B$  band to Figure 26(a), we have the relation of

$$\begin{aligned}
 (m - M)_{B, V1369 \text{ Cen}} & \\
 & = ((m - M)_B + \Delta B)_{V496 \text{ Sct}} - 2.5 \log 0.74 \\
 & = 14.15 - 4.1 \pm 0.2 + 0.325 = 10.38 \pm 0.2,
 \end{aligned} \tag{A15}$$

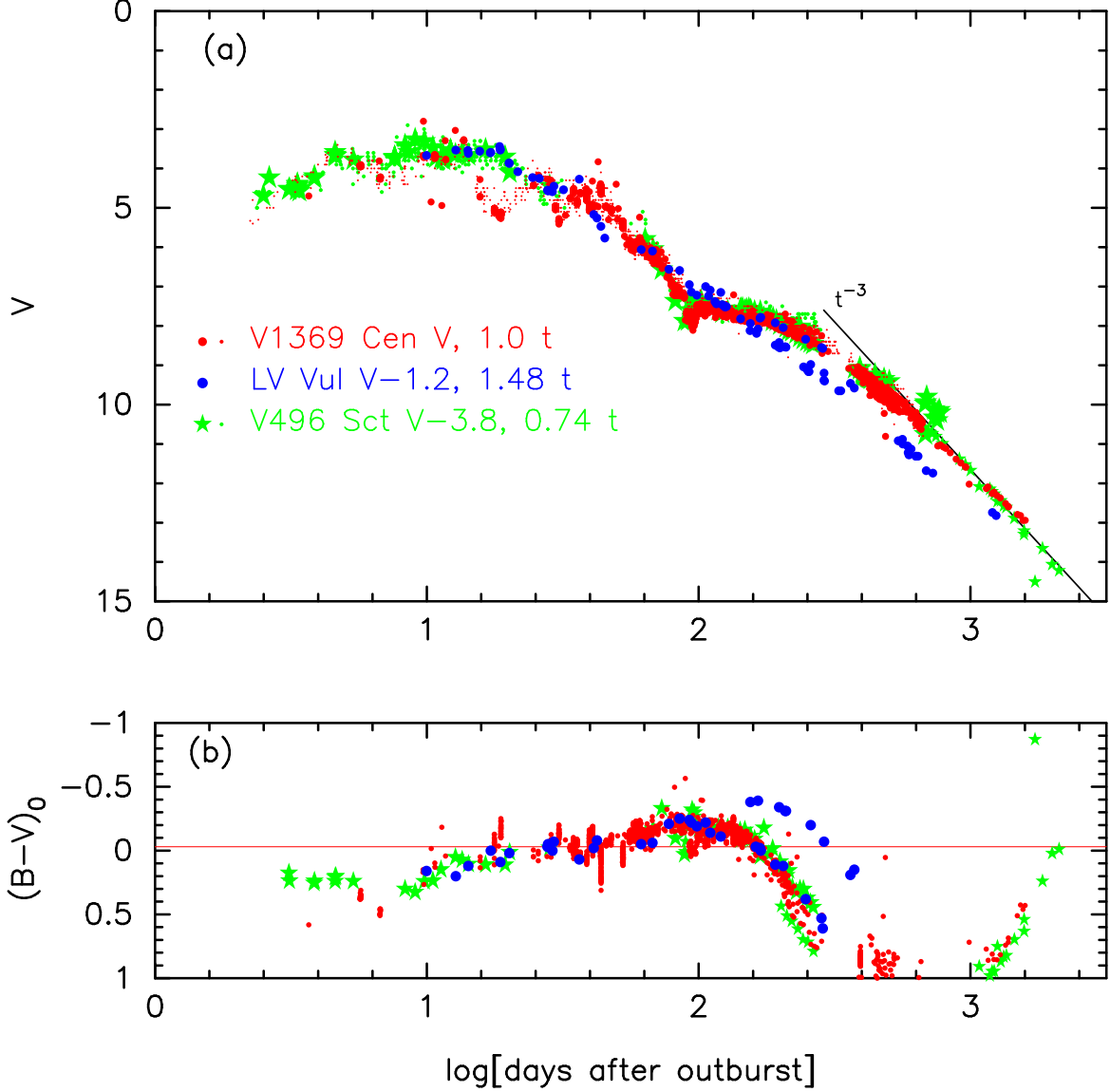


**Figure 25.** Same as Figure 19, but for V1369 Cen. The straight solid black line labeled “ $t^{-3}$ ” indicates the flux from homologously expanding ejecta, i.e., free expansion after the optically thick winds stop (see, e.g., Woodward et al. 1997; Hachisu & Kato 2006). The  $BV$  data of V1369 Cen are the same as those in Figure 24. We also plot the  $BV$  data of V496 Sct and LV Vul. The data of V496 Sct are the same as those in Figure 47 of Paper II.

where we adopt  $(m - M)_{B, V496 \text{ Sct}} = 13.7 + 1.0 \times 0.45 = 14.15$  from Section 7.12. Thus, we obtain  $(m - M)_B = 10.38 \pm 0.2$  for V1369 Cen. We obtain  $d = 0.97 \pm 0.1$  kpc from Equation (11) together with  $E(B - V) = 0.11$  and  $(m - M)_B = 10.38 \pm 0.2$ . We plot this relation of  $(m - M)_B = 10.38$  by the solid magenta line in Figure 7(c).

Applying Equation (4) to Figure 26(b), we have the relation of

$$\begin{aligned}
 (m - M)_{V, V1369 \text{ Cen}} &= ((m - M)_V + \Delta V)_{V496 \text{ Sct}} - 2.5 \log 0.74 \\
 &= 13.7 - 3.8 \pm 0.2 + 0.325 = 10.23 \pm 0.2,
 \end{aligned} \tag{A16}$$

where we adopt  $(m - M)_{V, V496 \text{ Sct}} = 13.7$  from Section 7.12. Thus, we obtain  $(m - M)_V = 10.23 \pm 0.2$  for V1369 Cen. We obtain  $d = 0.95 \pm 0.1$  kpc from Equation (5) together with  $E(B - V) = 0.11$ . We plot this relation of  $(m - M)_V = 10.23$  by the solid blue line in Figure 7(c).



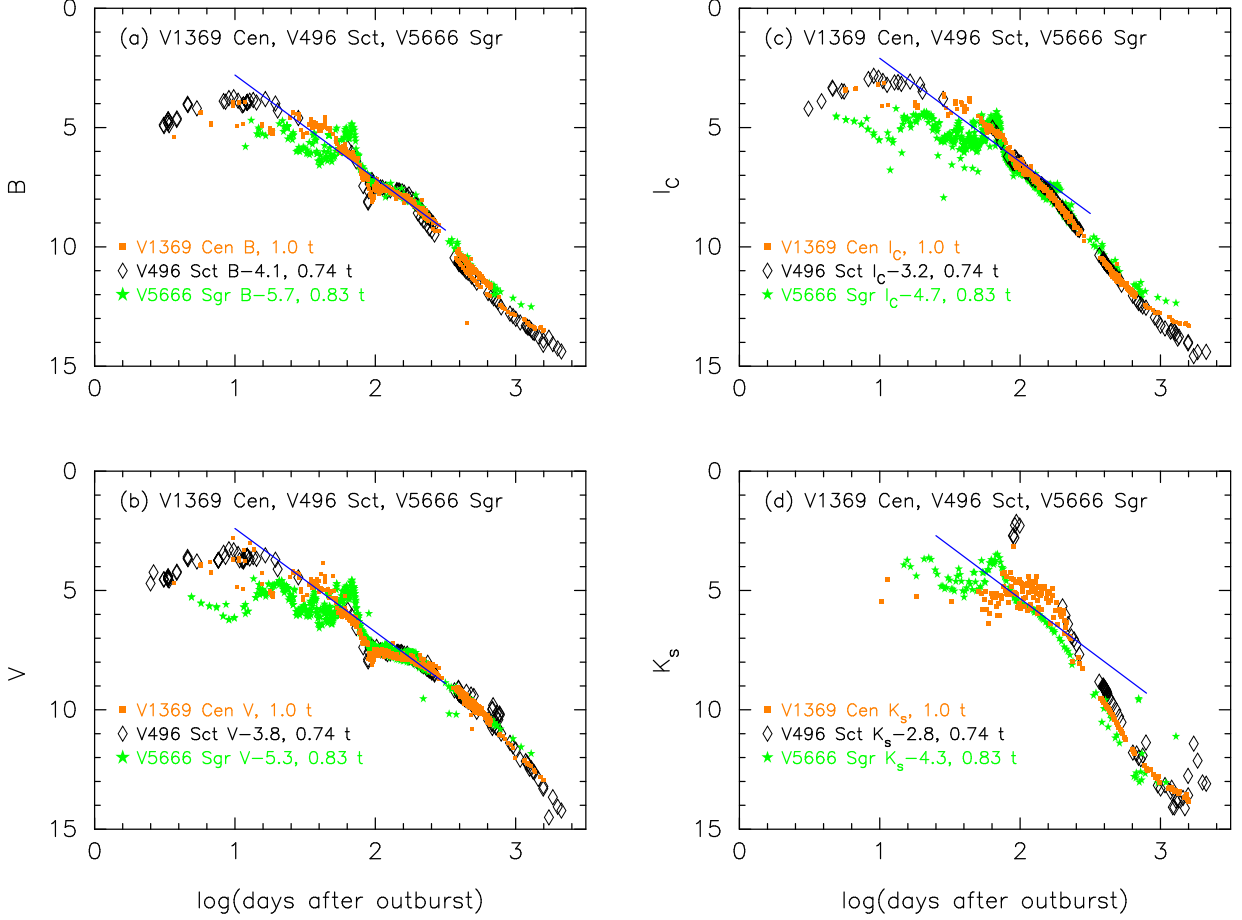


**Figure 26.** Same as Figure 18, but for a different set of V1369 Cen, V496 Sct, and V5666 Sgr. The  $BV$  data of V1369 Cen are the same as those in Figure 24. The  $BV$  data of V496 Sct are the same as those in Figure 51. The  $BV$  data of V5666 Sgr are the same as those in Figure 28. The  $I_C$  data of V1369 Cen are taken from AAVSO, VSOLJ, and SMARTS. The  $I_C$  data of V496 Sct are from Raj et al. (2012) and SMARTS. The  $I_C$  data of V5666 Sgr are from AAVSO, VSOLJ, and SMARTS. The  $K_s$  data are all taken from SMARTS.

From the  $I_C$  band data in Figure 26(a), we obtain

$$\begin{aligned}
 (m - M)_{I, V1369 \text{ Cen}} &= ((m - M)_I + \Delta I_C)_{V496 \text{ Sct}} - 2.5 \log 0.74 \\
 &= 12.98 - 3.2 \pm 0.2 + 0.325 = 10.11 \pm 0.2,
 \end{aligned} \tag{A17}$$

where we adopt  $(m - M)_{I, V496 \text{ Sct}} = 13.7 - 1.6 \times 0.45 = 12.98$ . Thus, we obtain  $(m - M)_{I, V574 \text{ Pup}} = 10.11 \pm 0.2$ . We obtain  $d = 0.97 \pm 0.1$  kpc from Equation (12) together with  $E(B - V) = 0.11$ . We plot this relation of  $(m - M)_I = 10.11$  by the solid cyan line in Figure 7(c).

V1369 Cen and V496 Sct showed a shallow dust blackout around 100 days ( $\log t \sim 2.0$ ) after the outbursts (Figure 26). Correspondingly, the  $K_s$  light curves have an enhancement above the line of universal decline law ( $F_\nu \propto t^{-1.75}$ ), as shown in Figure 26(d). In such a case, we do not use this part for overlapping. In the later phase, however, the decline trend of V1369 Cen becomes similar to those of V496 Sct and V5666 Sgr. We, thus, try to overlap as much as possible in the later phase. Applying Equation (9) for the  $K_s$  band, we obtain

$$\begin{aligned}
 (m - M)_{K, V1369 \text{ Cen}} &= ((m - M)_K + \Delta K_s)_{V496 \text{ Sct}} - 2.5 \log 0.74 \\
 &= 12.46 - 2.8 \pm 0.3 + 0.325 = 9.99 \pm 0.3,
 \end{aligned} \tag{A18}$$

where we adopt  $(m - M)_{K, V496 \text{ Sct}} = 13.7 - 2.75 \times 0.45 = 12.46$ . Thus, we obtain  $(m - M)_{K, V1369 \text{ Cen}} = 9.99 \pm 0.3$ . The distance is determined to be  $d = 0.98 \pm 0.3$  kpc from Equation (13) together with  $E(B - V) = 0.11$ . This distance

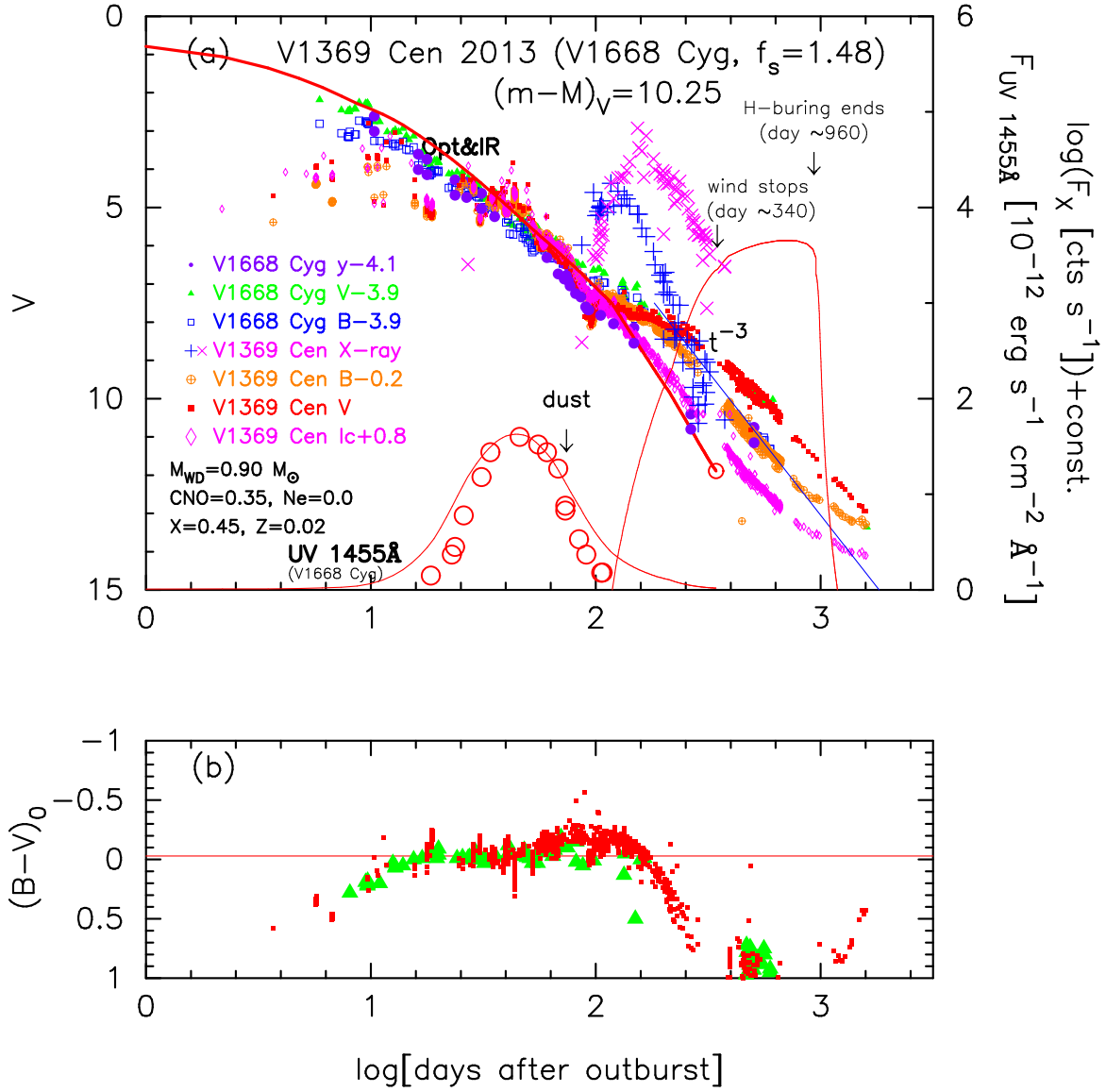


**Figure 27.** (a) The  $V$  and X-ray light and (b)  $(B - V)_0$  color curves of V1369 Cen. We also plot the  $V$  light curve and UV 1455Å data (large open red circles) of V1668 Cyg, the light curves of which are stretched by a factor of 1.48 in the time-direction against V1369 Cen. We add the  $B$  and  $I_C$  magnitudes of V1369 Cen taken from AAVSO, VSOLJ, and SMARTS. We add a  $0.90 M_\odot$  WD model (solid red lines) with the chemical composition of CO nova 3 (Hachisu & Kato 2016a), which reproduces the optical and NIR light curves of V1369 Cen. The  $V$  model light curve followed the shape of  $I_C$  magnitudes after the nebular phase started while the observed  $B$  and  $V$  magnitudes departed from it because of strong emission line effects. We add a straight solid black line labeled “ $t^{-3}$ ” that indicates the homologously expanding ejecta, i.e., free expansion after the optically thick winds stop.

is consistent with those determined from  $B$ ,  $V$ , and  $I_C$  bands. We plot this relation of  $(m - M)_K = 9.99$  by the solid cyan-blue line in Figure 7(c).

Figure 27 shows comparison with V1668 Cyg, one of well studied novae. The timescale of V1668 Cyg is stretched with  $f_s = 1.48$  and the  $V$  magnitude difference is  $\Delta V = -3.9$ . From the time-stretching method, we have the relation of

$$\begin{aligned}
 (m - M)_{V, V1369 \text{ Cen}} &= (m - M + \Delta V)_{V, V1668 \text{ Cyg}} - 2.5 \log 1.48 \\
 &= 14.6 - 3.9 \pm 0.2 - 0.43 = 10.27 \pm 0.2,
 \end{aligned}
 \tag{A19}$$

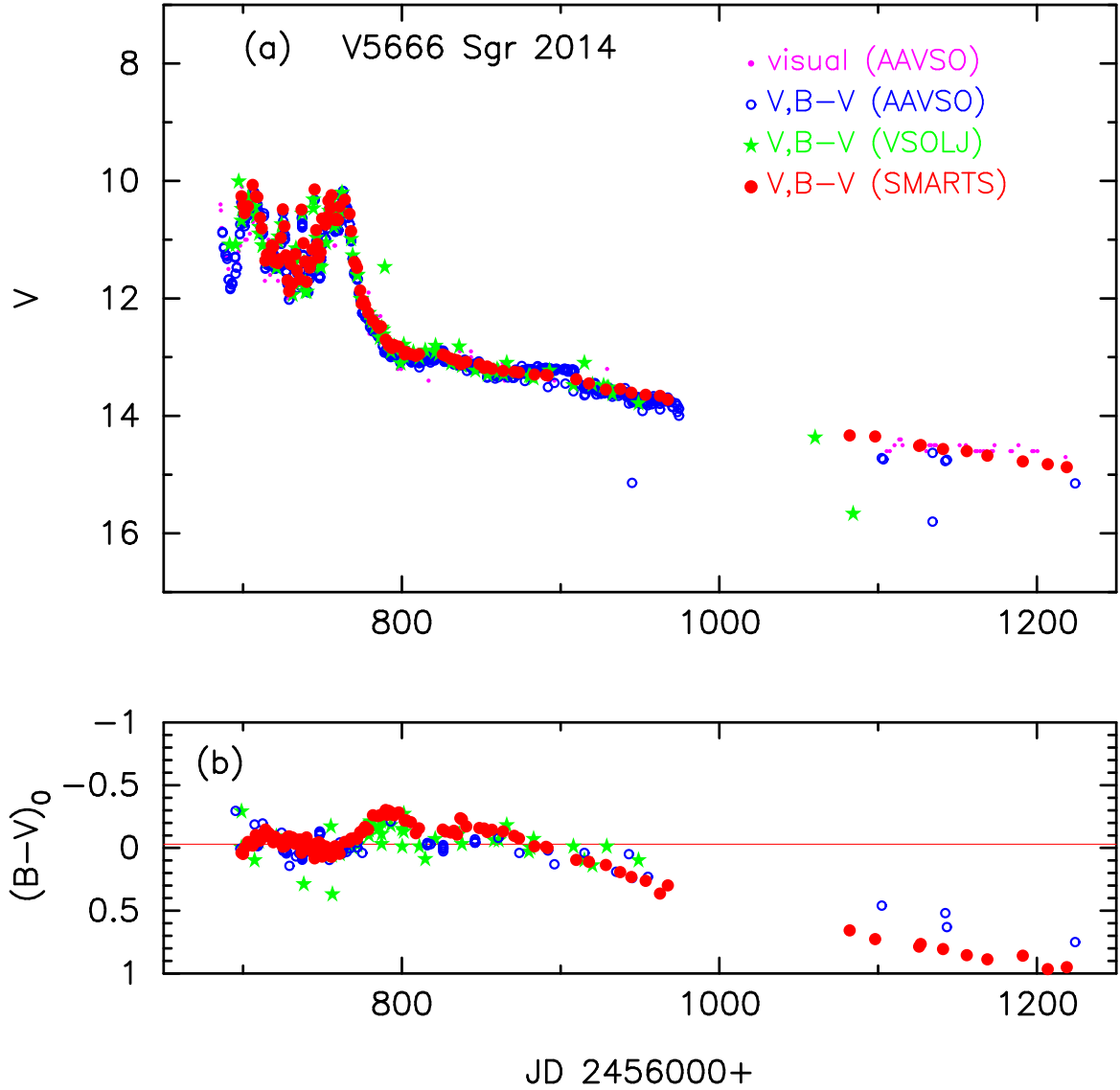


**Figure 28.** Same as Figure 17, but for V5666 Sgr. (a) The  $V$  and visual data of AAVSO (blue open circles and magenta dots) and  $V$  data of VSOLJ (filled green stars) are systematically shifted downward by 0.3 mag and 0.2 mag, respectively, to overlap them to the SMARTS data (filled red circles). (b) The  $(B - V)_0$  are dereddened with  $E(B - V) = 0.50$ . The  $B - V$  data of AAVSO (blue open circles) and VSOLJ (filled green stars) are systematically shifted up by 0.03 mag and 0.02 mag, respectively, to overlap them to the SMARTS data (filled red circles).

where we adopt  $(m - M)_{V,V1668 \text{ Cyg}} = 14.6$  from Section 2.3.3. Thus, we again confirm that  $f_s = 1.48$  against LV Vul and  $(m - M)_V = 10.27 \pm 0.2$ . To summarize, we adopt  $(m - M)_V = 10.25 \pm 0.1$  from various estimates based on the time-stretching method.

#### A.4. V5666 Sgr 2014

Figure 28 shows (a) the  $V$  and visual light and (b)  $(B - V)_0$  color curves of V5666 Sgr. The  $V$  and visual data of AAVSO (blue open circles and magenta dots) and  $V$  data of VSOLJ (filled green stars) are systematically shifted downward by 0.3 mag and 0.2 mag, respectively, to overlap them to the SMARTS data (filled red circles). Here,  $(B - V)_0$  are dereddened with  $E(B - V) = 0.50$  as obtained in Section 6. The  $B - V$  data of AAVSO (blue open circles) and VSOLJ (filled green stars) are systematically shifted upward by 0.03 mag and 0.02 mag, respectively, to overlap them to the SMARTS data (filled red circles).

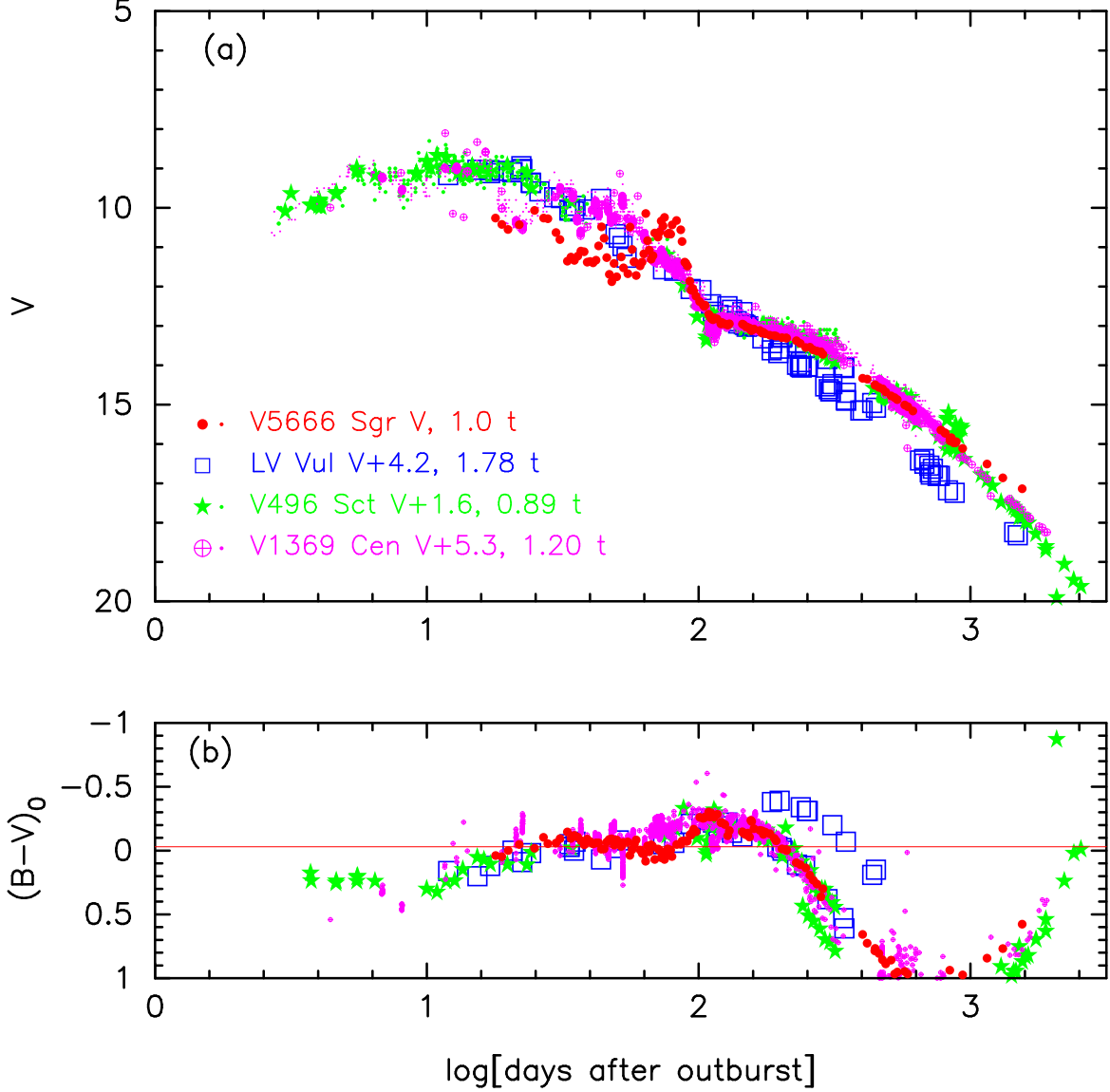


**Figure 29.** Same as Figure 25, but for V5666 Sgr. The  $BV$  data of V5666 Sgr are the same as those in Figure 28. The  $B - V$  colors of V5666 Sgr are dereddened with  $E(B - V) = 0.50$ . We also plot the  $BV$  data of LV Vul, V496 Sct, and V1369 Cen. The timescales of LV Vul, V496 Sct, and V1369 Cen are stretched by 1.78, 0.89, and 1.20, respectively, against V5666 Sgr.

Figure 29 shows (a) the  $V$  light curves of V5666 Sgr, LV Vul, V496 Sct, and V1369 Cen, and (b) their  $(B - V)_0$  color curves on logarithmic timescales. Here we assume that the V5666 Sgr outbursted on JD 2456681.0 (Day 0). Figure 29 compares V5666 Sgr with the similar  $V$  light curve novae, V496 Sct and V1369 Cen, in addition to LV Vul. We stretch the timescales of LV Vul, V496 Sct, and V1369 Cen by 1.78, 0.89, and 1.20, respectively, against V5666 Sgr, to overlap them with the V5666 Sgr  $V$  light and  $(B - V)_0$  color curves. From the time-stretching method, we have the relation of

$$\begin{aligned}
 (m - M)_{V, V5666 \text{ Sgr}} &= (m - M + \Delta V)_{V, LV \text{ Vul}} - 2.5 \log 1.78 \\
 &= 11.85 + 4.2 \pm 0.2 - 0.63 = 15.42 \pm 0.2 \\
 &= (m - M + \Delta V)_{V, V496 \text{ Sct}} - 2.5 \log 0.89 \\
 &= 13.7 + 1.6 \pm 0.2 + 0.13 = 15.43 \pm 0.2 \\
 &= (m - M + \Delta V)_{V, V1369 \text{ Cen}} - 2.5 \log 1.20 \\
 &= 10.25 + 5.3 \pm 0.2 - 0.20 = 15.35 \pm 0.2.
 \end{aligned} \tag{A20}$$

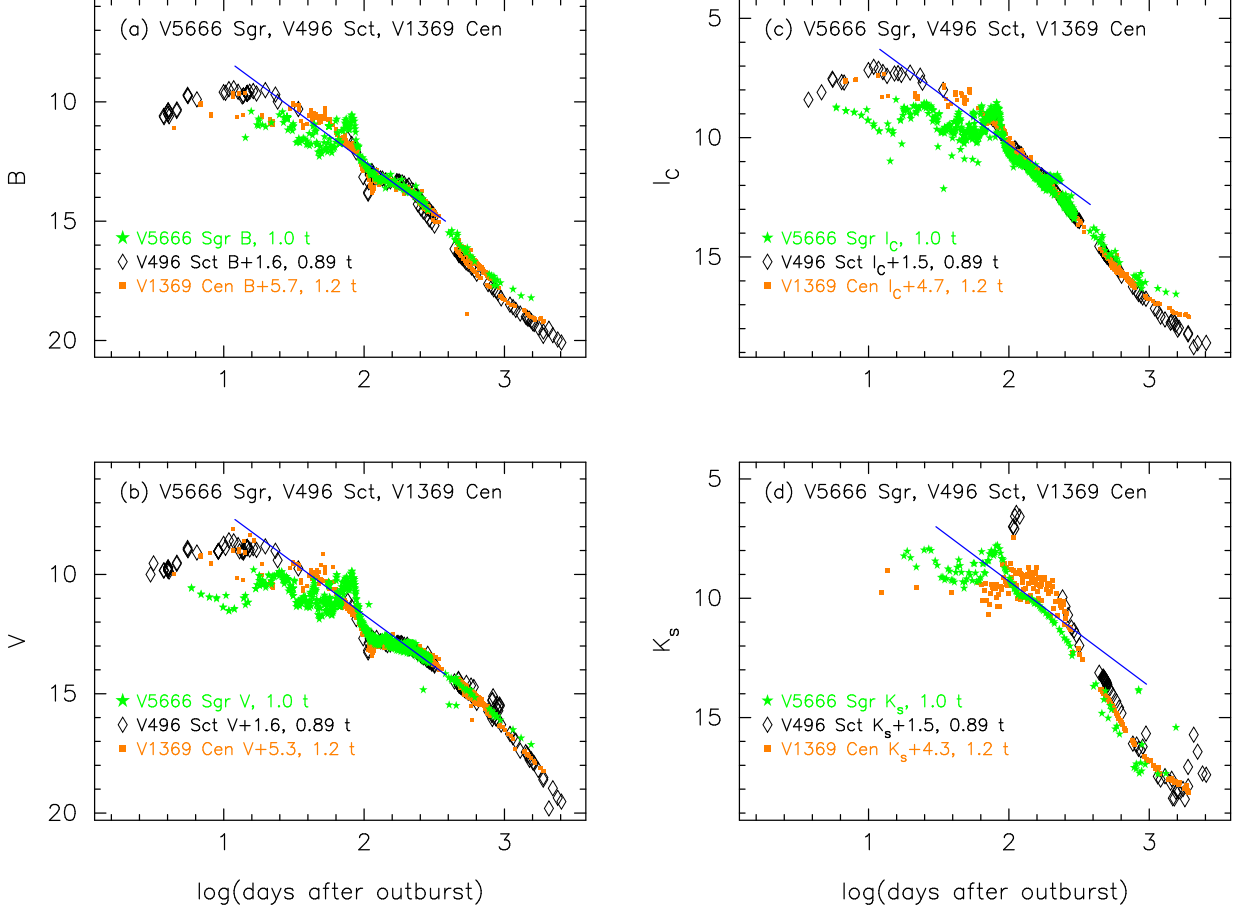


**Figure 30.** Same as Figure 26, but for V5666 Sgr. The data of V1369 Cen and V496 Sct are the same as those in Figure 26.

Thus, we obtained  $(m - M)_{V,V5666 \text{ Sgr}} = 15.4 \pm 0.1$ .

From Equations (1), (4), and (A20), we have the relation of

$$\begin{aligned}
 (m - M)_{V,V5666 \text{ Sgr}} & \\
 &\equiv (m_V - (M_V - 2.5 \log f_s))_{V5666 \text{ Sgr}} \\
 &= ((m - M)_V + \Delta V)_{LV \text{ Vul}} \\
 &= 11.85 + 4.2 \pm 0.2 = 16.05 \pm 0.2.
 \end{aligned} \tag{A21}$$

We further compare the V5666 Sgr light curves with other novae having similar light curves, V1369 Cen and V496 Sct. Figure 30 shows the same time-stretched light curves of  $B$ ,  $V$ ,  $I_C$ , and  $K_s$  bands as Figure 26. Applying Equation (7) for the  $B$  band to Figure 30(a), we have the relation of

$$\begin{aligned}
 (m - M)_{B,V5666 \text{ Sgr}} & \\
 &= ((m - M)_B + \Delta B)_{V496 \text{ Sct}} - 2.5 \log 0.89 \\
 &= 14.15 + 1.6 \pm 0.2 + 0.125 = 15.88 \pm 0.2 \\
 &= ((m - M)_B + \Delta B)_{V1369 \text{ Cen}} - 2.5 \log 1.2 \\
 &= 10.36 + 5.7 \pm 0.2 - 0.20 = 15.86 \pm 0.2,
 \end{aligned} \tag{A22}$$

where we adopt  $(m - M)_{B,V496 \text{ Sct}} = 13.7 + 1.0 \times 0.45 = 14.15$  from Section 7.12 and  $(m - M)_{B,V1369 \text{ Cen}} = 10.25 + 1.0 \times 0.11 = 10.36$  from Section 5. Thus, we obtain  $(m - M)_B = 15.87 \pm 0.1$  for V5666 Sgr. We obtain  $d = 5.8 \pm 0.6$  kpc from Equation (11) together with  $E(B - V) = 0.50$  and  $(m - M)_B = 15.87 \pm 0.1$ . We plot this relation of  $(m - M)_B = 15.87$  by the solid magenta line in Figure 7(d).

Applying Equation (4) to Figure 30(b), we have the relation of

$$(m - M)_{V,V5666 \text{ Sgr}}$$

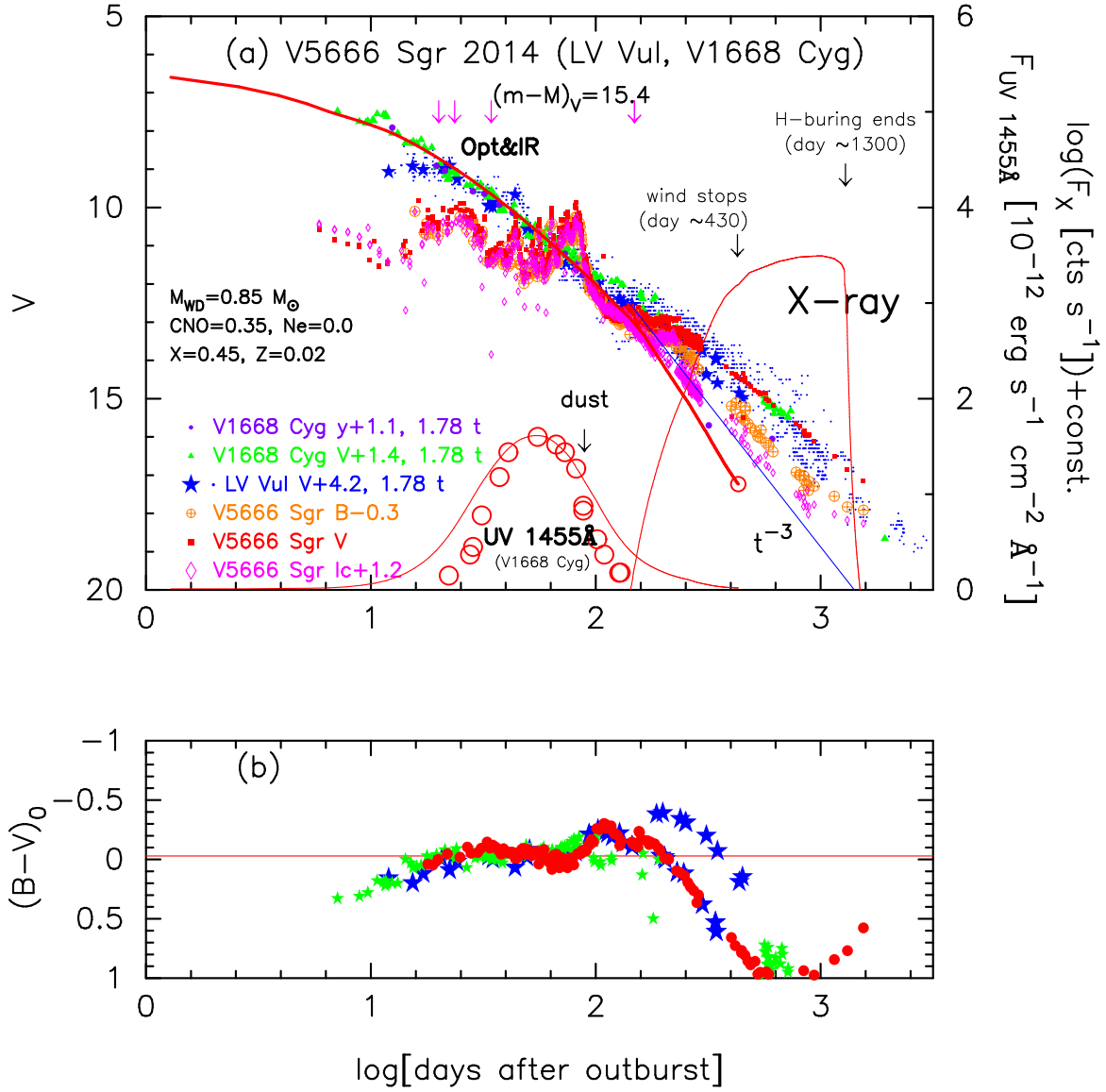


**Figure 31.** Same as Figure 27, but for V5666 Sgr. We also add (a) the  $V$  light and (b)  $(B - V)_0$  color curves of LV Vul and V1668 Cyg. Their light/color curves and the UV 1455Å flux (large open red circles) of V1668 Cyg are stretched by a factor of 1.78 against V5666 Sgr in the time-direction. We add the  $B$  and  $I_C$  magnitudes of V5666 Sgr taken from AAVSO, VSOLJ, and SMARTS. We add a  $0.85 M_\odot$  WD (solid red lines) models with the chemical composition of CO nova 3 (Hachisu & Kato 2016a), which approximately reproduce the optical and NIR light curves of V5666 Sgr. The *Swift* XRT observed V5666 Sgr five times as denoted by the downward magenta arrows, but did not detect X-rays.

$$\begin{aligned}
 &= ((m - M)_V + \Delta V)_{V496 \text{ Sct}} - 2.5 \log 0.89 \\
 &= 13.7 + 1.6 \pm 0.2 + 0.125 = 15.4 \pm 0.2 \\
 &= ((m - M)_V + \Delta V)_{V1369 \text{ Cen}} - 2.5 \log 1.2 \\
 &= 10.25 + 5.3 \pm 0.2 - 0.20 = 15.35 \pm 0.2,
 \end{aligned} \tag{A23}$$

where we adopt  $(m - M)_{V,V496 \text{ Sct}} = 13.7$  from Section 7.12 and  $(m - M)_{V,V1369 \text{ Cen}} = 10.25$  from Section 5. Thus, we obtain  $(m - M)_V = 15.38 \pm 0.1$  for V5666 Sgr. We obtain  $d = 5.8 \pm 0.6$  kpc from Equation (5) together with  $E(B - V) = 0.50 \pm 0.05$  and  $(m - M)_V = 15.38 \pm 0.1$ . We plot this relation of  $(m - M)_V = 15.38$  by the solid blue line in Figure 7(d).

From the  $I_C$  band data in Figure 30(c), we obtain

$$(m - M)_{I,V5666 \text{ Sgr}}$$

$$\begin{aligned}
 &= ((m - M)_I + \Delta I_C)_{V496 \text{ Sct}} - 2.5 \log 0.89 \\
 &= 12.98 + 1.5 \pm 0.2 + 0.125 = 14.61 \pm 0.2 \\
 &= ((m - M)_I + \Delta I_C)_{V1369 \text{ Cen}} - 2.5 \log 1.2 \\
 &= 10.07 + 4.7 \pm 0.2 - 0.20 = 14.57 \pm 0.2,
 \end{aligned} \tag{A24}$$

where we adopt  $(m - M)_{I,V496 \text{ Sct}} = 13.7 - 1.6 \times 0.45 = 12.98$  and  $(m - M)_{I,V1369 \text{ Cen}} = 10.25 - 1.6 \times 0.11 = 10.07$ . Thus, we obtain  $(m - M)_{I,V5666 \text{ Sgr}} = 14.59 \pm 0.1$ . We obtain  $d = 5.9 \pm 0.6$  kpc from Equation (12) together with  $E(B - V) = 0.50 \pm 0.05$  and  $(m - M)_I = 14.59 \pm 0.1$ . We plot this relation of  $(m - M)_I = 14.59$  by the solid cyan line in Figure 7(d).

We try to overlap the  $K_s$  light curves as much as possible in the later phase of Figure 30(d). Applying Equation (9) for the  $K_s$  band, we obtain

$$\begin{aligned}
 &(m - M)_{K,V5666 \text{ Sgr}} \\
 &= ((m - M)_K + \Delta K_s)_{V496 \text{ Sct}} - 2.5 \log 0.89 \\
 &= 12.46 + 1.5 \pm 0.3 + 0.125 = 14.09 \pm 0.3 \\
 &= ((m - M)_K + \Delta K_s)_{V1369 \text{ Cen}} - 2.5 \log 1.2 \\
 &= 9.95 + 4.3 \pm 0.3 - 0.20 = 14.05 \pm 0.3,
 \end{aligned} \tag{A25}$$

where we adopt  $(m - M)_{K,V496 \text{ Sct}} = 13.7 - 2.75 \times 0.45 = 12.46$ ,  $(m - M)_{K,V1369 \text{ Cen}} = 10.25 - 2.75 \times 0.11 = 9.95$ . Thus, we obtain  $(m - M)_{K,V5666 \text{ Sgr}} = 14.07 \pm 0.2$ . We obtain  $d = 6.0 \pm 0.6$  kpc from Equation (13) together with  $E(B - V) = 0.50 \pm 0.05$  and  $(m - M)_K = 14.07 \pm 0.2$ . We plot this relation of  $(m - M)_K = 14.07$  by the solid cyan-blue line in Figure 7(d).

Figure 31 also shows another comparison with LV Vul and V1668 Cyg. The light/color curves of LV Vul and V1668 Cyg are stretched by a factor of 1.78, so we obtain

$$\begin{aligned}
 &(m - M)_{V,V5666 \text{ Sgr}} \\
 &= (m - M + \Delta V)_{V,LV \text{ Vul}} - 2.5 \log 1.78 \\
 &= 11.85 + 4.2 \pm 0.2 - 0.63 = 15.42 \pm 0.2 \\
 &= (m - M + \Delta V)_{V,V1668 \text{ Cyg}} - 2.5 \log 1.78 \\
 &= 14.6 + 1.4 \pm 0.2 - 0.63 = 15.37 \pm 0.2,
 \end{aligned} \tag{A26}$$

from our time-stretching method. Thus, we again confirm  $(m - M)_{V,V5666 \text{ Sgr}} = 15.4 \pm 0.2$ .

## B. REANALYZED LIGHT CURVES OF 12 NOVAE

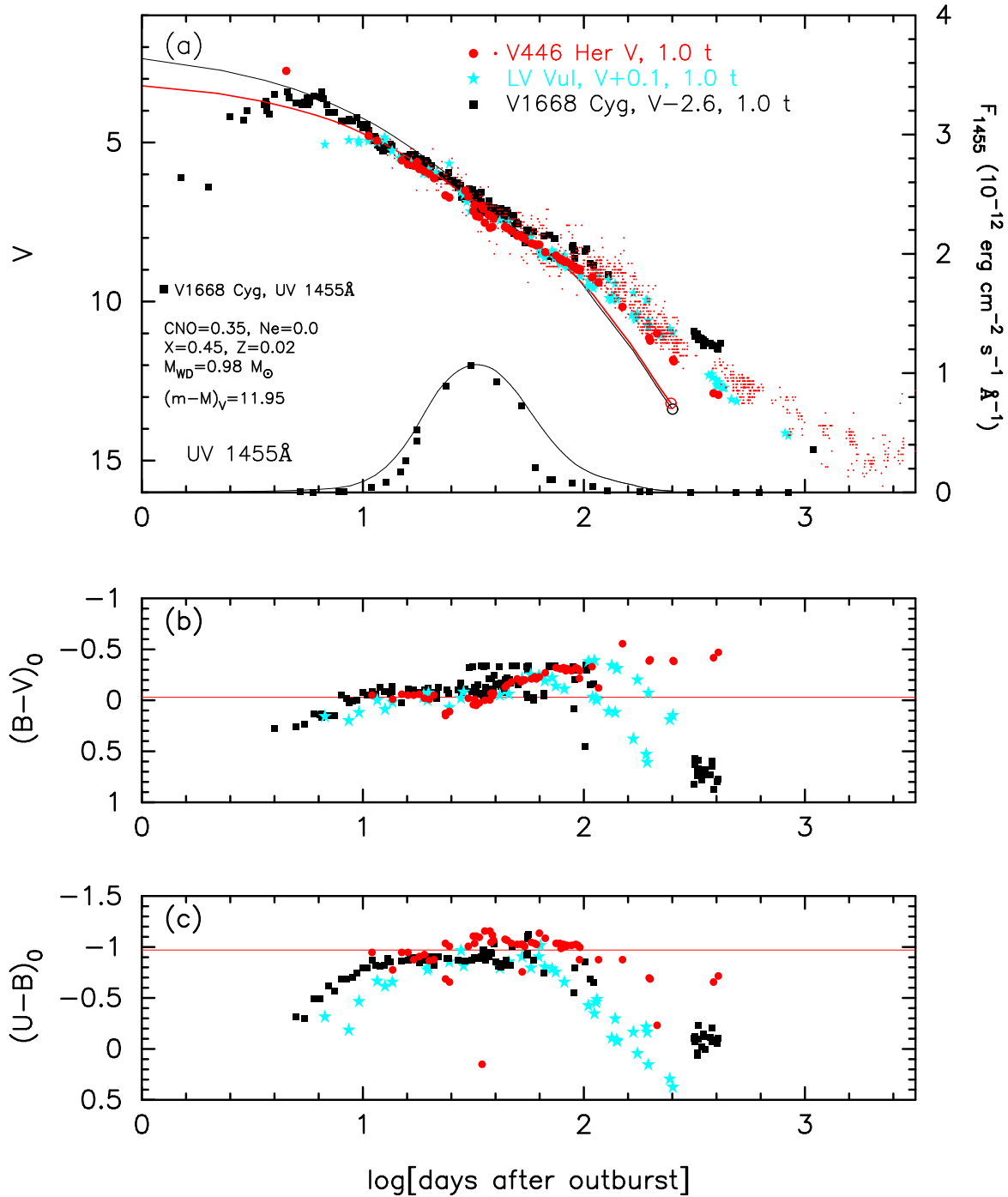
### B.1. V446 Her 1960

Figure 32 shows the light/color curves of V446 Her on a logarithmic timescale as well as LV Vul and V1668 Cyg. We overlap the light/color curves of these three novae as much as possible. Based on the time-stretching method, we have the relation of

$$\begin{aligned}
 &(m - M)_{V,V446 \text{ Her}} \\
 &= (m - M + \Delta V)_{V,LV \text{ Vul}} - 2.5 \log 1.0 \\
 &= 11.85 + 0.1 \pm 0.2 + 0.0 = 11.95 \pm 0.2 \\
 &= (m - M + \Delta V)_{V,V1668 \text{ Cyg}} - 2.5 \log 1.0 \\
 &= 14.6 - 2.6 \pm 0.2 + 0.0 = 12.0 \pm 0.2.
 \end{aligned} \tag{B27}$$

Thus, we obtain  $f_s = 1.0$  and  $(m - M)_V = 11.95 \pm 0.1$  for V446 Her. The new distance modulus is slightly larger than the previous value of  $(m - M)_V = 11.7 \pm 0.1$  (Paper II). This difference comes from the improved values of  $f_s$  and  $\Delta V$ . From Equations (14) and (B27), we have the relation of

$$\begin{aligned}
 &(m - M')_{V,V446 \text{ Her}} \\
 &\equiv (m_V - (M_V - 2.5 \log f_s))_{V446 \text{ Her}} \\
 &= (m - M + \Delta V)_{V,LV \text{ Vul}} \\
 &= 11.85 + 0.1 \pm 0.2 = 11.95 \pm 0.2.
 \end{aligned} \tag{B28}$$



**Figure 32.** Same as Figure 19, but for V446 Her (filled red circles). The data of V446 Her are the same as those in Figure 42 of Paper I, but we assume the outburst day of  $t_{\text{OB}} = \text{JD } 2436993.0$  for V446 Her. The  $(B-V)_0$  and  $(U-B)_0$  of V446 Her are dereddened with  $E(B-V) = 0.40$ . We also plot (a) the visual magnitudes (red dots) of V446 Her. We add (a) the  $V$  light, (b)  $(B-V)_0$ , and (c)  $(U-B)_0$  color curves of LV Vul and V1668 Cyg. We also add (a) the UV 1455Å fluxes (filled black squares) of V1668 Cyg. Assuming  $(m-M)_V = 11.95$  for V446 Her, we plot a model  $V$  light curve (solid red line) of a  $0.98 M_{\odot}$  WD with the envelope chemical composition of CO nova 3 (Hachisu & Kato 2016a). We also add another  $0.98 M_{\odot}$  WD model (solid black lines) with the chemical composition of CO nova 3, assuming  $(m-M)_V = 14.6$  for V1668 Cyg. This model (black lines) has a slightly larger initial envelope mass than the model (red line) for V446 Her.



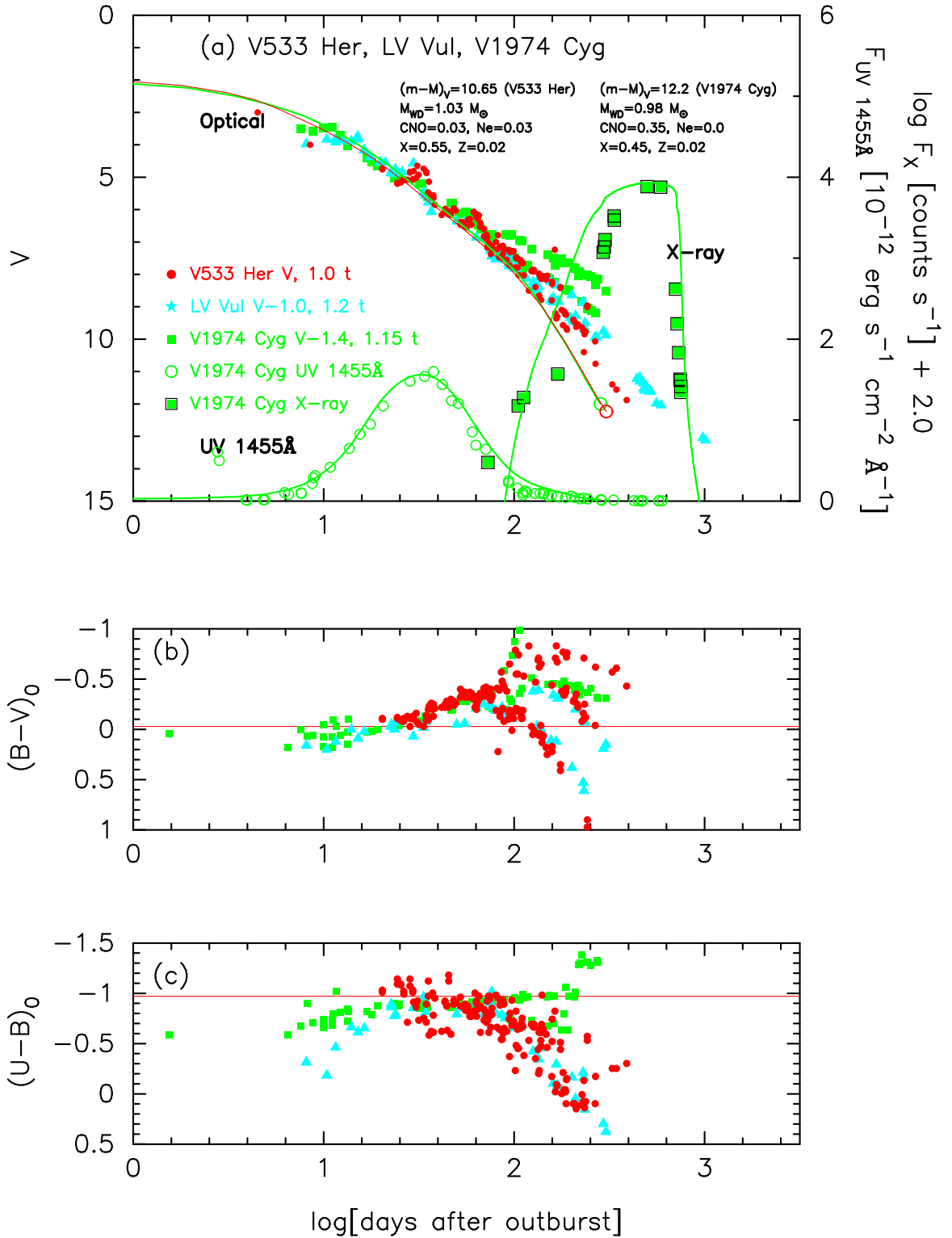


**Figure 33.** Same as Figure 19, but for V533 Her (filled red circles). We add the data of LV Vul and V1974 Cyg. The  $(B-V)_0$  and  $(U-B)_0$  data of V533 Her are dereddened by Equations (2) and (3) with  $E(B-V) = 0.038$ . We also add the UV 1455Å (open green circles) and supersoft X-ray (filled green squares with black outlines) fluxes of V1974 Cyg. The UV and X-ray data of V1974 Cyg are the same as those in Figure 13 of Paper I. Taking  $(m-M)_V = 10.65$  for V533 Her, we plot a model  $V$  light curve (solid red line) of a  $1.03 M_\odot$  WD with the envelope chemical composition of Ne nova 2 (Hachisu & Kato 2010). We also add a  $0.98 M_\odot$  WD model (solid green lines) with the chemical composition of CO nova 3 (Hachisu & Kato 2016a), taking  $(m-M)_V = 12.2$  for V1974 Cyg.

B.2. *V533 Her 1963*

We obtain  $f_s$  and  $(m - M)_V$  by the time-stretching method as in Figure 33, which shows the  $V$  light curve as well as the dereddened  $(B - V)_0$  and  $(U - B)_0$  color curves. We add the light/color curves of LV Vul and V1974 Cyg and overlap these light/color curves as much as possible. Applying the time-stretching method of Equation (4) to Figure 33(a), we have the relation of

$$\begin{aligned}
& (m - M)_{V, V533 \text{ Her}} \\
&= ((m - M)_V + \Delta V)_{LV \text{ Vul}} - 2.5 \log 1.20 \\
&= 11.85 - 1.0 \pm 0.3 - 0.20 = 10.65 \pm 0.3 \\
&= ((m - M)_V + \Delta V)_{V1974 \text{ Cyg}} - 2.5 \log 1.15 \\
&= 12.2 - 1.4 \pm 0.3 - 0.15 = 10.65 \pm 0.3.
\end{aligned} \tag{B29}$$

The new result of  $(m - M)_V = 10.65 \pm 0.2$  is almost the same as the previous result of  $(m - M)_V = 10.8 \pm 0.2$  (Paper II), but slightly improve the timescaling factors of  $f_s$  and vertical fit of  $\Delta V$ . We obtain  $f_s = 1.20$  against the template LV Vul. The distance is calculated to be  $d = 1.28$  kpc from Equation (5) together with  $(m - M)_V = 10.65$  and  $E(B - V) = 0.038$ . This value is almost the same as what Hachisu & Kato (2016b) concluded from various results in the literature.

From Equations (14) and (B29), we have the relation of

$$\begin{aligned}
& (m - M')_{V, V533 \text{ Her}} \\
&\equiv (m_V - (M_V - 2.5 \log f_s))_{V533 \text{ Her}} \\
&= ((m - M)_V + \Delta V)_{LV \text{ Vul}} \\
&= 11.85 - 1.0 \pm 0.3 = 10.85 \pm 0.3.
\end{aligned} \tag{B30}$$

B.3. *PW Vul 1984#1*

Figure 34 shows the light/color curves of PW Vul on a logarithmic timescale as well as LV Vul, V1500 Cyg, and V1668 Cyg. We deredden the colors of PW Vul with  $E(B - V) = 0.57$  as obtained in Section 7.3. In this figure, we regard that the  $V$  light curve of PW Vul oscillates between the  $V$  light curves of V1668 Cyg and V1500 Cyg during  $\log t$  (day)  $\sim 1.4$ – $2.1$ . Based on the time-stretching method, we have the relation of

$$\begin{aligned}
& (m - M)_{V, PW \text{ Vul}} \\
&= (m - M + \Delta V)_{V, LV \text{ Vul}} - 2.5 \log 2.24 \\
&= 11.85 + 2.0 \pm 0.3 - 0.88 = 12.97 \pm 0.3 \\
&= (m - M + \Delta V)_{V, V1668 \text{ Cyg}} - 2.5 \log 2.24 \\
&= 14.6 - 0.7 \pm 0.3 - 0.88 = 13.02 \pm 0.3 \\
&= (m - M + \Delta V)_{V, V1500 \text{ Cyg}} - 2.5 \log 3.7 \\
&= 12.3 + 2.1 \pm 0.3 - 1.43 = 12.97 \pm 0.3.
\end{aligned} \tag{B31}$$

Thus, we obtain  $f_s = 2.24$  against the template nova LV Vul and confirm the previous result of  $(m - M)_V = 13.0 \pm 0.2$  for PW Vul (Hachisu & Kato 2015, 2016b). From Equations (14) and (B31), we have the relation of

$$\begin{aligned}
& (m - M')_{V, PW \text{ Vul}} \\
&\equiv (m_V - (M_V - 2.5 \log f_s))_{PW \text{ Vul}} \\
&= (m - M + \Delta V)_{V, LV \text{ Vul}} \\
&= 11.85 + 2.0 \pm 0.3 = 13.85 \pm 0.3.
\end{aligned} \tag{B32}$$

We further obtain the distance moduli of  $BVI_C$  bands and examine the distance and reddening toward PW Vul. Figure 35 shows the three band light curves of PW Vul as well as V679 Car, YY Dor, and LMC N 2009a. For the  $B$  band, we apply Equation (7) to Figure 35(a) and obtain

$$\begin{aligned}
& (m - M)_{B, PW \text{ Vul}} \\
&= ((m - M)_B + \Delta B)_{YY \text{ Dor}} - 2.5 \log 11.7 \\
&= 18.98 - 2.8 \pm 0.2 - 2.67 = 13.51 \pm 0.2
\end{aligned}$$

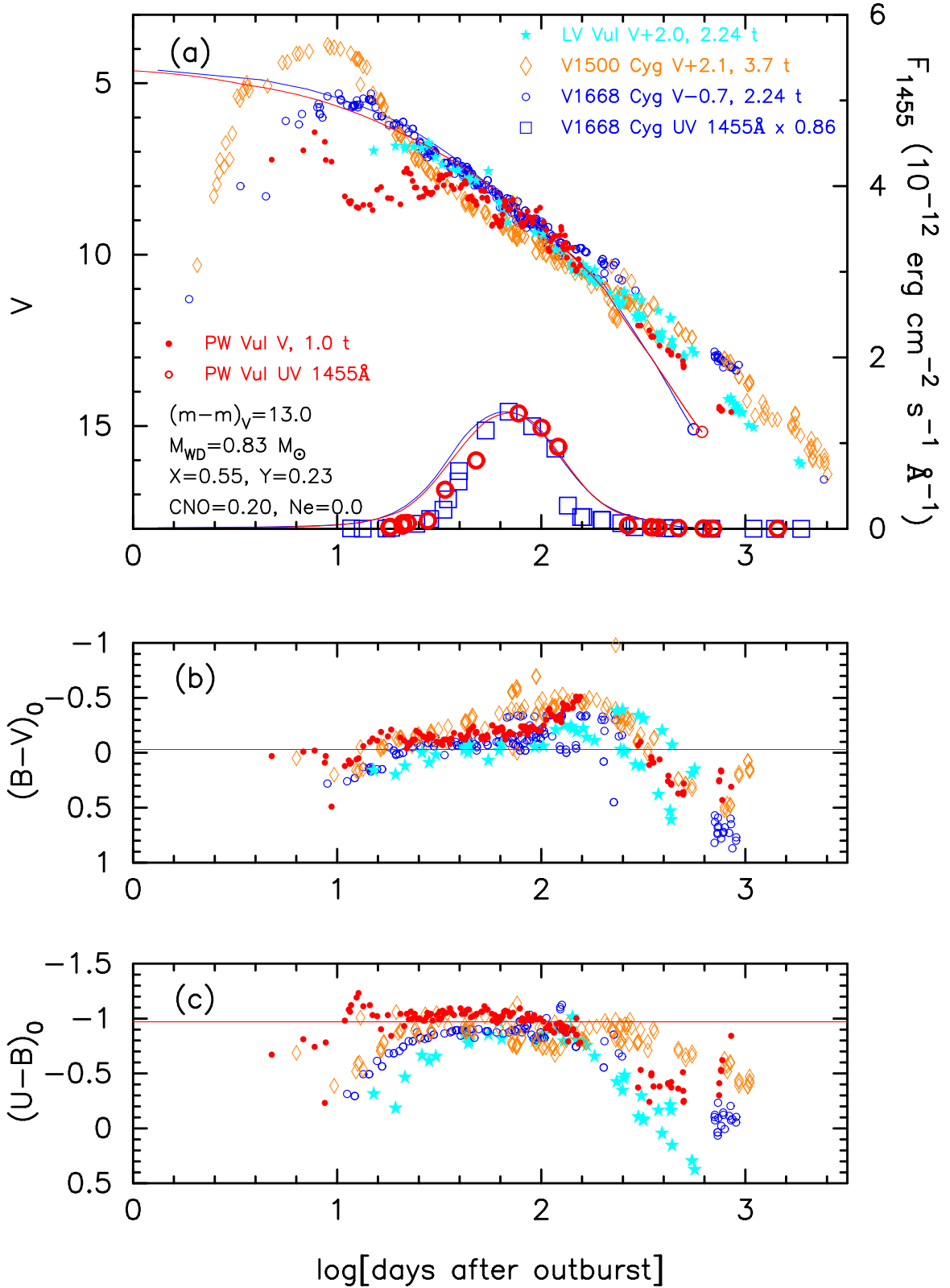


**Figure 34.** Same as Figure 19, but for PW Vul (filled red circles). We add the UV 1455Å flux of PW Vul (large open red circles) and V1668 Cyg (open blue squares). The data of PW Vul are the same as those in Figure 6 of Paper I. In panel (a), taking  $(m-M)_V = 13.0$  for PW Vul, we add model light curves (solid red lines) of a  $0.83 M_{\odot}$  WD with the envelope chemical composition of CO nova 4 (Hachisu & Kato 2015). We also add a  $0.98 M_{\odot}$  WD model (solid blue lines) with the chemical composition of CO nova 3 (Hachisu & Kato 2016a), taking  $(m-M)_V = 14.6$  for V1668 Cyg.

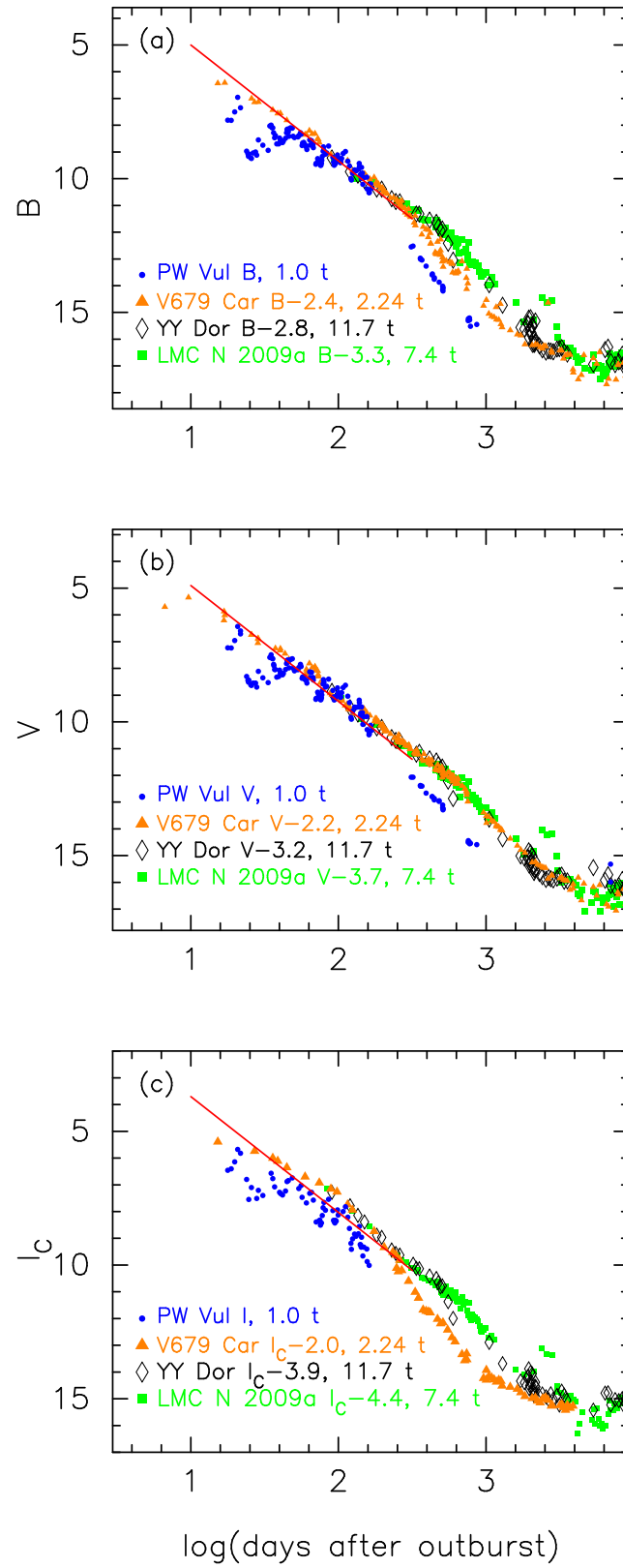


**Figure 35.** The  $BVI$  light curves of PW Vul are plotted together with those of V679 Car, YY Dor, and LMC N 2009a. The  $BV$  data of PW Vul are taken from Noskova et al. (1985), Kolotilov & Noskova (1986), and Robb & Scarfe (1995). The  $I$  data of PW Vul are taken from Robb & Scarfe (1995).

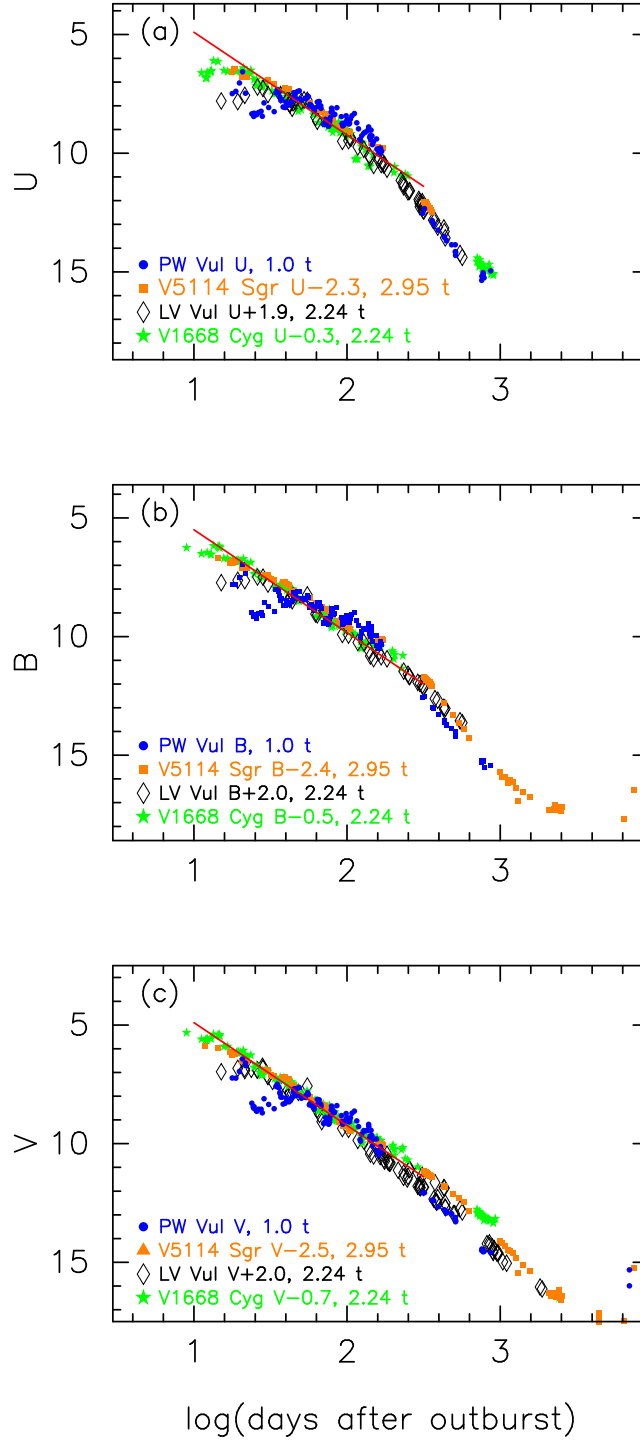


**Figure 36.** The  $UBV$  light curves of PW Vul are plotted together with those of V5114 Sgr, LV Vul, and V1668 Cyg. The  $UBV$  data of PW Vul are taken from Noslkova et al. (1985), Kolotilov & Noslkova (1986), and Robb & Scarfe (1995).

$$\begin{aligned}
 &= ((m - M)_B + \Delta B)_{\text{LMC N 2009a}} - 2.5 \log 7.4 \\
 &= 18.98 - 3.3 \pm 0.2 - 2.17 = 13.51 \pm 0.2 \\
 &= ((m - M)_B + \Delta B)_{\text{V679 Car}} - 2.5 \log 2.24 \\
 &= 16.79 - 2.4 \pm 0.2 - 0.87 = 13.52 \pm 0.2,
 \end{aligned} \tag{B33}$$

where we adopt  $(m - M)_{B, \text{V679 Car}} = 16.1 + 1.0 \times 0.69 = 16.79$ . Thus, we obtain  $(m - M)_{B, \text{PW Vul}} = 13.52 \pm 0.1$ .

For the  $V$  light curves in Figure 35(b), we similarly obtain

$$\begin{aligned}
(m-M)_{V,\text{PW Vul}} &= ((m-M)_V + \Delta V)_{\text{YY Dor}} - 2.5 \log 11.7 \\
&= 18.86 - 3.2 \pm 0.2 - 2.67 = 12.99 \pm 0.2 \\
&= ((m-M)_V + \Delta V)_{\text{LMC N 2009a}} - 2.5 \log 7.4 \\
&= 18.86 - 3.7 \pm 0.2 - 2.17 = 12.99 \pm 0.2 \\
&= ((m-M)_V + \Delta V)_{\text{V679 Car}} - 2.5 \log 2.24 \\
&= 16.1 - 2.2 \pm 0.2 - 0.87 = 13.03 \pm 0.2,
\end{aligned} \tag{B34}$$

where we adopt  $(m-M)_{V,\text{V679 Car}} = 16.1$  in Section 4. Thus, we obtain  $(m-M)_{V,\text{PW Vul}} = 13.0 \pm 0.1$ .

Applying Equation (8) for the  $I_C$  band to Figure 35(c), we obtain

$$\begin{aligned}
(m-M)_{I,\text{PW Vul}} &= ((m-M)_I + \Delta I_C)_{\text{YY Dor}} - 2.5 \log 11.7 \\
&= 18.67 - 3.9 \pm 0.3 - 2.67 = 12.1 \pm 0.3 \\
&= ((m-M)_I + \Delta I_C)_{\text{LMC N 2009a}} - 2.5 \log 7.4 \\
&= 18.67 - 4.4 \pm 0.3 - 2.17 = 12.1 \pm 0.3 \\
&= ((m-M)_I + \Delta I_C)_{\text{V679 Car}} - 2.5 \log 2.24 \\
&= 15.0 - 2.0 \pm 0.3 - 0.87 = 12.13 \pm 0.3,
\end{aligned} \tag{B35}$$

where we adopt  $(m-M)_{I,\text{V679 Car}} = 16.1 - 1.6 \times 0.69 = 15.0$ . However, we should not use this result because no  $I_C$  but only  $I$  data of PW Vul are available (Robb & Scarfe 1995) and the  $I$  light curve of PW Vul (filled blue circles) does not accurately follow the other  $I_C$  data which follow the universal decline law as shown in Figure 35(c).

We also plot the  $U$ ,  $B$ , and  $V$  light curves of PW Vul together with those of LV Vul, V1668 Cyg, and V5114 Sgr in Figure 36. We apply Equation (6) for the  $U$  band to Figure 36(a) and obtain

$$\begin{aligned}
(m-M)_{U,\text{PW Vul}} &= ((m-M)_U + \Delta U)_{\text{LV Vul}} - 2.5 \log 2.24 \\
&= 12.85 + 1.9 \pm 0.2 - 0.87 = 13.88 \pm 0.2 \\
&= ((m-M)_U + \Delta U)_{\text{V1668 Cyg}} - 2.5 \log 2.24 \\
&= 15.1 - 0.3 \pm 0.2 - 0.87 = 13.93 \pm 0.2 \\
&= ((m-M)_U + \Delta U)_{\text{V5114 Sgr}} - 2.5 \log 2.95 \\
&= 17.43 - 2.3 \pm 0.2 - 1.17 = 13.96 \pm 0.2,
\end{aligned} \tag{B36}$$

where we adopt  $(m-M)_{U,\text{LV Vul}} = 11.85 + (4.75 - 3.1) \times 0.60 = 12.85$ , and  $(m-M)_{U,\text{V1668 Cyg}} = 14.6 + (4.75 - 3.1) \times 0.30 = 15.10$ , and  $(m-M)_{U,\text{V5114 Sgr}} = 16.65 + (4.75 - 3.1) \times 0.47 = 17.43$ . Thus, we obtain  $(m-M)_{U,\text{PW Vul}} = 13.92 \pm 0.2$ . For the  $B$  light curves in Figure 36(b), we similarly obtain

$$\begin{aligned}
(m-M)_{B,\text{PW Vul}} &= ((m-M)_B + \Delta B)_{\text{LV Vul}} - 2.5 \log 2.24 \\
&= 12.45 + 2.0 \pm 0.2 - 0.87 = 13.58 \pm 0.2 \\
&= ((m-M)_B + \Delta B)_{\text{V1668 Cyg}} - 2.5 \log 2.24 \\
&= 14.9 - 0.5 \pm 0.2 - 0.87 = 13.53 \pm 0.2 \\
&= ((m-M)_B + \Delta B)_{\text{V5114 Sgr}} - 2.5 \log 2.95 \\
&= 17.12 - 2.4 \pm 0.2 - 1.17 = 13.55 \pm 0.2,
\end{aligned} \tag{B37}$$

where we adopt  $(m-M)_{B,\text{LV Vul}} = 11.85 + 1.0 \times 0.6 = 12.45$ ,  $(m-M)_{B,\text{V1668 Cyg}} = 14.6 + 1.0 \times 0.3 = 14.9$ , and  $(m-M)_{B,\text{V5114 Sgr}} = 16.65 + 1.0 \times 0.47 = 17.12$ . Thus, we obtain  $(m-M)_{B,\text{PW Vul}} = 13.55 \pm 0.2$ . We apply Equation (4) to Figure 36(c) and obtain

$$\begin{aligned}
(m-M)_{V,\text{PW Vul}} &= ((m-M)_V + \Delta V)_{\text{LV Vul}} - 2.5 \log 2.24 \\
&= 11.85 + 2.0 \pm 0.2 - 0.87 = 12.98 \pm 0.2 \\
&= ((m-M)_V + \Delta V)_{\text{V1668 Cyg}} - 2.5 \log 2.24
\end{aligned}$$

$$\begin{aligned}
 &= 14.6 - 0.7 \pm 0.2 - 0.87 = 13.03 \pm 0.2 \\
 &= ((m - M)_V + \Delta V)_{V5114 \text{ Sgr}} - 2.5 \log 2.95 \\
 &= 16.65 - 2.5 \pm 0.2 - 1.17 = 12.98 \pm 0.2.
 \end{aligned} \tag{B38}$$

Thus, we obtain  $(m - M)_{V, \text{PW Vul}} = 13.0 \pm 0.1$ . This result is essentially the same as those in Equations (B31) and (B34).

We plot these four distance moduli of  $U$ ,  $B$ ,  $V$ , and  $I_C$  bands in Figure 10(c) by the thin solid green, cyan, and thick solid blue, and thin solid blue-magenta lines, that is,  $(m - M)_U = 13.92$ ,  $(m - M)_B = 13.55$ , and  $(m - M)_V = 13.0$  and  $(m - M)_I = 12.12$ , respectively. These four lines cross at  $d = 1.8$  kpc and  $E(B - V) = 0.57$ .

#### B.4. V1419 Aql 1993

Figure 37 shows the light/color curves of V1419 Aql as well as LV Vul and V1668 Cyg. We regard that the  $V$  light curve of V1419 Aql follows V1668 Cyg and the upper branch of LV Vul during  $\log t$  (day)  $\sim 1.0$ – $1.4$ . Based on the time-stretching method, we have the relation of

$$\begin{aligned}
 &(m - M)_{V, V1419 \text{ Aql}} \\
 &= (m - M + \Delta V)_{V, LV \text{ Vul}} - 2.5 \log 1.41 \\
 &= 11.85 + 3.5 \pm 0.3 - 0.38 = 14.97 \pm 0.3 \\
 &= (m - M + \Delta V)_{V, V1668 \text{ Cyg}} - 2.5 \log 1.41 \\
 &= 14.6 + 0.8 \pm 0.3 - 0.38 = 15.02 \pm 0.3.
 \end{aligned} \tag{B39}$$

Thus, we obtain  $f_s = 1.41$  against the template nova LV Vul and  $(m - M)_V = 15.0 \pm 0.2$ . The new value is slightly larger than the previous estimate of  $(m - M)_V = 14.6 \pm 0.1$  by Hachisu & Kato (2016b), because the timescaling factor of  $f_s$  and  $\Delta V$  are improved. From Equations (14) and (B39), we have the relation of

$$\begin{aligned}
 &(m - M')_{V, V1419 \text{ Aql}} \\
 &\equiv (m_V - (M_V - 2.5 \log f_s))_{V1419 \text{ Aql}} \\
 &= (m - M + \Delta V)_{V, LV \text{ Vul}} \\
 &= 11.85 + 3.5 \pm 0.3 = 15.35 \pm 0.3.
 \end{aligned} \tag{B40}$$

#### B.5. V705 Cas 1993

Figure 38 shows the light/color curves of V705 Cas as well as LV Vul and PW Vul. We deredden the colors of V705 Cas with  $E(B - V) = 0.45$  as obtained in Section 7.5. Based on the time-stretching method, we have the relation of

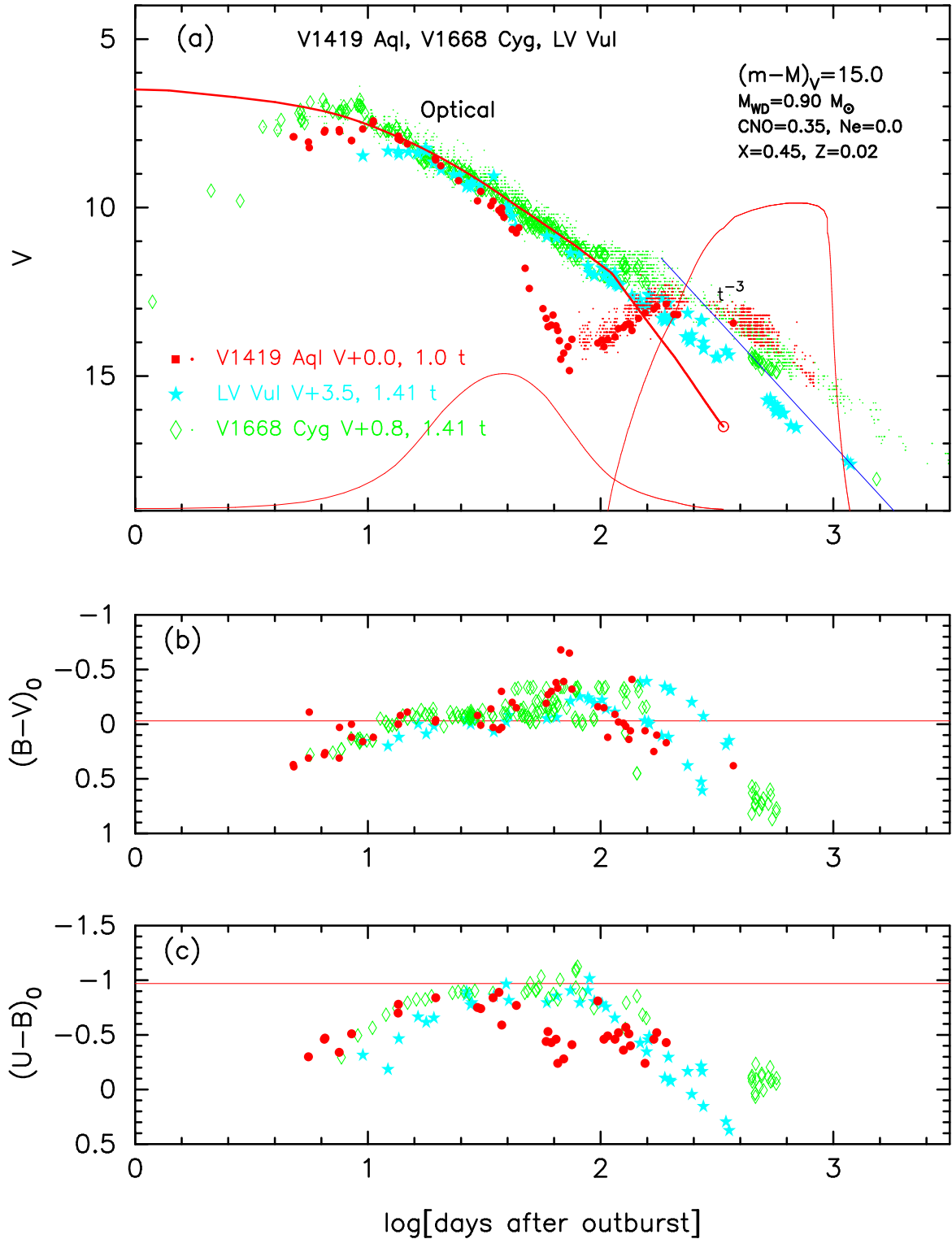
$$\begin{aligned}
 &(m - M)_{V, V705 \text{ Cas}} \\
 &= (m - M + \Delta V)_{V, LV \text{ Vul}} - 2.5 \log 2.8 \\
 &= 11.85 + 2.7 \pm 0.3 - 1.13 = 13.42 \pm 0.3 \\
 &= (m - M + \Delta V)_{V, PW \text{ Vul}} - 2.5 \log 1.26 \\
 &= 13.0 + 0.7 \pm 0.3 - 0.25 = 13.45 \pm 0.3.
 \end{aligned} \tag{B41}$$

Thus, we obtain  $f_s = 2.8$  against the template nova LV Vul and  $(m - M)_V = 13.45 \pm 0.2$ . This value is consistent with the previous value of  $(m - M)_V = 13.4 \pm 0.1$  estimated by Hachisu & Kato (2015). From Equations (14) and (B41), we have the relation of

$$\begin{aligned}
 &(m - M')_{V, V705 \text{ Cas}} \\
 &\equiv (m_V - (M_V - 2.5 \log f_s))_{V705 \text{ Cas}} \\
 &= (m - M + \Delta V)_{V, LV \text{ Vul}} \\
 &= 11.85 + 2.7 \pm 0.3 = 14.55 \pm 0.3.
 \end{aligned} \tag{B42}$$

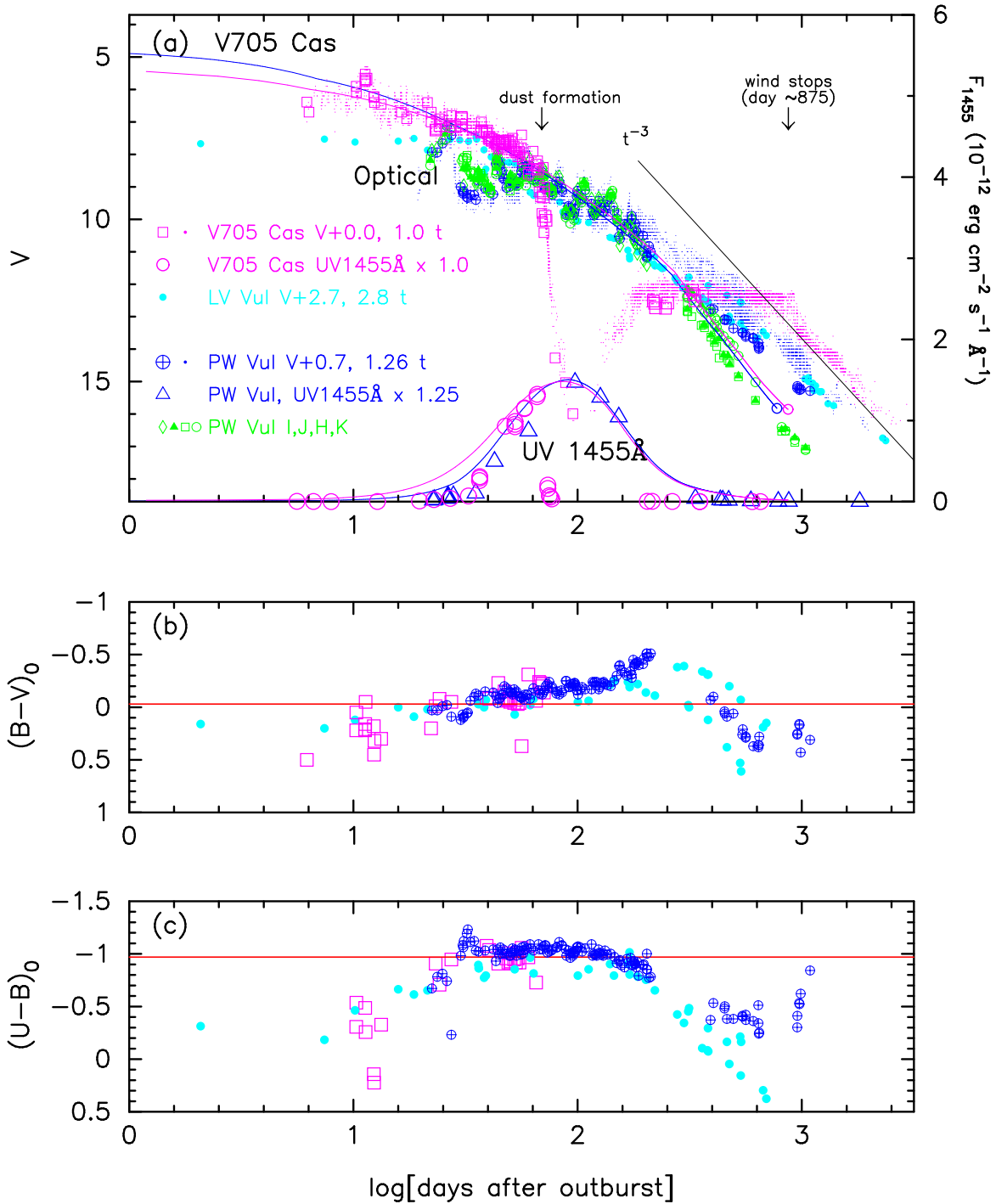
#### B.6. V382 Vel 1999

Figure 39 shows the light/color curves of V382 Vel as well as LV Vul, V1668 Cyg, and V1974 Cyg. The data of V382 Vel are the same as those in Figures 1 and 27 of Paper II. We add a straight solid black line labeled “ $t^{-3}$ ”



**Figure 37.** Same as Figure 19, but for V1419 Aql (filled red circles). The colors of V1419 Aql are dereddened with  $E(B - V) = 0.52$ . The data of V1419 Aql are the same as those in Figure 35 of Paper II. Adopting  $(m - M)_V = 15.0$  for V1419 Aql, we plot a  $0.90 M_{\odot}$  WD model (solid red lines) with the chemical composition of CO nova 3 (Hachisu & Kato 2016a). We add the UV 1455Å flux (left thin solid red line) and supersoft X-ray flux (right thin solid red line) of the  $0.90 M_{\odot}$  WD model.





**Figure 38.** Same as Figure 19, but for V705 Cas (open magenta squares for optical  $V$  and circles for UV). We also plot (a) the visual magnitudes (magenta dots for V705 Cas and blue dots for PW Vul). The data of V705 Cas and PW Vul are the same as those in Figure 13 of Hachisu & Kato (2015). In panel (a), taking  $(m - M)_V = 13.45$  for V705 Cas, we plot model light curves (solid magenta lines) of a  $0.78 M_{\odot}$  WD with the envelope chemical composition of CO nova 4 (Hachisu & Kato 2015). We also add a  $0.83 M_{\odot}$  WD (solid blue lines) with the same chemical composition of CO nova 4, taking  $(m - M)_V = 13.0$  for PW Vul.

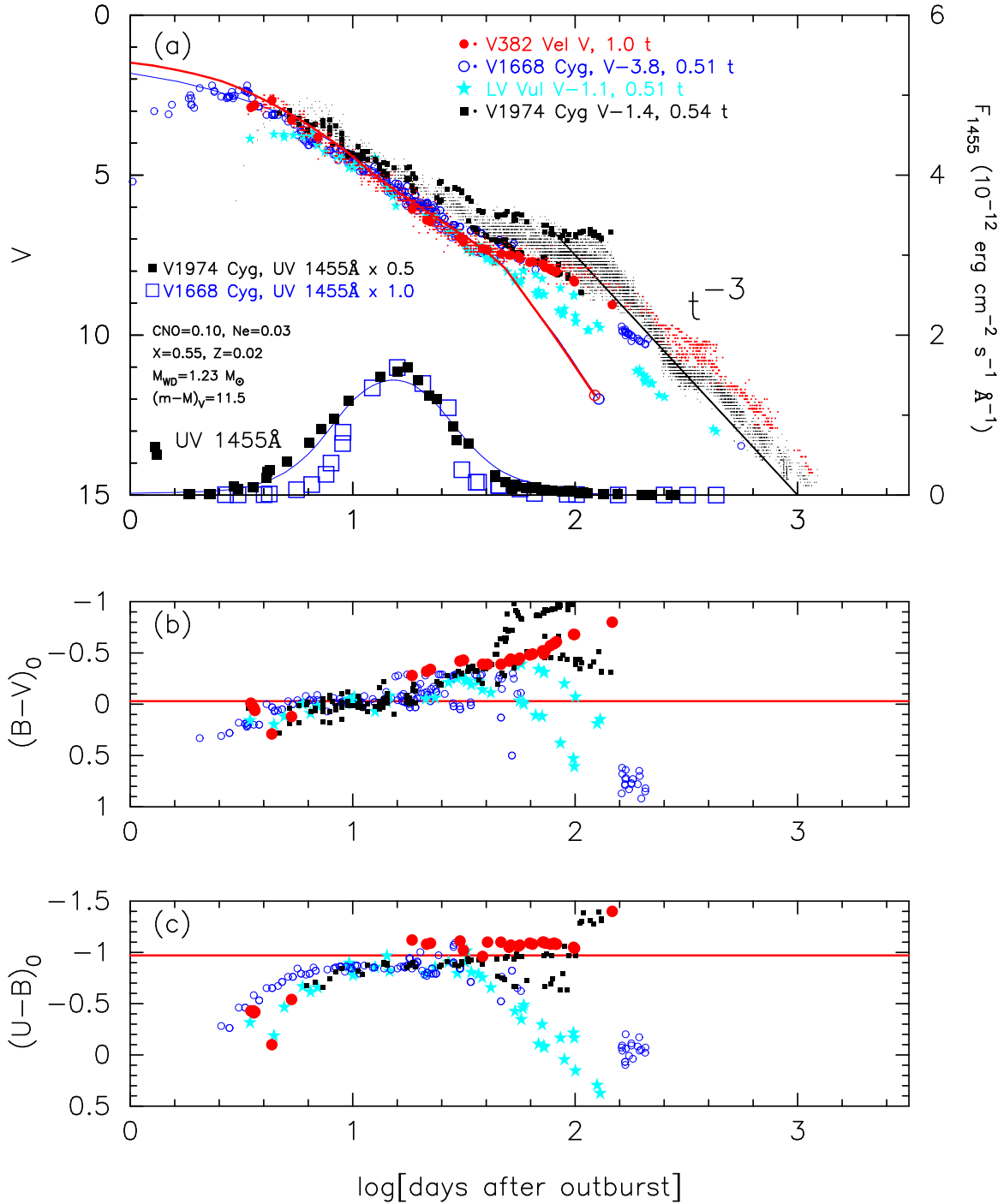


**Figure 39.** Same as Figure 19, but for V382 Vel. We also plot (a) the visual magnitudes (red dots for V382 Vel, blue dots for V1668 Cyg, and black dots for V1974 Cyg). The sources of V382 Vel data are the same as those in Figure 39 of Paper II. The other data are the same as those in Figures 19 and 23. Taking  $(m - M)_V = 11.5$  for V382 Vel, we plot a  $1.23 M_\odot$  WD model (solid red lines) with the chemical composition of Ne nova 2 (Hachisu & Kato 2010). We also add a  $0.98 M_\odot$  WD model (solid blue lines) with the chemical composition of CO nova 3 (Hachisu & Kato 2016a), taking  $(m - M)_V = 14.6$  for V1668 Cyg. We add a straight solid black line labeled “ $t^{-3}$ ” that indicates the homologously expanding ejecta, i.e., free expansion, after the optically thick winds stop.

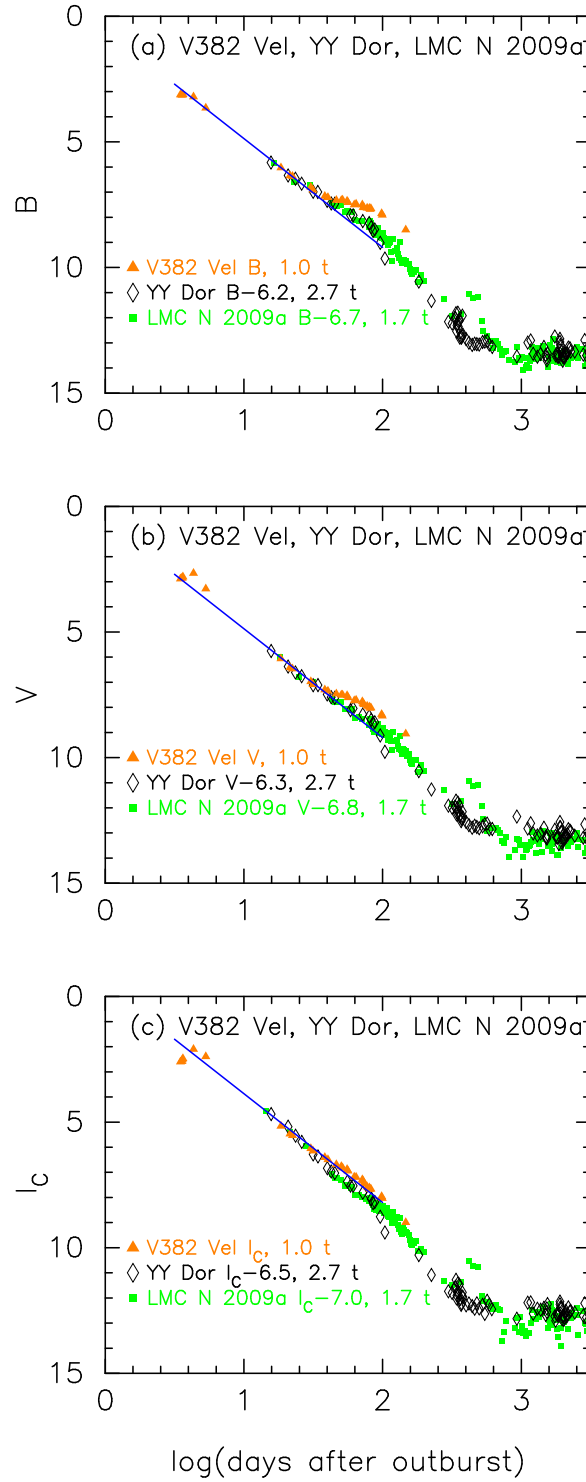


**Figure 40.** Same as Figure 21, but for V382 Vel. The  $BVI_C$  data of V382 Vel are taken from IAU Circular Nos. 7176, 7179, 7196, 7209, 7216, 7226, 7232, 7238, and 7277.

that indicates the homologously expanding ejecta, i.e., free expansion after the optically thick winds stop (see, e.g., Woodward et al. 1997; Hachisu & Kato 2006). The  $V$  light curves of these four novae roughly overlap each other except for the very early phase of LV Vul. Based on the time-stretching method, we have the relation of

$$(m - M)_{V,V382 \text{ Vel}}$$

$$\begin{aligned}
&= (m - M + \Delta V)_{V, \text{LV Vul}} - 2.5 \log 0.51 \\
&= 11.85 - 1.1 \pm 0.3 + 0.73 = 11.48 \pm 0.3 \\
&= (m - M + \Delta V)_{V, \text{V1668 Cyg}} - 2.5 \log 0.51 \\
&= 14.6 - 3.8 \pm 0.3 + 0.73 = 11.53 \pm 0.3 \\
&= (m - M + \Delta V)_{V, \text{V1974 Cyg}} - 2.5 \log 0.54 \\
&= 12.2 - 1.4 \pm 0.3 + 0.68 = 11.48 \pm 0.3.
\end{aligned} \tag{B43}$$

Thus, we obtain  $f_s = 0.51$  against the template nova LV Vul and  $(m - M)_V = 11.5 \pm 0.2$ . The result of  $(m - M)_V = 11.5 \pm 0.2$  is the same as  $(m - M)_V = 11.5 \pm 0.2$  in the previous work (Hachisu & Kato 2016a). From Equations (14) and (B43), we have the relation of

$$\begin{aligned}
&(m - M')_{V, \text{V382 Vel}} \\
&\equiv (m_V - (M_V - 2.5 \log f_s))_{\text{V382 Vel}} \\
&= ((m - M)_V + \Delta V)_{\text{LV Vul}} \\
&= 11.85 - 1.1 \pm 0.3 = 10.75 \pm 0.3.
\end{aligned} \tag{B44}$$

We obtain the reddening and distance from the time-stretching method. We plot the  $B$ ,  $V$ , and  $I_C$  light curves of V382 Vel together with those of the LMC novae YY Dor and LMC N 2009a in Figure 40. We apply Equation (7) for the  $B$  band to Figure 40(a) and obtain

$$\begin{aligned}
&(m - M)_{B, \text{V382 Vel}} \\
&= ((m - M)_B + \Delta B)_{\text{YY Dor}} - 2.5 \log 2.7 \\
&= 18.98 - 6.2 \pm 0.3 - 1.08 = 11.7 \pm 0.3 \\
&= ((m - M)_B + \Delta B)_{\text{LMC N 2009a}} - 2.5 \log 1.7 \\
&= 18.98 - 6.7 \pm 0.3 - 0.58 = 11.7 \pm 0.3.
\end{aligned} \tag{B45}$$

Thus, we obtain  $(m - M)_{B, \text{V382 Vel}} = 11.7 \pm 0.2$ . For the  $V$  light curves in Figure 40(b), we similarly obtain

$$\begin{aligned}
&(m - M)_{V, \text{V382 Vel}} \\
&= ((m - M)_V + \Delta V)_{\text{YY Dor}} - 2.5 \log 2.7 \\
&= 18.86 - 6.3 \pm 0.3 - 1.08 = 11.48 \pm 0.3 \\
&= ((m - M)_V + \Delta V)_{\text{LMC N 2009a}} - 2.5 \log 1.7 \\
&= 18.86 - 6.8 \pm 0.3 - 0.58 = 11.48 \pm 0.3.
\end{aligned} \tag{B46}$$

Thus, we obtain  $(m - M)_{V, \text{V382 Vel}} = 11.48 \pm 0.2$ . We apply Equation (8) for the  $I_C$  band to Figure 40(c) and obtain

$$\begin{aligned}
&(m - M)_{I, \text{V382 Vel}} \\
&= ((m - M)_I + \Delta I_C)_{\text{YY Dor}} - 2.5 \log 2.7 \\
&= 18.67 - 6.5 \pm 0.3 - 1.08 = 11.09 \pm 0.3 \\
&= ((m - M)_I + \Delta I_C)_{\text{LMC N 2009a}} - 2.5 \log 1.7 \\
&= 18.67 - 7.0 \pm 0.3 - 0.58 = 11.09 \pm 0.3.
\end{aligned} \tag{B47}$$

Thus, we obtain  $(m - M)_{I, \text{V382 Vel}} = 11.09 \pm 0.2$ .

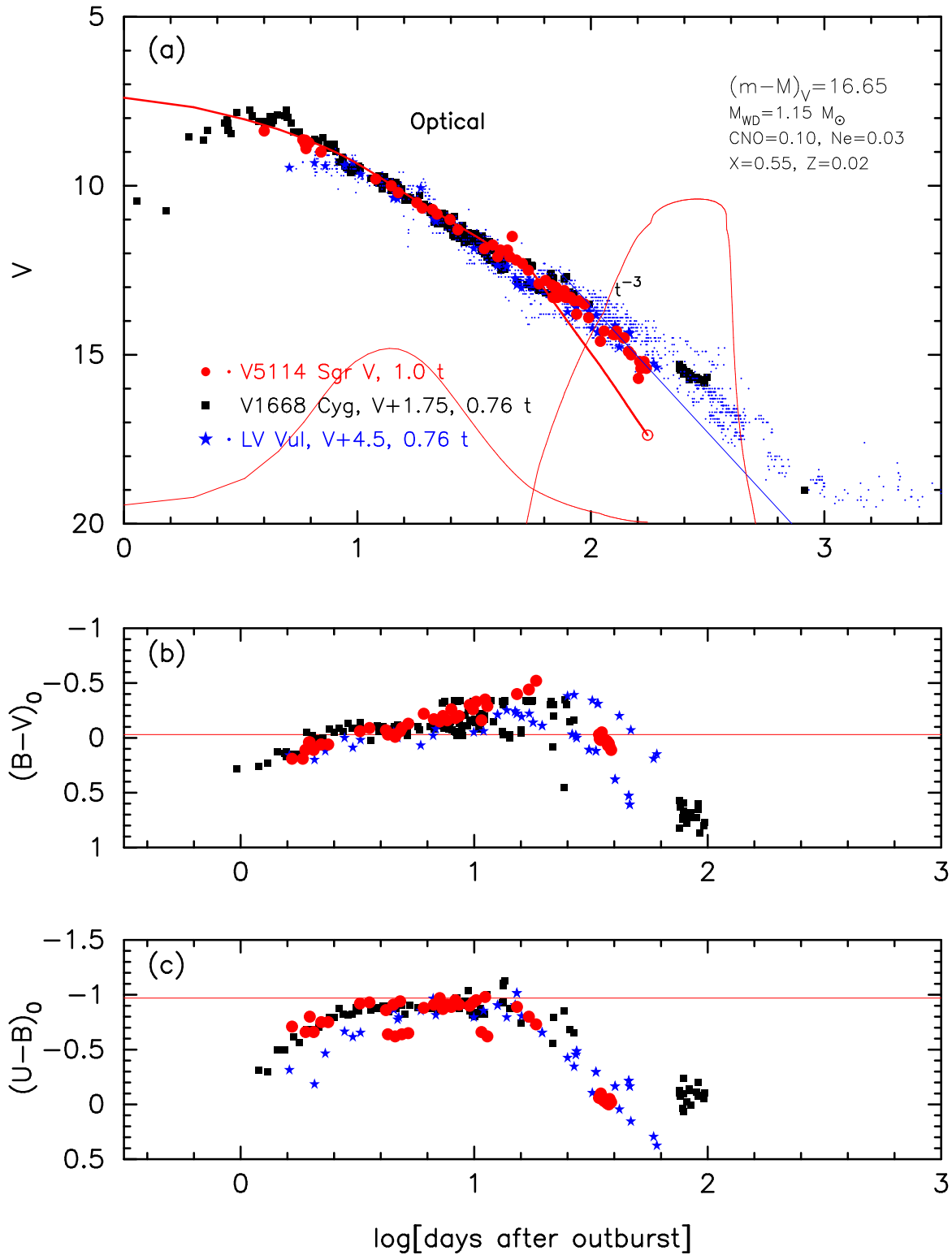
### B.7. V5114 Sgr 2004

Figure 41 shows the light/color curves of V5114 Sgr as well as LV Vul and V1668 Cyg. We regard that the  $V$  light curve of V5114 Sgr follows V1668 Cyg and LV Vul. Based on the time-stretching method, we have the relation of

$$\begin{aligned}
&(m - M)_{V, \text{V5114 Sgr}} \\
&= (m - M + \Delta V)_{V, \text{LV Vul}} - 2.5 \log 0.76 \\
&= 11.85 + 4.5 \pm 0.2 + 0.30 = 16.65 \pm 0.2 \\
&= (m - M + \Delta V)_{V, \text{V1668 Cyg}} - 2.5 \log 0.76 \\
&= 14.6 + 1.75 \pm 0.2 + 0.30 = 16.65 \pm 0.2.
\end{aligned} \tag{B48}$$

Thus, we obtain  $f_s = 0.76$  against the template nova LV Vul and  $(m - M)_V = 16.65 \pm 0.1$ . This value is slightly larger than the previous value of  $(m - M)_V = 16.5 \pm 0.1$  estimated by Hachisu & Kato (2016b). From Equations (14) and (B48), we have the relation of

$$(m - M')_{V, \text{V5114 Sgr}}$$



**Figure 41.** Same as Figure 19, but for V5114 Sgr (filled red circles). The data of V5114 Sgr are the same as in Figure 52 of Paper II, which were taken from Ederoclite et al. (2006), SMARTS (Walter et al. 2012), and IAU Circular Nos. 8306 and 8310. Adopting  $(m-M)_V = 16.65$  for V5114 Sgr, we plot a  $1.15 M_{\odot}$  WD model (solid red lines) with the chemical composition of Ne nova 2 (Hachisu & Kato 2010). We add the UV 1455Å flux (left thin solid red line) and supersoft X-ray flux (right thin solid red line) of the  $1.15 M_{\odot}$  WD model.

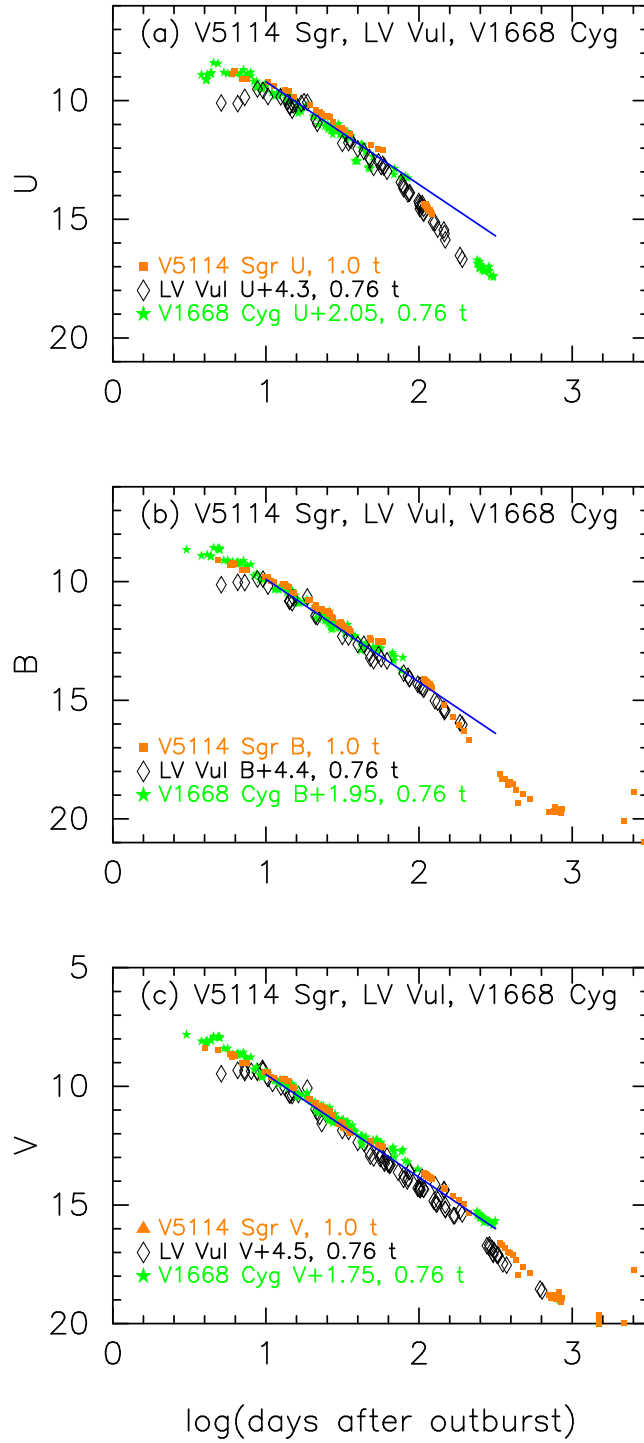


**Figure 42.** The  $UBV$  light curves of V5114 Sgr are plotted together with those of LV Vul and V1668 Cyg. The  $UBV$  data of V5114 Sgr are taken from Ederoclite et al. (2006) and IAU Circular No. 8310. The  $BV$  data of V5114 Sgr are taken from SMARTS (Walter et al. 2012) and IAU Circular No. 8306.

$$\begin{aligned}
 &\equiv (m_V - (M_V - 2.5 \log f_s))_{V5114 \text{ Sgr}} \\
 &= (m - M + \Delta V)_{V, LV \text{ Vul}} \\
 &= 11.85 + 4.5 \pm 0.2 = 16.35 \pm 0.2.
 \end{aligned}
 \tag{B49}$$

We obtain the reddening and distance from the time-stretching method. We plot the  $U$ ,  $B$ , and  $V$  light curves of V5114 Sgr together with those of LV Vul and V1668 Cyg in Figure 42. We apply Equation (6) for the  $U$  band to Figure 42(a) and obtain

$$\begin{aligned}
 (m - M)_{U, V5114 \text{ Sgr}} &= ((m - M)_U + \Delta U)_{LV \text{ Vul}} - 2.5 \log 0.76 \\
 &= 12.85 + 4.3 \pm 0.2 + 0.30 = 17.45 \pm 0.2 \\
 &= ((m - M)_U + \Delta U)_{V1668 \text{ Cyg}} - 2.5 \log 0.76 \\
 &= 15.1 + 2.05 \pm 0.2 + 0.30 = 17.45 \pm 0.2,
 \end{aligned} \tag{B50}$$

where we adopt  $(m - M)_{U, LV \text{ Vul}} = 11.85 + (4.75 - 3.1) \times 0.60 = 12.85$ , and  $(m - M)_{U, V1668 \text{ Cyg}} = 14.6 + (4.75 - 3.1) \times 0.30 = 15.10$ . Thus, we obtain  $(m - M)_{U, V5114 \text{ Sgr}} = 17.45 \pm 0.2$ . For the  $B$  light curves in Figure 42(b), we similarly obtain

$$\begin{aligned}
 (m - M)_{B, V5114 \text{ Sgr}} &= ((m - M)_B + \Delta B)_{LV \text{ Vul}} - 2.5 \log 0.76 \\
 &= 12.45 + 4.4 \pm 0.2 + 0.30 = 17.15 \pm 0.2 \\
 &= ((m - M)_B + \Delta B)_{LMC \text{ N } 2009a} - 2.5 \log 0.76 \\
 &= 14.9 + 1.95 \pm 0.2 + 0.30 = 17.15 \pm 0.2,
 \end{aligned} \tag{B51}$$

where we adopt  $(m - M)_{B, LV \text{ Vul}} = 11.85 + 1.0 \times 0.6 = 12.45$  and  $(m - M)_{B, V1668 \text{ Cyg}} = 14.6 + 1.0 \times 0.3 = 14.9$ . Thus, we obtain  $(m - M)_{B, V5114 \text{ Sgr}} = 17.15 \pm 0.2$ . We apply Equation (4) to Figure 42(c) and obtain

$$\begin{aligned}
 (m - M)_{V, V5114 \text{ Sgr}} &= ((m - M)_V + \Delta V)_{LV \text{ Vul}} - 2.5 \log 0.76 \\
 &= 11.85 + 4.5 \pm 0.2 + 0.30 = 16.65 \pm 0.2 \\
 &= ((m - M)_V + \Delta V)_{V1668 \text{ Cyg}} - 2.5 \log 0.76 \\
 &= 14.6 + 1.75 \pm 0.2 + 0.30 = 16.65 \pm 0.2.
 \end{aligned} \tag{B52}$$

Thus, we obtain  $(m - M)_{V, V5114 \text{ Sgr}} = 16.65 \pm 0.2$ . This result is essentially the same as that in Equation (B48). We plot these three distance moduli of  $U$ ,  $B$ , and  $V$  bands in Figure 12(c) by the magenta, cyan, and blue lines, that is,  $(m - M)_U = 17.45$ ,  $(m - M)_B = 17.15$ , and  $(m - M)_V = 16.65$  together with Equations (10), (11), and (5), respectively. These three lines cross at  $d = 10.9$  kpc and  $E(B - V) = 0.47$ .

### B.8. V2362 Cyg 2006

Figure 43 shows the light/color curves of V2362 Cyg on a logarithmic timescale as well as LV Vul and V1500 Cyg. We regard that the  $V$  light curve of V2362 Cyg follows that of V1500 Cyg. Based on the time-stretching method, we have the relation of

$$\begin{aligned}
 (m - M)_{V, V2362 \text{ Cyg}} &= (m - M + \Delta V)_{V, LV \text{ Vul}} - 2.5 \log 1.78 \\
 &= 11.85 + 4.2 \pm 0.3 - 0.63 = 15.42 \pm 0.3 \\
 &= (m - M + \Delta V)_{V, V1500 \text{ Cyg}} - 2.5 \log 2.95 \\
 &= 12.3 + 4.3 \pm 0.2 - 1.18 = 15.42 \pm 0.2.
 \end{aligned} \tag{B53}$$

Thus, we obtain  $f_s = 1.78$  against the template nova LV Vul and  $(m - M)_V = 15.4 \pm 0.2$ .

This new distance modulus in the  $V$  band is smaller than the previous value of  $(m - M)_V = 15.9 \pm 0.1$  in Paper II, because we improved both the timescaling factor of  $f_s$  and the vertical fit of  $\Delta V$ . The LV Vul upper branch in the time-stretched color-magnitude diagram corresponds to the redder (lower) branch after the onset of the nebular phase in the  $(B - V)_0$  color curves of Figure 43(b). We regard that the V2362 Cyg color curves overlap with this redder branch of LV Vul in the  $(B - V)_0$  color curve. Thus, we have more carefully determined the timescaling factor of  $f_s$  than the previous work (Paper II).

From Equations (14) and (B53), we obtain the relation of

$$(m - M')_{V, V2362 \text{ Cyg}}$$

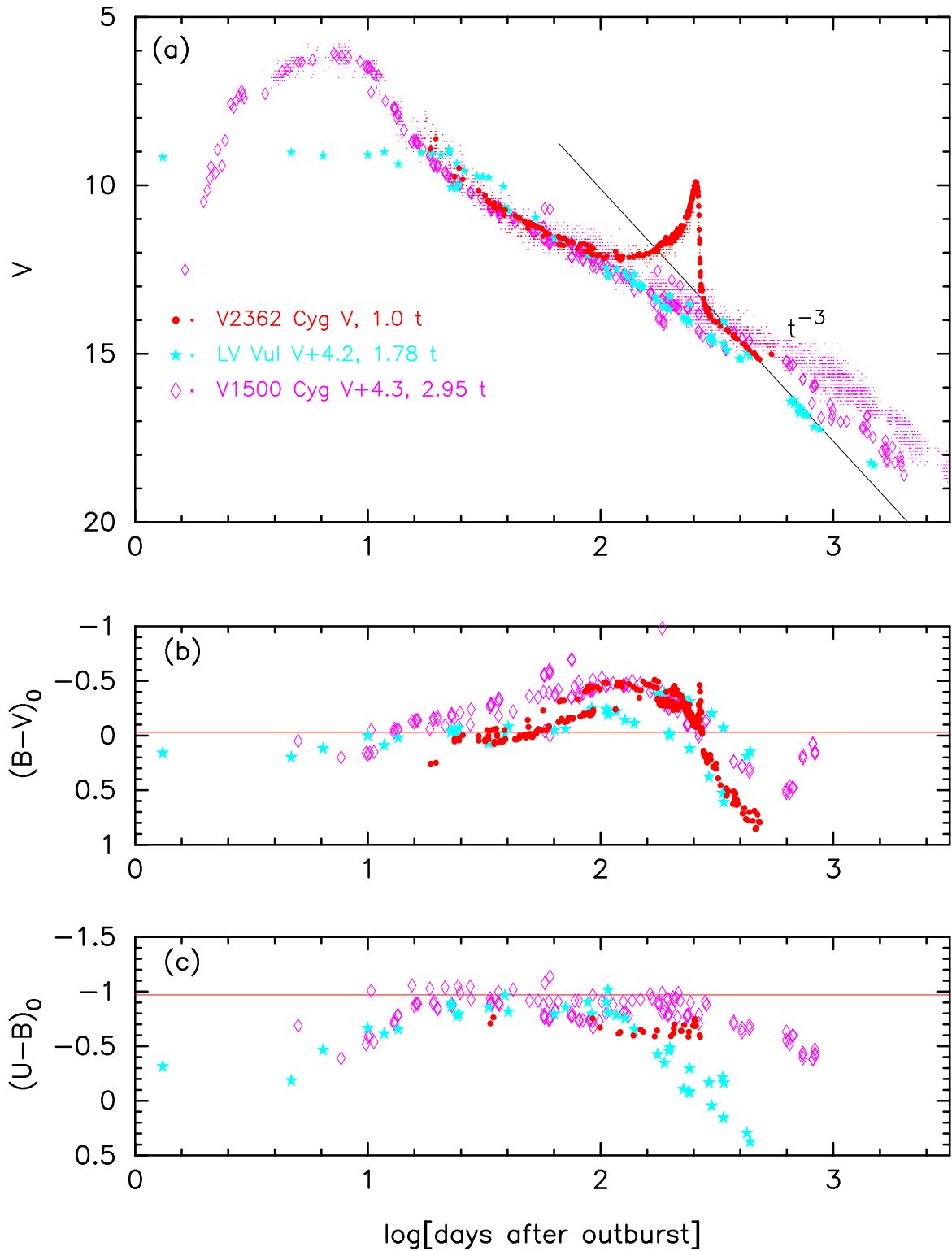


**Figure 43.** Same as Figure 19, but for V2362 Cyg (filled red circles) as well as LV Vul and V1500 Cyg. The  $(B - V)_0$  and  $(U - B)_0$  data of V2362 Cyg are dereddened with  $E(B - V) = 0.60$ . The data of V1500 Cyg and V2362 Cyg are the same as those in Figure 6 of Paper I and Figure 54 of Paper II, respectively. The free-free flux decays along the  $F_\nu \propto t^{-3}$  line after optically thick winds stop. See text for detail.



$$\begin{aligned}
 &\equiv (m_V - (M_V - 2.5 \log f_s))_{V2362 \text{ Cyg}} \\
 &= (m - M + \Delta V)_{V, LV \text{ Vul}} \\
 &= 11.85 + 4.2 \pm 0.3 = 16.05 \pm 0.3.
 \end{aligned} \tag{B54}$$

### B.9. V2615 Oph 2007

Figure 44 shows the light/color curves of V2615 Oph as well as LV Vul and V1419 Aql. The colors of V2615 Oph are dereddened with  $E(B - V) = 0.90$  as obtained in Section 7.9. The  $BV$  light curve data of this nova were obtained by Munari et al. (2008a). However, their  $B - V$  data show systematic differences among three observatories, a, b, and c (see their Figure 1). So, we shift the  $B - V$  data of group ‘‘a’’ (filled red circles in Figure 15(a)) by 0.15 mag bluer. The  $B - V$  data of group ‘‘b’’ and ‘‘c’’ (filled blue circles in Figure 15(a)) are not shifted. As a result, the  $B - V$  data of these three groups broadly overlap each other in Figures 44(b) and 15(a). We also add the  $V$  data taken from SMARTS (Walter et al. 2012). Based on the time-stretching method, we have the relation of

$$\begin{aligned}
 &(m - M)_{V, V2615 \text{ Oph}} \\
 &= (m - M + \Delta V)_{V, LV \text{ Vul}} - 2.5 \log 1.58 \\
 &= 11.85 + 4.6 \pm 0.2 - 0.50 = 15.95 \pm 0.2 \\
 &= (m - M + \Delta V)_{V, V1419 \text{ Aql}} - 2.5 \log 1.12 \\
 &= 15.0 + 1.1 \pm 0.2 - 0.13 = 15.97 \pm 0.2.
 \end{aligned} \tag{B55}$$

Thus, we obtain  $f_s = 1.58$  against the template nova LV Vul and  $(m - M)_V = 15.95 \pm 0.2$ . This value is smaller than the previous estimate of  $(m - M)_V = 16.5 \pm 0.1$  (Paper II). This is due not only to our careful  $(B - V)_0$  fitting that improves the timescaling factor of  $f_s$  but also to the revised vertical  $V$  fit to the LV Vul light curve. From Equations (14) and (B55), we have the relation of

$$\begin{aligned}
 &(m - M')_{V, V2615 \text{ Oph}} \\
 &\equiv (m_V - (M_V + 2.5 \log f_s))_{V2615 \text{ Oph}} \\
 &= (m - M + \Delta V)_{V, LV \text{ Vul}} \\
 &= 11.85 + 4.6 \pm 0.2 = 16.45 \pm 0.2.
 \end{aligned} \tag{B56}$$

We obtain the reddening and distance from the time-stretching method. We plot the  $B$ ,  $V$ , and  $I_C$  light curves of V2615 Oph together with those of V1368 Cen, V834 Car, and the LMC novae, YY Dor and LMC N 2009a, in Figure 45 on a logarithmic timescale. We apply Equation (7) for the  $B$  band to Figure 45(a) and obtain

$$\begin{aligned}
 &(m - M)_{B, V2615 \text{ Oph}} \\
 &= ((m - M)_B + \Delta B)_{V1368 \text{ Cen}} - 2.5 \log 0.66 \\
 &= 18.53 - 2.1 \pm 0.4 + 0.45 = 16.88 \pm 0.3 \\
 &= ((m - M)_B + \Delta B)_{V834 \text{ Car}} - 2.5 \log 2.5 \\
 &= 17.75 + 0.1 \pm 0.4 - 0.97 = 16.88 \pm 0.3 \\
 &= ((m - M)_B + \Delta B)_{YY \text{ Dor}} - 2.5 \log 8.3 \\
 &= 18.98 + 0.2 \pm 0.4 - 2.3 = 16.88 \pm 0.3 \\
 &= ((m - M)_B + \Delta B)_{LMC \text{ N } 2009a} - 2.5 \log 5.2 \\
 &= 18.98 - 0.3 \pm 0.4 - 1.8 = 16.88 \pm 0.3,
 \end{aligned} \tag{B57}$$

where we adopt  $(m - M)_{B, V1368 \text{ Cen}} = 17.6 + 0.93 = 18.53$  and  $(m - M)_{B, V834 \text{ Car}} = 17.25 + 0.50 = 17.75$  from Hachisu & Kato (2019). Thus, we obtain  $(m - M)_{B, V2615 \text{ Oph}} = 16.88 \pm 0.2$ . For the  $V$  light curves in Figure 45(b), we similarly obtain

$$\begin{aligned}
 &(m - M)_{V, V2615 \text{ Oph}} \\
 &= ((m - M)_V + \Delta V)_{V1368 \text{ Cen}} - 2.5 \log 0.66 \\
 &= 17.6 - 2.1 \pm 0.3 + 0.45 = 15.95 \pm 0.3 \\
 &= ((m - M)_V + \Delta V)_{V834 \text{ Car}} - 2.5 \log 2.5 \\
 &= 17.25 - 0.3 \pm 0.3 - 0.97 = 15.98 \pm 0.3 \\
 &= ((m - M)_V + \Delta V)_{YY \text{ Dor}} - 2.5 \log 8.3
 \end{aligned}$$

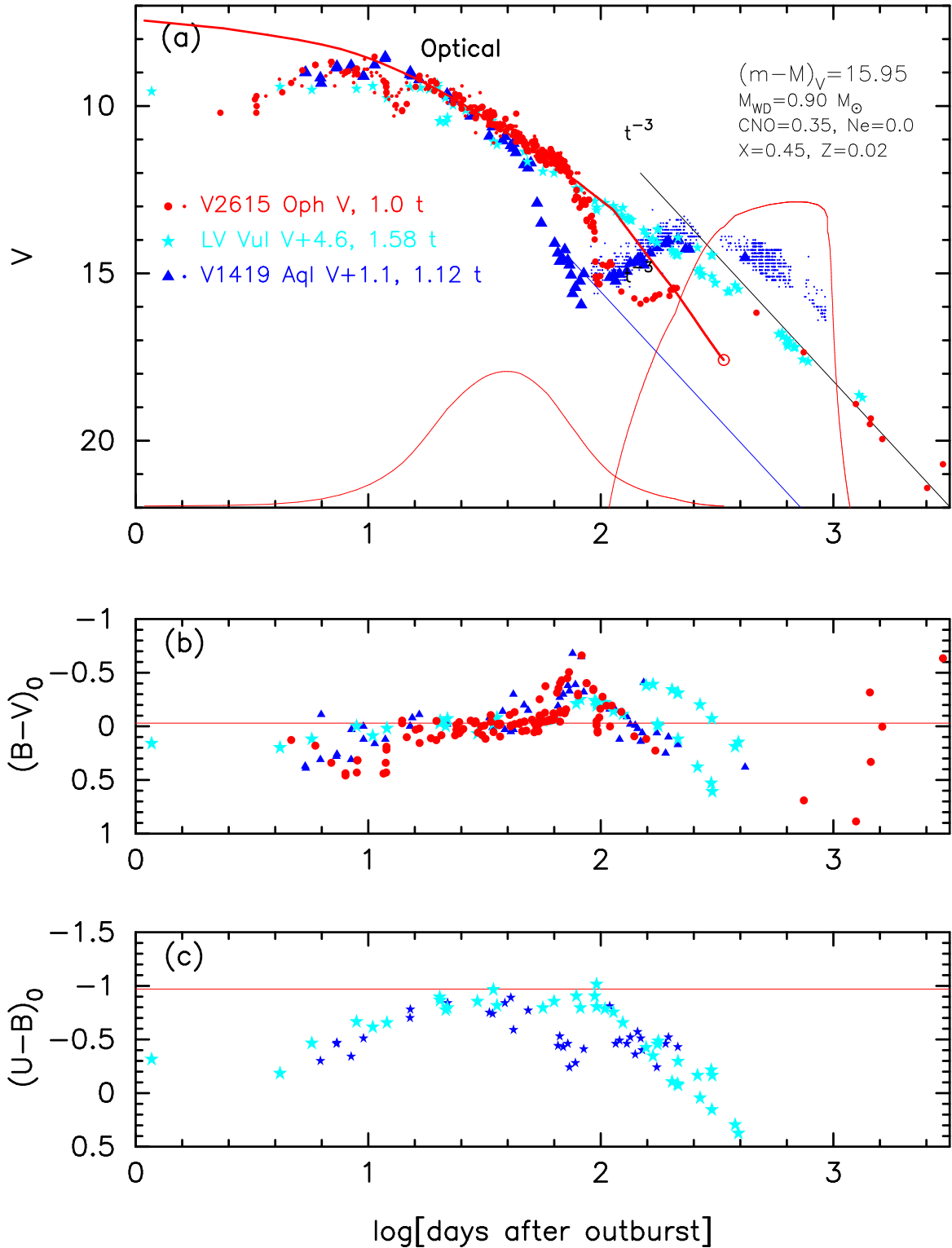


**Figure 44.** Same as Figure 19, but for V2615 Oph (filled red circles for V and small red dots for visual). The data of V2615 Oph are the same as those in Figure 63 of Paper II, but only the  $B - V$  data (filled red circles in Figure 15(a)) of group “a” of Munari et al. (2008a) are shifted by 0.15 mag bluer to overlap them to the other  $B - V$  data of group “b” and “c” (filled blue circles in Figure 15(a)). The other nova data are the same as those in Figure 37. We plot a  $0.90 M_{\odot}$  WD model (solid red lines) with the chemical composition of CO nova 3 (Hachisu & Kato 2016a), taking  $(m - M)_V = 15.95$  for V2615 Oph. We add the UV 1455Å flux (left thin solid red line) and supersoft X-ray flux (right thin solid red line) of the  $0.90 M_{\odot}$  WD model. See the text for more details.

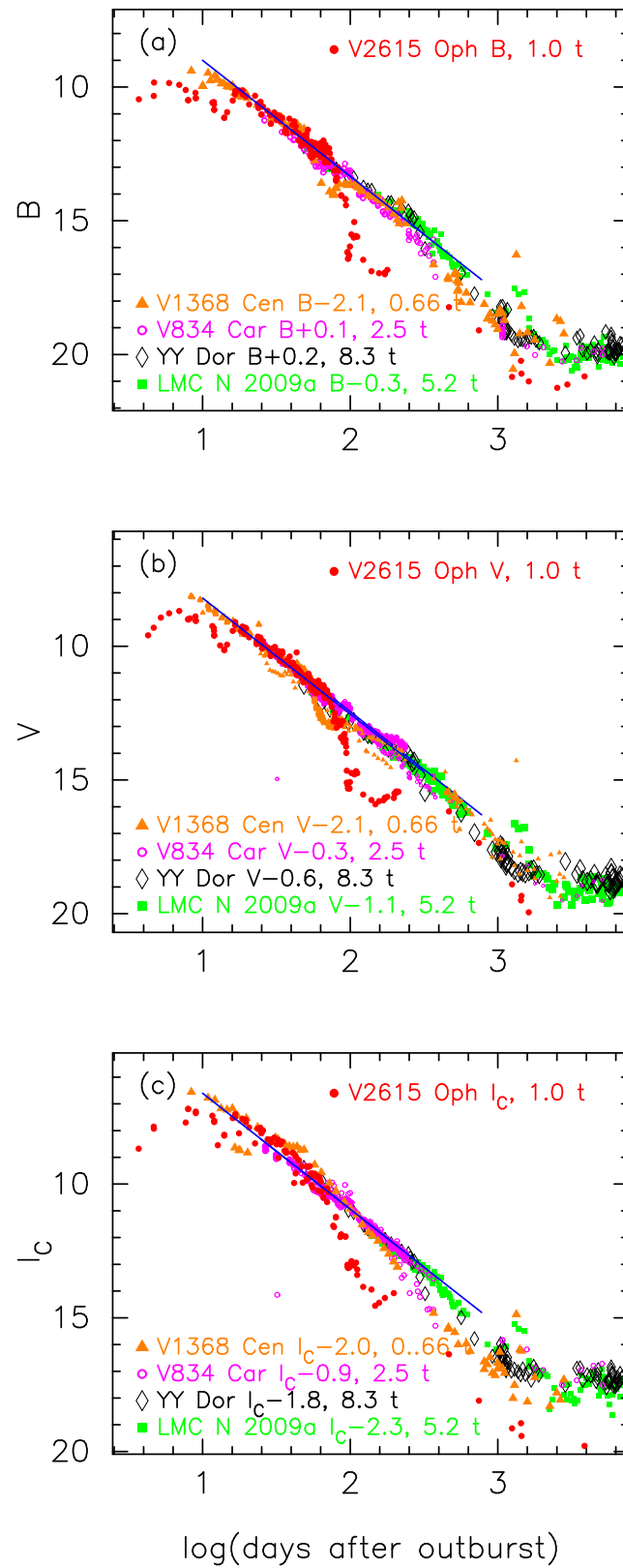


**Figure 45.** The  $BVI_C$  light curves of V2615 Oph are plotted together with those of V1368 Cen, V834 Car, YY Dor, and LMC N 2009a. The  $BVI_C$  data of V2615 Oph are taken from [Munari et al. \(2008a\)](#). The  $BVI_C$  data of V2615 Oph are also taken from SMARTS, AAVSO, and VSOLJ. The  $BVI_C$  data of V834 Car and V1368 Cen are taken from SMARTS and AAVSO.

$$\begin{aligned}
&= 18.86 - 0.6 \pm 0.3 - 2.3 = 15.96 \pm 0.3 \\
&= ((m - M)_V + \Delta V)_{\text{LMC N 2009a}} - 2.5 \log 5.2 \\
&= 18.86 - 1.1 \pm 0.3 - 1.8 = 15.96 \pm 0.3,
\end{aligned} \tag{B58}$$

where we adopt  $(m - M)_{V, V1368 \text{ Cen}} = 17.6$  and  $(m - M)_{V, V834 \text{ Car}} = 17.25$  from Hachisu & Kato (2019). Thus, we obtain  $(m - M)_{V, V2615 \text{ Oph}} = 15.96 \pm 0.2$ , being consistent with Equation (B55). We apply Equation (8) for the  $I_C$  band to Figure 45(c) and obtain

$$\begin{aligned}
&(m - M)_{I, V2615 \text{ Oph}} \\
&= ((m - M)_I + \Delta I_C)_{V1368 \text{ Cen}} - 2.5 \log 0.66 \\
&= 16.11 - 2.0 \pm 0.5 + 0.45 = 14.56 \pm 0.3 \\
&= ((m - M)_I + \Delta I_C)_{V834 \text{ Car}} - 2.5 \log 2.5 \\
&= 16.45 - 0.9 \pm 0.5 - 0.97 = 14.58 \pm 0.3 \\
&= ((m - M)_I + \Delta I_C)_{\text{YY Dor}} - 2.5 \log 8.3 \\
&= 18.67 - 1.8 \pm 0.5 - 2.3 = 14.57 \pm 0.3 \\
&= ((m - M)_I + \Delta I_C)_{\text{LMC N 2009a}} - 2.5 \log 5.2 \\
&= 18.67 - 2.3 \pm 0.5 - 1.8 = 14.57 \pm 0.3,
\end{aligned} \tag{B59}$$

where we adopt  $(m - M)_{I, V1368 \text{ Cen}} = 17.6 - 1.6 \times 0.93 = 16.11$ , and  $(m - M)_{I, V834 \text{ Car}} = 17.25 - 1.6 \times 0.50 = 16.45$  from Hachisu & Kato (2019). Thus, we obtain  $(m - M)_{I, V2615 \text{ Oph}} = 14.57 \pm 0.2$ . We plot these three distance moduli in Figure 14(a) by the thin solid magenta, blue, and cyan lines. These three lines cross at  $d = 4.3$  kpc and  $E(B - V) = 0.90$ .

#### B.10. V2468 Cyg 2008#1

Figure 46 shows the light/color curves of V2468 Cyg as well as LV Vul and V1500 Cyg. The  $(B - V)_0$  color is dereddened with  $E(B - V) = 0.65$  as obtained in Section 7.10. We regard that the early phase of the V2468 Cyg  $V$  light curve is superbright like V1500 Cyg and then oscillates between LV Vul and V1500 Cyg in the phase of  $\log t$  (day) = 1.0–2.0. The spectra of V1500 Cyg during the superbright phase (until day  $\sim 5$  and above the model  $V$  light curve of red line) are approximated with blackbody (Gallagher & Ney 1976; Ennis et al. 1977). After the superbright phase ended, the spectrum of V1500 Cyg changed to be of free-free emission, so that  $V$  magnitudes are fitted with our model light curve (solid red line). Our time-stretching method is applicable to the part of free-free emission dominated phase of optical light curves.

Based on the time-stretching method, we have the relation of

$$\begin{aligned}
&(m - M)_{V, V2468 \text{ Cyg}} \\
&= (m - M + \Delta V)_{V, \text{LV Vul}} - 2.5 \log 2.4 \\
&= 11.85 + 5.3 \pm 0.3 - 0.95 = 16.2 \pm 0.3 \\
&= (m - M + \Delta V)_{V, V1500 \text{ Cyg}} - 2.5 \log 4.0 \\
&= 12.3 + 5.4 \pm 0.3 - 1.5 = 16.2 \pm 0.3.
\end{aligned} \tag{B60}$$

Thus, we obtain  $f_s = 2.4$  against the template nova LV Vul and  $(m - M)_V = 16.2 \pm 0.2$ . The newly obtained value is larger than the previous value of  $(m - M)_V = 15.6 \pm 0.1$  estimated in Paper II because we improved the timescaling factor  $f_s$  and the vertical  $\Delta V$  fit. From Equations (14) and (B60), we have the relation of

$$\begin{aligned}
&(m - M')_{V, V2468 \text{ Cyg}} \\
&\equiv (m_V - (M_V - 2.5 \log f_s))_{V2468 \text{ Cyg}} \\
&= (m - M + \Delta V)_{V, \text{LV Vul}} \\
&= 11.85 + 5.3 \pm 0.3 = 17.15 \pm 0.3.
\end{aligned} \tag{B61}$$

We obtain the reddening and distance from the time-stretching method. We plot the  $B$ ,  $V$ , and  $I_C$  light curves of V2468 Cyg together with those of V1535 Sco, V834 Car, and the LMC novae, YY Dor and LMC N 2009a, in Figure 47 on a logarithmic timescale. We apply Equation (7) for the  $B$  band to Figure 47(a) and obtain

$$(m - M)_{B, V2468 \text{ Cyg}}$$

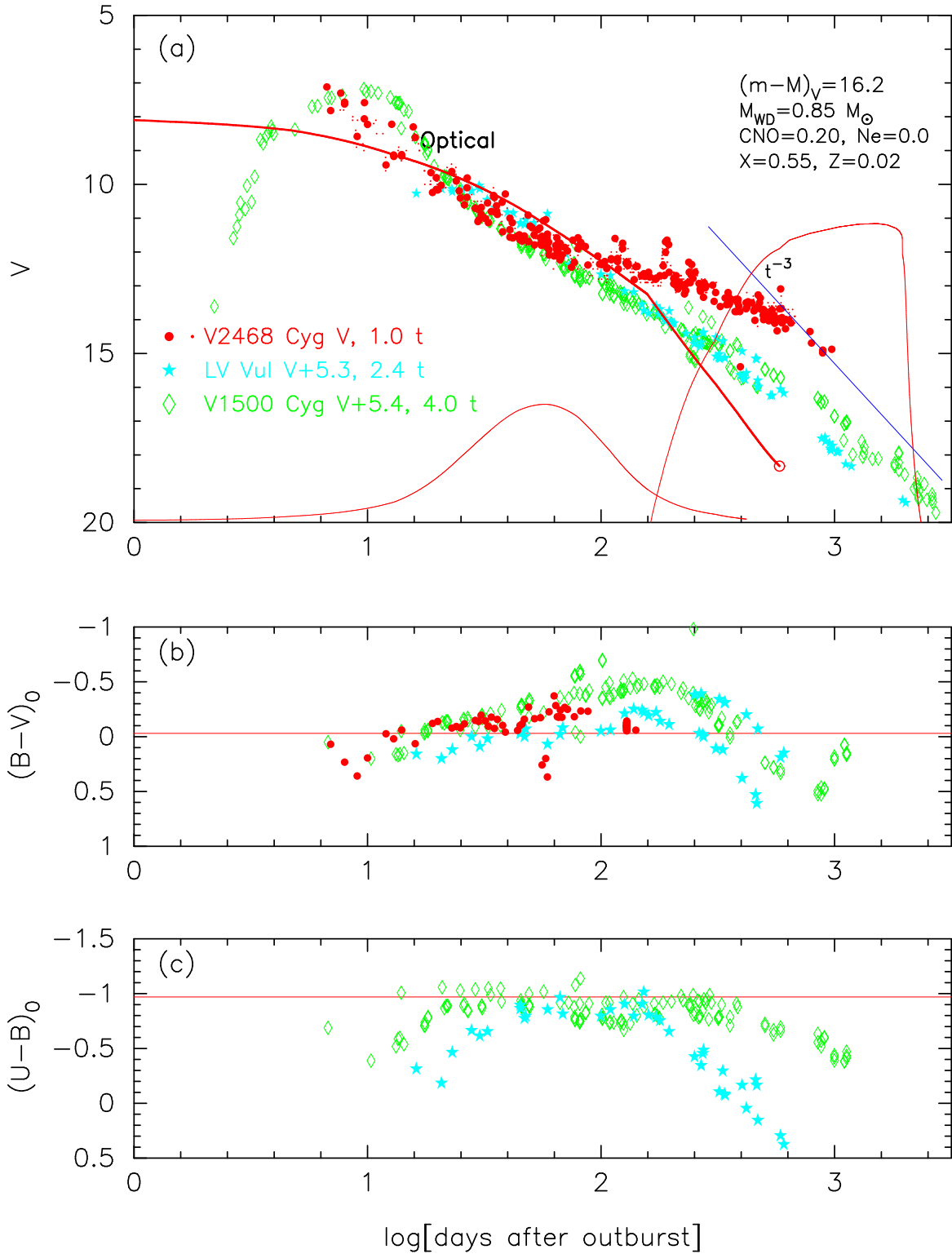


**Figure 46.** Same as Figure 19, but for V2468 Cyg (filled red circles for V and small red dots for visual). The data of V2468 Cyg are the same as those in Figure 68 of Paper II. We plot a 0.85  $M_{\odot}$  WD model (solid red lines) with the chemical composition of CO nova 4 (Hachisu & Kato 2015), taking  $(m - M)_V = 16.2$  for V2468 Cyg. We add the UV 1455Å flux (left thin solid red line) and supersoft X-ray flux (right thin solid red line) of the 0.85  $M_{\odot}$  WD model. See text for more details.

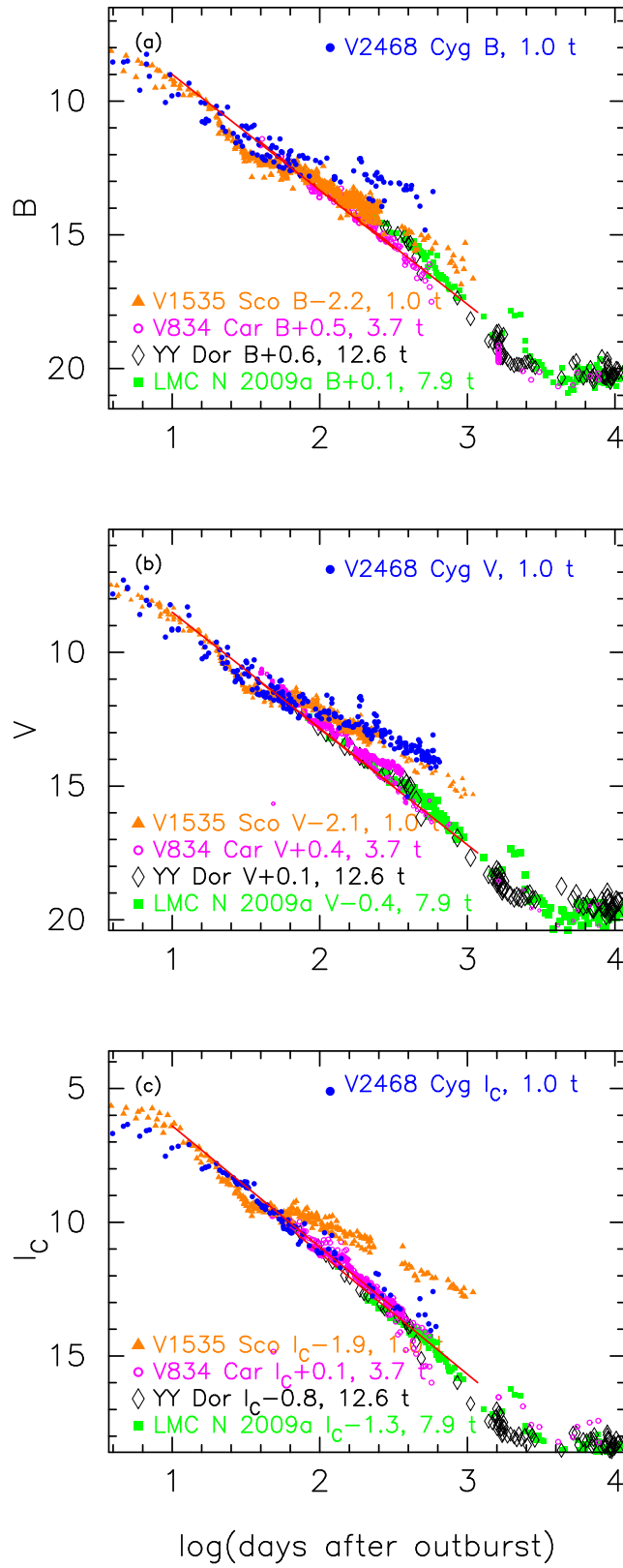


**Figure 47.** The  $BVI_C$  light curves of V2468 Cyg are plotted together with those of V1535 Sco, V834 Car, YY Dor, and LMC N 2009a. The  $BVI_C$  data of V2468 Cyg are taken from AAVSO and VSOLJ. The  $BVI_C$  data of V834 Car are taken from SMARTS and AAVSO. The  $BVI_C$  data of V1535 Sco are taken from SMARTS, AAVSO, and VSOLJ.

$$\begin{aligned}
 &= ((m - M)_B + \Delta B)_{V1535 \text{ Sco}} - 2.5 \log 1.0 \\
 &= 19.08 - 2.2 \pm 0.4 - 0.0 = 16.88 \pm 0.3 \\
 &= ((m - M)_B + \Delta B)_{V834 \text{ Car}} - 2.5 \log 3.7 \\
 &= 17.75 + 0.5 \pm 0.4 - 1.42 = 16.83 \pm 0.3 \\
 &= ((m - M)_B + \Delta B)_{YY \text{ Dor}} - 2.5 \log 12.6 \\
 &= 18.98 + 0.6 \pm 0.4 - 2.75 = 16.83 \pm 0.3 \\
 &= ((m - M)_B + \Delta B)_{LMC \text{ N } 2009a} - 2.5 \log 7.9 \\
 &= 18.98 + 0.1 \pm 0.4 - 2.25 = 16.83 \pm 0.3,
 \end{aligned} \tag{B62}$$

where we adopt  $(m - M)_{B,V1535 \text{ Sco}} = 18.3 + 0.78 = 19.08$  and  $(m - M)_{B,V834 \text{ Car}} = 17.25 + 0.50 = 17.75$  from [Hachisu & Kato \(2019\)](#). Thus, we obtain  $(m - M)_{B,V2468 \text{ Cyg}} = 16.85 \pm 0.2$ . For the  $V$  light curves in Figure 47(b), we similarly obtain

$$\begin{aligned}
 &(m - M)_{V,V2468 \text{ Cyg}} \\
 &= ((m - M)_V + \Delta V)_{V1535 \text{ Sco}} - 2.5 \log 1.0 \\
 &= 18.3 - 2.1 \pm 0.3 - 0.0 = 16.2 \pm 0.3 \\
 &= ((m - M)_V + \Delta V)_{V834 \text{ Car}} - 2.5 \log 3.7 \\
 &= 17.25 + 0.4 \pm 0.3 - 1.42 = 16.23 \pm 0.3 \\
 &= ((m - M)_V + \Delta V)_{YY \text{ Dor}} - 2.5 \log 12.6 \\
 &= 18.86 + 0.1 \pm 0.3 - 2.75 = 16.21 \pm 0.3 \\
 &= ((m - M)_V + \Delta V)_{LMC \text{ N } 2009a} - 2.5 \log 7.9 \\
 &= 18.86 - 0.4 \pm 0.3 - 2.25 = 16.21 \pm 0.3,
 \end{aligned} \tag{B63}$$

where we adopt  $(m - M)_{V,V1535 \text{ Sco}} = 18.3$  and  $(m - M)_{V,V834 \text{ Car}} = 17.25$  from [Hachisu & Kato \(2019\)](#). Thus, we obtain  $(m - M)_{V,V2468 \text{ Cyg}} = 16.21 \pm 0.2$ , being consistent with Equation (B60). We apply Equation (8) for the  $I_C$  band to Figure 47(c) and obtain

$$\begin{aligned}
 &(m - M)_{I,V2468 \text{ Cyg}} \\
 &= ((m - M)_I + \Delta I_C)_{V1535 \text{ Sco}} - 2.5 \log 1.0 \\
 &= 17.05 - 1.9 \pm 0.5 - 0.0 = 15.15 \pm 0.3 \\
 &= ((m - M)_I + \Delta I_C)_{V834 \text{ Car}} - 2.5 \log 3.7 \\
 &= 16.45 + 0.1 \pm 0.5 - 1.42 = 15.13 \pm 0.3 \\
 &= ((m - M)_I + \Delta I_C)_{YY \text{ Dor}} - 2.5 \log 12.6 \\
 &= 18.67 - 0.8 \pm 0.5 - 2.75 = 15.12 \pm 0.3 \\
 &= ((m - M)_I + \Delta I_C)_{LMC \text{ N } 2009a} - 2.5 \log 7.9 \\
 &= 18.67 - 1.3 \pm 0.5 - 2.25 = 15.12 \pm 0.3,
 \end{aligned} \tag{B64}$$

where we adopt  $(m - M)_{I,V1535 \text{ Sco}} = 18.3 - 1.6 \times 0.78 = 17.05$ , and  $(m - M)_{I,V834 \text{ Car}} = 17.25 - 1.6 \times 0.50 = 16.45$  from [Hachisu & Kato \(2019\)](#). Thus, we obtain  $(m - M)_{I,V2468 \text{ Cyg}} = 15.13 \pm 0.2$ .

### B.11. *V2491 Cyg 2008#2*

Figure 48 shows the light/color curves of V2491 Cyg as well as LV Vul and V1500 Cyg. Based on the time-stretching method, we have the relation of

$$\begin{aligned}
 &(m - M)_{V,V2491 \text{ Cyg}} \\
 &= (m - M + \Delta V)_{V,LV \text{ Vul}} - 2.5 \log 0.46 \\
 &= 11.85 + 4.7 \pm 0.4 + 0.85 = 17.4 \pm 0.4 \\
 &= (m - M + \Delta V)_{V,V1500 \text{ Cyg}} - 2.5 \log 0.76 \\
 &= 12.3 + 4.8 \pm 0.4 + 0.30 = 17.4 \pm 0.4.
 \end{aligned} \tag{B65}$$

Thus, we obtain  $f_s = 0.46$  against the template nova LV Vul and  $(m - M)_V = 17.4 \pm 0.3$ . The new distance modulus in the  $V$  band is larger than the previous value of  $(m - M)_V = 16.5 \pm 0.1$  (Paper II). This is because the reddening is revised to be  $E(B - V) = 0.45$  and the timescaling factor is improved to be  $f_s = 0.46$ . We carefully redetermine the

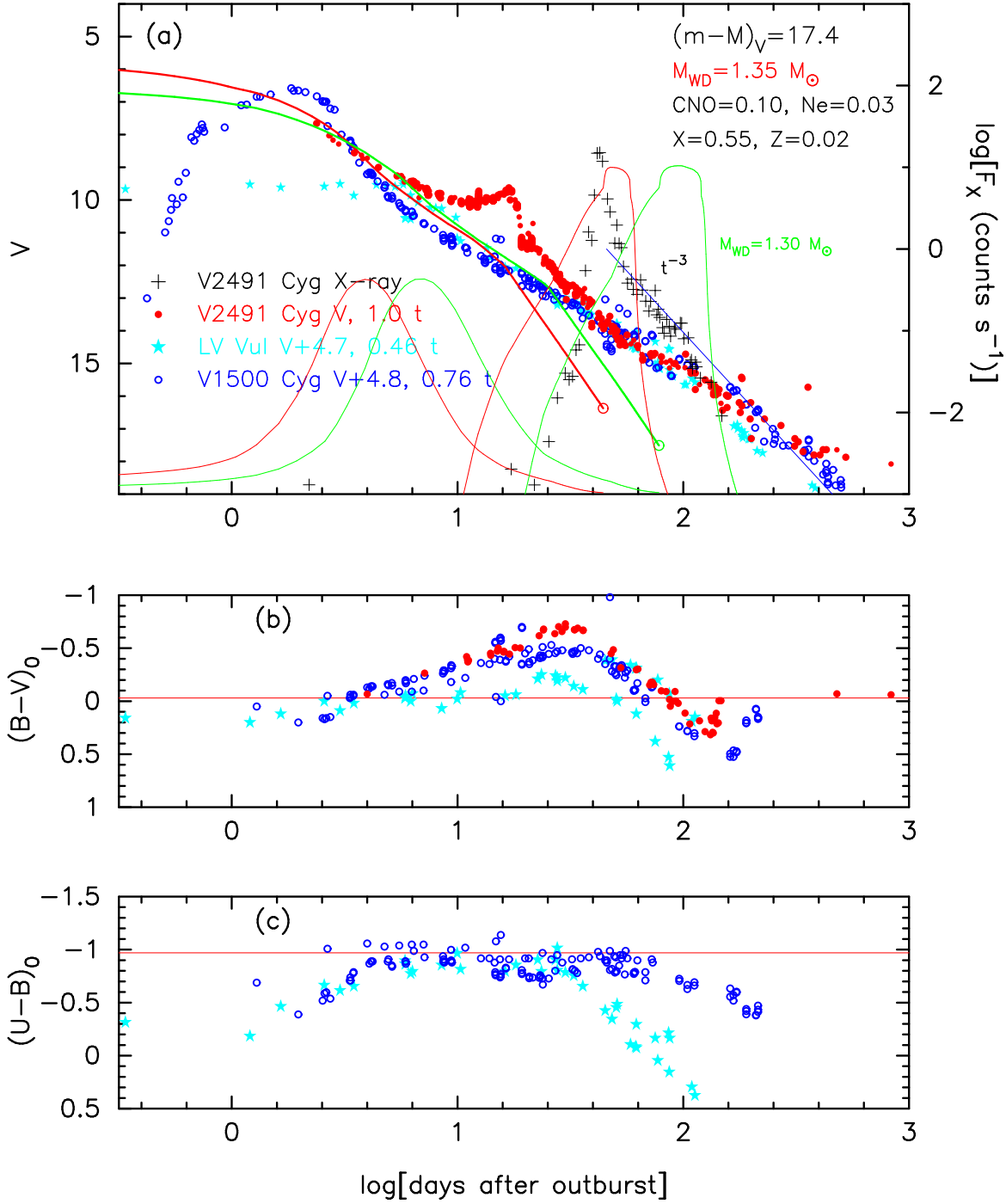


**Figure 48.** Same as Figure 19, but for V2491 Cyg (filled red circles). The  $(B - V)_0$  color of V2491 Cyg is dereddened with  $E(B - V) = 0.45$ . The data of V2491 Cyg are the same as those in Figure 70 of Paper II. We plot  $1.35 M_\odot$  and  $1.30 M_\odot$  WD models (solid red/green lines, respectively) with the chemical composition of Ne nova 2 (Hachisu & Kato 2010), taking  $(m - M)_V = 17.4$  for V2491 Cyg. We add the UV 1455Å flux (left thin solid red/green line) and supersoft X-ray flux (right thin solid red/green line) of the  $1.35/1.30 M_\odot$  WD models. See text for more details.

timescaling factor by fitting the  $(B - V)_0$  color curve of V2491 Cyg (filled red circles) with that of LV Vul (filled cyan stars) and V1500 Cyg (open blue circles) as shown in Figure 48(b). From Equations (14) and (B65), we obtain

$$\begin{aligned} (m - M')_{V, \text{V2491 Cyg}} \\ \equiv (m_V - (M_V - 2.5 \log f_s))_{\text{V2491 Cyg}} \end{aligned}$$



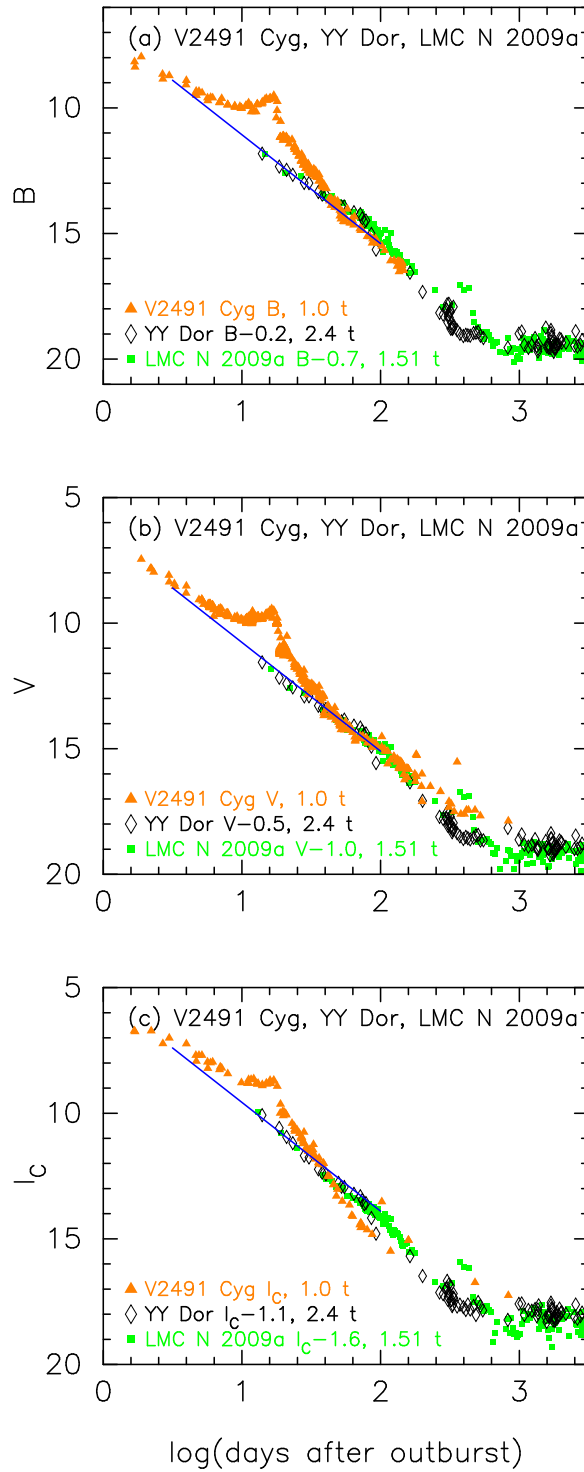


**Figure 49.** Same as Figure 21, but for V2491 Cyg. The  $BVI_C$  data of V2491 Cyg are taken from AAVSO, VSOLJ, and Munari et al. (2011).

$$\begin{aligned}
 &= (m - M + \Delta V)_{V, LV \text{ vul}} \\
 &= 11.85 + 4.7 \pm 0.4 = 16.55 \pm 0.4.
 \end{aligned}
 \tag{B66}$$

We obtain the reddening and distance from the time-stretching method. We plot the  $B$ ,  $V$ , and  $I_C$  light curves of V2491 Cyg together with those of the LMC novae YY Dor and LMC N 2009a in Figure 49 on a logarithmic timescale.

We apply Equation (7) for the  $B$  band to Figure 49(a) and obtain

$$\begin{aligned}
(m - M)_{B, V2491 \text{ Cyg}} &= ((m - M)_B + \Delta B)_{YY \text{ Dor}} - 2.5 \log 2.4 \\
&= 18.98 - 0.2 \pm 0.4 - 0.95 = 17.83 \pm 0.4 \\
&= ((m - M)_B + \Delta B)_{LMC \text{ N } 2009a} - 2.5 \log 1.51 \\
&= 18.98 - 0.7 \pm 0.4 - 0.45 = 17.83 \pm 0.4.
\end{aligned} \tag{B67}$$

Thus, we obtain  $(m - M)_{B, V2491 \text{ Cyg}} = 17.83 \pm 0.3$ . For the  $V$  light curves in Figure 49(b), we similarly obtain

$$\begin{aligned}
(m - M)_{V, V2491 \text{ Cyg}} &= ((m - M)_V + \Delta V)_{YY \text{ Dor}} - 2.5 \log 2.4 \\
&= 18.86 - 0.5 \pm 0.3 - 0.95 = 17.41 \pm 0.3 \\
&= ((m - M)_V + \Delta V)_{LMC \text{ N } 2009a} - 2.5 \log 1.51 \\
&= 18.86 - 1.0 \pm 0.3 - 0.45 = 17.41 \pm 0.3.
\end{aligned} \tag{B68}$$

Thus, we obtain  $(m - M)_{V, V2491 \text{ Cyg}} = 17.41 \pm 0.2$ . We apply Equation (8) for the  $I_C$  band to Figure 49(c) and obtain

$$\begin{aligned}
(m - M)_{I, V2491 \text{ Cyg}} &= ((m - M)_I + \Delta I_C)_{YY \text{ Dor}} - 2.5 \log 2.4 \\
&= 18.67 - 1.1 \pm 0.5 - 0.95 = 16.62 \pm 0.5 \\
&= ((m - M)_I + \Delta I_C)_{LMC \text{ N } 2009a} - 2.5 \log 1.51 \\
&= 18.67 - 1.6 \pm 0.5 - 0.45 = 16.62 \pm 0.5.
\end{aligned} \tag{B69}$$

Thus, we obtain  $(m - M)_{I, V2491 \text{ Cyg}} = 16.62 \pm 0.3$ .

We plot these three distance moduli of  $B$ ,  $V$ , and  $I_C$  bands in Figure 14(c) by the magenta, blue, and cyan lines, that is,  $(m - M)_B = 17.83$ ,  $(m - M)_V = 17.41$ , and  $(m - M)_I = 16.62$  together with Equations (11), (5), and (12). These three lines broadly cross at  $d = 15.9$  kpc and  $E(B - V) = 0.45$ .

### B.12. *V496 Sct 2009*

Figure 50 shows the light/color curves of V496 Sct as well as LV Vul and V1668 Cyg. In the early phase, the  $V$  light curve of V496 Sct overlaps that of LV Vul. In the middle phase, V496 Sct show a sharp and shallow dip due to dust blackout. In the later nebular phase, V496 Sct overlaps well with the upper branch of LV Vul, where the  $V$  light curve of LV Vul splits into two branches in the nebular phase due to the different responses of their  $V$  filters as discussed in Paper II. This is because strong [O III] lines contributes to the blue edge of  $V$  band filter in the nebular phase and small differences among the response functions of  $V$  filters make large differences in the  $V$  magnitudes. The  $(B - V)_0$  color curves of LV Vul also splits into two branches for  $\log t \gtrsim 2.0$ , that is, in the nebular phase. The lower branch of LV Vul in the  $(B - V)_0$  color curve is close to that of V496 Sct. We regard that the  $V$  light curve of V496 Sct follows V1668 Cyg and the upper branch of LV Vul and the  $(B - V)_0$  color curve of V496 Sct follows the lower branch of LV Vul.

Based on the time-stretching method, we have the relation of

$$\begin{aligned}
(m - M)_{V, V496 \text{ Sct}} &= (m - M + \Delta V)_{V, LV \text{ Vul}} - 2.5 \log 2.0 \\
&= 11.85 + 2.6 \pm 0.3 - 0.75 = 13.7 \pm 0.3 \\
&= (m - M + \Delta V)_{V, V1668 \text{ Cyg}} - 2.5 \log 2.0 \\
&= 14.6 - 0.1 \pm 0.3 - 0.75 = 13.75 \pm 0.3.
\end{aligned} \tag{B70}$$

Thus, we obtain  $f_s = 2.0$  against the template nova LV Vul and  $(m - M)_V = 13.7 \pm 0.2$ . The new value is much smaller than the previous estimate of  $(m - M)_V = 14.4 \pm 0.1$  (Paper II). This is because we improved the timescaling factor of  $f_s$  and the vertical  $V$  light curve fitting. From Equations (14) and (B70), we have the relation of

$$\begin{aligned}
(m - M')_{V, V496 \text{ Sct}} &\equiv (m_V - (M_V - 2.5 \log f_s))_{V496 \text{ Sct}}
\end{aligned}$$

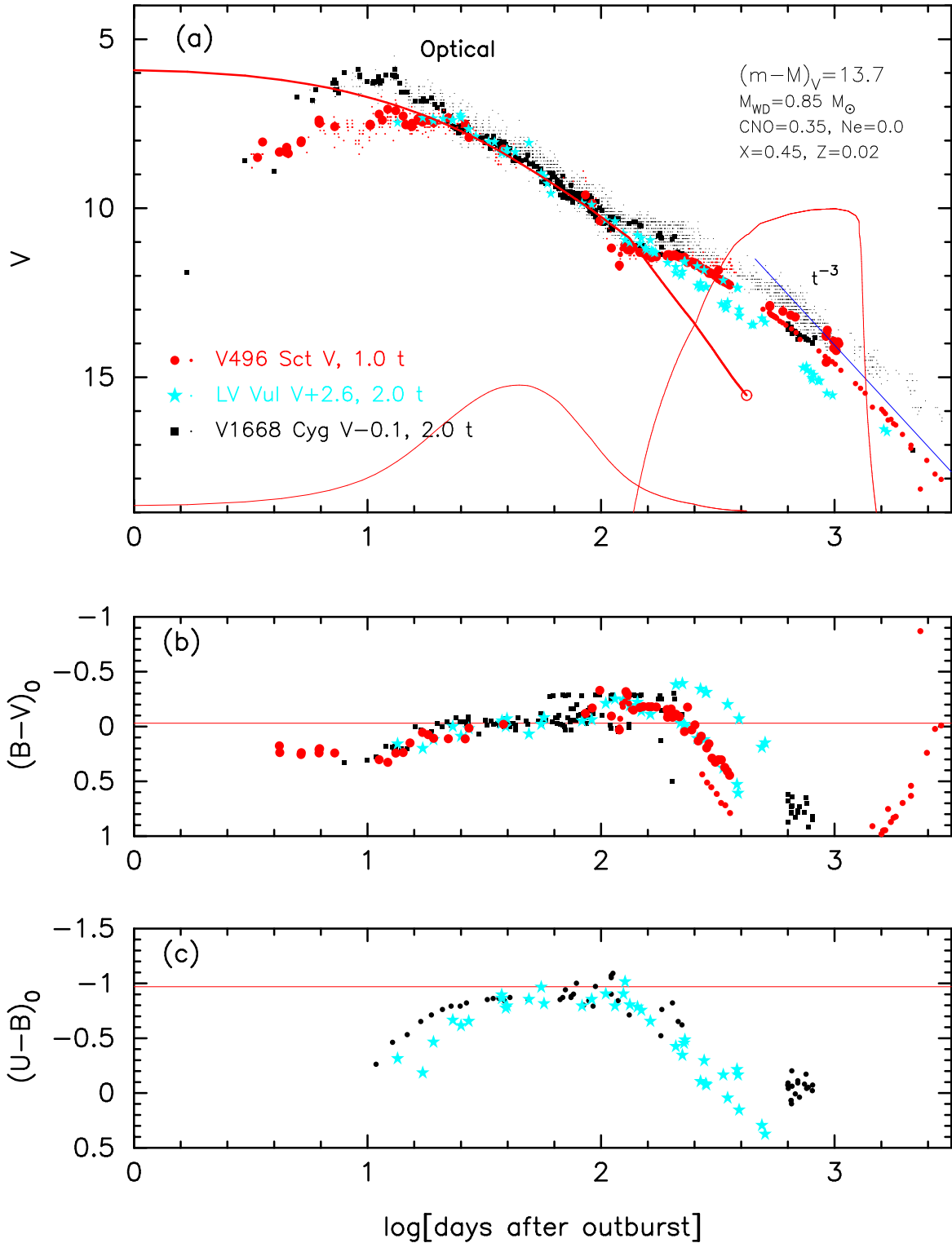


**Figure 50.** Same as Figure 19, but for V496 Sct (filled red circles for  $V$  and small red dots for visual). The data of V496 Sct are the same as those in Figure 73 of Paper II. We plot a  $0.85 M_{\odot}$  WD model (solid red lines) with the chemical composition of CO nova 3 (Hachisu & Kato 2016a), taking  $(m - M)_V = 13.7$  for V496 Sct. We add the UV 1455Å flux (left thin solid red line) and supersoft X-ray flux (right thin solid red line) of the  $0.85 M_{\odot}$  WD model. See the text for more details.

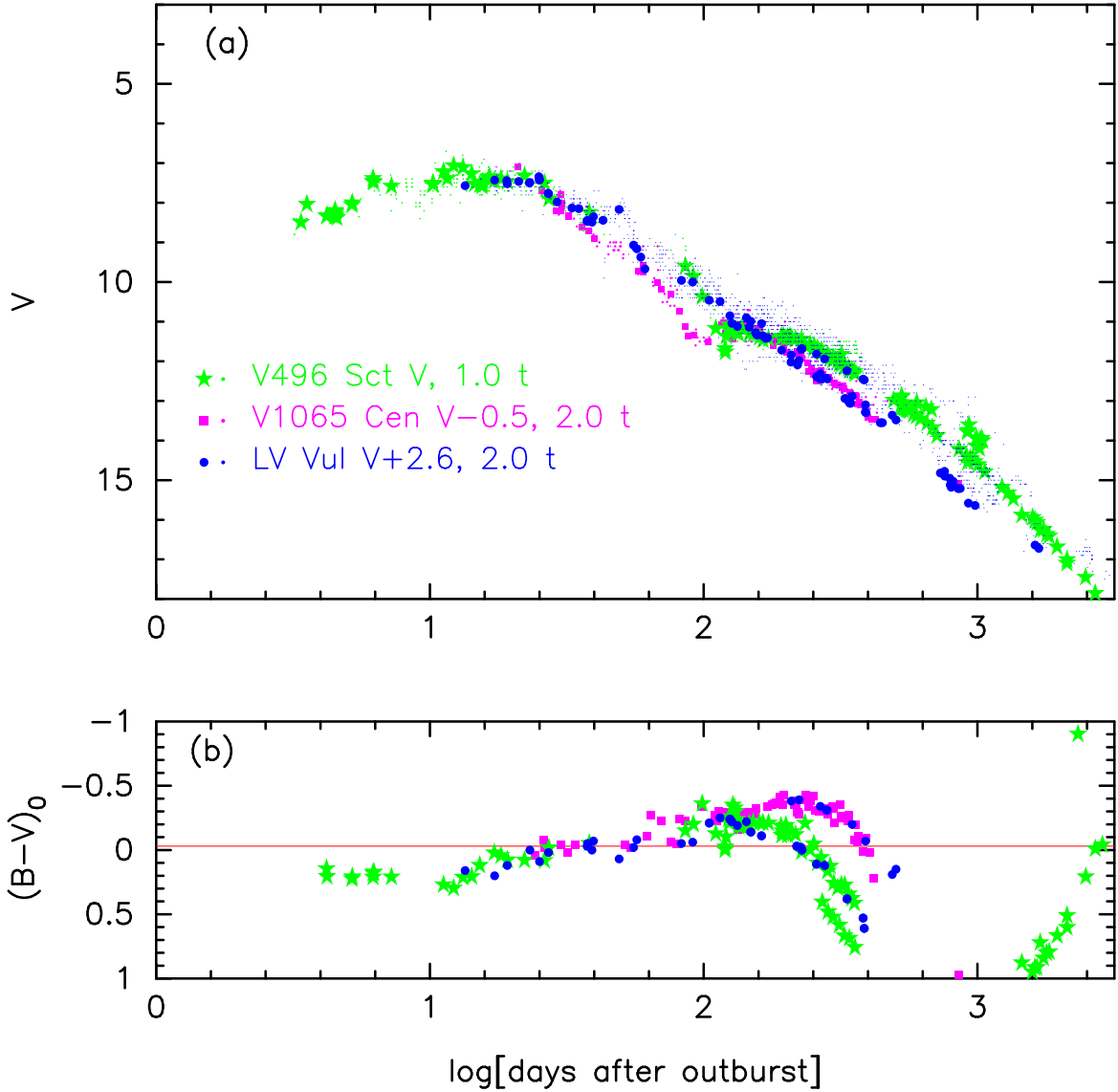


**Figure 51.** Same as Figure 50, but for a different set of V496 Sct, V1065 Cen, and LV Vul. The data of V496 Sct are the same as those in Figure 50. We also plot the  $BV$  data of V1065 Cen and LV Vul. The data of V1065 Cen are the same as those in Figure 4 of Hachisu & Kato (2018a).

$$\begin{aligned}
 &= (m - M + \Delta V)_{V, \text{LV Vul}} \\
 &= 11.85 + 2.6 \pm 0.3 = 14.45 \pm 0.3.
 \end{aligned} \tag{B71}$$

Figure 51 shows the light/color curves of V496 Sct as well as LV Vul and V1065 Cen. The light/color curves of V1065 Cen show different paths of V496 Sct. We regard that the  $V$  light curve of V1065 Cen follows the lower branch of LV Vul and the  $(B - V)_0$  color curve evolves along the upper branch of LV Vul in the nebular phase ( $t > 100$  day). For V1065 Cen, Hachisu & Kato (2018a) derived  $(m - M)_V = 15.0 \pm 0.2$  and  $E(B - V) = 0.45 \pm 0.05$  (and  $f_s = 1.0$  against LV Vul) as summarized in Table 1. Applying Equation (4) to Figure 51, we have the relation of

$$\begin{aligned}
 &(m - M)_{V, \text{V496 Sct}} \\
 &= (m - M + \Delta V)_{V, \text{LV Vul}} - 2.5 \log 2.0 \\
 &= 11.85 + 2.6 \pm 0.2 - 0.75 = 13.7 \pm 0.2 \\
 &= (m - M + \Delta V)_{V, \text{V1065 Cen}} - 2.5 \log 2.0 \\
 &= 15.0 - 0.5 \pm 0.2 - 0.75 = 13.75 \pm 0.2.
 \end{aligned} \tag{B72}$$

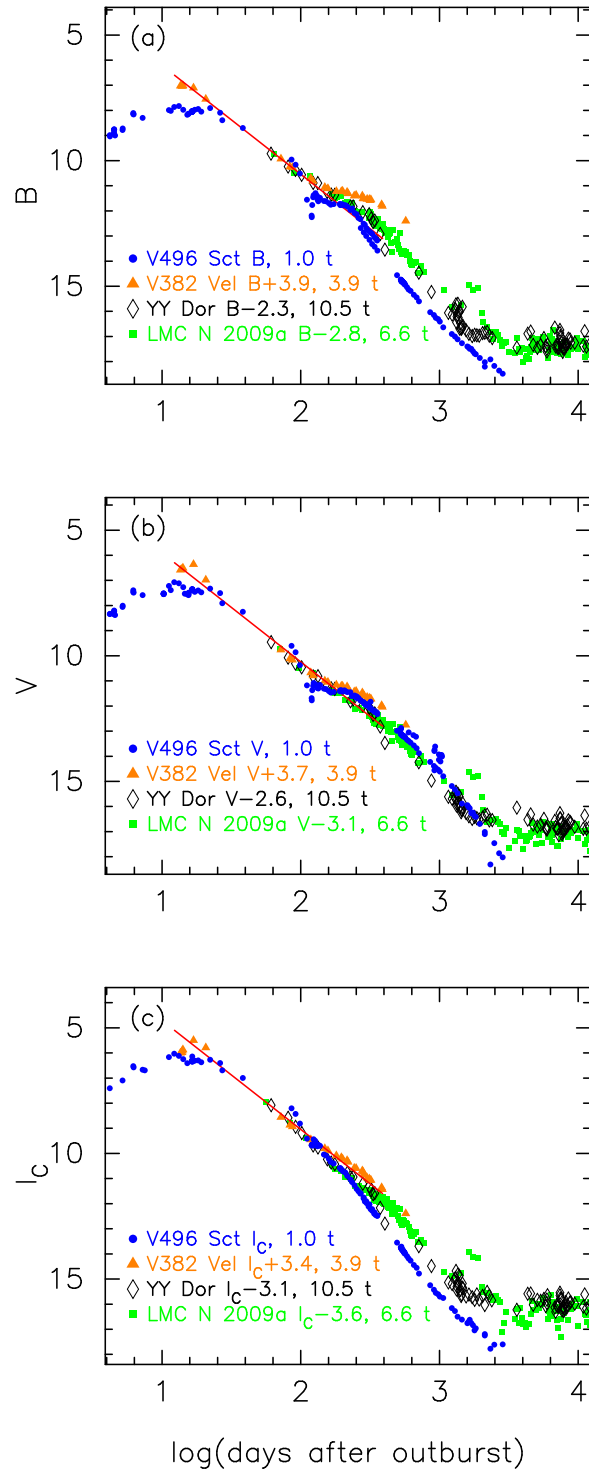


**Figure 52.** Same as Figure 21, but for V496 Sct. The  $BVI_C$  data of V496 Sct are taken from AAVSO, SMARTS, and Raj et al. (2012).

This value of  $(m - M)_V = 13.7 \pm 0.2$  is consistent with Equation (B70).

Figure 52 plots the  $B$ ,  $V$ , and  $I_C$  light curves of V496 Sct together with those of V382 Vel, and the LMC novae YY Dor and LMC N 2009a. We apply Equation (7) for the  $B$  band to Figure 52(a) and obtain

$$(m - M)_{B, \text{V496 Sct}}$$

$$\begin{aligned}
&= ((m - M)_B + \Delta B)_{\text{YY Dor}} - 2.5 \log 10.5 \\
&= 18.98 - 2.3 \pm 0.2 - 2.55 = 14.13 \pm 0.2 \\
&= ((m - M)_B + \Delta B)_{\text{LMC N 2009a}} - 2.5 \log 6.6 \\
&= 18.98 - 2.8 \pm 0.2 - 2.05 = 14.13 \pm 0.2 \\
&= ((m - M)_B + \Delta B)_{\text{V382 Vel}} - 2.5 \log 3.9 \\
&= 11.75 + 3.9 \pm 0.2 - 1.47 = 14.18 \pm 0.2.
\end{aligned} \tag{B73}$$

Thus, we obtain  $(m - M)_{B, \text{V496 Sct}} = 14.15 \pm 0.1$ , For the  $V$  light curves in Figure 52(b), we similarly obtain

$$\begin{aligned}
&(m - M)_{V, \text{V496 Sct}} \\
&= ((m - M)_V + \Delta V)_{\text{YY Dor}} - 2.5 \log 10.5 \\
&= 18.86 - 2.6 \pm 0.2 - 2.55 = 13.71 \pm 0.2 \\
&= ((m - M)_V + \Delta V)_{\text{LMC N 2009a}} - 2.5 \log 6.6 \\
&= 18.86 - 3.1 \pm 0.2 - 2.05 = 13.71 \pm 0.2 \\
&= ((m - M)_V + \Delta V)_{\text{V382 Vel}} - 2.5 \log 3.9 \\
&= 11.5 + 3.7 \pm 0.2 - 1.47 = 13.73 \pm 0.2.
\end{aligned} \tag{B74}$$

Thus, we obtain  $(m - M)_{V, \text{V496 Sct}} = 13.71 \pm 0.1$ . We apply Equation (8) for the  $I_C$  band to Figure 52(c) and obtain

$$\begin{aligned}
&(m - M)_{I, \text{V496 Sct}} \\
&= ((m - M)_I + \Delta I_C)_{\text{YY Dor}} - 2.5 \log 10.5 \\
&= 18.67 - 3.1 \pm 0.2 - 2.55 = 13.02 \pm 0.2 \\
&= ((m - M)_I + \Delta I_C)_{\text{LMC N 2009a}} - 2.5 \log 6.6 \\
&= 18.67 - 3.6 \pm 0.2 - 2.05 = 13.02 \pm 0.2 \\
&= ((m - M)_I + \Delta I_C)_{\text{V382 Vel}} - 2.5 \log 3.9 \\
&= 11.1 + 3.4 \pm 0.2 - 1.47 = 13.03 \pm 0.2.
\end{aligned} \tag{B75}$$

Thus, we obtain  $(m - M)_{I, \text{V496 Sct}} = 13.02 \pm 0.2$ .

## REFERENCES

- Ando, H., & Yamashita, Y. 1976, PASJ, 28, 171
- Andreä, J., Drechsel, H., Snijders, M. A. J., & Cassatella, A. 1991, A&A, 244, 111
- Arhipova, V. P., & Zaitseva, G. V. 1976, Soviet Astron. Lett., 2, 35
- Austin, S. J., Wagner, R. M., Starrfield, S. et al. 1996, AJ, 111, 869
- Becker, H. J., & Duerbeck, H. W. 1980, PASP, 92, 792
- Belokon, E. T., & Larionov, V. M. 1977, Soviet Astronomy, 21, 355
- Bode, M. F., Darnley, M. J., Beardmore, A. P., et al. 2016, ApJ, 818, 145
- Bohlin, R. C., Savage, B. D., & Drake, J. F. 1978, ApJ, 224, 132
- Burlak, M. A. 2008, Astronomy Letters, 34, 249
- Cassatella, A., Altamore, A., & González-Riestra, R. 2002, A&A, 384, 1023
- Chincarini, G. 1964, PASP, 76, 289
- Chincarini, G., & Rosino, L. 1964, Annales d'Astrophysique, 27, 469
- Chochol, D., Grygar, J., Pribulla, T., et al. 1997, A&A, 318, 908
- Chochol, D., Hric, L., Urban, Z., et al. 1993, A&A, 277, 103
- Chen, B.-Q., Huang, Y., Liu, X.-W., et al. 2018, MNRAS, 483, 4277
- Cheung, C. C., Jean, P., Shore, S. N., et al. 2013, The Astronomer's Telegram, 5649, 1
- Cohen, J. G. 1985, ApJ, 292, 90
- Cohen, J. G. 1988, The extragalactic distance scale, Proceedings of the ASP 100th Anniversary Symposium, eds. S. van den Bergh & C. J. Prechet (San Francisco, ASP), ASP conference series, 4, 114
- della Valle, M., & Livio, M. 1995, ApJ, 452, 704
- della Valle, M., Pasquini, L., Daou, D., & Williams, R. E. 2002, A&A, 390, 155
- Diaz, M. P., Costa, R. D. D., & Jatenco-Pereira, V. 2001, PASP, 113, 1554
- Downes, R. A., & Duerbeck, H. W. 2000, AJ, 120, 2007
- Ederoclite, A., Mason, E., della Valle, M., et al., A&A, 459, 875
- Ennis, D., Becklin, E. E., Beckwith, S., et al. 1977, ApJ, 214, 478
- Evans, P. A., Beardmore, A. P., Page, K. L., et al. 2009, MNRAS, 397, 1177
- Eyres, S. P. S., Davis, R. J., Bode, M. F., & Lloyd, H. M. 1996, IAUC, 6292, 2
- Fernie, J. D. 1969, PASP, 81, 374
- Franckowiak, A., Jean, P., Wood, M., Cheung, C. C., & Buson, S. 2018, A&A, 609, A120
- Friedjung, M. 1966, MNRAS, 132, 143
- Furuyama, S., & Pearce, A. 2014, CBET, 3802, 1
- Gallagher, J. S., & Holm, A. V. 1974, ApJ, 189, L123
- Gallagher, J. S., & Ney, E. P. 1976, ApJ, 204, L35
- Green, G. M., Schlafly, E. F., Finkbeiner, D. P., et al. 2015, ApJ, 810, 25
- Green, G. M., Schlafly, E. F., Finkbeiner, D. P., et al. 2018, MNRAS, 478, 651
- Guido, E., Howes, N., Nicolini, M., et al. 2013, IAUC, 9265, 1
- Güver, T., & Özel, F. 2009, MNRAS, 400, 2050
- Hachisu, I., & Kato, M. 2006, ApJS, 167, 59
- Hachisu, I., & Kato, M. 2009, ApJL, 694, L103
- Hachisu, I., & Kato, M. 2010, ApJ, 709, 680
- Hachisu, I., & Kato, M. 2014, ApJ, 785, 97 (Paper I)
- Hachisu, I., & Kato, M. 2015, ApJ, 798, 76
- Hachisu, I., & Kato, M. 2016a, ApJ, 816, 26
- Hachisu, I., & Kato, M. 2016b, ApJS, 223, 21 (Paper II)
- Hachisu, I., & Kato, M. 2017, in Proceedings of the Palermo Workshop 2017 on “The Golden Age of Cataclysmic Variables and Related Objects - IV”, ed. F. Giovannelli et al. (Trieste: SISSA PoS), 315, 47
- Hachisu, I., & Kato, M. 2018a, ApJ, 858, 108
- Hachisu, I., & Kato, M. 2018b, ApJS, 237, 4
- Hachisu, I., & Kato, M. 2019, ApJS, submitted
- Hachisu, I., Kato, M., Kiyota, S., et al. 2006b, ApJL, 651, L141
- Hachisu, I., Kato, M., Kiyota, S., et al. 2008b, RS Ophiuchi (2006) and the Recurrent Nova Phenomenon, ASP Conf. Ser. 401, eds. A. Evans et al. (San Francisco, ASP), p.206.
- Hachisu, I., Kato, M., & Luna, G. J. M. 2007, ApJ, 659, L153
- Harrison, T. E., Bornak, J., McArthur, B. E., & Benedict, G. F. 2013, ApJ, 767, 7
- Hric, L., Petrík, K., Urban, Z., Hanžl, D., A&AS, 133, 211
- Ibarra, A., & Kuulkers, E. 2008, The Astronomer's Telegram, 1473, 1
- Ibarra, A., Kuulkers, E., Beardmore, A., et al. 2008, The Astronomer's Telegram, 1478, 1
- Imara, N., & Blitz, L. 2007, ApJ, 662, 969
- Izzo, L., Mason, E., Vanzì, L., et al. 2013, The Astronomer's Telegram, 5639, 1
- Kato, M., & Hachisu, I., 1994, ApJ, 437, 802
- Kato, M., Saio, H., Hachisu, I., & Nomoto, K. 2014, ApJ, 793, 136
- Kimeswenger, S., Dalnodar, S., Knapp, A., et al. 2008, A&A, 479, L51

- Kolotilov, E. A., & Noskova, R. I. 1986, *Soviet Astronomy Letters*, 12, 370
- Krautter, J., Beuermann, K., Leitherer, C., et al. 1984, *A&A*, 37, 307
- Kreiner, J. M., Kurpińska, M., & Winiarski, M. 1966, *Acta Astronomica*, 16, 137
- Kuulkers, E., Ness, J.-U., Ibarra, A., et al. 2013, *The Astronomer's Telegram*, 5628, 1
- Liszt, H. S. 2014, *ApJ*, 780, 10
- Lynch, D. K., Russell, R. W., Rudy, R. J., Woodward, C. E., & Schwarz, G. J. 2008b, *IAUC*, 8935, 1
- Marshall, D. J., Robin, A. C., Reylé, C., Schultheis, M., & Picaud, S. 2006, *A&A*, 453, 635
- Mason, E., Shore, S. N., De Gennaro Aquino, I., et al. 2018, *ApJ*, 853, 27
- Munari, U., & Zwitter, T. 1997, *A&A*, 318, 269
- Munari, U., Yudin, B. F., Kolotilov, E. A., et al. 1994a, *A&A*, 284, L9
- Munari, U., Tomov, T. V., Hric, L., Hazucha, P. 1994b, *Inf. Bull. Variable Stars*, 3977, 1
- Munari, U., Henden, A., Valentini, M., et al. 2008a, *MNRAS*, 387, 344
- Munari, U., Siviero, A., Henden, A., et al. 2008b, *A&A*, 492, 145
- Munari, U., Siviero, A., Dallaporta, S., et al. 2011, *New Astronomy*, 16, 209
- Naik, S., Banerjee, D. P. K., & Ashok, N. M. 2009, *MNRAS*, 394, 1551
- Naik, S., Banerjee, D. P. K., Ashok, N. M., Das, R. K. 2010, *MNRAS*, 404, 367
- Naito, H., Mizoguchi, S., Arai, A., et al. 2012, *A&A*, 543, A86
- Ness, J.-U., Schwarz, G. J., Retter, A., et al. 2007a, *ApJ*, 663, 505
- Ness, J.-U., Starrfield, S., Jordan, C., Krautter, J., & Schmitt, J. H. M. M. 2005, *MNRAS*, 364, 1015
- Nishiyama, S., Tamura, M., Hatano, H., et al. 2009, *ApJ*, 696, 1407
- Noskova, R. I., Zaitseva, G. V., & Kolotilov, E. A. 1985, *Soviet Astronomy Letters*, 11, 257
- Orio, M., Parmar, A. N., Greiner, J., et al. 2002, *MNRAS*, 333, L11
- Özdörmez, A., Güver, T., Cabrera-Lavers, A., Ak, T. 2016, *MNRAS*, 461, 1177
- Özdörmez, A., Ege, E., Güver, T., & Ak, T. 2018, *MNRAS*, 476, 4162
- Page, K. L., Beardmore, A. P., Osborne, J. P., & Schwarz, G. J. 2014, *The Astronomer's Telegram*, 5966, 1
- Piatti, A., & Geisler, D. 2013 *AJ*, 145, 17
- Pietrzyński, G., Graczyk, D., Gieren, W., et al. 2011, *Nature*, 495, 76
- Pfau, W. 1976, *Inf. Bull. Variable Stars*, 1106, 1
- Poznanski, D., Prochaska, J. X., Bloom, J. S. 2012, *MNRAS*, 426, 1465
- Raj, A., Ashok, N. M., Banerjee, D. P. K., et al. 2012, *MNRAS*, 425, 2576
- Rieke, G. H., & Lebofsky, M. J. 1985, *ApJ*, 288, 618
- Robb, R. M., & Scarfe, C. D. 1995, *MNRAS*, 273, 347
- Rudy, R. J., Lynch, D. K., Russell, R. W., Woodward, C. E., & Covey, K. 2008b, *IAUC*, 8938, 2
- Saito, R. K., Minniti, D., Angeloni, R., et al. 2013, *A&A*, 554, A123
- Saizar, P., Starrfield, S., Ferland, G. J., et al. 1991, *ApJ*, 367, 310
- Sale, S. E., Drew, J. E., Barentsen, G., et al. 2014, *MNRAS*, 443, 2907
- Schaefer, B. E. 2018, *MNRAS*, 481, 3033
- Schmeer, P., & Gualdoni, C. 2008, *IAUC*, 8999, 4
- Schlafly, E. F., & Finkbeiner, D. P. 2011, *ApJ*, 737, 103
- Schmidt, Th. 1957, *Z. Astrophys.*, 41, 181
- Schultheis, M., Chen, B. Q., Jiang, B. W., et al. 2014, *A&A*, 566, A120
- Schwarz, G. J., Ness, J.-U., Osborne, J. P., et al. 2011, *ApJS*, 197, 31
- Seaton, M. J. 1979, *MNRAS*, 187, 73
- Selvelli, P., & Gilmozzi, R. 2013, *A&A*, 560, A49
- Shen, L.-Z., et al. 1964, *Acta Astronomica Sinica*, 12, 83
- Shore, S. N., Schwarz, G., Bond, H. E., et al. 2003, *AJ*, 125, 1507
- Shore, S. N., Schwarz, G. J., Walter, F. M., et al. 2014, *The Astronomer's Telegram*, 6413, 1
- Slavin, A. J., O'Brien, T. J., Dunlop, J. S. 1995, *MNRAS*, 276, 353
- Slovak, M. H. & Vogt, S. S. 1979, *Nature*, 277, 114
- Steiner, J. E., Campos, R., & Cieslinski, D. 1999, *IAUC*, 7185, 2
- Tarasova, T. N. 2014b, *Astronomy Reports*, 58, 302
- Tempesti, P. 1972, *A&A*, 20, 63
- Tempesti, P. 1979, *Astronomische Nachrichten*, 300, 51
- The, P. S., & van der Klis, M. 1976, *Inf. Bull. Variable Stars*, 1089, 1
- Tomkin, J., Lambert, D. L., & Woodman, J. 1976, *A&A*, 48, 319
- Tomov, T., Swierczynski, E., Mikołajewski, M., & Ilkiewicz, K. 2015, *A&A*, 576, A119
- van den Bergh, S., & Younger, P. F. 1987, *A&AS*, 70, 125
- van Genderen, A. M. 1963, *Bull. of the Astr. Inst. of the Netherlands*, 17, 293



- Waagen, E. O., Henden, A., Maury, A., et al. 2008, IAUC, 8999, 1
- Wade, R. A., Ciardullo, R., Jacoby, G. H., & Sharp, N. A. 1991, AJ, 102, 1738
- Walter, F. M., Battisti, A., Towers, S. E., Bond, H. E., & Stringfellow, G. S. 2012, PASP, 124, 1057
- Williamon, R. M. 1977, PASP, 89, 44
- Williams, R. E. 1992, AJ, 104, 725
- Woodward, C. E., Gehrz, R. D., Jones, T. J., Lawrence, G. F., & Skrutskie, M. F. 1997, ApJ, 477, 817
- Wu, C.-C., Holm, A. V., Panek, R. J., et al. 1989, ApJ, 339, 443
- Young, P. J., Corwin, H. G., Bryan, J., & de Vaucouleurs, G. 1976, ApJ, 209, 882